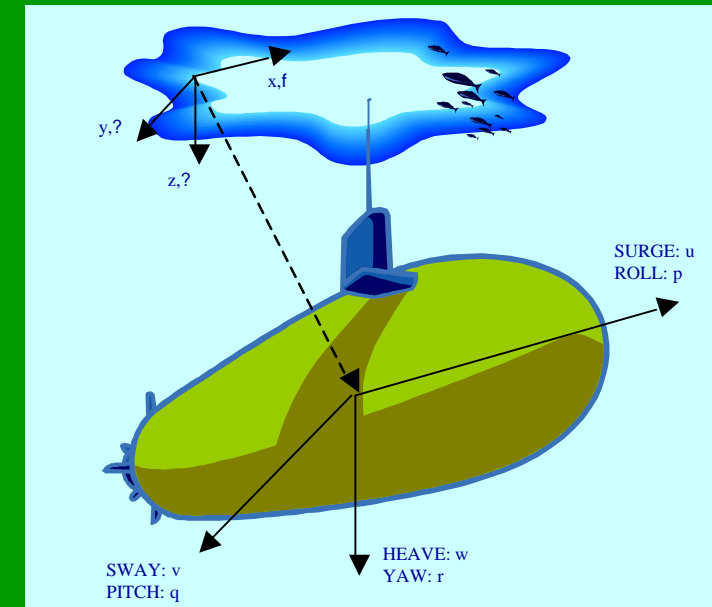# Automation for the Maritime Industries

AUTOMAR Thematic Network (CICYT-DPI2002-10620-E) was aiming to foster Spanish research and innovation activity in the maritime industrial sector in order to strengthen their role in Europe. During the three years of the AUTOMAR Network many activities have been carried out, and all the partners have actively contributed. This book collects in its 14 Chapters excellent, state of the art, contributions that show clearly the high level of scientific knowledge in this field reached by the Spanish RTD, both at the Universities and at the Research Institutions.

It can be expected that the book content will serve to promote the knowledge and applications of the complex control and mechatronic systems at present under development in Spain, and it will also serve as a sound background for those young scientists entering in this exciting field of automation of the maritime industries.

Edited by
J Aranda, M A Armada, J M de la Cruz

Automation for the Maritime Industries

Automation for the Maritime Industries

Edited by

J Aranda
Departamento de Informática y Automática
UNED. Madrid

M A Armada
Instituto de Automática Industrial
Consejo Superior de Investigaciones Científicas

J M de la Cruz
Facultad de Ciencias Físicas
Universidad Complutense de Madrid

First Published 2004

About the Editors

Joaquín Aranda received the Licentiate degree from the Complutense University of Madrid, and the PhD degree from the UNED (*Universidad Nacional de Educación a Distancia*). He served as Teaching Assistant in the Department of Computer Science and Automatic Control (Departamento de Informática y Automática), University of Madrid, and as Assistant Professor, Associate Professor and Senior Professor at the UNED. He was deputy director of the Computer Science University School (*Escuela Universitaria de Informática*) of UNED, and director of Computer Science High School (*Escuela Técnica Superior de Ingeniería Informática*). He is author or co-author of more than 70 publications (including books chapters, papers in journals and conference proceedings). His scientific activities cover various aspects within the control engineering field: robust control, computer control, modelling and simulation of continuous processes, and application of control and simulation to high speed craft, airplane and robotic. He is working in several research projects relating to these topics.

Manuel A Armada received his PhD in Physics from the University of Valladolid (Spain) in 1979. Since 1976 he has been involved in research activities related to Automatic Control (singular perturbations and aggregation, bilinear systems, adaptive and non-linear control, multivariable systems in the frequency domain, and digital control) and Robotics (kinematics, dynamics, and tele-operation). He has been working in more than forty RTD projects (including international ones like EUREKA, ESPRIT, BRITE/EURAM, GROWTH, and others abroad the EU, especially with Latin America (CYTED) and Russia, where he is member of the Russian Academy of Natural Sciences. Dr Armada owns several patents, and has published over 200 papers (including contributions to several books, monographs, journals, international congresses, and workshops). He is currently the Head of the Automatic Control Department at the Instituto de Automatica Industrial (IAI-CSIC), his main research direction being concentrated in robot design and control, with especial emphasis in fields like flexible robots and on walking and climbing machines.

Jesús M. de la Cruz received his PhD in Physics from the Complutense University of Madrid in 1984. He has been Associated Professor in the area of Automation and System Engineering, Faculty of Science (UNED) during the period 1986-1990. He is Full Professor at the Faculty of Physics (Complutense University of Madrid) since 1992. He has been Director of the Departmental Section of Informatics and Automatic at the Faculty of Physics (Complutense University of Madrid), 1993-1997, and Director of the Department of Computer Architecture and Automatic, 1997-2001. He has participated and managed in many research projects, like those related with: High Speed Ship (Bazan, 1998-2000), gas distribution optimisation (Repsol-YPF), Pharmacy Logistics (COFARES, 2001-2002), robust control for aeronautics (EC Garteur FM (AG08)). Prof. de la Cruz has directed 10 PhD Thesis in the area of Automatic Control, and published over 20 papers in international journals. He is co-author of a book on computer vision. His present research is focused on control systems and statistical learning. He is a member of IEEE.

vi

Contents

Preface

AUTOMAR Thematic Network (CICYT- DPI2002- 10620- E) was organised with the idea of putting together all the Spanish research groups and firms involved somehow in the maritime sector in order to increase co-operation level and knowledge dissemination. The AUTOMAR Partners are the following Institutions:

- Universidad Nacional de Educación a Distancia.
    - Departamento de Informática y Automática
- Universidad Complutense de Madrid
    - Departamento de Arquitectura de Computadores y Automática
- Universidad de Cantabria
    - Departamento de Tecnología Electrónica, Ingeniería de Sistemas y Automática
- Universidade da Coruña
    - E. S. Marina Civil
- Consejo Superior de Investigaciones Científicas
    - Instituto de Automática Industrial
- Universidad Politécnica de Madrid
    - Departamento de Automática, Ingeniería Electrónica e Informática Industrial
    - Departamento de Arquitectura y Contrucción Navales
- Universidad Politécnica de Cataluña
    - Departamento de Ingeniería de Sistemas, Automática e Informática Industrial
- Universidad de Cádiz
    - Facultad de Ciencias Naúticas
- Canal de Experiencias Hidrodinámicas de El Pardo

AUTOMAR was aiming to foster Spanish research and innovation activity in the maritime industrial sector in order to strengthen their role in Europe. During the three years of the AUTOMAR Network many activities have been carried out, and all the partners have actively contributed. This book, prepared to be presented at the last AUTOMAR meeting, collects in its 14 Chapters excellent, state of the art, contributions that show clearly the level of scientific knowledge in this field reached by the Spanish RTD, both at the Universities and at the Research Institutions. We would like to thank all of authors and the participant Institutions for their contributions and help. Special thanks are for the Ministry of Education and Science for the AUTOMAR network funding under project DPI2002- 10620- E.

Joaquín Aranda
Manuel A. Armada
Jesús M. de la Cruz

November 2004

x

Chapter 1

Advances on Mechanical and Thermal Load Monitoring Applied to Marine Diesel Engines

RAMÓN FERREIRO GARCÍA
University of A Coruña, Spain, Dept. of Industrial Engineering
MANUEL HARO CASADO
University of Cadiz, Spain, Dept of System Engineering

The aim of the work deals with the problem of develop and implement a software based tool to monitor thermal and mechanical aspects and detect load severity on journal bearings deciding the properly action in Marine Diesel Engines, using advanced aspects of functional and hardware redundancy applied on fault detection, fault isolation, decision making and system recovery without applying on-line vibration monitoring of main and crankshaft bearings. To achieve such objectives, functional redundant back-propagation neural networks are used as universal functional approximation devices in combination with rule based strategies to find specific variables and process parameter changes useful in decision-making.

1 INTRODUCTION

1.1 Motivation and Objectives

Between actual trends in development of engine room monitoring and alarm systems are multifunctional devices and/or virtual instrumentation based in software sensors-predictors and artificial intelligence (AI) arranged as combination of neural networks based models or predictors with expert knowledge or rule based systems. Development of digital processing algorithms and tools has created the possibility to obtain the new quality of operating condition measurements. Instead of using many single-quantity meters traditionally applied in ship engine control room, a few multifunctional microprocessor based or PC based devices configured into virtual instrumentation could be applied.

This work is focused on main engine monitoring of typical hardware sensors related with combustion performance and main bearings monitoring including diagnosis as an alternative to on-line mechanical vibration analysis. The idea of detecting load severity on journal bearings deals with the need to early detection of bearings malfunction or some engine parts supporting overloads influencing crankshaft and main bearings. Consequently the objectives of the work are:

(a) To develop a methodology in condition monitoring to be applied on crankshaft bearings diagnosis for Marine Diesel Engines as an alternative to vibration monitoring systems and combustion related variables monitoring.

(b) To develop a software based tool for on-line fault detection, fault isolation, decision making and system recovery avoiding to apply on-line vibration monitoring of crankshaft bearings.

(c) To develop and apply in the monitoring system algorithms based on artificial intelligence (AI), supporting typical functions such as trouble shooting, prediction and decision making procedures focussed on system recovery.

(d) To assess severity limits with regard to journal bearings condition using some redundant thermal and mechanical model based approaches necessary to develop the mentioned software tool.

1.2 Background on systems monitoring

Products quality specifications associated to the complexity of process operation are exponentially increasing. In order to alleviate the operating requirements associated with these demands, plant health is being relayed upon the ultimate state of the art monitoring technology. In order to achieve required performance specifications, processes must tolerate instrumentation faults to operate fault free or safely.

Process supervision is the task responsible for correct operation by means of process monitoring tasks. The types of faults encountered in industrial applications are commonly classified into some of the following groups:

- Process parameter changes
- Disturbance parameter changes
- Actuator malfunctions
- Sensor malfunctions

The sequence of subtasks to be carried out to ensure the right process operation is the main body of process supervision usually referred to as the process monitoring tasks, which include: faults detection, fault identification, fault diagnosis and fault removing by process intervention, process recovery or process reconfiguration.

Process monitoring is based in data acquisition and data processing procedures. Process monitoring tasks can be classified into one or several following approaches:

- Data-driven
- Analytical
- Knowledge-based

*Data-driven.-*The proficiency of the data-driven, analytical and knowledge-based approaches depends on the quality and type of available models, and on the quantity and quality of data available.

Principal Component Analysis (PCA) is the most widely used data-driven technique. PCA is an optimal dimensionality reduction technique in terms of capturing the variance of the data, and it accounts for correlations among variables [1], [2]. The structure abstracted by PCA can be useful in identifying either the variables responsible for the fault and /or the variables most affected by the fault.

Fisher Discriminant Analysis (FDA) is a dimensionality reduction technique developed and studied within the pattern classification community [3]. FDA determines the portion of observation space that is most effective in discriminating amongst several data classes. Discriminant analysis is applied to this portion of the observation space for fault diagnosis

Partial Least Squares (PLS) are data decomposition methods for maximising covariance between predictor block and predicted block for each component [4], [5], [6], [7].

Analytical.- Analytical methods that use residuals as features are commonly referred to as analytical redundancy methods. The residuals are the outcomes of consistency checks between the plant observations and its math-model. The residuals will be sufficiently large values under presence of faults and small or negligible in the presence of disturbances, noise

and or modelling errors [8], [9], [10]. There are three main ways commonly used to generate residuals:

- Parameter estimation
- Observers
- Parity relations

In the case of parameter estimation, the residuals are the difference between the nominal model parameters and the estimated model parameters. Deviations in the model parameters is an indication used as the basis for detecting and isolating faults [11], [12], [13], [14].

In the observer-based methods, system output is reconstructed from measurements or a subset of measurements with the help of observers. The differences between actual measured output and estimated output are the residuals [15], [16], [17].

Parity relations strategy checks the consistency of process math-model (the mathematical equation of the system) with real time measurements. The parity relations are subjected to a linear dynamic transformation with the transformed residuals used in detection and isolation tasks [18], [19], [20]. Mentioned and commented analytical approaches requires error free mathematical models in order to be effective.

Knowledge-based.- Knowledge-based methods, extensively applied on process monitoring tasks include the following:

- Causal analysis
- Expert systems
- Pattern recognition

This techniques are based on qualitative models, which can be obtained through causal modelling of the systems, expert knowledge, a detailed model describing the system, or fault-symptom based cases.

Causal analysis techniques are based on the causal modelling of fault-symptom relationships. Causal analysis techniques including signed directed graphs and the symptom tree are primarily used in fault diagnosis [21], [22], [23].

Expert systems are used under a human reasoning scheme (shallow-knowledge expert system). Domain experts experience can be formulated in terms of knowledge stored into a rule base, combined with first principles knowledge, and applied successfully on fault diagnosis [24], [25]. In contrast to shallow-knowledge expert systems, deep-knowledge expert systems are based on a model such as engineering fundamentals, a structural description of the system, or a complete behavioural description of its components in faulty and normal operation conditions [26]. More advanced expert systems using machine learning techniques are advantageously used to shallow and deep knowledge expert systems, in which neural network based learning algorithms are extensively used [27].

Pattern recognition techniques use association between data patterns and faults classes without an explicit modelling of internal process states or structure. Artificial neural networks and self-organizing maps based in the unsupervising learning known as Kohonen self-organising map are the main tools [28].

An extensively used technique for process diagnosis based in neural networks apply the back-propagation neural network scheme [29]. In this work, back propagation neural networks will be used as the main tool associated to rule based decision making strategies [30], [31].

None of the mentioned methods are affective (alone or individually used) in large scale systems supervision without being combined between them. Usually the best process monitoring schemes include the use of multiple methods for fault detection, identification and diagnosis.

Next sections deals with following work: Paragrah 2 shows the modelling task using Neural Networks (NN) functional approximation to solve general modelling problems including virtual sensors and predictors. Paragraph 3 describes a diagnosing methology using functional and hardware redundancy. Paragraph 4 describes the proposed analytical modelling task using thermal and mechanical load properties for crankcase or main journal bearings. Paragraph 5 describes the developed software based tool with an application example on a MAN B&W type Marine Diesel Engine

2 FUNCTIONAL APPROXIMATION BY NEURAL NETWORK BASED MODELLING

It is not common to operate with linear processes because a system is linear if all of its elements are linear and non-linear if any element is non-linear. Due to such reason industrial processes are usually non-linear. On the other hand, real lumped parameter systems doesn't exists. Process parameters usually encountered in industrial systems are generally distributed instead of lumped, and finally, such systems are non-stationary, which means that its parameters are time-variant. Under this scenario any attempt to model an industrial system by analytical means could not succeed unless it will be assumed a considerable modelling error. Mentioned drawbacks could be minimised or at least slowed down by applying an alternative modelling approach under functional approximation. Functional approximation has been extensively applied in many industrial applications where it can be pointed out some recent works due to [32] among other authors. Nevertheless, in this work functional approximation is being applied exploiting its maximum modelling power to describe real time applications: Here varying time parameters of time variant systems are considered as system variables from a modelization point of view. Such modelling concept is carried out by means of conveniently trained BPNN. Under such assumption a process can be described by a set of variables classified as command inputs, disturbances, controlled outputs, internal process variables, variable parameters, constant parameters, and in general all variables and parameters related by any functional dependence between them and stored into a database under some restrictive conditions.

Causal processes can be modelled by means of universal functional approximation devices. A modelling property of causality is used in this work to predict not only steady state process input-output relationships but transient state dynamics also.

In order to reaffirm the concept of neural network based modelling (NNBM), let us consider a causal process being described by a functional approximation procedure where V_1 is the output variable, $V_2, V_3, \ldots V_N$ are input variables including its derivatives and $P_1, P_2, \ldots P_J$ are process parameters. Under such notation, the following transient state inputs/output relationship may be expressed for every sample cycle as:

$$V_1 = f(V_2, V_3, \cdots V_N, P_1, P_2, \cdots P_M) \tag{1}$$

Given a database containing causal data supplied from the process defined by expression (1), following relationships can be stated as output predictions according the following expressions:

$$V_1 = f(V_2, V_3, \cdots V_N, P_1, P_2, \cdots P_J),$$
$$V_2 = f(V_1, V_3, \cdots V_N, P_1, P_2, \cdots P_J),$$
$$P_1 = f(V_1, V_2, \cdots V_N, P_2, P_J),$$
$$P_J = f(V_1, V_2, \cdots V_N, P_1, P_2)$$

$$(2)$$

where $V_1 = f(V_2, V_3, V_N, P_1, P_2, \ldots P_J)$ in (2) is a direct model predictor (DMP), and any other relational functions in (2) are inverse model predictors (IMP).

Neural networks will not be an accurate predictor, if operating input/output data are outside their training data range. Therefore, the training data set should possess sufficient operational range including the maximum and minimum values for both inputs/output variables.

Variables dimensions for database size (DBS) are selected according required precision to the function implemented on the basis of a NNBM. Usually, database size could be defined as the product between the number of variables involved in a function and number of data sets (*NDS*) involving all function variables. According this definition, follows that

$$NDS = \prod_{i=1}^{NV} DP_i,$$
$$DBS = NV \cdot \prod_{i=1}^{NV} DP_i$$

$$(3)$$

where DP_i is the number of valid datapoints for variable (i) and *NV* is the number of input and output variables including variable parameters involved in a function.

Every sampled data set, in order to be acquired and stored into a database, must satisfy the condition of functional dependency representing the real-time dynamic behaviour. In order to ensure such condition a signal conditioning task by proper filtering is to be carried out. Such signal-conditioning task requires that every variable would be enabled to enter the database when all inputs/output variables satisfy the condition of being acquired into the same sample cycle. If one and only one data point fail entering the database, then all data set is eliminated.

The amount of achieved data must be representative of correct plant dynamic patterns. When database is filled with updated data, old data in database is overwritten by new data. A large number of valid data sets provide much better accuracy in the training phase. According the variable to be predicted, reorganisation of inputs-output sets of variables from data contained into database must be performed in order to initiate the training phase, where the NN output is the variable to be predicted and the rest of process variables or variable parameters are inputs.

To summarise the data acquisition task and training procedure under the back-propagation algorithm, figure 1 illustrates the general scheme to be implemented.
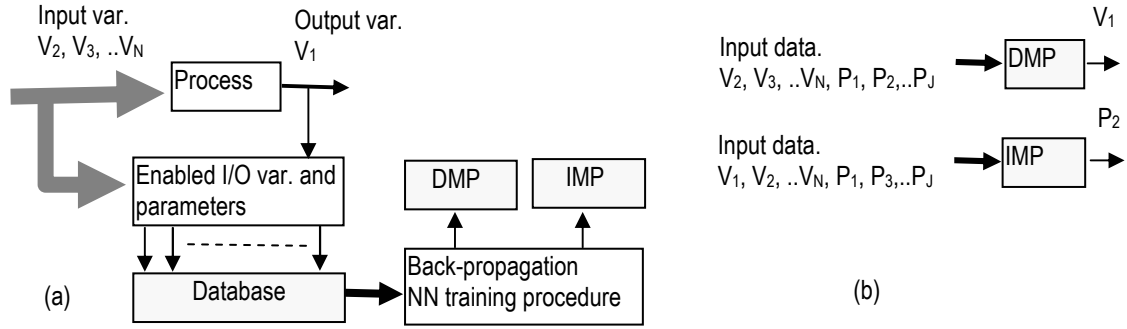
Fig. 1. Single process continuous data acquisition, data storing, and NN training phase. (a) Data acquisition and NN Training. (b) Application of DMP and IMP.

2.1 Proposed Parameter Estimation Technique

Conventional parameter estimation method is appropriate if the process faults are associated with changes in model parameters, such as in the case of multiplicative faults and when appropriate math-models are available. Nevertheless in the case of distributed parameter, non-linear and time-variant systems conventional methods such as least-squares are not efficient. Modelling errors will be drastically reduced by modelling the systems on the basis of functional approximation. Functional approximation of the form described by expression (2) based in BPNN is proposed as a general methodology to detect deviation between nominal system parameters and actual estimated system parameters. Let's admit a system defined as a function of its measurable input/output variables and its measurable parameters

$$V_1 = f(V_2, V_3, \cdots V_N, P_1, P_2, \cdots P_M), \tag{4}$$

Achieving the database with the variables and parameters associated to expression (4) and consequent training of an appropriate BPNN, yields the following neural network based function capable for output the estimates of a single parameter $\hat{P}_1$.

$$\hat{P}_1 = f(V_1, V_2, \cdots V_N, P_2, P_J), \tag{5}$$

Figure 2 shows the scheme of a neural network function block structured to be trained by means of a back propagation algorithm and real-time operation to estimate a single parameter.
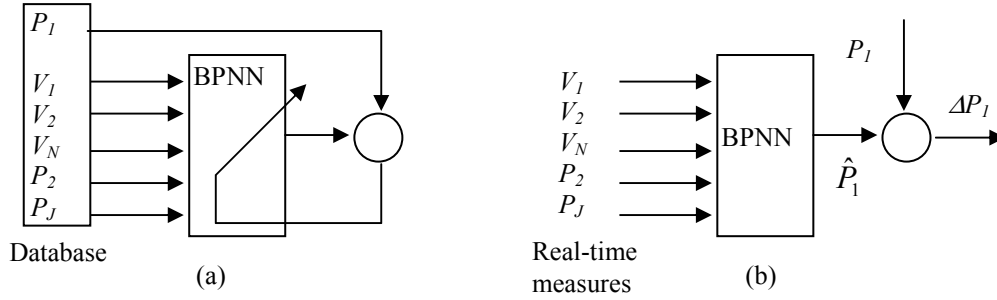
Fig. 2. Parameter estimation function block: (a), training phase. (b), real time parameter estimation

If a process fault is associated to the parameter variation, then a residual given as the difference between nominal and actual estimated parameter values

$$\Delta P_J = P_J - \hat{P}_J , \qquad (6)$$

is an indication of parameter changes and consequently of the existence of a fault or anomaly due to parameter changes located on the origin of that parameter variation. Even if no faults are present in the plant, the ΔP_J will not be equal to zero due to process disturbances and noise. That means, the process is stochastic and a threshold must be used to indicate if a fault exists. It is considered that a fault is detected when a single ΔP_J is larger than some threshold.

The parameters associated with the threshold violation are those associated with the responsible fault. Knowledge acquired as described will be used on the software based tool architecture.

3 FAULT DETECTION AND ISOLATION STRATEGY USING FUNCTIONAL AND HARDWARE REDUNDANCY

3.1. Concepts on functional and hardware redundancy

The performance of all input/output devices of a multivariable severe monitoring system is of critic relevance. For that reason redundancy is a common alternative to fault tolerant control systems monitoring. Consequently, proposed strategy concerns to both aspects of redundancy combined between them as required:
- Functional redundancy
- Hardware redundancy

Functional redundancy deals with two or more functions describing the same process, while hardware redundancy is referred to two or more hardware devices applied in measuring the same variable.

Supervision task is being carried out in two phases: fault detection and fault isolation. Depending on process characteristics there will be necessary to propose functional and hardware redundancy.

Fault detection is inferred by evaluating functions achieved by functional redundancy with parity relations.

Fault isolation is inferred by logic evaluation of hardware redundancy with parity relations on pairs of devices, which means that fault isolation concerns to discrimination of a faulty sensor by means of a novel method. The main objective in applying functional redundancy is to detect and isolate the group of devices that fails. So that, in order to ensure the dynamic equilibrium, action/reaction forces inherent to dynamic processes are balanced by functional approximation based models according NNBM.

3.2. Isolation of a faulty group of devices

Given a general dynamic process modelled by means of functional approximation procedures under NNBM1, NNBM2 NNBM3 and NNBM4 where Y_A and Z_R are action and reaction functions, Y and Z are NNBM outputs of the action/reaction functions, Y' and Z' are redundant NNBM outputs of Y and Z, it follows that

$$DMP1 : Y = f(Y_1, Y_2, ...Y_N)$$
$$DMP2 : Y' = f(Y_1', Y_2', ...Y_N')$$
$$DMP3 : Z = f(Z_1, Z_2, ...Z_N)$$
$$DMP4 : Z' = f(Z_1', Z_2', ...Z_N')$$

(7)

where $Y_1, Y_2,..Y_N$, are inputs from measuring devices to DMP1, $Y_1', Y_2',..Y_N'$ are inputs from redundant measuring devices to DMP2, $Z_1, Z_2,..Z_N$ are inputs from measuring devices to DMP3, and $Z_1', Z_2',..Z_N'$ are inputs from redundant hardware devices to DMP4.

Given a dynamic process where an input or action force Y_A (manipulated variable) is modelled as $Y = f(Y_1, Y_2, ...Y_N)$, the output or reaction force Z_R is modelled as $Z = f(Z_1, Z_2, ...Z_N)$, which is a function of process variables, then, the condition for dynamic equilibrium requires the assumption:

$$Y_A = Z_R$$

(8)

In order to establish reasoning bases regarding devices performance, following propositions are considered:

The condition for functional redundancy between groups of devices requires the existence of instrumentation groups modelled such that rigorously $Y' = Y$, $Z' = Z$, equations which in practice are relaxed to the approach

$$Y' \cong Y, \quad Z' \cong Z$$

(9)

The condition for the existence of hardware redundancy requires

$$Y_1 \cong Y_1', Y_2 \cong Y_2', ...Y_N \cong Y_N'$$
$$Z_1 \cong Z_1', Z_2 \cong Z_2', ...Z_N \cong Z_N'$$

(10)

A necessary condition but not sufficient to confirm the correct operation of instrumentation is the correctness of the involved NNBMs, which means the absence of modelling errors in the functional approximation devices. Under the necessary condition consisting in the absence of

modelling errors and assuming that $Y \cong Z$ and that only irrelevant short periods of time $Y \neq Z$, then it is admitted that both main groups of devices operate correctly with an exception. Furthermore, if $Y' \cong Z'$ and that only irrelevant short periods of time $Y' \neq Z'$, then it is admitted that both groups of redundant devices operate correctly with an exception. Consequently, if $Y \cong Z$, $Y \cong Y'$ and $Z \cong Z'$ then the redundant groups of devices Y' and Z' operate correctly because $Y \cong Z'$ and $Y' \cong Z$. The mentioned exception concerns to the possibility of collapse of all devices in both groups. In such a case, then $Y = Z = 0$, $Y' = Z' = 0$.

Proof: given $Y \cong Z$, $Y \cong Y'$ and $Z \cong Z'$ then $Y' \cong Z'$ which is the balance asseveration between Y_A and Z_R.

Theorem 1:

Under the assumption of $Y \neq Z$, at least one of both groups of devices of measuring system fails.

Proof: $Y_A = Z_R$, that means dynamic equilibrium must be balanced or dynamic balance cannot be violated. Consequently, if no fault exists, $Y \cong Z$. So hat, if processing system (NNBM) do not fail, then data acquisition system (measuring devices of Y, Z or both) fails. Consequently from theorem 1 follows that If $Y' \neq Z' \Rightarrow$ at least one of both groups of redundant measuring system fails. Furthermore, if $Y' \neq Z'$ AND $Y \neq Z \Rightarrow$ at least one of main groups and one of its redundant groups of measuring devices fails.

Individually faulty groups isolation is carried out by functional redundant analysis of residuals applied on all groups of measuring devices. In the task of faulty groups isolation, the following theorem is to be proposed and applied:

Theorem 2

Any residual R_{ij} approaching null value, guarantee the correct operation of both groups of devices involved in such residual.

Proof: $Y \cong Z$ is a guarantee of correctness measuring instrumentation groups Y and Z. So that, if $Y \cong Z$ then $R \cong Y-Z \cong 0$.

As consequence of theorem 2 it can be stated that when comparing three groups of devices G_1, G_2 and G_3, the group of devices that fails is the one excluded from the two groups that approaches null value. According last proposition it follows that given the groups of devices Y, Y', Z, and Z', where Y' and Z' are redundant groups of Y and Z respectively, yields the faulty group as:

$$G_1 \Leftarrow R_{YY'} \wedge R_{YZ} \wedge \overline{R}_{Y'Z}$$
$$G_2 \Leftarrow R_{YY'} \wedge R_{Y'Z} \wedge \overline{R}_{YZ} \qquad\qquad (11)$$
$$G_3 \Leftarrow R_{YZ} \wedge R_{Y'Z} \wedge \overline{R}_{YY'}$$

where R_{IJ} are the residuals achieved by parity relations applied by means of functional redundancy and the symbol $\wedge$ is a logic AND operator. So that, applying logical evaluation of achieved residuals by means of the rule based procedure shown by expression (8), faults detection and isolation at groups level is being carried out. The meaning of expression (8) is illustrated by means of figure 3.
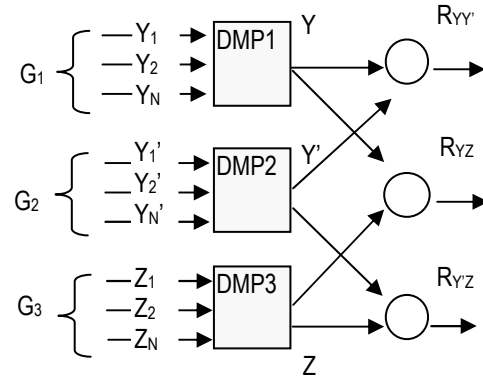
Fig. 3. Fault detection and isolation between redundant groups of devices

Using an alternative redundant group, individual faulty groups isolation is completed under the same reasoning base.

$$G_2 \Leftarrow R_{Y'Z} \wedge R_{Y'Z'} \wedge \overline{R}_{ZZ'}$$
$$G_3 \Leftarrow R_{Y'Z} \wedge R_{Z'Z} \wedge \overline{R}_{Y'Z'} \qquad (12)$$
$$G_4 \Leftarrow R_{ZZ'} \wedge R_{Z'Y'} \wedge \overline{R}_{ZY'}$$

The meaning of expression (12) is illustrated in the figure (4)
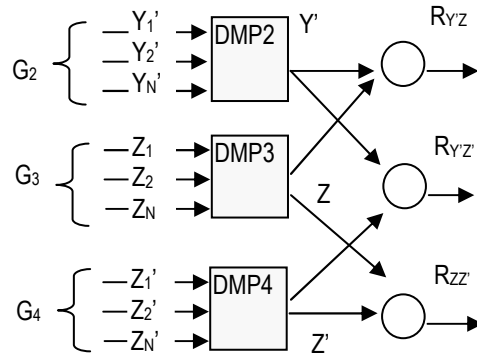
Fig. 4. Fault detection and isolation between alternative redundant groups of devices

Using the simplified combination of both main and its redundant groups, yields

$$G_1 \Leftarrow R_{YY'} \wedge R_{YZ} \wedge \overline{R}_{Y'Z}$$
$$G_2 \Leftarrow R_{YY'} \wedge R_{Y'Z} \wedge \overline{R}_{YZ}$$
$$G_3 \Leftarrow R_{YZ} \wedge R_{Y'Z} \wedge \overline{R}_{YY'}$$
$$G_4 \Leftarrow R_{Y'Z'} \wedge R_{ZZ'} \wedge \overline{R}_{Y'Z}$$

$$(13)$$

The meaning of such asseveration concluded by the expression (10) is depicted by figure 5
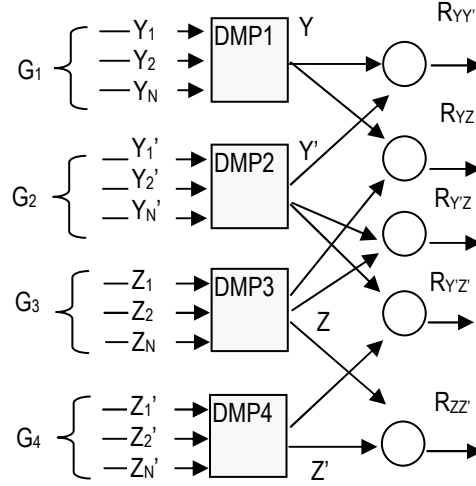
Fig. 5. Fault detection and isolation between both, main and its redundant groups

3.3. Isolation of a faulty device

Nevertheless, fault isolation at device level requires to add a step more which consists in exploit the concept of hardware redundancy, where the faulty device is isolated by the following rule-based inferential procedure:

$$Y_1 \Leftarrow G_1 \wedge R_{Y1}$$
$$Y_2 \Leftarrow G_1 \wedge R_{Y2}$$
$$\vdots$$
$$Y_n \Leftarrow G_1 \wedge R_{Yn}$$
$$Y_1' \Leftarrow G_2 \wedge R_{Y1}$$
$$Y_2' \Leftarrow G_2 \wedge R_{Y2}$$
$$\vdots$$
$$Y_n' \Leftarrow G_2 \wedge R_{Yn}$$

$$(14)$$

where $R_{Y1} = Y_1 - Y_1'$, $R_{Y2} = Y_2 - Y_2'$, $R_{Yn} = Y_n - Y_n'$

$$Z_1 \Leftarrow G_3 \wedge R_{Z1}$$
$$Z_2 \Leftarrow G_3 \wedge R_{Z2}$$
$$\vdots$$
$$Z_n \Leftarrow G_3 \wedge R_{Zn}$$
$$Z_1{}' \Leftarrow G_4 \wedge R_{Z1}$$
$$Z_2{}' \Leftarrow G_4 \wedge R_{Z2}$$
$$\vdots$$
$$Z_n{}' \Leftarrow G_4 \wedge R_{Zn}$$

(15)

where $R_{Z1} = Z_1 - Z_1{}'$, $R_{Z2} = Z_2 - Z_2{}'$, $R_{Zn} = Z_n - Z_n{}'$

3.3.1. Decision-making and reconfiguration

Decision task under a single faulty device with redundancy consists in enabling the redundant stand-by device when a fault appear in a device of a main group of devices as soon as possible in order to avoid additional disturbances due to instrumentation faults, avoiding the potential imminent shut down of the plant. So that, in the same sample cycle where expression (11) or (12) detects a fault, reconfiguration must be carried out.

In this section it has been shown that combining hardware redundancy with functional redundancy, ambiguity is avoided and the FD & FI problem is deterministically solved under some constraints such as:

- Residuals evaluation must be performed only under steady state dynamics.
- Determinism exists only under a unique fault and not more than one at a time under normal process operation.

4 SEVERITY ASSESSMENT ON HYDRODYNAMIC JOURNAL BEARINGS

4.1 Introduction

This section is devoted to manipulation of mechanical load severity limits from a maintenance and monitoring software tool point of view. A journal bearing consists of an approximated cylindrical bearing body or sleeve around a rotating cylindrical shaft. Journal bearings are found in all motors, generators and internal combustion engines in which a fluid lubricant is used to avoid wear as much as possible. Wear is the unwanted removal of material from solid surfaces by mechanical means. It is one of the leading reasons for the failure and replacement of internal combustion engines. It has been estimated that the cost of wear, which include repair and replacement, along with equipment downtime, constitute the most important cost due to maintenance tasks. Wear is due to four primary types: sliding wear, abrasion, erosion and corrosive wear. A hydrodynamic journal bearing maintains separation of shaft from bearing because the lubricant viscosity and the speed of the shaft create pressure in the converging portion of the fluid film which carries load.

After an initial transition or "running-in" period, sliding wear tends to reach a steady state rate which is approximated by the following (Holm/Archad) wear equation as

$$V = \frac{K \cdot W \cdot s}{H}$$

(16)

where V is the volume of worm material, K is the dimensionless wear coefficient, s is a sliding distance, W is the normal load between the surfaces and H is the hardness of the two contacting surfaces. From (16) follows that wear can be affected by reducing the wear coefficient K and the normal load W.

Journal bearings are subjected to unbalanced operating loads whose consequences could be summarised as abnormal physical deterioration. When load distribution is not uniform among the complete set of journal bearings mechanical and thermal symptoms will appear.

- Mechanical symptoms are detected by means of vibration analysis.
- Thermal symptoms are detected by means of temperature gradient deviation of each journal bearing.

The torque developed by friction between shaft and journal is described as

$$P_F = K_F \cdot C \cdot R \tag{17}$$

where P_F is the friction torque resistance, K_F is the .hydrodynamic friction coefficient and R is the shaft radio. The friction power is

$$Pow = P_F \cdot \omega = K_F \cdot C \cdot R \cdot 2 \cdot \pi \cdot n \tag{18}$$

where ω is the angular velocity and n is number of revolutions per second.

The thermal flow generated due to shaft-journal friction transferred to the lubricant is

$$q_E = q_L \cdot Ce \cdot \Delta t \tag{19}$$

where q_L is the mass flow of lubricant, Ce is the lubricant specific heat and Δt is the thermal gradient (difference between input and output lube oil temperatures)

Hence, the relation between mechanical and thermal load is described by means of an energy balance equation as. According energy conservation principle (18) and (19) can be balanced as

$$K_F \cdot C \cdot R \cdot 2 \cdot \pi \cdot n = q_L \cdot Ce \cdot \Delta t \tag{20}$$

Last expression has some practical qualitative sense because it let us to observe how load, speed and lube oil flow exerts influence on thermal gradient according

$$\Delta t = f(C, n, q_L) = \frac{K_F \cdot R}{Ce} \cdot \frac{C \cdot n}{q_L} = c \cdot \frac{C \cdot n}{q_L} \tag{21}$$

Mechanical engineering uses sometimes a design criterion or approach based on the product $p.v$, where p is the mean pressure and v is the peripheral velocity

That is, being $v = 2\pi \cdot R \cdot n$ y $p = \dfrac{C}{2R \cdot L}$, where L is the journal width, the criterion $p.v$ is inserted in (20) as

$$K_F \cdot 2 \cdot L \cdot p \cdot v = q_L \cdot Ce \cdot \Delta t \qquad (22)$$

which let us to achieve operation parameters as following

$$pv = \frac{q_L \cdot Ce \cdot \Delta t}{K_F \cdot 2 \cdot L} \qquad (23)$$

Criterion *p.v* should not be exceeded to ensure a safely operation condition. Avoiding to reach such limit requires to actuate on lube oil flow. This severity assessment method has the inconvenient of requiring some experience about the knowledge of value *p.v*.

4.2 Practical criteria applied on journals load severity

4.2.1 Nominal load criterion
From experimental research some criteria were achieved. Among them a practical criterion to asses load severity on journal bearings is based in the nominal load that is its maximum continuous rating (MCR). For instance an engine running at 100% of its MCR power is developing a friction work which is transferred to lube oil according (19) as

$$q_{E(MCR)} = q_L \cdot Ce \cdot \Delta t \qquad (24)$$

If it is admitted a constant lube oil flow rate at MCR power, only the thermal gradient could vary. Consequently the thermal gradient can be associated to the load dissipated by lube oil refrigeration capacity yielding

$$\Delta t_{(MCR)} = \frac{q_{E(MCR)}}{q_L \cdot Ce} \qquad (25)$$

From equation (25) the degree of load severity could be achieved by comparison between actual with nominal thermal gradient by means of the relation

$$\frac{\Delta t_{(MCR)}}{100} = \frac{\Delta t}{sev} \qquad (26)$$

where the load severity *sev* is expressed as percent load of nominal load

$$sev = \frac{100 \cdot \Delta t}{\Delta t_{(MCR)}} \qquad (27)$$

4.2.2 Absolute load severity criterion ESDU
This criterion is based on experimental results from [33] ESDU, "A general guide to the choice of journal bearings type, Item 67073, The Institution of Mechanical Engineers, London, 1965". In nomogram shown in figure 8, it is represented the mechanical load on the

14

journal bearing as function of shaft diameter and shaft speed. According ESDU criterion, the maximum load C_M is defined as

$$C_M = f(D,n) = f_1(D,\omega) \tag{28}$$

The load limit defined by (28) can be inserted into (21) to achieve the maximum allowable thermal gradient

$$\Delta t_M = f(C_M, n, q_L) = \frac{K_F \cdot R}{Ce} \cdot \frac{C_M \cdot n}{q_L} = c \cdot \frac{C_M \cdot n}{q_L} \tag{29}$$

Figure 8 shows the nomogram in which the maximum allowable load (N) is plotted against shaft diameter (m) and shaft speed (rps).
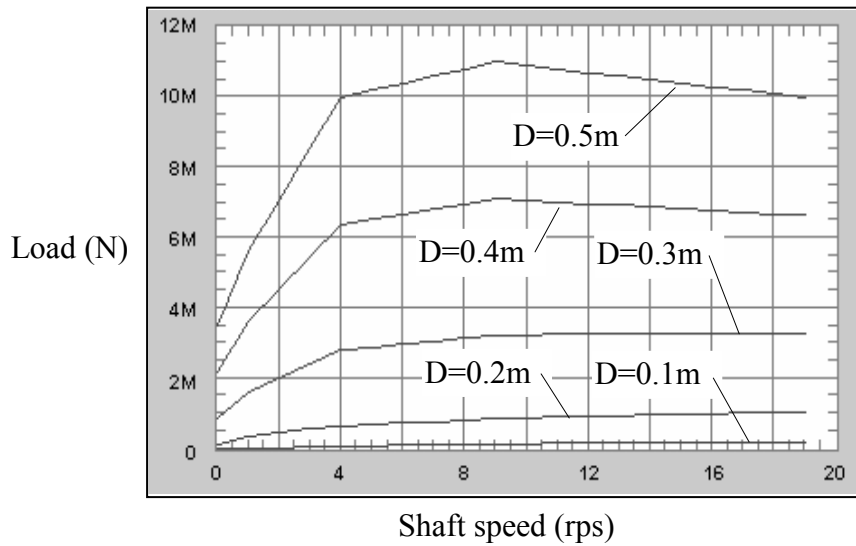
Fig 8. General guide to journal bearing-type selection.

From information shown in figure 8, the *pv* criterion could be assessed by combining (29) with (23) according

$$pv_M = \frac{q_L \cdot Ce \cdot \Delta t_M}{K_F \cdot 2 \cdot L} \tag{30}$$

for which it is necessary to know the dimensions of journal bearing. The criteria described so far is applied on rule based decision making strategies processed by means of proposed software tool.

Some criteria to assess load severity has been applied on developing a software based tool described in next section, in which, automatically load limits are under alert and decisions making is applied according proposed criteria which is taken into account.

5 SOFTWARE TOOL CHARACTERISTICS

5.1 Automatic monitoring of internal combustion engines

The automatic monitoring and alarm systems for engine room should be potentially prepared for use in unattended machinery space (UMS) and cooperation with one man bridge operation (OMBO). Instead of an engineering on duty for four hours, it can monitor and log important quantities at predetermined intervals, automatically record quantities and provide a printed log of variables at present intervals for main engine and associated auxiliary machinery.

According to the requirement of the ship automation integration and unattended machinery space, the new development of automatic monitoring system will satisfy the characteristics:

▪ Centralised and distribution control.- Application of distributed control system (DCS) will not only collect the data or information for central management but also deliver them to all the appointed places for display or alarm. At the same time it can control the operation of relevant machine on the spot.

▪ Intelligence of the management.- Application of AI may finally set up a diagnosis forecast system which has the function of trouble shooting, trouble duagnosis and trend analysis.

The DCS architecture has the following characteristics

▪ Each working station complets its task, which is undertaken ibdependently, the control function is distributed and the sharing of load is reasonable. It can cooperate in decisdion making functions.

▪ Each working station can deliver all the information through communication network and work in coodination. It inproves the function of the system and obtains the optimal process of the information to reach the purpose of the information being commonly shared.

▪ The hardware and software is of open type, standard and modulized design. All systems can be assembled flexible, it can also be strong adapted and extended.

▪ Fault alllowance based design in hardware, including operation station, control station and communication chain,. Also it is adopted twin-installations considering the electro-magnetic compatibility to improve the high reliabilty of whoole system.

The basis of UMS and OMBO application is shown in figure 9. On mentioned figure, KA and KB means knowledge acquisition and knowledge base respectively. Compared with traditional monitoring systems in engine room, the monitoring system based on AI has the following functions:

▪ Trouble shooting
▪ Fault diagnosis and prediction
▪ Put it in right operation (decision making and actuation to achieve system recovered)
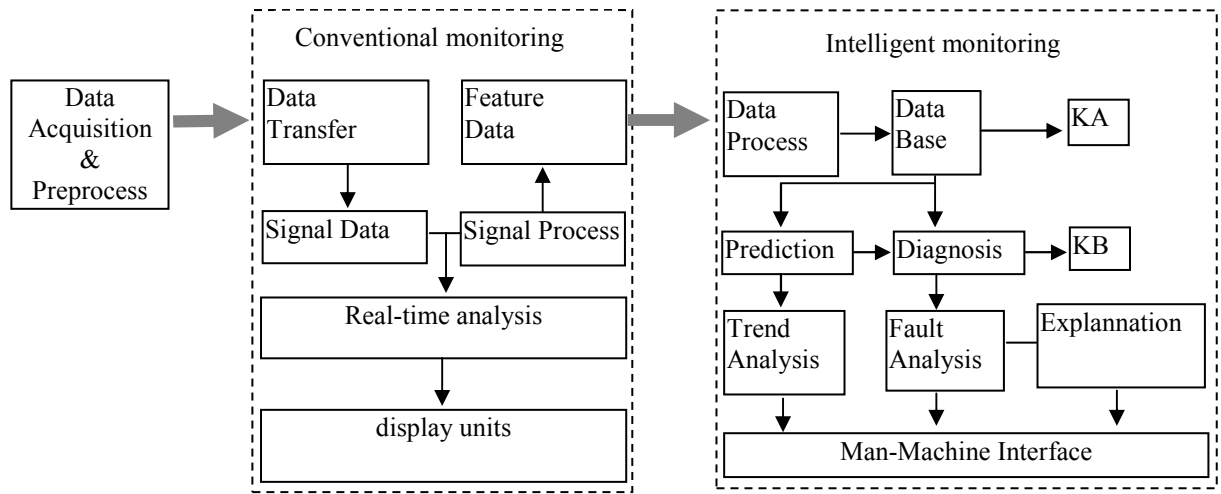
Fig. 9. Monitoring system based on intelligent integration

5.2. Characteristics of Man-Machine Interface

The proposed software tool is developed with the help of a virtual engineering environment (VEE). It consists in a set of parallel algorithms scheduled according theory aspects described in past sections and a Man-Machine-Interface (MMI). Some layouts of MMI for developed monitoring system appears as shown in next figures of this section. A main menu offers the possibility for selecting the proper view to be displayed by operators.

In figure 10 it is shown a set of thermal-mechanical functions which relate the main bearings condition with cylinder temperature and cylinder maximum pressure. According such data, variances and standard deviations are shown.

Fig. 10. Variance and Standard deviations of Main Engine functions

In figure 11 are shown the results of coherence analysis in order to automatically validate the data achieved, being applied functional redundancy.
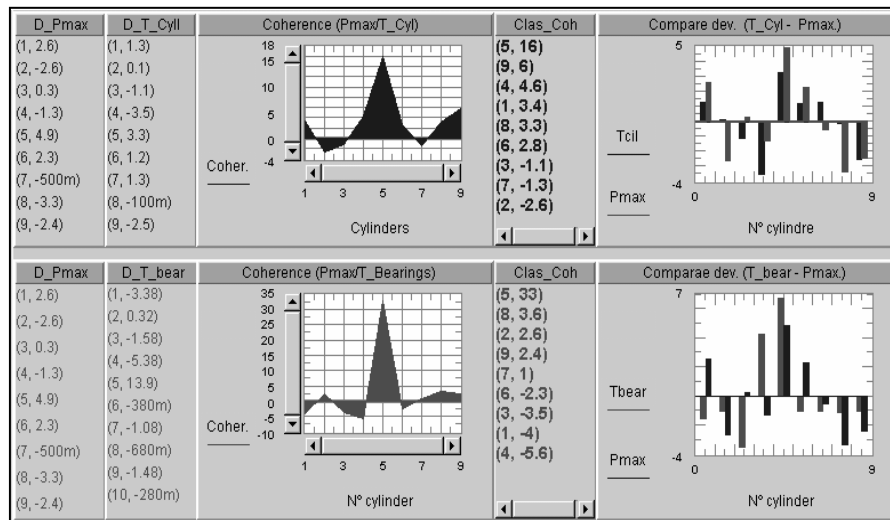
Fig. 11. Results of Coherence Analysis

Figure 12 shos the temporal evolution of loads on main bearings and its respective variances.
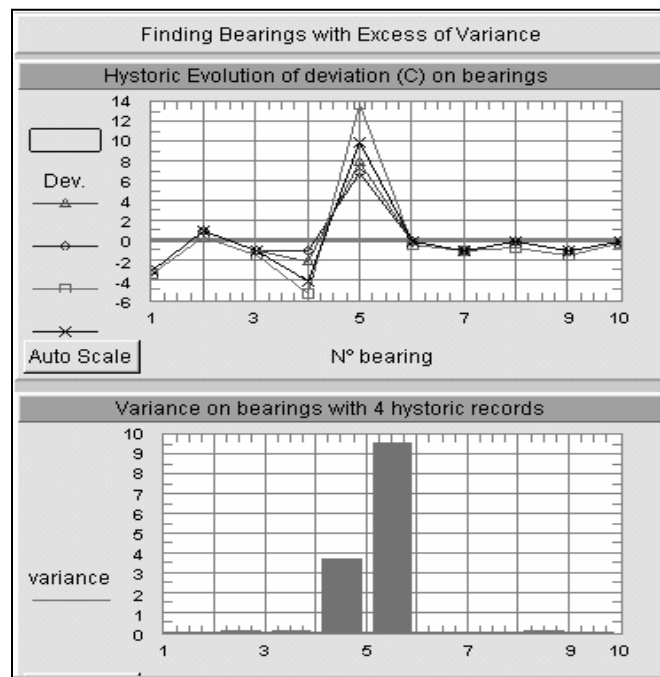
Fig. 12. Load variance s of main bearings.

Finally in figure 13 it is shown a panel view representing the load severity of main bearings according a selected criterion, which in this case is (pv). As consequence of an AI-ES based analysis, for every bearing, an alert is active indicating the bearing condition with respect to the actual supported load.
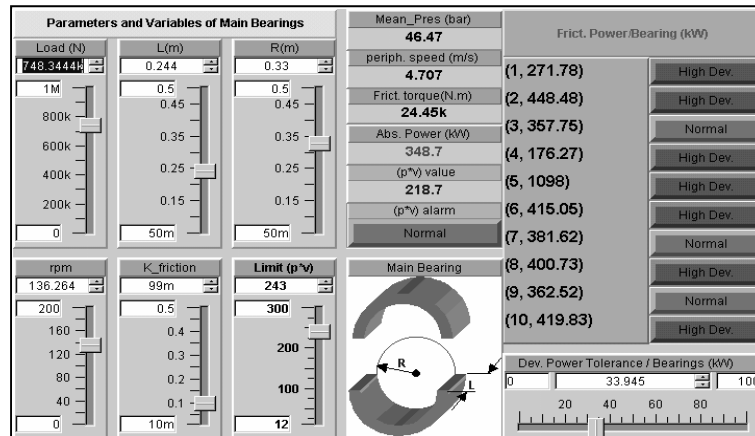
Fig. 13. Operating condition of journal bearings

5.3. Complementary tools

There are other tools which offers some advantages when they embed some of the contributions proposed in the work. A special case of such tools is DeltaV [34]. This tool contains sub-tool which is specially designed to manage virtual instruments: DeltaV Neural. It is suitable to operate under Foundation Fieldbus standard instrumentation.

DeltaV Neural provides easy-to-use tools for developing and training the neural network (NN) model. The most relevant characteristics are:

- Easily creates virtual sensors using NN
- NN executes right in the DeltaV controller as a function block
- Automated pre-processing, design, training and verification
- Expert mode allows interaction in the NN development

DeltaV Neural gives us a practical way to create virtual sensors for measurements previously available only through the use of lab analysis or online analysers. DeltaV Neural is easy to understand and use, allowing process engineers to produce extremely accurate results even without prior knowledge of NN theory.

. Some Advantages of using DeltaV Neural are:

DeltaV Neural offers an entirely new approach to the implementation of virtual sensors with neural networks. Using the DeltaV Neural function block we can identify up to 20 individual process measurements to be correlated with lab entry or continuous analyser data per every NN used. No step testing or manual disturbance of the process is necessary in order to implement the NN.

DeltaV Neural is implemented as a Function Block that executes in the DeltaV controller. This allows to use the standard tools of DeltaV Control Studio to define the necessary input variables along with manual lab entry data or data from a continuous analyser.

The DeltaV Continuous Historian automatically collects data on the inputs used by the Neural Net Function Block completely eliminating the need to configure a process historian .

Alternatively you may import existing historical data into DeltaV Neural using commonly available tools such as Microsoft Excel for data preparation.

DeltaV Neural will automatically perform the training needed to build the network and stop when over training is detected. The historical data used to train the model can be easily viewed, and any portions containing abnormal operating conditions may be excluded using easy graphical tools.

Upon completion of the automated network training, the sensitivies of each process input may be viewed graphically. DeltaV Neural is capable of eliminating any variables shown to have little or no effect on the output.

Additionally, experts have the option to specify such detailed parameters as outlier limits, max/min number of hidden neurons, and maximum training epochs. It is not a mandatory requirement for the use to specify any of the preceding values: they are intended for the use of expert users only.

Verification of actual and predicted values vs. samples gives the user an easily understable picture of how the network behaves. Verification may be done against original data or any other user selectable timeframe.

DeltaV Neural is licensed by the function block, and several NN blocks may be executed in the same controller simultaneously.

6 CONCLUSIONS

In this work, a software tool which combines the ANN and ES techniques to set up an ANN based expert system for main engine fault diagnosis has been developed and implemented.
Some advantages of the ANN-ES combination are:

- It can accumulate the knowledge by learning the previous fault information.
- Every ANN can be trained independently when using the multi-layer structure.
- The rules of diagnosis reasoning will be automatically obtained during the training process of the network.
- Knowledge and the rules will be stored in the net topology and the connecting weight values, thus avoiding the problem of "match impact" and "combination explosion". It is suitable for on-line operation.

With mentioned advantages the proposed combination ANN-ES play an important role in the ship information management.

Development of monitoring and alarm systems for main engine including the related devices and installations, because of the ship hostile environment, requires to apply some protective means and selective measuring techniques.

Progress in digital processing algorithms and tools gave possibilities to obtain new solutions for monitoring and alarm systems such as multifunctional microprocessor devices cooperating with global engine room monitoring and control systems, often configured also into virtual instrumentation.

ACKNOWLEDGEMENT

REFERENCES

[1] Jackson J. E., 1956. Quality control methods for two related variables. *Industrial Quality Control*., 7:2-6,

[2] Jackson J. E., 1959. Quality control methods for several related variables. *Technometrics*. 1:359-377.

[3] Duda R. O. And Hart P. E., 1973. *Pattern Classification and Scene Analysis*. John Wiley & Sons, New York.

[4] Wise B. M. And Gallagher N. B. 1996. The process chemometrics approache to process monitoring and fault detection. *Journal of Process Control*, 6:329-348

[5] MacGregor J. F., 1994. Statistical Process Control of multivariate processes. *Proc. Of the IFAC Int. Symp. On Advanced Control of Chemical Processes*, pp 427-435, New York. Pergamon Press.

[6] Piovoso M. J. and Kosanovich K. A. 1994. Applications of multivariate statistical methods to process monitoring and controller design. *Int. Journal of Control*, 59:743-765

[7] Piovoso M. J. and Kosanovich K. A. 1992. Monitoring process performance in real time. *Proc. Of the American Control Conference,*, pp. 2359-2363, Piscataway, New Jersey. IEEE Press.

[8] Frank P. M., 1993. Robust model based fault detection in dynamic systems. *On line fault detection and supervision in the chemical process industries*. pp.1-13. Pergamon Press. Oxford. IFAC Symposium series Number 1.

[9] Deckert J.C. 3et all. 1977. F-8 DFBW sensor failure identification using analytic redundancy. *IEEE Trans. On Automatic Control*, 22: 795-803.

[10] Hodouin D. And Makni 1996. S. Real time reconciliation of mineral processing plant data using bilinear material balance equations coupled to empirical dynamic models. *Int. Journal of Mineral Processing* , 48: pp. 245-264.

[11] Bakiotis C. et all. 1979. Parameter and Discriminant Analysis for jet engine mechanical state diagnosis. *Proc. Of the IEEE Conf. On Decision and Control,* pp 11-1. Piscataway, New jersey. IEEE Press.

[12] Isserman R 1998. Process Fault Detection based on modelling and estimation methods.: A survey. *Automatica*, 20: 387.404.

[13] Isserman R 1993. Fault diagnosis of machines via parameter estimation and knowledge processing.-Tutorial paper. *Automatica,*29: pp. 815-835.

[14] Mehra R. K. And Peschon J. 1971. An Innovation approach to fault detection and diagnosis in dynamic systems. *Automatica*, 7: pp. 637-640

[15] Frank P. M., 1990. Fault diagnosis in dynamic systems using analytical and knowledge based redundancy.- A survey and some new results. *Automatica*, 26:459-474.

[16] Clark R.N. et all. 1975. Detecting instrument malfunctions in control systems. *IEEE Trans. On Aerospace and Electrooninc Systems*, 11:465-473.

[17] Ding X. And Guo L. 1996. Observer based fault detection optimised in the frequency domain. *Proc. Of the 13th IFAC World Congress*, Vol N, pp. 157-162. Piscataway, New Jersey. IEEE Press.

[18] Gertler. J. J. 1998. *Fault Detection and Diagnosis in Engineering Systems.* Marcel Decker, Inc. New York.

[19] Mironovski L. A. 1979. Functional diagnosis of linear dynamic systems. *Automation and Remote Control*, 40: 1198-1205.

[20] Mironovski L. A. 1980. Functional diagnosis of linear dynamic systems- A survey. *Automation and Remote Control*, 41: 1122-1142

[21] Lee G. et all.1999. Multiple-fault diagnosis under uncertain conditions by the quantification of qualitative relations. *Ind. Eng. Che.Res.*, 38: pp988-998.

[22] Mo K. J. et all. 1998. Robust fault diagnosis based on clustered symptom trees. *Control Engineering Practice*, 5: pp199-208

[23] Mo K. J. et all. 1997. Development of operation-aided system for chemical processes. *Expert Systems with Applications*. 12: pp 455-464

[24] Kramer M. A. and Finch F. E. 1988. Development and classification of expert systems for chemical process fault diagnosis. *Robotics and Computer integrated Manufacturing.* 4: pp 437-446

[25] Li. T. 1989. Expert Systems for Engineering Diagnosis: Styles, requirements for tools, and adaptability. Ed Tzafestas S. G. *Knowledge-based Systems Diagnosis, Supervision, and Control*, pp. 27-37. Plenum Press, New York

[26] Kramer M. A and Palowitch J.B.L. 1987. A rule-based approach to fault diagnosis using the signed direct graph. *AIChE. Journal.* 37: pp.1067-1078

[27] Bakshi B.R. and Stephanopoulos G. 1994. Representation of process trends, IV Induction of real time patterns from operating data for diagnosis and supervisory control. *Computers and Chemical Engineering.*18: pp 303-332.

[28] Doyle R. J. et all. 1993. Causal modelling and data-driven simulation for monitoring of continuous systems. *Computers in Aerospace.*, 9:395-405

[29] Nekovie, R., and Sun, Y., (1995). Back propagation Network and its Configuration for Blood Vessel Detection in Angiograms, IEEE Trans. on Neural Networks, Vol 6, No 1.

[30] Ali Zilouchian and Khalid Bawazeer (2001). Application of neural networks in oil refineries. *Intelligent Control Systems Using Soft Computing Methodologies*, ed. by Ali Zilouchian Mo Jamshidi. CRC Press, 2001, pp 139-158. USA

[31] Demuth, H. And Beale, M., (1998). *Neural Network Toolbox for Use with MATLAB*, the Math Works Inc., Natick, MA, USA.

[32] Bawazeer, K. H. and Zilouchian, A., (1997) Prediction of Crude Oil Production Quality Parameters Using Neural Networks, *Proc. Of IEEE int. Conf. On Neural Networks.*, New Orleans.

[33] ESDU, "A general guide to the choice of journal bearings type, Item 67073, The Institution of Mechanical Engineers, London, 1965

[34] DeltaV. Terrence L. Blevis, Gregory K. McMillan, Willy K. Wojsznis, and Michael W. Brown. (2003). Advanced Control Unleashed:Plant Peformance management for Optimum Benefit. ISA- The Instruementation, Systems, and Automation Sdociety. USA.

Chapter 2

Ship pedestrian flow simulation. The Sifbup-S application

A. LÓPEZ PIÑEIRO
Universidad Politécnica de Madrid. Dep. SON (ETSIN)
F. PÉREZ ARRIBAS
Universidad Politécnica de Madrid. Dep. EBIN (ETSIN)
R. DONOSO MORILLO-V., R. TORRES FERNÁNDEZ
Aula Izar

The main objective of this paper is to present the conceptual design, models and user oriented software tools developed inside the SIFBUP research project, which main aim is the analysis and simulation of the passengers flow aboard ships, specially focused in the resolution of problems related with ship evacuation in emergency situations. A summary of the main ship evacuation problems, related regulations and different numerical model types for the study of passengers movement proposed by R&D groups are also presented.

NOMENCLATURE

D – Pax density
E+L – Embankment and boat launching phase
ES – Embankment Station
ETSIN – Naval Architecture and Marine Engineering School
FSS – Fire Safety Ship Code
HSC – High Speed Craft
IMO – International Maritime Organization
MES – Marine Evacuation System
MS – Mustering Station
MSC – Maritime Safety Committee
MSC-c1033 – Circular 1033 of the MSC
M&A – Mustering and Abandon phases of ship evacuation
PAX. – Passenger (by extension any pedestrian type)
Ro-Ro – Roll on – Roll off ship
S – Pax speed
SEP – Ship Evacuation Plan
SIFBUP – Flow Simulation for Passenger Ships project
SOLAS – Safety of Life at Ships Code

1 INTRODUCTION

Since long time ago, Izar shipyards and the ETSIN R&D Group on Aboard Human Factors have a close collaboration in the study of ship evacuation problems. Under the support of the Spanish R&D Program for the Shipyard Industry, sponsored by the Ministry of Science and

Technology and controlled by the "Gerencia del Sector Naval", we started in 2002 the Sifbup project (DINN-17) with a team composed by:

−   Izar, the Spanish main group of shipyards, as main partner with expert knowledge in ship design.
−   The ETSIN as scientific partner and responsible of the development of the software tools.
−   Trasmediterranea, the main Spanish company of passenger ships, with direct experience on passenger ship operation.

During the project life, the team was extended with the addition of Next Limit Company, experts on 3D simulation.

The main project objective is to develop a family of tools designed to aid the study of aboard people and vehicles flow. We have developed different tools oriented to the various necessities along the ship' life, such us:

−   The Sifbup-D, for the evacuation study in the first phases of the ship project.
−   The Sifbup-S, a 2D simulation of people movement in normal aboard operation and in emergency situations.
−   The Sifbup-S3D, to see the people movement in a "virtual reality" environment.
−   The Sifbup-V, to analyse the load and unload operations of trucks, cars and other vehicles inside ferries and other Ro-Ro ships.

In this paper we present the original work made for the 2D simulation of pax movement aboard and its results.

2   PEDESTRIAN MOVEMENT MODELS

If we study the different approaches to pedestrian movement analysis, that is the base for aboard evacuation study, we can classify the used models in tree groups: macro-models, micro-models and meso-models.

Macro-models consider the behaviour of people movement analysing the global response of a group that occupies a local or sector. The main parameters are speed, maximum flow and passengers' density. From land evacuation studies, different functions have been proposed for the curve speed vs. density (figure 1). In optimal path analysis it is normal to consider constant speed and maximum flow.

In any case, the most important simplification is the modelization of people as a compressible fluid, with a maximum flow and density. Any situation that tries to overpass it, produces a "catastrophic" response (queue formation), This methodology is known as "hydraulic model".

Micro-model approach presents the movement of every person. There are three main approaches: linear (1), corpuscular (2) and the cellular ones (3). At the moment the last one is the most popular on technical developments (4). It is based in the division of the available space for motion in squared cells that can be occupied (or not) by a person.
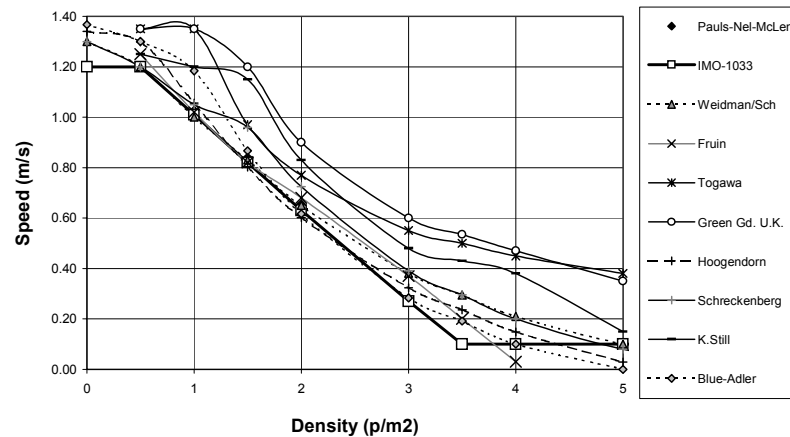
Figure 1. Speed vs. pax density.

The movement of every person is influenced by its objectives (direction, attraction, etc.) and by the occupation of the near cells (people, walls,..). It is a discrete model (in space and time) well adapted for programming with "agent modelling" techniques. The Meso-model makes a mixture of previous models (5), (6). Generally it uses the macro for calculus and the micro for presentation.

One important modelization aspect is the variability of human behaviour. Data of figure 1 are mean values, but people speed can be a function of: age, gender, health, platform stability, etc. (7), (8). Due to this reason, input data for the micro-models must be heuristic and tools based in it must use Monte-Carlo simulation methodology or other similar ones to obtain reliable statistical results.

3 THE SHIP EVACUATION PROBLEM

The well-known disasters of the Herald of Free Enterprise, Scandinavian Star and the Estonia have set a new regulation about passengers safety and crew training of passengers ships that include ship evacuation and evacuation aids.

IMO (International Maritime Organisation) and one of its committees (MSC: Maritime safety committee) has published in June 2002 a document titled "Interim guidelines for evacuation analysis for new and existing passenger ships" (MSC–c1033), that includes two analysis methods. This guide mentions that further investigations and developments are necessary. Other IMO regulations have been publishes in order to improve the evacuation process on different passenger ships (Ro-pax, HSC, large passenger ships, etc.).

In all transport and public building it is compulsory to have a scheduled evacuation plan and during an emergency situation all people must follow it. From the post-catastrophic analysis of significant events, the experts, (9), underline the following differences between the scheduled plan and the usual reality:

− Most of people do not start walking the emergency alarm sounds. There is an important delay to react to the alarm indication, known as "awareness time", and it exists the trend to continue with the previous activity. The decision to start evacuation is delayed if the environment is not well known.

− People usually follow a known route better than follow the emergency exit symbols.

− In general, people move with a strong influence of their relatives or friends behaviour. Group is more significant that individual.

− Evacuation symbols are not followed, especially if they are text ones.

− Physical and psychological constraints are very important, with significative variation between different people types. Young people not only walk quickly but also take decisions in less time. Childs wait hidden until their parents starts moving. People that ingested alcohol or drugs reduce significant their own mobility speed and increase their response time.

− People can go through a smoky area of reduced visibility, especially if they know well the place or if someone acting as a leader guides them.

− In crowded situations, it is not common the generation of a panic situation. This is a normal "newspaper headline" but not the reality. Massive deaths are normally related more with delays in the emergency notice and restrictions in the escape routes capacity.
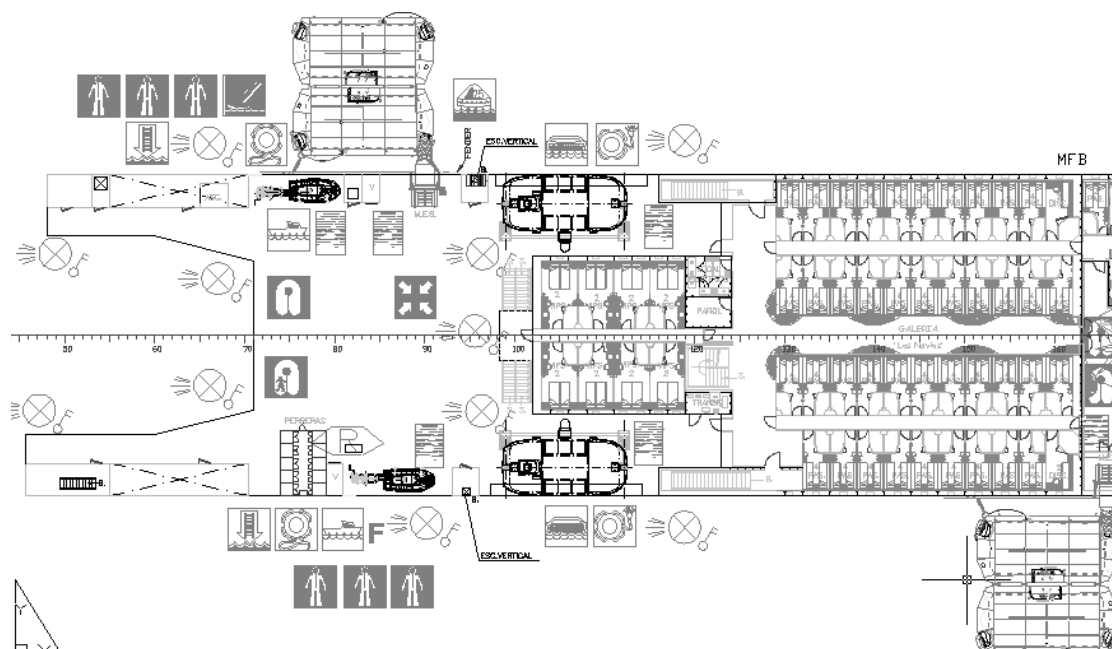
Figure 2. Partial view of a ship evacuation plan.

Other important aspects to consider are the differences between land situations and ship evacuation (10). The environment and the human behaviour are quite different due to:

− Distribution and evacuation aids that are unknown for the normal passenger.

− Different crisis origin.

− Movements are difficult in a non-horizontal and unsteady platform.

− The ship is isolated and frequently in a "rough sea".

− People (passengers and crew) with multilingual and multicultural origin.

− Different ship operation situations.

Due to the mentioned reasons, passenger ship evacuation is a complex process (figure 2). According to IMO regulations (11) it must be scheduled in mustering and abandon phases (M&A). The first is an uncontrolled movement of people from the initial places to assembly stations. In the second stage the passengers have to be guided (controlled) by crewmembers that develop a supervised plan avoiding unnecessary crowds and queues.

Evacuation may happen at any time while sailing. So, facilities for it must be always ready. The crew must be trained with frequent aboard exercises. They will know the evacuation ways and their duties at these situations. Maintenance of the evacuation ways and lifesaving systems is also an important matter.

According to IMO, the main part of the Ship Evacuation Plan (SEP) is: "an operating guide, either printed or in computer format, where missions and duties of the crew, basic operations sequence and operating criteria (with examples, if possible) are indicated". The main interfaces of the SEP with passengers' evacuation are the information sings in the escaping routes and the instructions in the case of ship evacuation. A good SEP must:

− Be easily managed; with a clear abandon group definition and their travel schedule (without crossing or overlapping between groups).
− Calculate, with a suitable reliability level, the arrival time to the mustering stations for the different passengers groups.
− Calculate and minimise the time between the ship abandon command and the moment that the last person abandons the ship.

During emergency stage, the situation must be managed according to the SEP through appropriate decisions and commands according the two phases of the M&A process. From the start of the emergency signal and during the mustering phase there will be few control (formally there will be uncontrolled passenger movement). Passengers go to the assembly stations following the main or the secondary evacuation plan and signals.

Then, the crew verify passenger's number and their lifejackets use. When the Master give the "ship abandon" order, the crew lead the passengers towards the embarkation points (evacuation stations) in "controlled groups" through the ship evacuation routes, moving at a near-optimal speed and flow. For this controlled passenger' flow, there are two different options: one member of the crew acts as a "leader" for a group of passengers, or different crewmembers are placed in critical points of the evacuation route in order to guide the passengers and regulate their flow. As a consequence of the mentioned above, the need of specific models and tools for the ship evacuation analysis is clear.

4 IMO REGULATIONS

The Maritime Safety Committee, once approved MSC-c909 on Interim Guidelines for a simplified evacuation analysis of Ro-Ro passenger ships as a guide for the implementation of SOLAS regulation II-2/28-1.3, requested the Sub-Committee on Fire Protection (FP) to

develop guidelines also on evacuation analysis for passenger ships in general and for high-speed passenger crafts.

IMO has also approved MSC/Circ.1001 on Interim Guidelines for a simplified evacuation analysis of high-speed passenger craft.

The Committee, at its seventy-fifth session (May 2002), approved Interim Guidelines on evacuation analyses for new and existing passenger ships, including Ro-Ro passenger ships, as set out in the annexes to the present circular (MSC-c1033). It offers the possibility of using two different methods:

− A simplified evacuation analysis.
− An advanced evacuation analysis.

The Committee, as far as both methods need to be extensively validated, agreed that the Guidelines would have an interim nature and that the evacuation analysis methods should be reviewed in the future with the light of the results of experience using the present Guidelines, ongoing research and development aiming at applying only the advanced evacuation method and, when available, analyses of actual events utilizing it.
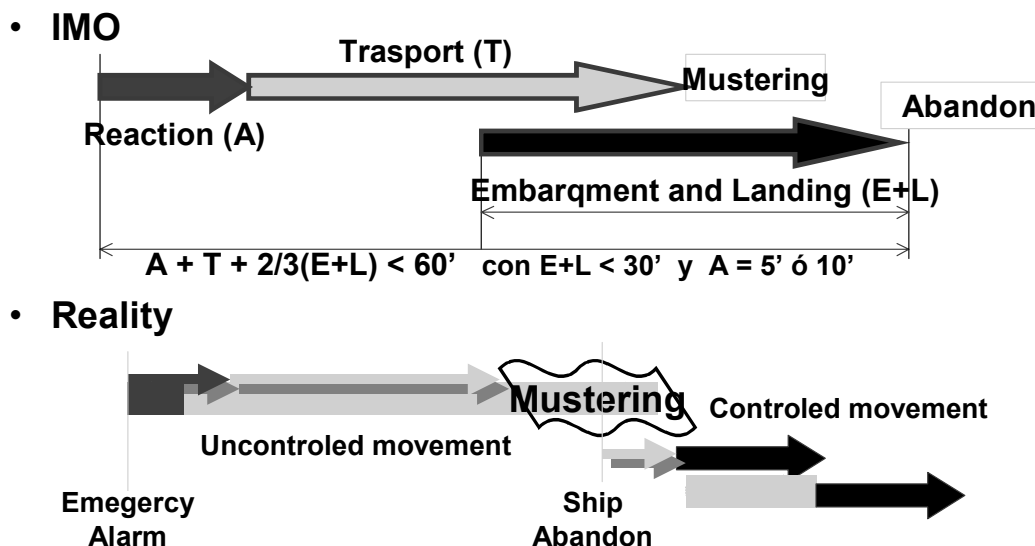
Figure 3. Comparison between IMO SEP and real situations.

The simplified analysis is based in a macro-model adapted from the buildings evacuation method (12). For the calculation of the evacuation time, the following components are considered:

− The awareness time (A) is the one that people need to react to an emergency situation. This time begins with the initial presentation of an emergency (e.g. alarm signal) and ends when the passenger has accepted the situation and begins moving towards an assembly station.

28

- The travel time (T) is defined as the time it takes all persons on board to move from where they are when the alarm is activated, to the assembly stations and then onto the embarkation stations. For its calculations, a hydraulic macromodel is used, based on a speed-density function modelled with data of table 1.
- The embarkation and launching time (E+L) is the sum of the time required to provide ship abandonment for the total number of persons on board.

The evacuation process, as illustrated in figure 3, should be complied with:

- Calculated total evacuation time: $A + T + 2/3 (E + L) \leq n$ $E + L \leq 30'$
- For Ro-Ro passenger ships, n = 60.
- For passenger ships other than Ro-Ro passenger ships, n = 60 if the ship has no more than 3 main vertical zones; and 80, if the ship has more than 3 main vertical zones.

Table 1. Values of initial specific flow and initial speed as a function of density.

Type of facility	Initial density D (p/m2)	Initial specific flow Fs (p/(ms))	Initial speed of persons S (m/s)
Corridors	0	0	1.2
	0.5	0.65	1.2
	1,9	1.3	.67
	3.2	0.65	0.20
	≥3.5	0.32	0.10

With the underline advanced evacuation analysis each occupant is studied as an individual that has a detailed representation of the layout of a ship and simulates the interaction between people and the ship environment.

This method of estimating the evacuation time is based on several idealized benchmark scenarios and the following assumptions are considered:

- Passengers and crew are represented as unique individuals with specified individual abilities and different response times.
- Passengers and crew will evacuate via the main escape routes, as referred to in SOLAS regulation II-2/1.
- Passenger load and initial distribution is based on chapter 13 of the FSS Code.
- Full availability of escape routes is considered unless otherwise is stated.
- A safety margin is included in the calculations to consider model limitations, and the limited number and nature of the benchmark scenarios considered. These issues include:

  - The crew will immediately be at the evacuation duty stations ready to assist the passengers.
  - Passengers follow the signage system and crew instructions (i.e. alternative route selection apart from the stated ones is not considered in the analysis).

- Smoke, heat and toxic fire products that are present in fire situations are not considered to impact passenger/crew performance.
- Family group behaviour is not considered in the analysis.
- Ship motions, heel, and trim are not considered.

At least, four scenarios should be considered for the analysis. Two scenarios, namely night (case 1) and day (case 2), as specified in chapter 13 of the FSS Code; and, two further scenarios (case 3 and case 4) based on reduced escape route availability are considered for the day and night case, as specified in the appendix.

The Guide permits a big freedom in the model choice with the following limits:

- Each person is represented in the model individually.
- The abilities of each person are determined by a set of parameters, some of which are probabilistic.
- The movement of each person is recorded.
- The parameters should vary among the individuals of the population.
- The basic rules for personal decisions and movements are the same for everyone, described by a universal algorithm.
- The time difference between the actions of any two persons in the simulation should be not more than one second of simulated time, e.g. all persons proceed with their action in one second (a parallel update is necessary).

The assumptions made for the simulation should be stated. Assumptions that contain simplifications the Interim Guidelines for the advanced evacuation analysis should not be made.

Also the Guide explain a validation procedure with 11 test designed to check that pax moves:

- With speed, flow and reaction times corrects.
- In a logical mode against obstacles and counter-flow.
- With whole results in complex scenarios consistent whit changes in the flow parameters.

In order to facilitate their use, the parameters are grouped into the same 4 categories as used in other industrial fields:

- GEOMETRICAL: layout of escapes routes, their obstruction and partial unavailability, initial passenger and crew distribution conditions.
- POPULATION: ranges of parameters of persons and population demographics. It is quite developed as could see in the table 2.
- ENVIRONMENTAL: static and dynamic conditions of the ship.
- PROCEDURAL: crewmembers available to assist in emergency.

Table 2. Example of population data.

Population groups - passengers	Walking speed on flat terrain (e.g. corridors)		
	Minimum (m/s)	Mean (m/s)	Maximum (m/s)
Females younger than 30 years	0.93	1.24	1.55
Females 30-50 years old	0.71	0.95	1.19
Females older than 50 years	0.56	0.75	0.94
Females older than 50, mobility impaired (1)	0.43	0.57	0.71
Females older than 50, mobility impaired (2)	0.37	0.49	0.61
Males younger than 30 years	1.11	1.48	1.85
Males 30-50 years old	0.97	1.3	1.62
Males older than 50 years	0.84	1.12	1.4
Males older than 50, mobility impaired (1)	0.64	0.85	1.06
Males older than 50, mobility impaired (2)	0.55	0.73	0.91
Population groups - crew	Walking speed on flat terrain (e.g. corridors)		
	Minimum (m/s)	Mean (m/s)	Maximum (m/s)
Crew females	0.93	1.24	1.55
Crew males	1.11	1.48	1.85

The travel time, both that predicted by models and as measured in reality, is a random quantity due to the probabilistic nature of the evacuation process. In total, a minimum of 50 different simulations should be carried out for each of the four-benchmark cases. A safety margin is added to account for the assumptions. It is 600 s for cases 1 and 2 and 200 s for cases 3 and 4

Finally the Guide reflects that the documentation of the algorithms should contain:

− The variables used in the model to describe the dynamics, e.g. walking speed and direction of each person.
− The functional relation between the parameters and the variables.
− The type of update, e.g. the order in which the persons move during the simulation (parallel, random sequential, ordered sequential or other).
− The representation of stairs, doors, assembly stations, embarkation stations, and other special geometrical elements and their influence on the variables during the simulation (if there is any) and the respective parameters quantifying this influence.
− A detailed user guide/manual specifying the nature of the model and its assumptions and guidelines for the correct use of the model and interpretations of results should be readily available.

The results of the analysis should be documented by means of:

− Details of the calculations.
− The total evacuation time.
− The identified congestion points.

5 CELLULAR MODEL FOR COMPLEX SPACES

As mentioned advanced evacuation analysis have to be able to study the behaviour of every single person involved in the evacuation, and everyone can have different characteristics that

will affect mainly to his or her speed (young people, elder people, crew,...). With a cellular model, the space is divided is squared cells, and passengers are studied individually like. The ship and evacuation modelization is divided in these stages:

5.1 Strategic level

The general arrangement of the ship or a part of it, with cabins, corridors and public spaces is imported (via a .dxf file normally) and floor is divided in squared cells of 0.4 by 0.4 meters (figure 4, left). This is a standard value in evacuation studies (13), (14) that derives from the maximum density in crows when the movement reaches a stop (15). One person thereby occupies one cell and two different passengers cannot occupy the same cell.

Other cells contain different information, depending on the way it influences the person standing on it. If it is not accessible, it represents an obstacle like a wall or furniture. Others affect the speed of a person walking through them; for example, stairs and these cells can be used to connect different decks or levels, with a different speed if it is upstairs or downstairs.

The discretization and the cell size often lead to discussions. The main argument against the use of cells is the exclusion of small variations in the width of corridors or doors. This is improved with a coefficient that affects the speed and it is a function of the corridor or door with where the passenger is moving.

The problem concerning with orientation of a person is the global route choice. How a person evades obstacles and other passengers is considered in the operative level as is described in the next point, but the way that a person chooses where to go and to get there is the decisive problem. In the case of evacuation, this is called the evacuation plan that can be the main evacuation plan or secondary evacuation plan if the main is not possible because of fire or flooding for example. Inside the ship, the evacuation plan is clearly indicated through fluorescent arrows on the corridors, and route maps inside cabins and other spaces.

The cellular model works with the information generated by the macromodel, which works in a hydraulic way, with branches and nodes in specific points. These points are corners, cross points, connection points... From one node to other, a shortest path algorithm sets the optimum way, and a connection matrix between nodes can be obtained. This way, an optimum evacuation plan is designed. Macromodels can study different evacuation plans in case of emergency where some nodes are blocked, setting a secondary or alternative evacuation plan.
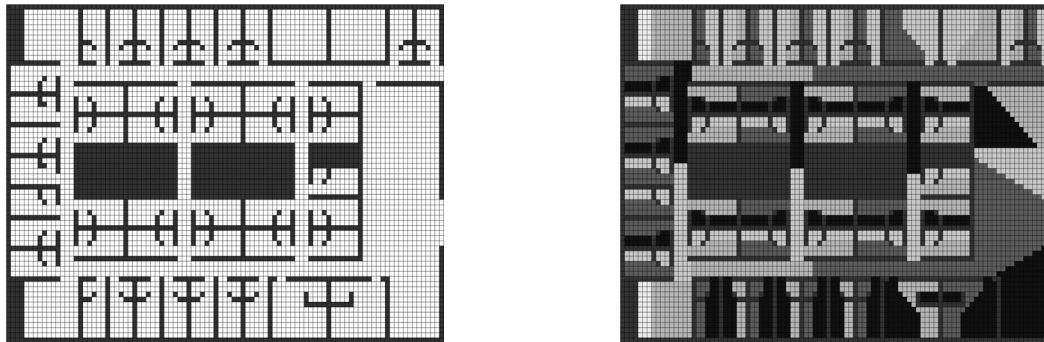
Figure 4. Discretization in cells and tactical level.

In this strategic level, decisions about the destiny points of the passengers (mustering and embarkment stations) are made. So, this strategic level is quite related with macromodels (16)

5.2 Tactical level
The direction in which passengers have to move in order to reach their goal is contained in the cells (figure 4, right). So, a person knows where to move in the next time step and these motions will lead the final goal (mustering or embarkation stations). Crewmembers have different routes towards the mentioned stations according their duty schedule at emergency, and sometimes, practically ever, there are encountered flows between crew and passengers. That is the reason because the model must solve encountered flows as it will be seen in the point IMO requirements, and every cell can have stored more than one route.

In some approaches route information in given through potentials. This means that only goal cells have to be marked, and the potential will automatically spreads the directions from one accessible cell to the following and by this throughout the whole structure.

Cellular model reads this information, and assigning the nodes position in the cells, the optimum way can be translated in information for the cells' directions, assigning the evacuation plan, or plans, to the cells. A different treatment is made for cells inside the cabins to assign directions from the cabin cells to the cabin door. Passengers read the mentioned information contained in the cells and follow the evacuation plan from their initial places towards the mustering stations.

When passengers reach the mustering stations, they wait in their cells until they can go to the different embarkation stations, as long as the lifeboat or other devices are being prepared. Then passengers are divided as a function of the MES capacity and when the MES is prepared, passengers can leave their cells, and go to the assigned embarkation stations. There, an egress-time is considered, to take into account the delay while entering a lifeboat or sliding on a marine evacuation system. These times are experimental ones (17).

Environmental conditions can be considered in this tactical level. If the ship is heeled portboard during evacuation, the directions of the cells can be changed, "pushing" or changing the tendency of motion portboard. Rolling motion can be also considered, by doing a periodical change of the tactical level (meanly in the speed effect) with the modal period of

the Sea State where evacuation occurs. The effect of the environment can also affect speed in the operative level (7)

5.3 Operative level

The individual behaviour of every passenger when going from cell to cell is studied in this level. Passenger's speed is influenced by passengers' density around, and by the number of cells in the advance direction that the person can move. One passenger cannot jump others to move forward them, and must go through left or right, if possible. If not, he must wait or move laterally in some cases.

For every passenger, two matrixes are obtained at every moment. A sight matrix and a motion matrix are used (figure 5). These have standard values and can be reduced in the case of low visibility because of smoke and some authors affect speed function with an experimental coefficient. In Figure 3, reserved cells are presented as arcs and selected path for advance with an arrow.

Passengers' density is calculated in a cell matrix that surrounds the passengers (sight matrix). With this passenger's density, speed can be obtained through an expression based in experimental results. According table 1 we use the following:

$$S = S0 \cdot 1 \; ; D \quad 0.5 \; pax/m2 \tag{1}$$
$$S = S0 \cdot (\; 1.153 - 0.306 \cdot D); 0.5 < D \quad 3.5 \; pax/m2$$
$$S = S0 \cdot 0.082; 3.5 < D \; pax/m2$$

Where S0 is a probabilistic function of the passenger type (crew, age, gender,...) and the values are also provided by MSC-c1033 Annex 2 (11) and D is the passengers density measured in the sight matrix. As far as the advance is a multiple of the cells length, sometimes a passenger will advance more than the exact value assigned by the speed function, and other times less. This lack or excess in the advance distance should be taken into account to correct the advance in the next time steep.

But a passenger can advance only the number of free cells in the direction of motion which is assigned in the tactical level, so this calculation is made in the motion matrix, and the lower of these two values (cells assigned by the speed function and free cells) is the number of cells that a passenger advances in this time step. So, a passenger can choose advance through the column or row of cells (path) of the centre, left, or right, chosen with an optimum path algorithm.

Every passenger reserves also the cell just in front of her for the next time step, and this cell can not be occupied or crossed by other passenger. This is a polite behaviour, trying not to disturb the advance of the rest of the passengers crossing their way, and in case of encountered flows, trying not to be face to face of other passenger.
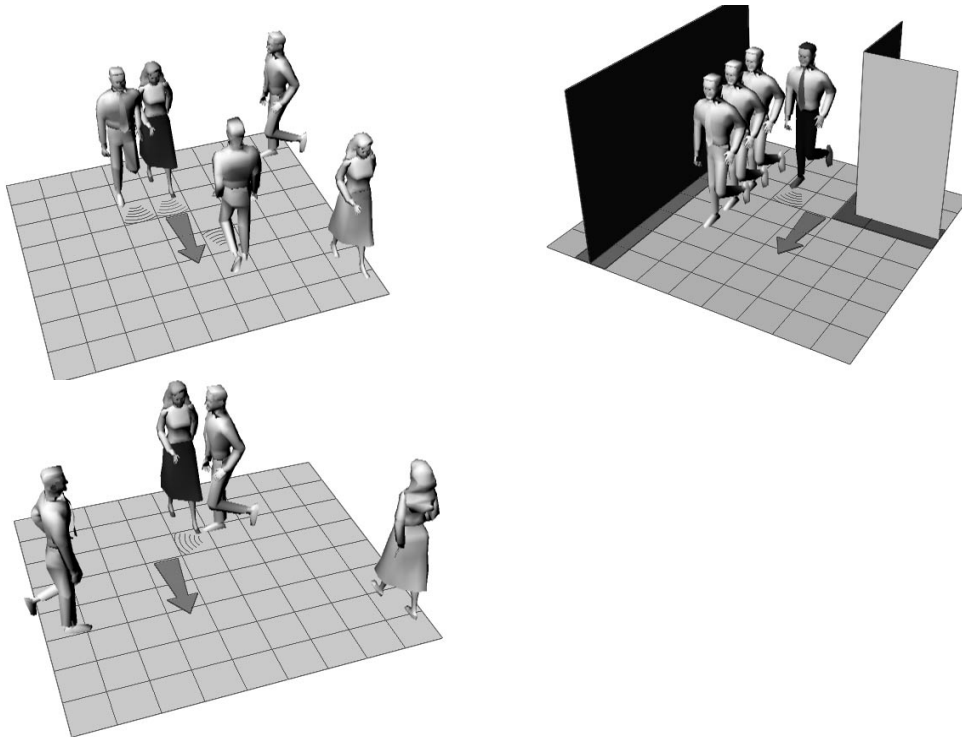
Figure 5. Examples of the operative level.

A passenger can avoid other passengers and obstacles (if possible) and following the evacuation plan, arrive to the final place inside the ship. Regarding IMO requirements, varying the values of S0 in [1] and by this random way, the type of passengers, at least 50 simulations must be made.

6   THE SIFBUP-S APPLICATION

Once we developed the cellular model for the movement of persons in complex geometry environments, we made its implementation in a computer application (the Sifbup-S), using Visual-Basic programming language.

Our objective was to develop a flexible application, modular, integrated and oriented to the user (18). The participation in the project of a shipyard, a ship owner and a company leader in visualization software were fundamental for its practical aspects. As a specification summary, the Sifbup-S has been designed to solve the following objectives:

-   It fulfils with the advanced method of the MSC-c1033.

    −   Its concept design is opened, allowing the simulation of the movement of persons in 2D in complex stages (ships, platforms, buildings, etc.) connecting different levels with staircases or ramps.

- For the definition of the case and its analysis, it uses a modular structure with several data files, that allows the use of previous work to modify or expand the present project. The program works in two different modes: Edition and Calculation (the last one includes the 2D simulation and the results analysis).
- This structure allows to be integrated with other applications, such us CAD ones importing design in .dxf format, and the Sifbup-D and Sifbup-3D. There is also the option to export in .xls format for its post process with data sheets.
- Manual introduction and edition of cells' properties is also possible.
- The user can start with a general analysis of the ship zones, using quick input data and then the user can improve the model, working with greater precision (doors, speed coefficients, etc.) at the critical zones.
- Apart from the global response times, we can obtain detailed results using counters, and watching the dynamic symbols on the graphical output interface.
- The 2D simulation allows a global and detailed vision of the evolution of a situation, with several tools that make easy the visualization and identification of different variables related with evacuations, such us pax density or critical zones.
- The graphic interface design is highly ergonomic with Windows structure and an extensive mouse use.

In figure 6 we see the application general aspect in the edition and calculation modes.
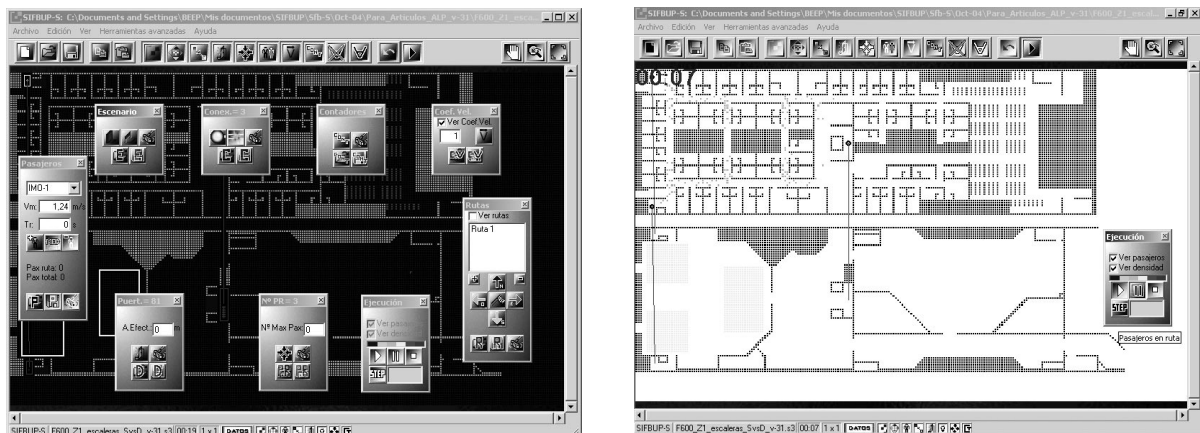
Figure 6. Sifbup-S edition an execution interfaces.

The edition process can be accomplished in manual form, if we have not any previous data files, or in an automated way if we have previous studies from other applications. In the first case it is compulsory to provide the following data (Fig. 7):

- Layout representation.
- Routes definition (field of directions)
- Pax placement in theirs start points
- Connections (staircases) between decks or floors.
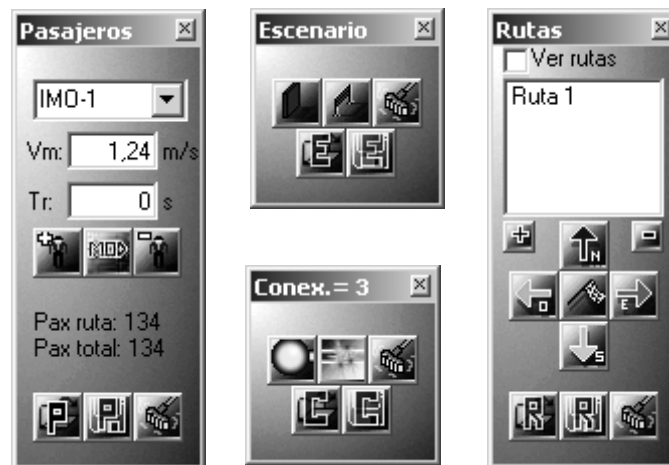
Figure 7. Interface windows for basic tools.

The first step can be made importing a drawing in .dxf format drawing and/or using the copy and paste tools.

For the second one, an advanced tool of "automatic routes generator" has been created, based on a shorter path algorithm.

For the two last statements we can start with the pax distribution generated in an evacuation study using the Sifbup-D application, with the pax placed in their cabins. If we don't have this study, there are tools for the automatic pax placement in public rooms or in cabins connected to a corridor. In both cases it is enough to define graphically the extremes of line were passengers will be distributed, and indicate the number of pax.
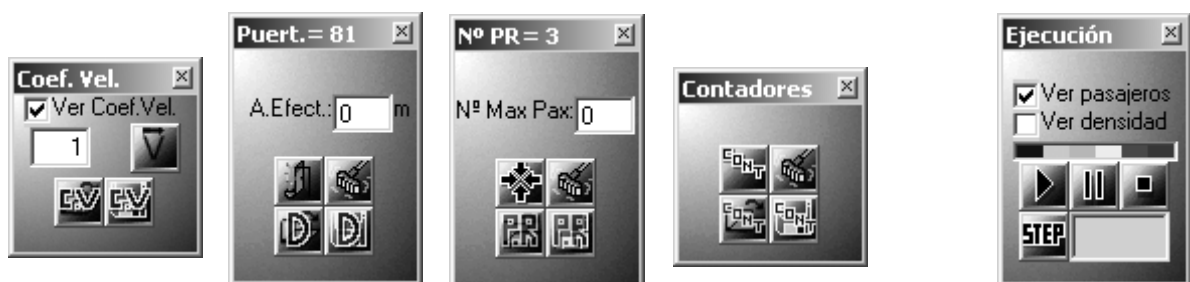
Figure 8. Interface windows for advanced tools and execution mode.

If the user wants to improve the post-process analysis, he can use the following additional options (figure 8):

−   Counters: to watch the pax time evolution through a specific place of the ship.
−   Doors: to represent with greater accuracy the maximum flow in any narrow place.

- Speed coefficients: to adjust the real corridor width and the staircase effect on speed. This is only necessary in critical spaces (narrow corridors) with a poor width representation of the cellular model.
- Assembly stations: these allow keeping the pax in the arrival zones, using these data as starting point for later studies (Embankment phase). This way, the complex problem of ship evacuation can be temporarily divided in several ones, studying with detail the intermediate results.
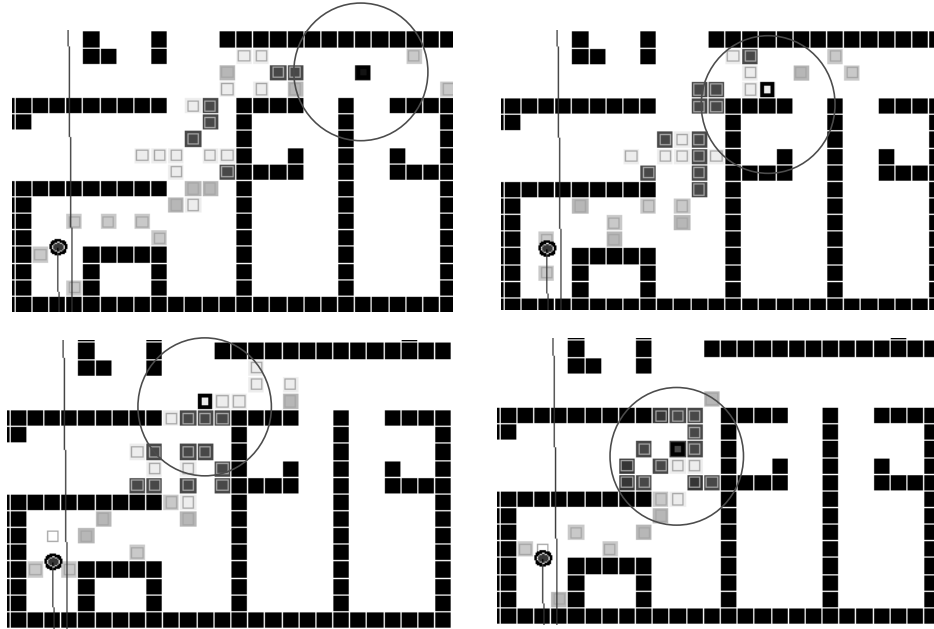
Figure 9. Advance images of a tagged pax.

To start the calculation mode once the project definition is finished, it is enough to start the simulation. We will see in the screen all pax movements (figure 9). In order to make easy this graphic analysis the application has the following post-process facilities active during the calculation mode:

-       Scroll and zoom (also operative in the edition mode).
-       Stop (pause) and step-by-step execution.
-       Image capturing (photo).
-       Reload of the initial pax location.
-       Special tag to emphasize selected pax.
-       Information (lower bar) of all data related with a selected cell.
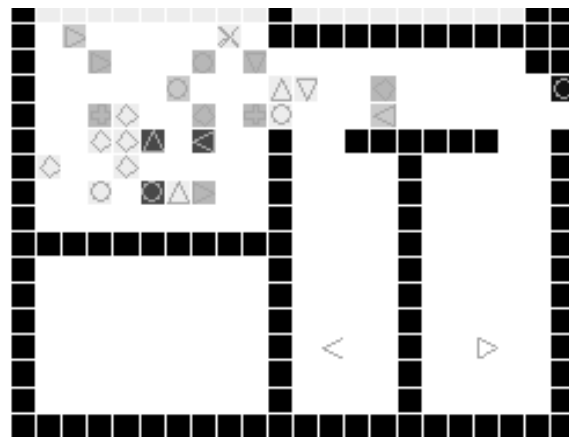
Figure 10. Example of pax symbology.

When it is in execution mode each pax has a triple symbol tag (figure 10):

- The symbol shape: represents the pax type, which is related to his maximum speed.
- The symbol colour: shows the pax origin (route).
- The cell background: informs about the density around a cell.

The symbol and/or the background can be hidden for different visualization types and to improve the execution speed.

When calculation phase is finished, a special mark appears on all the cells which density have overcomes a threshold limit during a significant period of time. By this way is easy to identify the crowded zones that will affect seriously to the evacuation process.

By default the calculation mode works with a deterministic method. This helps the post-process and initial analysis. According to the advanced methodology indicated by the regulation MSC-c1033, the application has also a random analysis mode. This randomises automatically the properties of each pax and allows a statistic analysis of the total time of the evacuation, with multiple speed and awareness time distribution for a given study.

Figure 11. 3D evacuation simulation.

The program also exports the following information:

−   Evolution of the pax number along time in the points were counters are placed.
−   Multiple "photos" of the process. In figure 9 are shown four to indicate the advance of the tagged pax.
−   Video image of all the evacuation process (using external tools).
−   Statistic results.
−   Final pax position.
−   Path of every single pax during the simulation. Starting with this data file we can work with the application Sifbup-3D to generate a simulation in 3D, as shown in figure 11 with the scene visualization controlled by the user (virtual reality).

7 CONCLUSIONS

The necessity of special models to study the movement of people on complex and size limited scenarios has been showed, with the special requirements to use them on ship emergency evacuation simulations.

The accomplishment of the existing regulation has to be implemented in the models.

Our approach to solve this problem, based on an improved cellular agent model, is a good solution, not only on the theoretical face, but also on their easiness to use it to develop a used oriented application for the pedestrian flow aboard simulation.

REFERENCES

(1) Pérez, F.; López, A. "A 2D model to study the evacuation of ship passengers". Second International Conference "Navy ands Shipbuilding Nowadays" NSN'2002, St. Petersburg, 2001.

(2) Okazaki, S.; Matsushita, S. "A study of simulation model for pedestrian movement with evacuation and queuing". www.anc-d.fukui.ac.jp/ ^sat/ECS93.pdf.

(3) Blue V.J. and Adler J.L. "Cellular automata microsimulation for modelling bi-directional pedestrian walkways, Transportation Research B 35/3, 293, 2001.

(4) López, A.; Pérez, F. "Designer and master aids to improve the Evacuation of passenger ships". World Maritime Technical Conference. S. Francisco, 2003.

(5) Letizia, L. "Developments in Evacuation Systems and Techniques", Safer-Eurororo Workshop, Madrid, 2000.

(6) López, A.; Pérez, F. "Models and tools for the ship evacuation simulation". : 3rd. International Congress on Maritime Technological Innovations and Research, Bilbao, 2002.

(7) Brumley A. and Koss L., "The influence of human factors on the motor ability of passenger during the evacuation of ferries and cruise ships", Conference on Human Factors in Ship Design and Operation, London, 2000.

(8) Yoshida K. et al. "Study on evaluation of escape route in passenger ships by evacuation simulation and full-scale trials", www.rime.gr.jp , 2002.

(9) Pauls J. "SFPE on fire protection engineering handbook. Chapter 13: movement of people". NFPA, New York, 1993.

(10) López, A. "Simulación del movimiento de las personas a bordo. Aplicación a la evacuación en situaciones de emergencia". X Jornadas Universidad Politécnica de Madrid – Fuerzas Armadas, Madrid, 2002.

(11) IMO "Maritime Safety Committee Circ. 1033". IMO, London, 2002.

(12) Pérez, F.; López, A. "Cellular models applied to the evacuation of ship passengers". International Congress on Ship and Shipping Research, Palermo, 2003.

(13) Hellesoy A.: "Evacuation Analysis as a Design Tool". Hyper 2002 conforcence, Bergen, 2002.

(14) Konig T. et al.: "Assessment of Evacuation of Processes on Passenger Ships by Microscopic simulation". Pedestrian and Evacuation Dynamics. Ed. Sharma. 2001.

(15) Helbing, D. Verkehrsdynamik,: "Neue physikalische Modellierungskontezpe". Springer Verlag, Berlin 1996.

(16) López, A.; Robledo, F. et al.: "Investigación multi-institucional sobre ferry de alta velocidad". 36 Sesiones Técnicas de Ingeniería Naval. AINE, Cartagena 1999.

(17) Marón, A.; Valle, J.; Riola, J.M. et al.: "Evacuación en buques de pasaje: Necesidades e investigación", Rev. Ingeniería Naval nº798 Nov-02, Madrid, 2002.

(18) López, A.; Pérez, F. "Ship evacuation optimisation. Tools for master an designer aid". 2nd International Conference in Pedestrian and Evacuation Dynamics (PED'03), London, 2003.

Chapter 3

Evolutionary computation in a multiobjective problem for autonomous underwater vehicle trajectories

J. M. GIRON-SIERRA, J. FERNANDEZ-PRISUELOS, B. ANDRES-TORO, J. M. DE LA CRUZ
D. A.C.Y.A., Fac. CC. Fisicas. Universidad Complutense de Madrid, 28040 Madrid. Spain
J.M. RIOLA
CEHIPAR, El Pardo, Madrid. Spain

Part of a research project on cooperative marine robotics is the scenario of a submarine rendez-vous. This paper considers this case, where a high-manoeuvrability autonomous underwater vehicle (AUV) should meet a submarine platform for energy, samples and data service. Since the AUV is equipped with a set of thrusters, the problem of an adequate command of the thrusters appears. Given initial and final points for the AUV underwater trajectory, the problem is to determine the set of forces and times to be exerted by the thrusters to get an adequate trajectory. Several constraints and simultaneous objectives to be optimized must be considered. Given the complexity of the multi-objective optimisation problem, it seems opportune to use Genetic Algorithms.

1 INTRODUCTION

An interesting case of cooperation between marine crafts is a rendez-vous between a submarine platform, which can be in charge of bio monitoring, and a service AUV. A high-manoeuvrability AUV is considered by our research. This AUV has no flaps, no rudder, but a set of thrusters for surge, pitch, yaw, sway and heave motions. The AUV must depart from an initial point, near the surface, and reach the submerged platform following a certain trajectory to be determined. Likewise, the control action of the thrusters must be determined to cause that trajectory. Several considerations and criteria appear concerning what should be an adequate trajectory. Consequently, there is a multi-objective optimisation problem. In this problem, motions are coupled and thrusters have limited authority.

Along several optimisation problems that have been found by the research of our team, it has been useful to apply Genetic Algorithms (B. Andres-Toro, et al., 2000a; Esteban, et al., 2002). After some years applying genetic algorithms (GA), a MATLAB toolbox was developed: EVOCOM (De Andres, et al., 2000b). This is a multipurpose evolutionary algorithm toolbox. It has been successfully applied to the AUV control problem. The representation of this problem in terms of chromosomes and fitting function is a relevant aspect covered in this paper.

The scientific literature provides a good mathematical and modelling background for the AUV dynamics and control (Fossen, 2002). However, most of the papers and textbooks consider

submergible vehicles with fins and rudders, which is not our case. With respect to the application of Genetic Algorithms to the AUV context, there are contributions considering trajectories planning. For instance (Alvarez, et al., 2004) deals with 3D scenarios, with sea currents and underwater mountains. There are some other papers in a similar vein (Kwiesielewicz, et al., 2000; Tan, et al., 2004). These contributions focus on trajectories, this paper focus instead on control planning (using thrusters). Cooperative marine robotics is a new field that is beginning to consider different problems, such the scenarios of (Kyrkjebo, et al., 2004) on ship rendezvous operations, (Stilwell, et al., 2003) with platoons of AUVs, or (Soetanto, et al., 2003) with the coordinated control of marine robots. This belongs to the spirit of multi-agent robotic systems (Liu and Wu, 2001; Weiss, 1999; Billard, 2004), with elements of formation control (Tanner, et al., 2004).

The order in this paper is the following. First, an explanation of the problem and its mathematical procedures, then a GA treatment of the problem in order to apply the method to several cases with different obstacle avoidance situations, and finally some conclusions according with the results obtained.

2 PROBLEM STATEMENT

2.1. Rendez-vous scenario
The research considers a high-manoeuvrability AUV that departs from an initial point near the surface, and that should meet a submerged platform. The final rendez-vous must be with the AUV in horizontal attitude and zero speed. An adequate trajectory (not much energy invested, not much time) must be determined together with the action of the thrusters causing the trajectory.

The high manoeuvrability AUV has four thrusters that can be reversed, so its displacement is allowed in five degrees of freedom excluding roll motion. Figure 1 and figure 2 show two views of the AUV (notice that the thrusters are attached to the AUV structure, so their action depends of the AUV attitude).
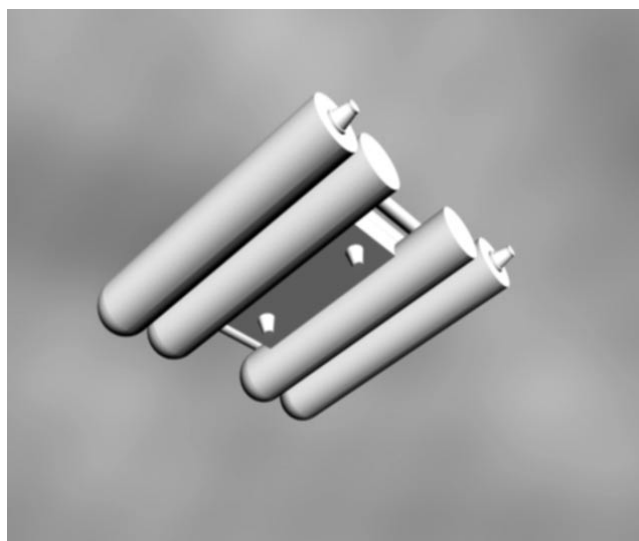
Figure 1. View of the AUV

44
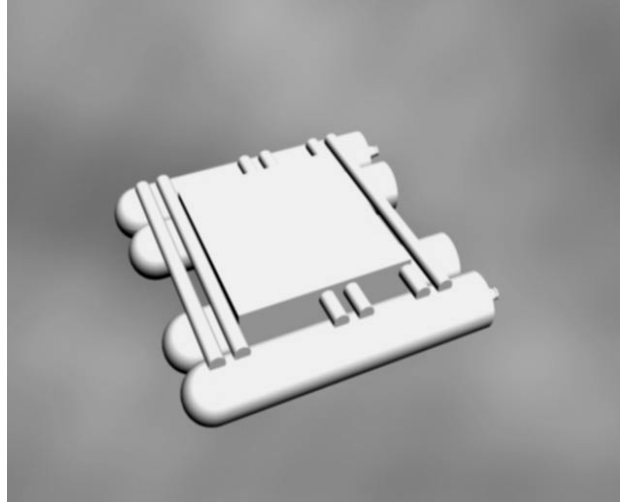
Fig.2. View of the AUV

2.2. Mathematical model

The motion of the body-fixed frame of reference is described relative to an inertial frame or earth-fixed reference frame. The general motion of the AUV is expressed by the following vectors (SNAME 1950):

$$\eta_1 = [x, y, z]^T ; \quad \eta_2 = [\phi, \theta, \psi]^T ; \quad \upsilon_1 = [u, v, w]^T ; \quad \upsilon_2 = [p, q, r]^T ;$$

$$\tau_1 = [X, Y, Z]^T ; \quad \tau_2 = [K, M, N]^T$$

where η_1 and η_2 denote the position and orientation respect in earth-fixed coordinates, υ_1 and υ_2 the speed in the same reference and τ_1 and τ_2 the forces and moments vectors applied. See next figure for the AUV coordinate systems (Fig. 3)
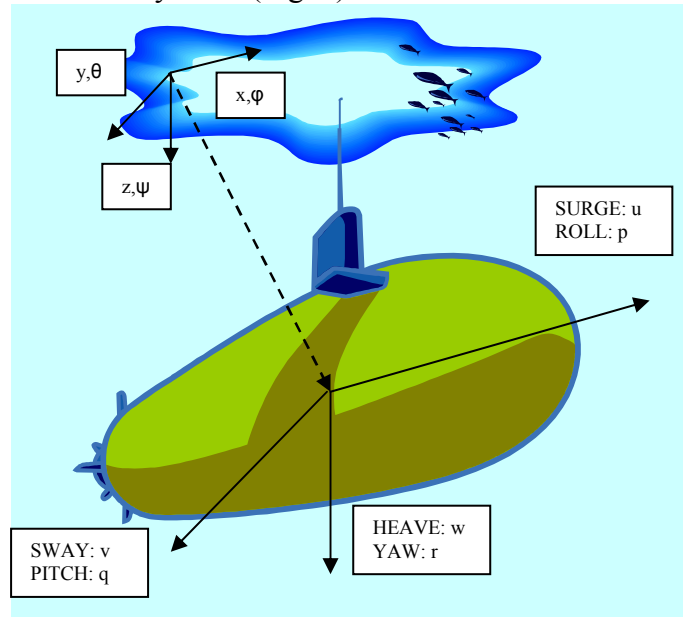
Fig. 3. Axis coordinate systems

The following coordinates transforms relate translational and rotational velocities between body-fixed and earth-fixed reference systems

$$
\begin{bmatrix} x' \\ y' \\ z' \end{bmatrix} = J_1(\eta_2) \cdot \begin{bmatrix} u \\ v \\ w \end{bmatrix} \qquad \begin{bmatrix} \phi' \\ \theta' \\ \psi' \end{bmatrix} = J_2(\eta_2) \cdot \begin{bmatrix} p \\ q \\ r \end{bmatrix}
$$

where $J_1(\eta_1)$ and $J_2(\eta_2)$ are the following matrix

$$
J_1(\eta_2) = \begin{bmatrix} (\cos\psi \cdot \cos\theta) & (-\sin\psi \cdot \cos\phi + \cos\psi \cdot \sin\theta \cdot \sin\phi) & (\sin\psi \cdot \sin\phi + \cos\psi \cdot \sin\theta \cdot \cos\phi) \\ (\sin\psi \cdot \cos\theta) & (\cos\psi \cdot \cos\phi + \sin\phi \cdot \sin\theta \cdot \sin\psi) & (-\cos\psi \cdot \sin\phi + \sin\psi \cdot \sin\theta \cdot \cos\phi) \\ (-\sin\theta) & (\cos\theta \cdot \sin\phi) & (\cos\theta \cdot \cos\phi) \end{bmatrix}
$$

$$
J_2(\eta_2) = \begin{bmatrix} 1 & (\sin\phi \cdot \tan\theta) & (\cos\theta \cdot \tan\theta) \\ 0 & (\cos\phi) & (-\sin\phi) \\ 0 & (\sin\phi / \cos\theta) & (\cos\phi / \cos\theta) \end{bmatrix}
$$

Note that the last matrix is not defined in $\theta = \pm 90°$, but the vehicle motion does not ordinarily approach this singularity.

Taking a general model for the six DOF which involves the influence of added mass, Coriolis effects, hydrodynamic forces, wind and currents perturbations, gravitational and control forces (Fossen, 2002), the below expression is presented:

$$
M \cdot v' + C(v) \cdot v + D(v) \cdot v + g(\eta) = \tau + \omega
$$

and considering a two-dimensional scenario with only three relevant control actions (surge and heave forces, pitch moment), neglecting Coriolis forces (short distances) and wind/currents effects, and taking into account only the linear damping terms, the following equations of motion are obtained

$$
\begin{bmatrix} m - Xu' & -Xw' & m \cdot z_g - Xq' \\ -Xw' & m - Zw' & -m \cdot x_g - Zq' \\ m \cdot z_g - Xq' & -m \cdot x_g - Zq' & Iyy - Mq' \end{bmatrix} \begin{bmatrix} u' \\ w' \\ q' \end{bmatrix} + \begin{bmatrix} -Xu & -Xw & -Xq \\ -Zu & -Zw & -Zq \\ -Mu & -Mw & -Mq \end{bmatrix} \cdot \begin{bmatrix} u \\ w \\ q \end{bmatrix} +
$$

$$
+ \begin{bmatrix} 0 & 0 & 0 \\ 0 & 0 & -(m - Xu') \cdot u \\ 0 & (Zw' - Xu') \cdot u & m \cdot x_g \cdot u \end{bmatrix} \cdot \begin{bmatrix} u \\ w \\ q \end{bmatrix} + \begin{bmatrix} 0 \\ 0 \\ W \cdot \overline{BG}_Z \cdot \sin\theta \end{bmatrix} = \begin{bmatrix} F_1 \\ F_2 \\ F_3 \end{bmatrix}
$$

In order to implement a SIMULINK model, accelerations in each DOF can be expressed as:

$$u' = \left(\frac{F_1 + Xu \cdot u + Xw \cdot w + Xq \cdot q - \left(m \cdot z_g - Xq'\right) \cdot q' + Xw' \cdot w'}{m - Xu'} \right)$$

$$w' = \left(\frac{F_3 + (m - Xu') \cdot u \cdot q + Zw \cdot w + Zu \cdot u + (m \cdot x_g + Zq') \cdot q' + Xw' \cdot u'}{m - Zw'} \right)$$

$$q' = \left(\frac{F_5 - W \cdot z_g \cdot \sin q - (m \cdot x_g \cdot u - Mq) \cdot q - [(Zw' - Xu') \cdot u - Mw] \cdot w + Mu \cdot u + \left(m \cdot x_g + Zq'\right) \cdot w' - \left(m \cdot z_g - Xq'\right) \cdot u'}{I_{yy} - Mq'} \right)$$

that are three coupled equations for the AUV trajectory. The numerical values of the constants are showed below (Table 1.). This set of non-dimensional hydrodynamic derivatives has been calculated by different experimental and theoretical formulae, applied with the main characteristics of the showed AUV (Triantafyllou and Hover, 2002):

Table 1. Numerical values for
non-dimensional derivatives
in equations of AUV motion

Constant	Numerical value
Xu'	-7.6*exp(-3)
Xw'	1.7*exp(-1)
Xq'	2.5*exp(-2)
Xu	5.0*exp(-3)
Xw	2.0*exp(-1)
Xq	7.0*exp(-2)
Zw'	-2.4*exp(-1)
Zq'	-6.8*exp(-3)
Zu	-6.5*exp(-3)
Zw	-3.0*exp(-1)
Zq	-1.4*exp(-1)
Mq'	-1.7*exp(-2)
Mu	-1.0*exp(-1)
Mw	-3.5*exp(-2)
Mq	-1.7*exp(-1)

The mass value is equal to *40 kg*, and it can be assumed that *W=B= 400 N* in the simulation. The center of mass and the center of buoyancy (origin of the body fixed coordinate system) are not coincident ($x_g=0.1$ *m*, $y_g=0$ *m*, $z_g=0.02$ *m*).

2.3. The problem

The problem is to predict the proper AUV thruster's actions for a good rendez-vous with an underwater platform, starting from an initial point near the surface. An important aspect of the solution is the multi-objective scheme proposed (explained in the section below).

3 ESTABLISHING A GENETIC ALGORITHM PLANNING METHOD

The key issues for the successful application of GA are to define a good codification in terms of chromosomes, and to establish an adequate fitting function. It is important to take advantage of the open opportunities offered by GA to include "a priori" knowledge about the problem (in the case of this research, this knowledge leads to a specific semantics of the chromosomes and to define constraints and criteria to be optimized).

3.1. Fitting function

The optimization criteria are explained in the following list, and are implemented like a multi-objective function:

- Trajectories avoiding obstacles.
- AUV trajectories without points over the sea surface or under the sea bottom.
- Good arrival at the submarine platform, with zero final speed and zero final pitch angle.
- Short trajectory length, with not much time involved.
- Low energy requirements.

The objectives are grouped into two sets. The first set includes primary objectives; the second set includes secondary objectives. A Pareto front is determined for the first set (but the second set is considered: between two individuals with equal fitting function value, the individual with better value in the second set is preferred). When the Pareto front has been determined for the first set, another Pareto front is determined for the second set (considering values in the first set). This is repeated, till results converge.

3.2. Codification of the solution

The total trajectory from the starting point to the final point is divided in a different number of intervals. In each of these intervals a set of forces and moments F_{surge}, F_{heave} and F_{pitch} are applied during a time "t" (called in 3.2. as X, Z and M, respectively). This is, during the first t_1 seconds, the $F_{1,1}$ surge force, the $F_{1,3}$ heave force and the $F_{1,5}$ pitch moment are applied. During the second interval, along t_2 seconds, increments $\Delta F_{2,1}$, $\Delta F_{2,3}$ and $\Delta F_{2,5}$ are added to the surge force, the heave force and the pitch moment respectively. This is repeated in the rest of intervals (with increments $\Delta F_{j,1}$, $\Delta F_{j,3}$ and $\Delta F_{j,5}$).

So, the selected codification for the individuals of the population is showed in the next figure

| $\Delta F_{1,1}$ | $\Delta F_{1,3}$ | $\Delta F_{1,5}$ | $\Delta F_{2,1}$ | $\Delta F_{2,3}$ | $\Delta F_{2,5}$ | | $\Delta F_{j,1}$ | $\Delta F_{j,3}$ | $\Delta F_{j,5}$ | | $\Delta F_{N,1}$ | $\Delta F_{N,3}$ | $\Delta F_{N,5}$ | t_1 | t_2 | | t_j | | t_N |

$\xleftarrow{\hspace{6cm}}$ *Forces* $\xrightarrow{\hspace{1cm}}$ $\xleftarrow{\hspace{0.5cm}}$ *Times* $\xrightarrow{\hspace{2cm}}$
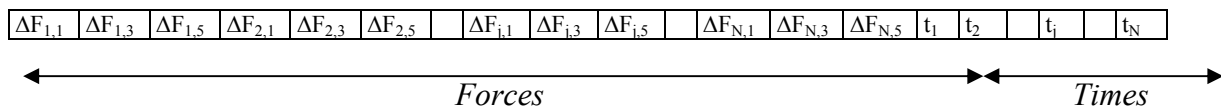
Fig. 4. Individual structure

So, with this codification, in the "jth" interval the forces and moments applied during a time $T = t_j + t_{j-1}$ are

$$F_{j,surge} = \Delta F_{j,1} + \Delta F_{j-1,1}$$
$$F_{j,heave} = \Delta F_{j,3} + \Delta F_{j-1,3}$$
$$F_{j,pitch} = \Delta F_{j,5} + \Delta F_{j-1,5}$$

3.3. Algorithm specifications

The standard GA algorithm is described in (Goldberg, 1989; Michalewicz, 1999). The algorithm specifications are according to the EVOCOM toolbox methodology (B. Andres-Toro, et al., 2000) and only will be explained some basic considerations about the evolutionary algorithm.

Evolutionary algorithms are adaptative methods which can be used to obtain the solution of a search or optimisation problem. They work with a population of individuals, each representing a possible solution of the given problem. The best individuals, according with an utility/fitness function, are selected to create new individuals with the genetic operators, recombining and modifying the information stored in the old ones. The new individuals are then inserted in the population with some of the old ones, and all of them compete for breeding in a new step of the algorithm. This process continues until a stop condition is reached, and the best individuals found for the algorithm are considered the solution of the problem. The basic steps in a standard GA algorithm are showed in Fig. 4.:
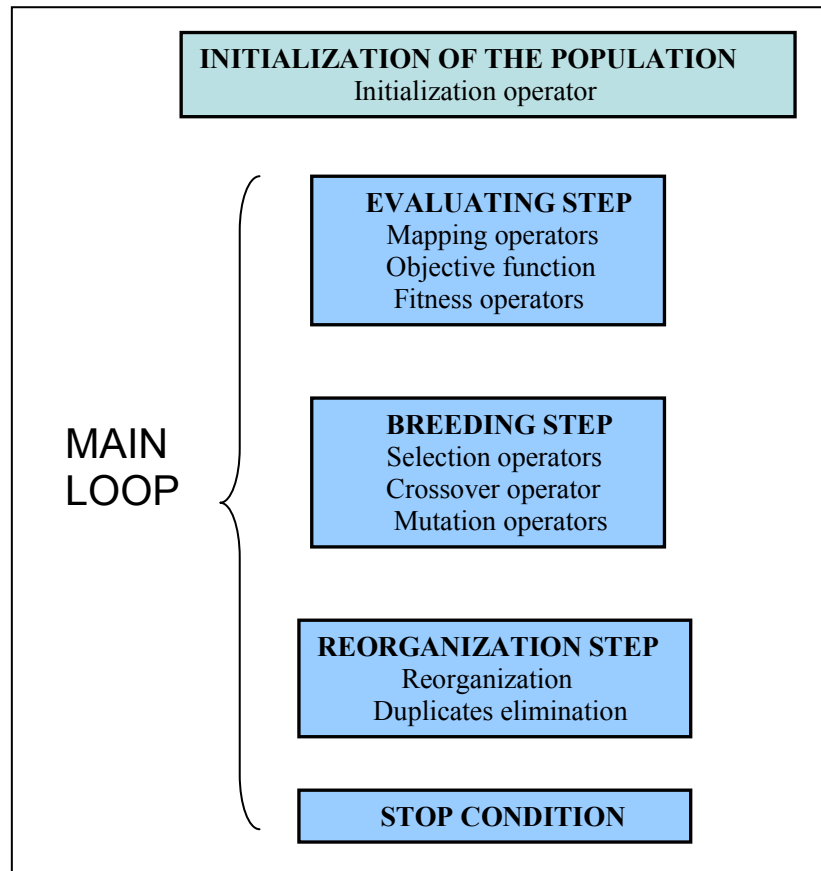
Fig. 4. Main scheme of the GA algorithm

In the AUV optimisation problem, the population includes 40 individuals, with a elitist selection method and tree points for crossing operations. The crossing probability used is 0.8 and the mutation probability is 0.008.

4 APPLICATION TO SEVERAL CASES

Several cases have been defined to check the optimisation procedure. Basically the cases consider several interesting situations corresponding to different final positions to be reached. Table 2 summarizes the different cases.

Table 2. Several rendez-vous cases

Final point (m)	Length(m)	Time (s)	Intervals
X=1; Y=1.	1.44	33.3	8
X=1; Y=2.	2.28	39.8	10
X=1; Y=5.	5.11	68.8	20
X=2; Y=1.	2.48	40.5	12
X=2; Y=2	2.92	48.4	15
X=2; Y=5.	5.53	65.5	25
X=5; Y=1.	5.30	64.1	20
X=5; Y=2.	5.57	70.1	20
X=5; Y=5.	7.31	93.27	35
X=10; Y=5.	12.00	134.7	50
X=10; Y=10.	16.06	163.7	60
X=15; Y=5.	17.53	128.3	58
X=15; Y=10.	18.83	148.5	60
X=30; Y=20.	36.7	209.6	88
X=40; Y=20.	50.41	203.0	95
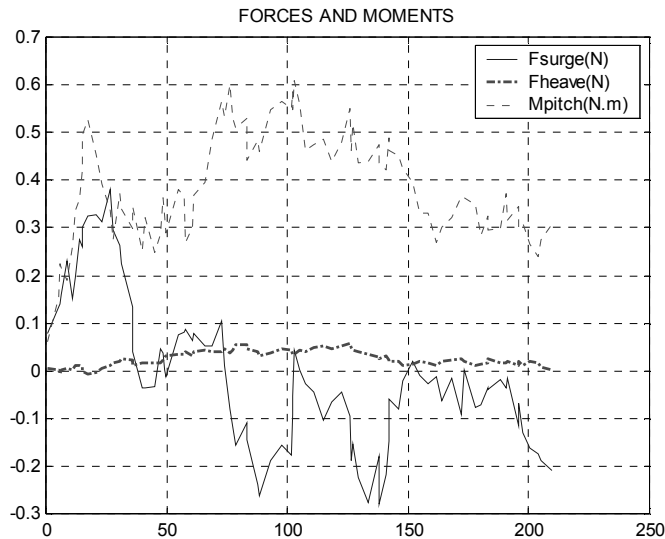
Fig. 5. A solution for the X=30, Y=20 case

In all cases the GA procedure reaches successful solutions in less than 1200 generations (10 minutes in a Pentium IV at 512 Mhz). Figure 5 shows an example of solution: the forces planning for a trajectory reaching X=30, Y=20 in 148.5 seconds. Notice the jagged curves in figure 3. This is a typical result when using GA to approximate the optimal solution. It is easy to refine this solution with a local optimisation algorithm, obtaining smoother curves.

For the solution described in figure 6, the cog trajectory of the AUV is as depicted in figure 4. The curve is smooth because the marine craft inertia integrates the forces. Figure 7 shows the evolution of the surge, heave and pitch speeds due to the application of the forces exerted. It can see that the AUV ends with zero final speed in each degree of freedom (DOF).
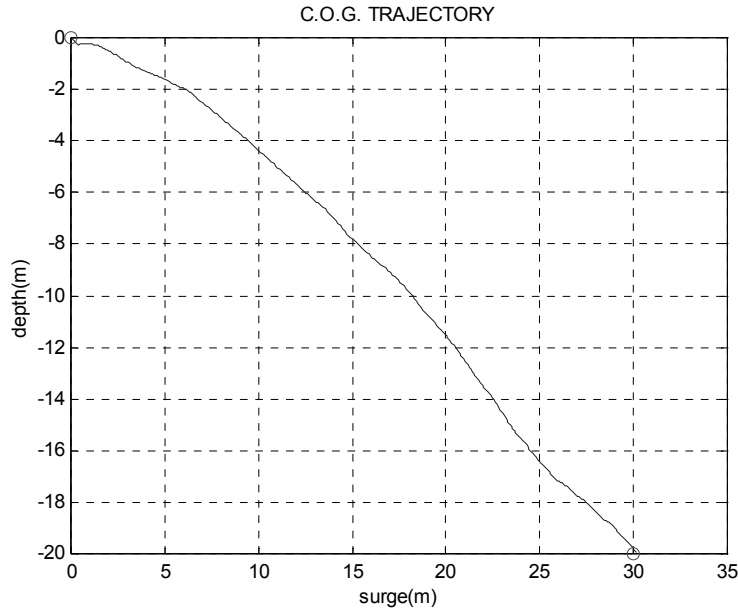
Fig. 6. Trajectory of the AUV c.o.g.
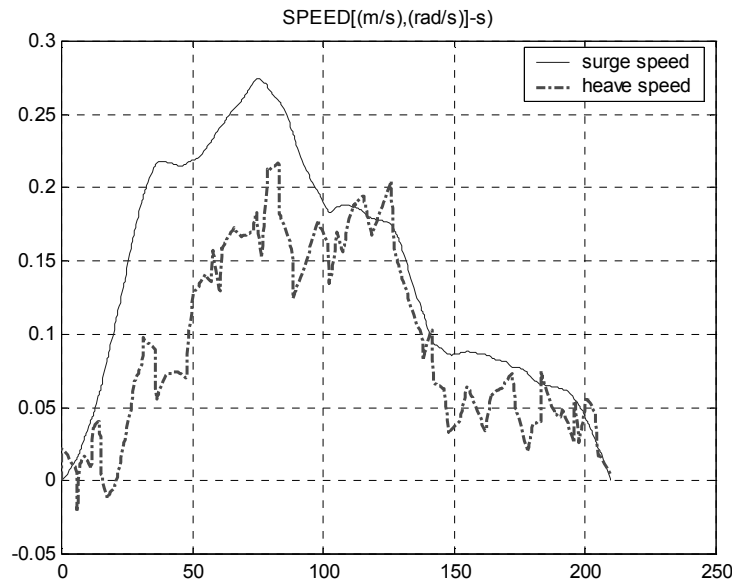
Fig. 7. Speed plotting of the AUV c.o.g.

It is important to know that in case of the pitch DOF, the values obtained in every case are smaller than 1*exp(-3) rad, so its graphical representation is not interesting. The evolution of the pitch speed has a similar behaviour (no significant values).

5 OBSTACLE AVOIDANCE

Obstacles have been added to the problem. Different types of obstacles have been considered, for example, a real obstacle could be sited at the bottom, like an underwater hill. Another type could be located at the sea surface, it may be a ship. One more complicated case may be like the depicted in figure 15, with both types of obstacles. Solution in terms of forces, trajectories and velocities will be exposed in the figures showed below
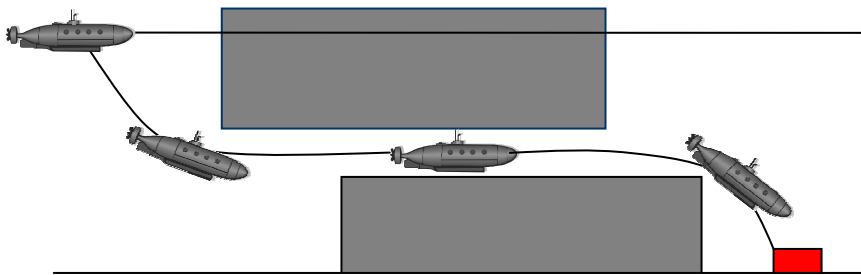
Fig. 8. AUV avoiding obstacles.
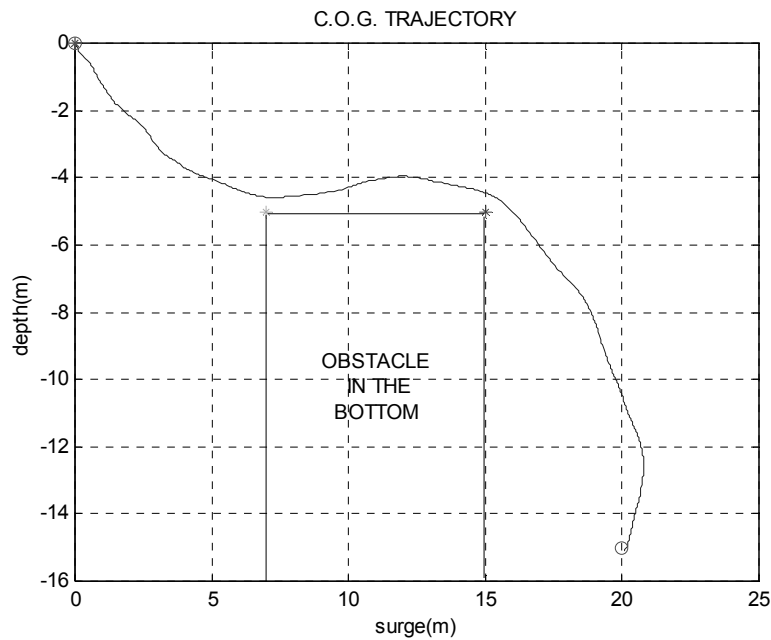
Fig. 9. Avoidance of an obstacle located at the sea bottom

In figure 9 it can be seen the trajectory obtained in the simulation for the case that the vehicle avoids an obstacle like is plotted in the figure, and with destiny point (X=20 m forward, Y=15 m depth). Figure 10 shows the solution for this case in terms of forces, and figure 11 plots the speed evolution (notice that the total time is necessary is 219 s).
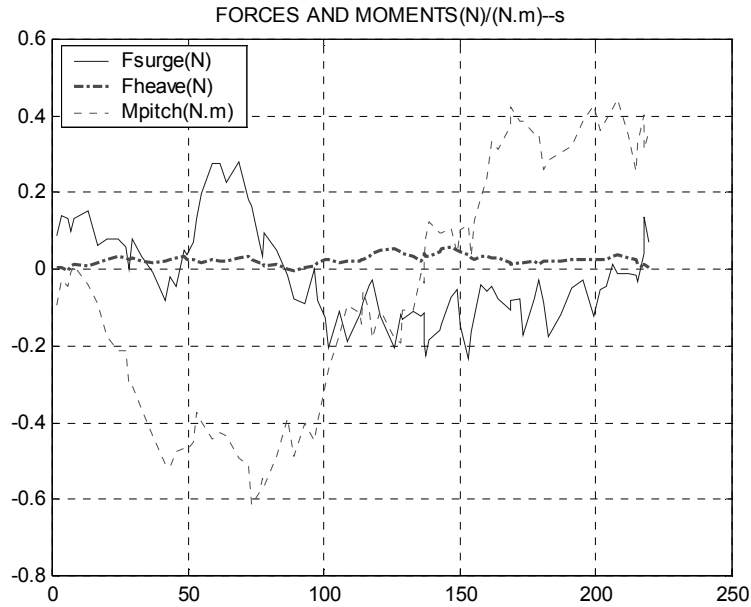
**Fig. 10. Thrusters actions for the avoidance
of an obstacle located at sea bottom**
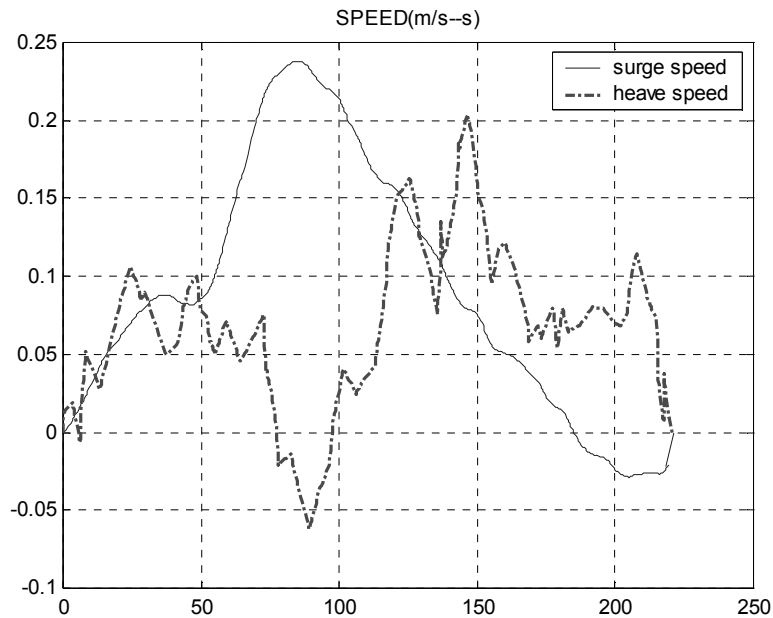
**Fig. 11. Speed plotting of the AUV c.o.g. for the case
of the avoidance on the bottom obstacle**

In a similar way, figures 12, 13 and 14 represent the same data for the case of the avoidance of a floating obstacle
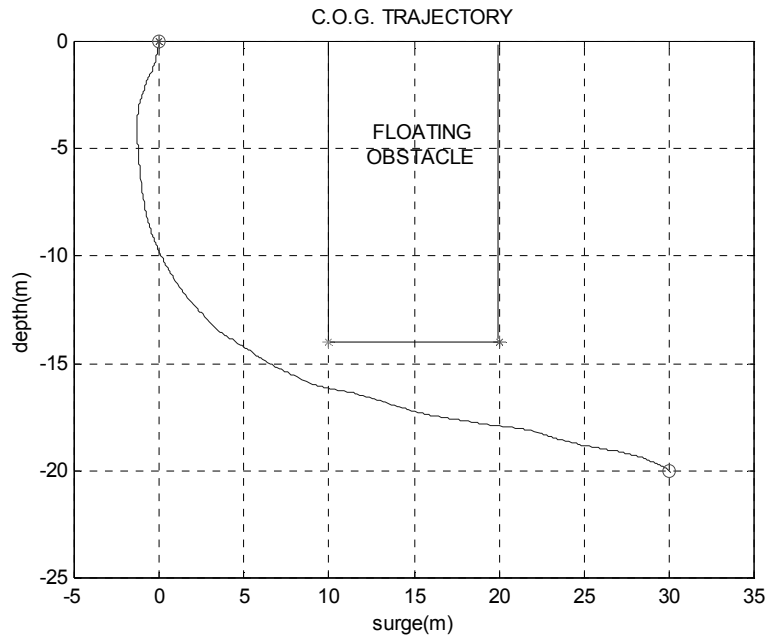
Fig.12. Trajectory of the AUV c.o.g. for the avoidance of a floating obstacle
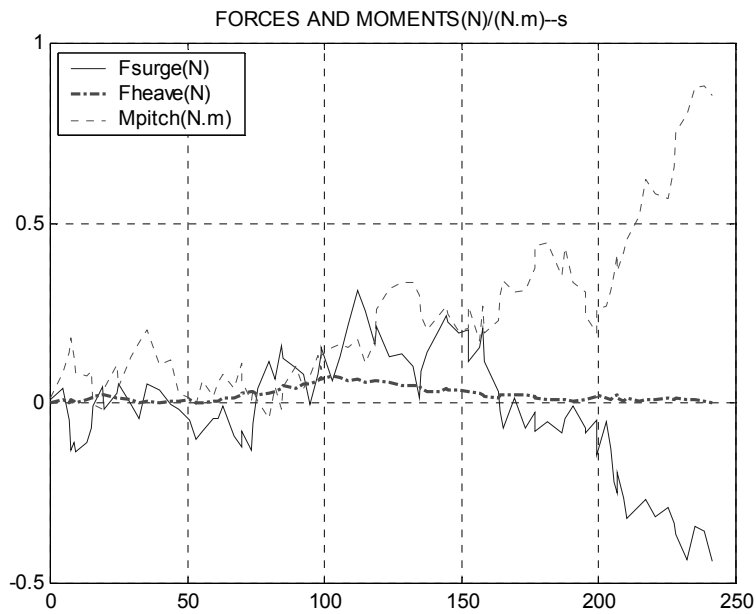
Fig. 13. Solution in terms of forces for the avoidance of an obstacle located at sea surface
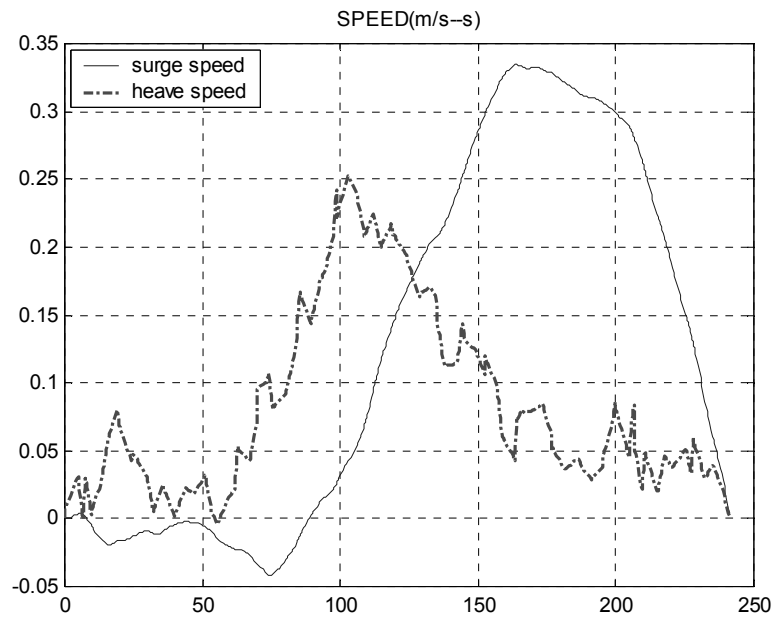
**Fig. 14. Speed plotting of the AUV c.o.g. for the case
of the avoidance on the bottom obstacle**

Obstacles are easily included in the optimisation procedure. In the next case two obstacles are considered (figures 15, 16 and 17):
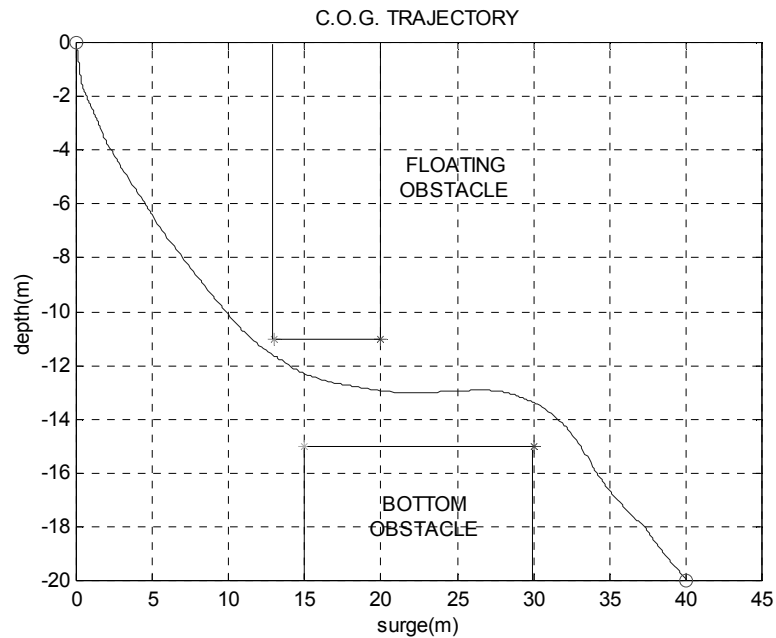
Fig. 15. Trajectory avoiding two obstacles
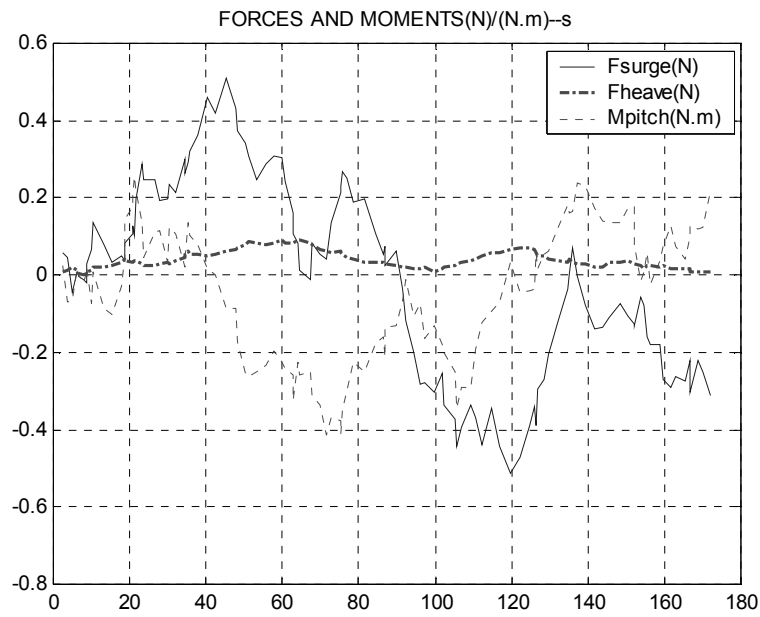
Fig. 16. Thrusters actions for the trajectory showed in figure 15
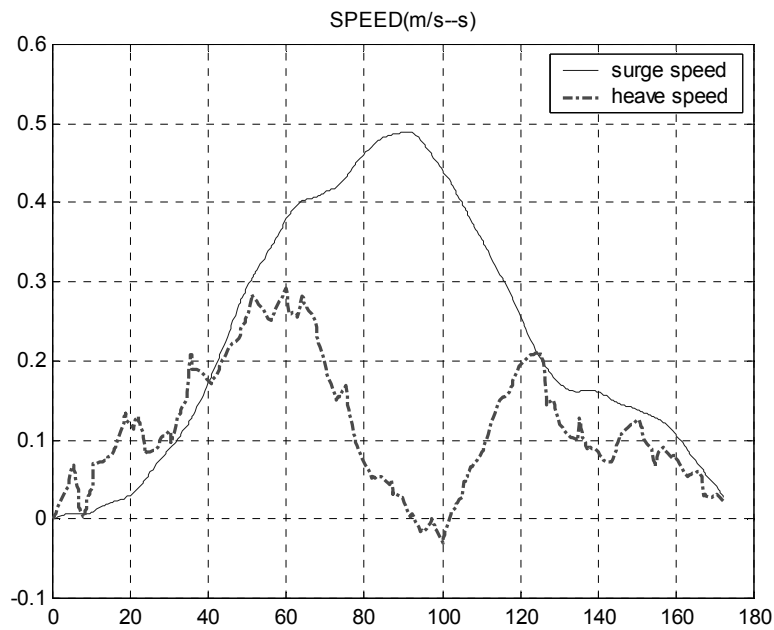
Fig. 17. Speed-time plotting for trajectory showed in figure 15

Notice the zero final speed obtained in every case. In fact, the multi-objective function implemented in GA has the speed requirements in the first level of priority. This is, the algorithm considers with the same relevance the avoidance of the obstacles, the destiny point arrival, the zero final pitch angle and the zero final speed in each degree of freedom, so a good solution must include the last characteristic.

Another possibility considered is the successive use of the GA for the solution of a more complicated case. In a situation with an arbitrary number of obstacles, general GA can be used in order to avoid all the bodies, but also, from the previous knowledge of the problem, GA may be used for reach individual sub-goals which also offer a good solution.

For example, look at the figure 18. The trajectory showed has been obtained with partial optimisations: the first one considering the avoidance of the first floating body and the first obstacle located at bottom. The final values of speed and position are used as starting points for the next optimisation that starts the AUV from this point and avoids the rest of the obstacles. The last optimisation completes the solution of the problem.
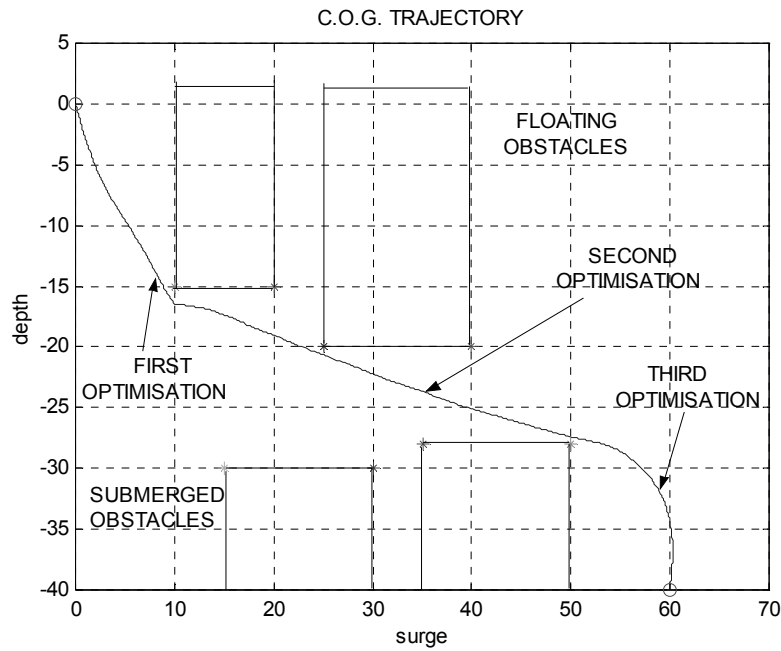
Fig. 18. Avoidance of various obstacles with a successive use of the GA

Figure 19 shows the solution for surge forces that must be exerted in each partial optimisation to obtain the total solution. Figures 20 and 21 plot the same data for heave forces and pitch moment. Figures 22 and 23 show the evolution of the surge and heave speed respectively, ending with zero speed like in the other cases.

With this alternative methodology the results are as good as in a single use of the GA, and it offers another possibility in the application procedure of the GA. The real time employed for obtain the solution was around 8 min. in the same computer (Pentium IV at 512 Mhz). In figures 22 and 23 we can see that the total time necessary for this simulated case will be 645 seconds, and this is because the time for the GA increases depending of the complexity and dimensions of the obstacles, because it is necessary to implement the total trajectory with a high number of intervals and the individual size increases. Depending of the nature of the problem, the number of callings to the GA would be different, but maintaining the same philosophy.
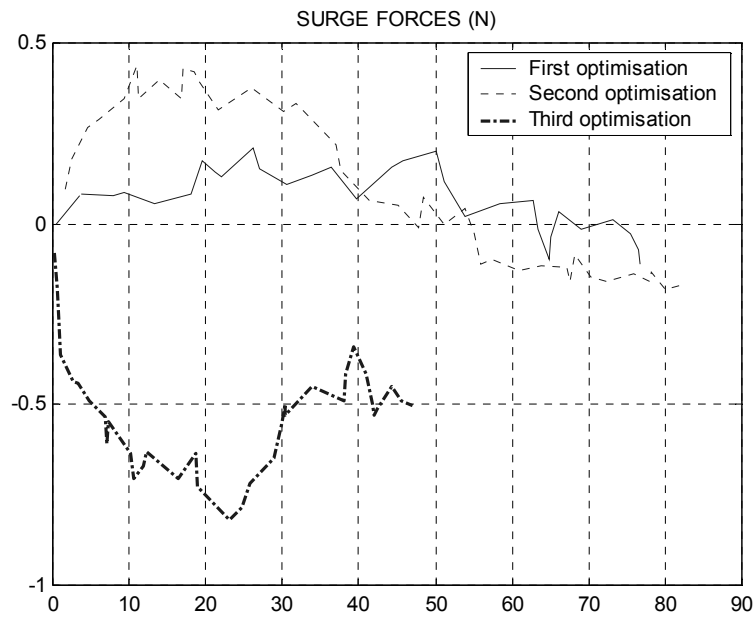
Fig. 19. Surge forces in the progressive optimisation problem
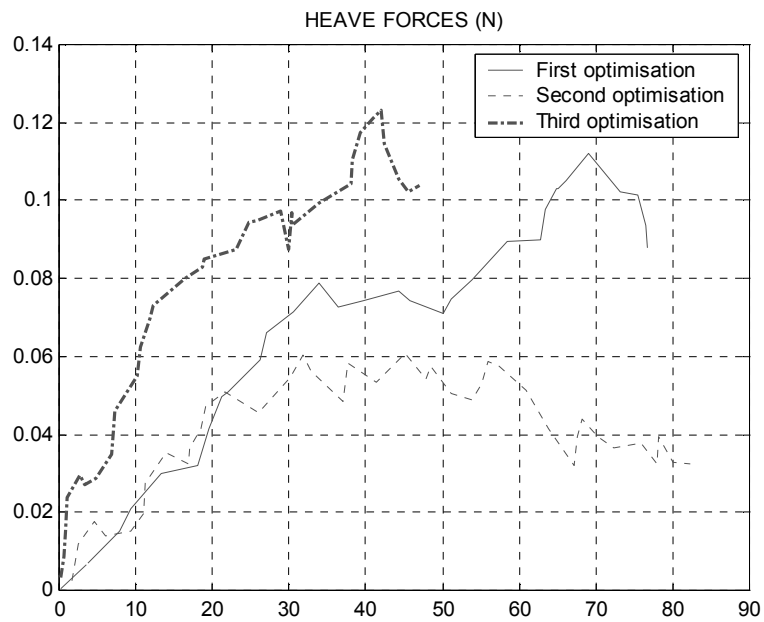
Fig. 20. Heave moments in the progressive optimisation problem
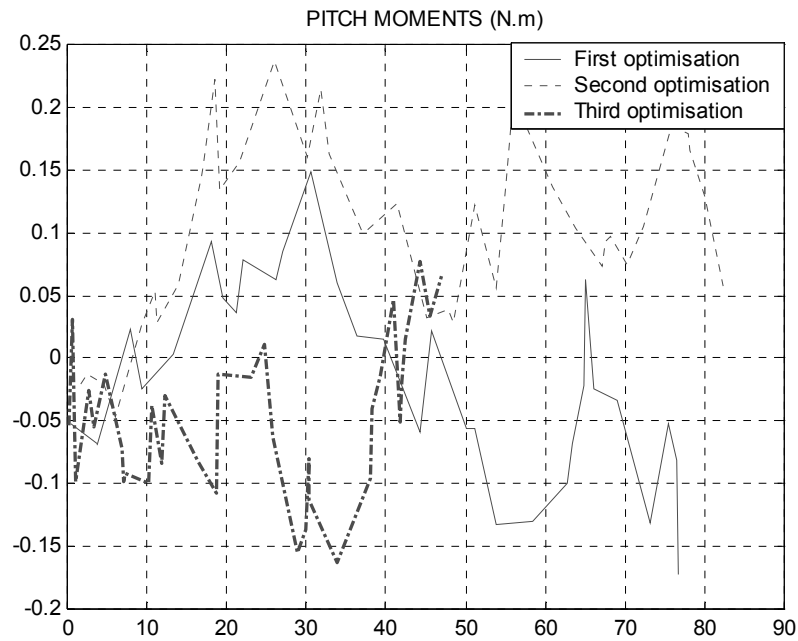
Fig. 21. Heave moments in the progressive optimisation problem
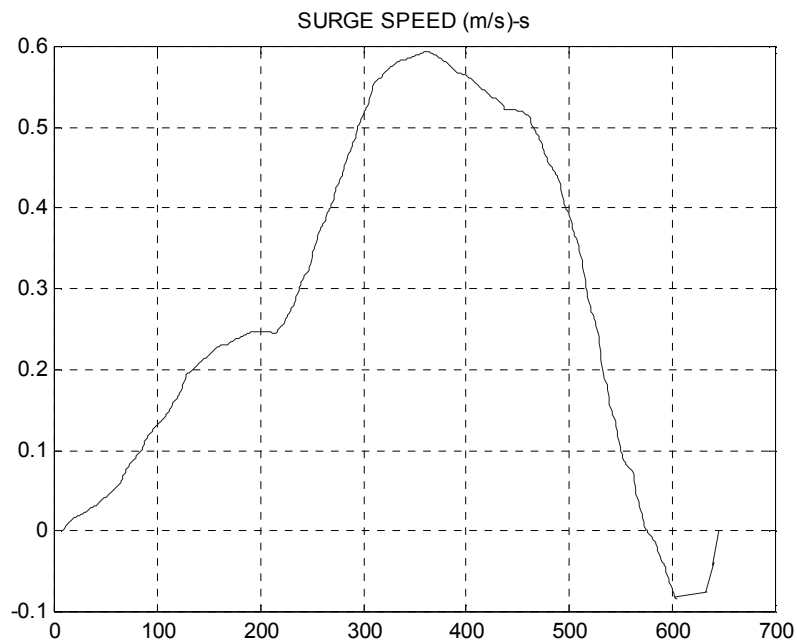
Fig. 22. Surge speed plotting for the figure 18 trajectory
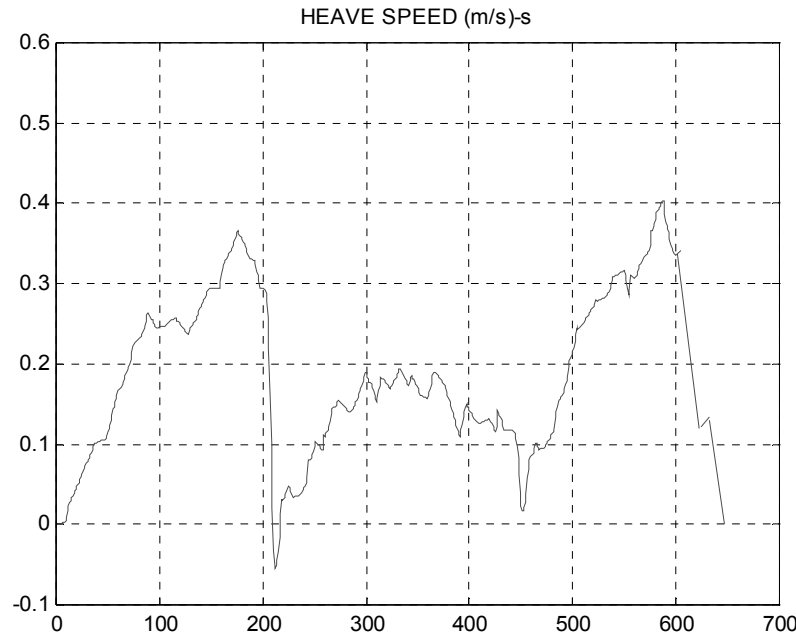
Fig. 23. Heave speed plotting for the figure 18 trajectory

6 CONCLUSIONS

Part of a research on marine craft cooperation is a submarine rendez-vous scenario. In particular, the research considers a high-manoeuvrability AUV, being in service of a submarine platform. The AUV has no rudder and no fins, only thrusters. This paper considered the genetic planning of the thrusters actions, to obtain an adequate trajectory between two given points. The system has motion coupling, and the thrusters have limited authority. This leads to a multi-objective optimisation problem with several constraints.

A statement of the problem in genetic terms has been devised. Using the EVOCOM toolbox, developed in house, satisfactory solutions have been obtained for a set of paradigmatic cases.

The procedure obtained is easy to apply, including "a priori" knowledge. Obstacle avoidance has been studied, with good results. The result obtained by the procedure is a vector of references for the thrusters, easy to transfer to the AUV before operation.

It is clear that next studies should focus on control issues along the trajectory, compensating deviations with respect to the planned thrusters actions.

ACKNOWLEDGEMENTS

REFERENCES

[1] Alvarez, A., A. Caiti and R. Onken (2004). Evolutionary path planning for autonomous underwater vehicles in variable ocean, *IEEE Trans. Oceanic Eng.*, vol. 29, n.2, April, 418-429.

[2] Billard, E.A. (2004). Patterns of agent interaction scenarios as use case maps, *IEEE Trans. System, Man and Cybernetics,* PartB, vol. 34, n4, August, 1933-1939.

[3] B. Andres-Toro, B., S. Esteban, J.M. Giron-Sierra and J.M. De la Cruz (2000a). Modelling the motions of a fast ferry with the help of genetic algorithms, *In Proceedings Third IMACS MATMOD*, Vienna, 783-786.

[4] Besada-Portas, E., B. Andrés-Toro, B., Lopez-Orozco, J. M. EVOCOM ver 2.0. A Multipurpose Evolutionary Algorithm Toolbox. *D.A.C.Y.A. Fac. CC. Físicas, Univ. Complutense Madrid. Spain.*

[5] B. Andres-Toro, B., S. Esteban, D. Rivera, J.I. Hidalgo and M. Prieto (2000b). Parallel Genetic Algoritms: an application for model parameter identification in process control, In *Proceedings GECCO 2000*, 65-69.

[6] Esteban, S., B. Andres-Toro, E. Besada-Portas, J.M. Giron-Sierra and J.M. De la Cruz (2002). Multiobjective control of flaps and T-foil in high speed ships, In *Proceedings IFAC 2002 World Congress*, Barcelona.

[7] Fossen, T.I. (2002). *Marine Control Systems,* Marine Cybernetics AS, Trondheim.

[8] Goldberg, D.E. (1989). *Genetic Algorithms in Search, Optimization and Machine Learning*, Addison-Wesley.

[9] Kwiesielewicz, M., W. Piotrowski , R. Smierzchalski and R. Sutton (2000). AUV path planning for navigational constraints by evolutionary computation, In *Proceedings IFAC MCMC 2000*, 323-326.

[10] Kyrkjebo, E., M. Wondergem, K.Y. Pettersen and H. Nijmeijer (2004). Experimental results on synchroniztion control of ship rendezvous operations, In *Proceedings IFAC CAMS 2004*, Ancona, Italy, 453-458.

[11] Liu, J. and J. Wu (2001). *Multi-Agent Robotic Systems*, CRC Press.

[12] Michalewicz, Z. (1999). *Genetic Algorithms + Data Structures = Evolution Program*, Springer-Verlag.

[13] Soetanto, D., L. Lapierre and A. Pascoal (2003). Coordinated motion control of marine robots (2003), In *Proceedings IFAC MCMC2003*, Gerona, Spain, 250-255.

[14] Stilwell, D.J. and B.E. Bishop (2000). Platoons of underwater vehicles, IEEE Cotrol Systems Magazine, vol. 20, December, 45-52.

[15] Tan, C.S., R. Sutton and J. Chudley (2004). An incremental stochastic motion planning technique for autonomous underwater vehicles, In *Proceedings IFAC CAMS 20004*, Ancona, Italy, 483-488.

[16] Tanner, G.T., J. Pappas and V. Kumar (2004). Leader-to-formation stability, *IEEE Trans. Robotics and Automation*, vol. 20, n.3, June, 443-455.

[17] Weiss, G. (1999). *Multiagent Systems*. MIT Press.

Chapter 4

An Overview about Dynamic Positioning of Ships

JOAQUÍN ARANDA, JOSÉ MANUEL DÍAZ, SEBASTIÁN DORMIDO CANTO, ROCÍO MUÑOZ, CARLOS HERNÁNDEZ CUESTA
Departamento de Informática y Automática. UNED. Madrid, Spain

A ship is continuously exposed to environmental disturbances. The objective of a Dynamic Positioning System is to maintain the desired position and heading applying adequate propeller thrust and without using device as anchor. Dynamic Positioning can be described as an integration of a number of shipboard systems to obtain the ability of accurate maneuverability.

1. INTRODUCTION

Dynamic Positioning System (DPS) is the system to automatically keep ship or offshore structure at the fixed position with the thrust of propeller or thruster and without using such fixing device as anchor.

Dynamic positioning may either be absolute in that the position is locked to a fixed point over the bottom, or relative to a moving object like another ship. One may also position the ship at a determined angle towards wind and waves.

DPS have been commercially available since the 1960s, and today a DP system is a natural component in the delivery of many new vessels. The first ship to fulfil the accepted definition of dynamic positioning was the "Eureka" (1961), of about 450 tons displacement and length 130 feet. This ship was fitted with an analogue control system, interfaced with a taut wire reference. Equipped with steerable thrusters fore and aft in addition to her main propulsion.

In 1980 the number of Dynamic positioning capable ships was about 65, in 1985 the number had increased to about 150. Currently it stands at over 1.000 and is still expanding.

It is interesting to note the diversity of ships types and functions using Dynamic Positioning. A list of activities include: coring, platform supply, shuttle tanker offtake, floating production, heavy lift cargo transport, exploration drilling, production drilling, diver support, pipeline, rocket launch platform positioning, repair/maintenance support to military vessels, ship-to ship transfer, manoeuvring conventional ships cable lay and repair, pre and post operational survey, multi-role, accommodation services, hydrographic survey, wreck survey, savage and removal, dredging, rockdumping, subsea installation, lifting, well simulation and workover, passenger cruises, mine countermeasures, oceanographical research, and seabed mining.

The Dynamic Positioning Systems have become more sophisticated and complicated, as well as more reliable.

The DPS development came in the mid 1970's with the application of Kalman filters and linear quadratic optimal controllers. These systems were computationally demanding compared to the computer resources then available [1-7]. In the 1990's a renewed interest for the subject was shown by the application of alternative control strategies; designs based on H∞-control was introduced [8,9], controller minimising self-induced rolling and pitching were proposed [10], and control strategies based on non-linear methods were suggested [11-13]. The non-linear techniques developed for dynamic positioning in [14] were successfully applied to a full scale turret-anchored FPSO. In [15] was showed a two-layered controller for moored ships dedicated to minimise a general cost function punishing important operational parameters such as rolling, riser traction and fuel consumption.

In general, depending on the supported functionality we may crudely divide dynamic positioning market into two segments: an high-end market demanding tailor-made solutions and high operational safety; and in the other end, there are lightweight systems offering a selection of the functionality available in the high-end brand. These systems typically offer simple station keeping functionality, course-keeping auto-pilots, and manual control.

The advantages of fully DP operated ships are the ability to operate in deep-water, the flexibility to quickly establish position and leave location, and to start up in higher sea states than if a mooring system should be connected.

2. BASIC PRINCIPLES OF DYNAMIC POSITIONING

A Dynamic Positioning Systems can be described as an integration of a number of shipboard systems to obtain the ability of accurate manoeuvrability. The main functions performed by a DPS are showed in Figure 1. The position and heading of ship are estimated based on the ship model, the position and heading measurements, and the forces acting on the ship. The control commands to the thrusters are calculates based on the difference between the desired position and heading and the estimated position and heading. The thrusters provide the necessary forces to counter the external forces and moment acting on the ship
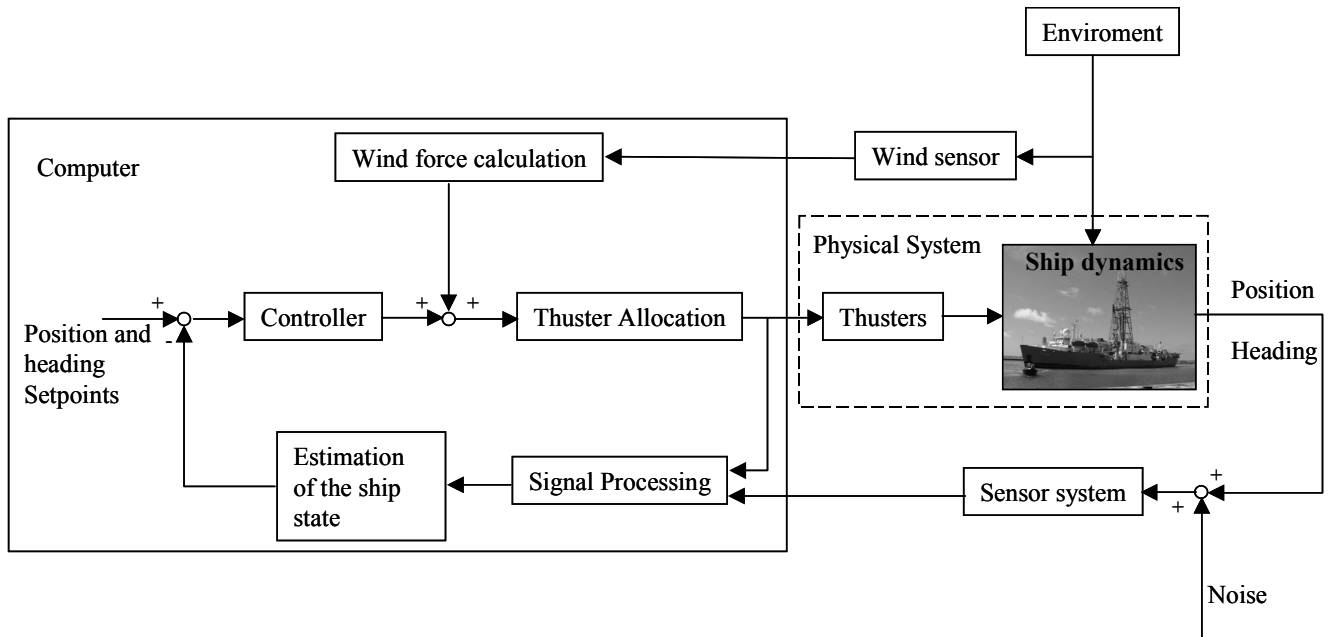
Figure 1. Schematic diagram of a Dynamic Positioning Systems

The measured signals are processed by the signal processing module, this block performs tests identifying high variance, wild point, frozen signals, and signal drift. Erroneous signals are rejected. Roll and pitch compensation of position measurements is also performed in this block.

The main objective of the Estimation module is to provide estimates of ship's positions, heading and velocities. The rapid, purely oscillatory motion induced by wave has to be filtered out. In order to estimate ship position, The DPS uses information about the sensor system, that is a Position Measurement Equipment or Position Reference System, and its own internal model of the ship. The measurements are noisy. The source of noise depends on the sensors and on the method used for measuring position.

A conventional feedback controller is of PD-type using the position and heading estimates. Some kind of integral action is required to compensate for static environmental disturbance. The controller feedforward normally consists reference and feed-forward.

The trhuster allocation block maps the controller the controller outputs (such as force and moment demands) into thuster set points such as propeller speed, azimuth nad rudder angles, pitch ratio.

3 MODELING OF MARINE VEHICLES

The number of published investigations about ship modelling is immense. For example, a nonlinear model in 6 degree of freedom is shown in[16], a survey of ship models and experimental techniques for identification of ship dynamics are described in several publications [17-19].

The hydrodynamic and derivatives coefficients occurring in the equations of motion cannot be calculated analytically and hence tests with the physical model are carried out in towing tanks, rotating arms tanks and Planar Motion Mechanism (PMM). Experimental techniques (as described in [20]) can be used to determine these coefficients.

The use of system identification techniques to determine ship-dynamics has been increasing, and different input signals are defined (see for example the early work of Aström and Kälström [21], or [22], where classical least squares algorithms are used). However, the extra complexity associated with non-linear systems, with constrains and no initial information of model structure, means that exhaustive search is not always feasible. In these cases genetic identification strategy can be used to obtain initial values.

Experiments in towing tanks are concerned with the determination of the motion transfer functions. Usually, tests in regular waves are made to experimental determination of the motion transfer functions. In this case, it is necessary to record the sinusoidal motions of the model and to determine the motion amplitudes experienced for a variety of different waves frequencies. The incident waves can be measured using a wave probe mounted on the towing carriage. This introduces a phase shift in the recorded motions and it is necessary to correct for this effect in the analysis.

In general, the ship model is a set of equations of motion that is used to predict the motion of the ship when know forces and moment are applied. In order to achieve good performance of the DPS the model has to be as detailed as practically possible. The model parameters are verified by sea trials. However the model only represents some behaviour of the ship, so the model is an approximation and is not perfect.

Without loss of generality, the dynamics of a surface ship are described by a model based on the horizontal motion with the motion variables of surge, sway and yaw. The movement of the ship is determined by the hydrodynamic forces and moments, the input variables of which are shaft angular velocity, related to propeller thrust, and the rudder deflection angle. These physical input variables subject to constraints. The ship motion can be defined over two coordinate frames using a body-fixed frame of surge-sway (X_0Y_0) and a global reference frame of North-East (XY)

The three degrees of freedom non-linear ship motion equations can be written as [17]:

$$m\left(\frac{du}{dt} - vr - x_G r^2\right) = X\left(u, v, r, \frac{du}{dt}, \delta, n\right)$$

$$m\left(\frac{dv}{dt} + ur + x_G \frac{dr}{dt}\right) = Y\left(v, r, \frac{dv}{dt}, \frac{dr}{dt}, \delta\right)$$

$$I_z \frac{dr}{dt} + mx_G\left(\frac{dv}{dt} + ur\right) = N\left(v, r, \frac{dv}{dt}, \frac{dr}{dt}, \delta\right)$$

where t is time index, u, v denote surge and sway velocity, r is yaw angular velocity, m and Iz are mass of ship and the moments of inertia about the normal axis of X_0Y_0 plane, x_G is the

Cartesian coordinate of the centre of gravity along X_0 axis, δ denotes the rudder deflection angle and n is the shaft velocity, $X(.)$, $Y(.)$ and $N(.)$ are external forces (along the surge X_0, sway Y_0 axis) and moment (for yaw rotation X_0-Y_0).

For underwater vehicle moving in six degree of freedom at high speed, the motion is highly nonlinear and coupled. However, in many applications the vehicle will only be allowed to move at low speed. If the vehicle has three planes of symmetry, then some coupled elements can be neglected (see [17]).

4 POSITION REFERENCE SYSTEM

Accurate, reliable and continuos position information is essential for dynamic positioning. A DPS requires data at a rate of once per second to achieve high precision. The dynamic position ships have some position reference system independent of the normal navigation system.

The most commonly used position reference for DPS is DGPS (Differential Global Position System) [23]. In order to improve GPS accuracy to levels useful for dynamic positioning, differential corrections are applied to GPS data. This is done by establishing reference stations at know points.

The basic concept of DGPS is the use of 2 receivers, one at a known location and one at an unknown position, that see GPS satellites in common. By fixing the location of one of the receivers, the other location may be found either by computing corrections to the position of the unknown receiver or by computing corrections to the pseudoranges. By using DGPS, effects of selective availability can be removed. For short baseline distances between receivers, some of the biases from the atmosphere can be removed as well. This cancellation effect is the result of both receivers seeing the same things. If one receiver location is known, then the bias in the pseudorange to the known receiver can be calculated and used to correct the solution of the unknown receiver location. Using double differenced observables can eliminate selective availability effects as well as other biases. Double differences are primarily used for surveying and geodetic research using phases; however, they are not limited to those applications. First, single differences are formed by subtracting observation equations from two separate receivers to a single satellite. Taking the difference between two single differences for a specific receiver pair gives the carrier phase double difference.

Some DGPS services accept multiple differential inputs obtained from an array of reference stations widely separated. Network DGPS systems provide greater stability and accuracy, and remove more of the ionospheric error than obtainable from a single reference station. The accuracy obtained by a DGPS is of 1 to 3 meters dependent upon the distances to the reference stations, ionospheric conditions, and the constellation of satellites available.

Others position reference systems used in dynamic positioning are: Hydroacoustic Position Reference, Taut Wire, Laser-based systems and Artemis.

In general, DPS combine position reference data from two or more position reference systems.

The ship heading is provided by one or more gyro compasses, which transmit data to the DPS.

5 ESTIMATION

The measurement from Position Reference System are noisy. This noise depends on the sensors and method used for measuring position. Then, the problem is how do you estimate the position and attitude state of the ship whit an approximate knowledge of the ship dynamics and with noisy measurements. The answer to this problem is the use of Kalman filtering techniques. In a Dynamic Positioning application a Kalman filter is used to estimate the state of the vessel (for which a dynamics model has been developed) based on noisy measurements from reference systems and sensors.

In 1960, R.E. Kalman published his famous paper describing a recursive solution to the discrete data linear filtering problem [24]. Since that time, due in large part to advances in digital computing, the Kalman filter has been the subject of extensive research and application, particularly in the area of autonomous or assisted navigation. A very "friendly" introduction to the general idea of the Kalman filter can be found in Chapter 1 of [25], while a more complete introductory discussion can be found in [26], which also contains some interesting historical narrative. You can see also [27].

The Kalman filter estimates a process by using a form of feedback control: the filter estimates the process state at some time and then obtains feedback in the form of (noisy) measurements. As such, the equations for the Kalman filter fall into two groups: time update equations and measurement update equations. The time update equations are responsible for projecting forward (in time) the current state and error covariance estimates to obtain the a priori estimates for the next time step. The measurement update equations are responsible for the feedback—i.e. for incorporating a new measurement into the a priori estimate to obtain an improved a posteriori estimate.

The time update equations can also be thought of as predictor equations, while the measurement equations can be thought of as corrector equations. Indeed the final estimation algorithm resembles that of a predictor-corrector algorithm for solving numerical problems.

The specific equations for the time and measurement updates are:

Time update:

$$\dot{\hat{x}}_k = A\hat{x}_{k-1} + Bu_{k-1}$$
$$P_k^- = AP_{k-1}A^T + Q$$

Measurement update:

$$K_k = P_k^- H^T (HP_k^- H^T + R)^{-1}$$
$$\hat{x}_k = \hat{x}_k^- + K_k(z_k - H\hat{x}_k^-)$$
$$P_k = (I - K_k H)P_k^-$$

After each time and measurement update pair, the process is repeated with the previous a posteriori estimates used to project or predict the new a priori estimates. This recursive nature

is one of the very appealing features of the Kalman filter—it makes practical implementations much more feasible than (for example) an implementation of a Wiener filter which is designed to operate on all of the data directly for each estimate. The Kalman filter instead recursively conditions the current estimate on all of the past measurements.

The measurement noise covariance R is usually measured prior to operation of the filter. Measuring the measurement error covariance R is generally practical (possible) because we need to be able to measure the process anyway (while operating the filter) so we should generally be able to take some off-line sample measurements in order to determine the variance of the measurement noise.

The determination of the process noise covariance Q is generally more difficult as we typically do not have the ability to directly observe the process we are estimating. Sometimes a relatively simple (poor) process model can produce acceptable results if one "injects" enough uncertainty into the process via the selection of Q. Certainly in this case one would hope that the process measurements are reliable.

In either case, whether or not we have a rational basis for choosing the parameters, often times superior filter performance (statistically speaking) can be obtained by tuning the filter parameters Q and R. The tuning is usually performed off-line, frequently with the help of another (distinct) Kalman filter in a process generally referred to as system identification.

6 CONTROLLER DESIGN

The main purpose of a positioning control system is that a ship maintains a specified position and compass heading unaffected by the disturbances action upon it. The positioning control problem is one of attenuating these disturbances by applying proper counteracting forces.

Increased computational power has provided the opportunity to implement more sophisticated control algorithms. More demanding control strategies such as model predictive control and online numerical optimization techniques have been commercialized.

Different controllers are proposed in the literature. See for example [28-32]. Some of these controllers have been successfully installed on several commercial DP systems.

Many DPS rely on multivariable PID algorithms in conjunction with an observer providing state estimates [30]. The basic principle of a PID control law is to generate a thrust for which the different terms are respectively proportional to the 3-dimensional position and heading deviation vector as referred to the ship position relative to the desired setpoint (the proportional term), to the velocity deviation vector (the differential term), and to the accumulated deviation vector (the integral term). All these vectors are referred to a specific time instant t. Based on this principle, the required thruster force vector in the body-fixed frame can be formulated as sum of the three terms corresponding to proportional, derivative and integral actions.

The H_∞ design approach provides a step forward in the technology of dynamic ship positioning systems that are equally important as the introduction of the Kalman filtering

optimal control schemes. The advantages of the latter were so obvious that ship operators demanded this capability and the consequence was that the Kalman filtering system was widely applied and used in practice [32].

The H_∞ robust design technique was developed for uncertain systems and its main objective was to provide a design that is more robust than that can be obtained with LQG/Kalman filtering methods or other techniques. The fundamental problem with Kalman filtering methods is that there is no formal method in the problem description in which modeling errors in the plant can be taken into account. In many cases as will be explained below, information is available in the frequency ranges where ship models are poor. However, there is no method for incorporating this information in Kalman filtering/optimal control schemes. The consequence is that many hours can be spent on commissioning. Moreover, it is likely that unpredictable performance will occur in unusual sea-state conditions.

Intelligent techniques as fuzzy control can be used also. FLC provides a nonanalytic alternative to the classical control theory [33].

Fuzzy control is based on an I/O function that maps each very low-resolution quantization interval of the input domain into a very low-low resolution quantization interval of the output domain. As there are only 7 or 9 fuzzy quantization intervals covering the input and output domains the mapping relationship can be very easily expressed using the "if-then" formalism. (In many applications, this leads to a simpler solution in less design time.) The overlapping of these fuzzy domains and their linear membership functions will eventually allow to achieve a rather high-resolution I/O function between crisp input and output variables

ACKNOWLEDGMENTS

REFERENCES

[1] Balchen, J. G., N. A. Jenssen and S. Sælid (1976). Dynamic positioning using Kalman filtering and optimal control theory. In: IFAC/IFIP Symposium on Automation in O.shore Oil Field Operation. Amsterdam, Holland. pp. 183— 186.

[2] Balchen, J. G., N. A. Jenssen, E. Mathisen and S. Sælid (1980). A dynamic positioning system based on Kalman filtering and optimal control. Modeling Identification and Control 1(3), 135—163.

[3] Sælid, S., N. A. Jensen and J. G. Balchen (1983). Design and analysis of a dyanmic positioning system based on Kalman filtering and optimal control. IEEE Trans. on Automatic Control 28(3), 331—339.

[4] Grimble, M. J., R. J. Patton and D. A. Wise (1980). The design of dynamic positioning control systems using stochastic optimal control theory. Optimal Control Applications and Methods 1, 167—202.

[5] Fung, P. T.-K. and M. J. Grimble (1983). Dynamic ship positioning using a selftuning Kalman filter. IEEE Trans. on Automatic Control 28(3), 339—349.

[6] Sørensen, A. J., S. I. Sagatun and T. I. Fossen (1996). Design of a dynamic positioning system using model-based control. J. of Control Engineering Practice 4(3), 359—368.

[7] Fossen, T. I., S. I. Sagatun and A. J. Sørensen (1996). Identification of dynamically positioned ships. Control Engineering Practice 4(3), 369—376.

[8] Katebi, M. R., M. J. Grimble and Y. Zhang (1997). H∞ robust control design for dynamic ship positioning. In: IEE Proc. on Control Theory and Applications. pp. 110—120.

[9] Donha, D. C. and E. A. Tannuri (2001). Non-linear semi-submersible positioning system design using an H∞ controller. In: Proc. of the 5th IFAC Conf. On Control Applications in Marine Systems (CAMS2001). Glasgow, UK.

[10] Sørensen, A. J. and J. P. Strand (2000). Positioning of small-waterplane-area marine constructions with roll and pitch damping. J. of Control Engineering Practice 8(2), 205—213.

[11] Fossen, T. I. and Å. Grøvlen (1998). Nonlinear output feedback control of dynamically positioned ships using vectorial observer backstepping. IEEE Trans. On Control Systems Technology 6(1), 121—128.

[12] Fossen, T. I. and J. P. Strand (1999). Passive nonlinear observer design for ships using Lyapunov methods: Experimental results with a supply vessel. Automatica 35(1), 3—16.

[13] Fossen, T. I. and J. P. Strand (2001). Nonlinear passive weather optimal positioning control (WOPC) system for ships and rigs: Experimental results. Automatica 37(5), 701—715.

[14] Sørensen, A. J., J. P. Strand and T. I. Fossen (1999). Thruster assisted position mooring system for turret-anchored FPSOs. In: Proc. of the 1999 IEEE Int. Conf. on Control Applications (CCA'99). Honolulu, Hawaii. pp. 1110—1117.

[15] Tannuri, E. A., C. P. Pesce and D. C. Donha (2001). Assisted dynamic positioning system for a FPSO based on minimization of a cost function. In: Proc. of the 5th IFAC Conf. On Control Applications in Marine Systems, CAMS2001. Glasgow, UK.

[16] Fossen, T.I. and Fjellstad, O.E. 1995. Nonlinear modelling of marine vehicles in 5 degrees of freedom. Journal of Mathematical Modelling of Systems. Vol. 1. No. 1.

[17] Fossen, T.I. 1994. Gidance and Control of Ocean Vehicles. John Wiley and sons.

[18] Webster, W.C. (editor). 1992. Shiphandling Simulation. Application to waterway design. National Academy Press.

[19] Lloyd, A.R.J.m. 1989. Seakeeping: Ship Behaviour in Rough Weather. Ellis Horwood.

[20] E.V. Lewis (editor) (1989). Principles of Naval Architecture. Second Revision. Volume III. Motions in Waves and Controllability. The Society of Naval Architects and Marine Engineers.

[21] Aström, K.J. and Källström, C.G. 1976. Identification of ship steering dynamics. Automatica. Vol. 12. Pp.9-22.

[22] Aranda, J., J.M. de la Cruz, and J.M. Díaz. Identification of Multivariable Models of Fast Feries. European Journal of Control (2004) vol. 10, no.2, pp. 187-198.

[23] Bradford W. Parkinson and James J. Spilker Jr. (Editors). Global Positioning System: Theory and Applications (Volumes I & II). 1996, AIAA.

[24] Kalman, R. E. 1960. "A New Approach to Linear Filtering and Prediction Problems". Transaction of the ASME—Journal of Basic Engineering, pp. 35-45 (March 1960)

[25] Maybeck, Peter S. 1979. Stochastic Models, Estimation, and Control, Volume 1, Academic Press, Inc.

[26] Sorenson, H. W. 1970. "Least-Squares estimation: from Gauss to Kalman," IEEE Spectrum, vol. 7, pp. 63-68, July 1970.

[27] Gelb, A. 1974. Applied Optimal Estimation, MIT Press, Cambridge, MA.

[28] Sørensen AJ, Leira B, Strand JP, Larsen CM. Modelling and control of riser angles and stresses in dynamic positioning. In: Proc. 5ht IFAC Conf. on Manoeuvring and Control of Marine Craft—MCMC'2000. Aalborg, Denmark; 2000a. p. 275–280.

[29] Sørensen AJ, Strand JP. Positioning of small-waterplane-area marine constructions with roll and pitch damping. J of Control Eng Practice 2000;8(2):205–13.

[30] Leira, B.J., A.J. Sorensen, C.M. Larsen. A reliability-based control algorithm for dynamic positioning of floating vessels. Structural Safety 26 (2004): 1-28.

[31] Sorensen, A.J.; B. Leira, J.P. Strand, C.M. Larsen. Optimal setpoint chasing in dynamic positioning of deep water drilling and intervention vessels. Int. J. Robust Nonlinaer Control 2001; 11:1185-1205.

[32] M.R, Katebi, I. Yamamomoto, M. Matsuura, M.J. Grimble. Robust dynamic ship positioning system design and applications. Int. J. Robust Nonlinaer Control 2001; 11:1257-1284.

[33] L.A. Zadeh, "Outline of a new approach to the analysis of complex systems and decision processes," *IEEE Trans. Syst., Man., Cyber.,* vol.SMC-3, no. 1, pp. 28-44, 1973.

Chapter 5

Two Ships Towing Together; A Cooperation Scenario in a Marine Environment

J.M. GIRON-SIERRA, J. JIMÉNEZ, A. DOMINGUEZ,
J.M. RIOLA[1], J.M. DE LA CRUZ, B. DE ANDRES-TORO
Dep. A.C.Y.A., Fac. CC. Fisicas. U. Complutense de Madrid, Ciudad Universitaria, 28040 Madrid. Spain
[1]CEHIPAR El Pardo (Madrid) Spain.

Marine environments offer suggestive scenarios for Automatic control and Cooperation strategies to be applied. The present paper focus on a particular one: Two ships towing together an off-shore oil retaining boom. Basic dynamical equations are presented for the combined displacement of both ships plus the boom. Computer simulation of basic manoeuvres works out the basic control implications of the problem and suggests cooperation among the ships as a suitable and reliable technique to fulfil ships goals and minimize boom strain.

1 INTRODUCTION

From ancient times, sailing has been a fascinating human activity. Ages of continuous effort have been required to evolve from the simple floating rafts to the actual complex vessels. As in many other human activities, experience has been the key to master the sea and science the way to explain and improve the achievements of experience.

But perhaps for being sailing a so ancient art, automation and control have been introduced mainly in recent times and only partially. The control effort still relies in human beings and this is especially true when marine manoeuvring is the topic.

Concerning feedback control applied to marine vessels, Fossen (2002) lists a wide number of examples of commercially available systems: Ship and underwater vehicle autopilots for course-keeping and turning control, way-point tracking trajectory and path control system for marine vessels, depth autopilots for underwater vehicles, torpedo control systems, attitude control system for underwater vehicles, dynamic positioning systems for marine vessels, positioning mooring systems for floating vessels, fin and rudder-roll stabilization systems, wave-induced vibration damping systems for high-speed craft, buoyancy control systems including trim and heel correction systems, propulsion control systems and forward speed control systems, propeller and thrusters control systems and energy and power management systems.

From the point of view of control problems; marine environments offer a wide source of suggestive scenarios:

- Ship's course control, rises as a first interesting problem: To determine the optimum course according to sea state, fuel consumption, time to delivery, etc. Navigation in shallow waters or along channels requires in both cases a sound strategy of course control to avoid run aground or to prevent collisions.

- Seakeeping problems (Lloyd, 1998), has been the scope of recent efforts: To improve ship's stability and global performance by means of proper actuators such as fins, T-foils or flaps (De la Cruz, et al. 2004; Haywood, et al., 1995; Ryle, 1998). Such actuators require also some kind of control smartness to be operated properly.

- Manoeuvring is perhaps a still more varied field. It can include a single vessel or several ones in a wide range of scenarios:

The apparently simple operation of freight or person offshore transfer, involved a coordinated manoeuvre between two vessels. The degree of complexity depends on several factors; weather conditions, ships features, kind of freights to be transferred and human factors could be pointed out. Recent papers on related topics are (Kyrkjebo, 2003, 2004; Morishita, 2004).

Offshore rescue scenarios, which often involve the deployment of small fast rescue craft from a parent vessel demand a set of operational requirements that determines the success of the rescue craft operation; save and efficient launch and release from the parent vessel, transit to casualty, rescue of the casualty, transit back to the parent vessel, and recovery of the rescue craft.

The mutual manoeuvring between two or more sailing vessels to avoid a possible collision, taking into account the operational constraints and course objectives, compose also a complex system. In this context, towing cases are of new interest (Johansen, 2003).

Device deployment constitutes another interesting scenario of waterborne operation. The deployment of nets, set of buoys, barriers etc. which may be employed to mark or confine a particular sea area (for example, after an oil leakage). This scenario includes also the removal of wrecks and other recycling operations. Several watercrafts may cooperate to hold, transport and eventually deploy the device in a proper way.

Operational requirements in this case demand the capability of involved watercrafts to perform a proper dynamic positioning, the ability of them to deal with the device to be deployed in a well coordinated way and capability to react against possible modifications on the area to be bounded. The success demands the correct use and operation of the whole system as in the previously described operations.

It is clear, that thinking in terms of automation, the aforementioned scenarios are far beyond the scope of feedback control and emergent concepts or techniques such cooperation, interchange of information, multi-agent systems, self-awareness, reactive/deliberative answer capacity, etc. could play an interesting role to furnish a new generation of vessels able to perform such manoeuvres safer and better.

The need of cooperative control in marine operations has been recognized recently by several authors and institutions. (Soentanto, et al., 2003; Stilwell and Bishop, 2000) are illustrative references. A way to deal with this kind of problems is to look at the more general robotics field, where cooperation between mobile agents is attracting research interest from years ago. Reference books of interest are (Weiss, 1999; Liu and Wu, 2001); recent relevant articles focusing on formations and agent interaction are (Tanner, et al., 2004; Billard, 2004).

The present paper contains the first steps towards a complete study of a deployment scenario; two boats cooperate to deploy a floating barrier. The study departs from a simplified version of ships and barrier dynamic equations.

2 PROBLEM APPROACH

For marine vessels moving in 6 degrees of freedom (DOF), 6 independent coordinates are necessary to determine position and orientation. The first three coordinates correspond to the position and the time derivatives to the speeds along the x, y and z axes. The last three coordinates and their time derivatives describe orientation and rotational speeds. The 6 different motion components are usually defined as, surge, sway, heave, roll, pitch and yaw.

Figure 1 shows the 6 degrees of freedom as they have been described.
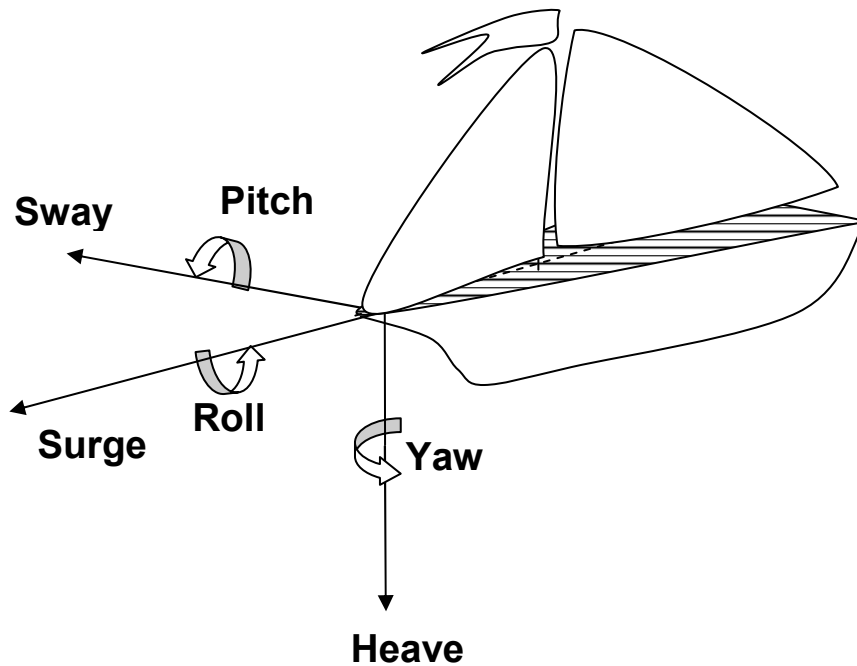
Fig. 1. Motion variables for marine vessels

In the present work, only surge, sway and yaw are taken into account for being more directly related with ship course description. Pitch, roll and heave, are more related with ship oscillation induced by waves motion. In the actual world, every six movements are coupled but in this first approach to the problem pitch, roll and heave will not be taken into account for simplicity reasons.

2.1 Simplified scenario

The scenario is made up by two identical ships which tow together a floating boom. This last, consists of a certain number of identical floating rigid elements. Two consecutive elements are jointed by a hinge, so that one can swing relative to the other. The whole set of elements form a sort of chain in which each rigid element acts as a link. Each one of the two tip links of the boom is jointed to the stern of one ship. Fig.2 shows a schematic view of the described scenario.
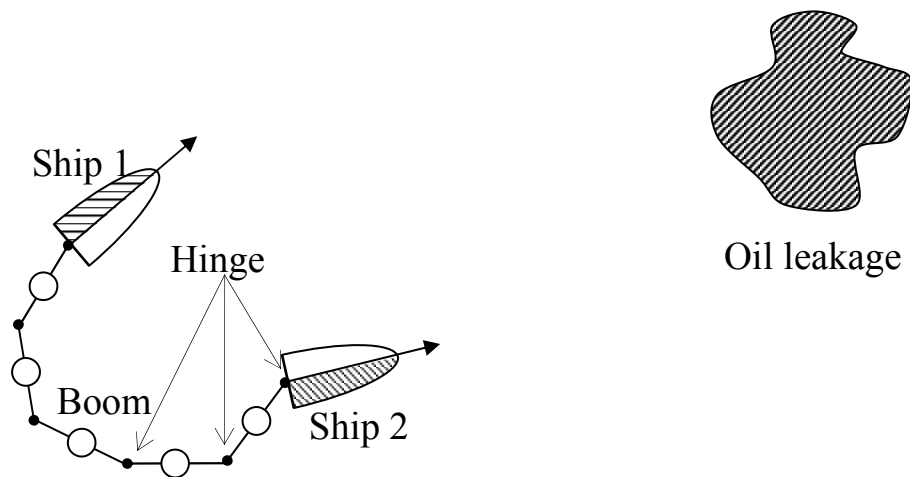
Fig. 2. Schematic scenario view

For ships and boom links, only their lengths will be considered as relevant for dynamical analysis.

Ships are described by their mass, mass inertia moment and three drag coefficients that represent the resistance to motion through the fluid along surge, sway and yaw coordinates. Propulsion in surge direction is considered in terms of power and steer action is also represented in terms of power to generate a moment in the yaw direction. The combined effect of propulsion power and steer power determines the ship course; both variables will be the input variables to be operated for control purposes.

Booms links are defined also by their mass, mass inertia moment and drag coefficients similar to those employed in the ships. Strains in the ends of the links complete the description for the boom dynamic.

2.2 Mathematical approach

The motion of a ship, in the x-y plane, can be described with the following equations:

$$m_b a_{bx} = [F_m - \mu_l(v_{by} sen(\theta) + v_{bx} \cos(\theta))] \cos(\theta) - \mu_t l_s (v_{bx} sen(\theta) - v_{by} \cos(\theta)) sen(\theta) \quad (1)$$

$$m_b a_{by} = [F_m - \mu_l(v_{by} sen(\theta) + v_{bx} \cos(\theta))] sen(\theta) - \mu_t l_s (-v_{bx} sen(\theta) + v_{by} \cos(\theta)) \cos(\theta) \quad (2)$$

$$M - \mu_a l_s \omega_b = I_b \alpha_b \quad (3)$$

where m_b represents the mass of the ship, a_{bx} and a_{by} represent the acceleration in axes x and y, F_m is the surge force applied to the ships, M is the yaw moment, μ_l, μ_t, μ_a are the drag coefficients in surge, sway and yaw, l_s is the length of the ship, I_b is the moment of inertia. Obviously, equations (1-3) describe a naïve model for the ship dynamic, where added mass and no linear hydrodynamic damping has been neglected.

There is another simplification which is important to notice: The moment M, applied in the yaw direction, drives the changes of course for the ship. Usually, it is caused by the action of a rudder, by the deflexion of water jets, etc. This means that moment M is usually coupled in some way with the surge force. The nature of such coupling depends on the ship particular features. In the present case, surge force and yaw moment have been decoupled and both act independently.

Figure 3 shows the geometry of the problem where the angle θ represents the course, v_b is the ship velocity, mcb is the position of the ship centre of mass.
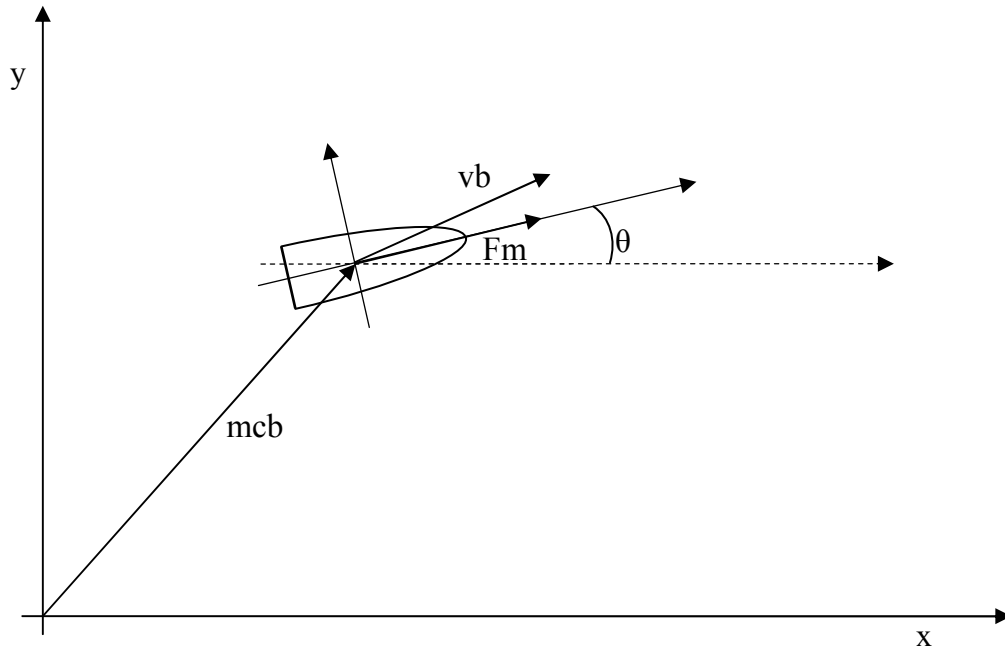
Fig. 3. Ship main variables

The motion of the boom, which is attached to the ships, is deduced by first considering a link and then combining several links. A closing condition is imposed to assure boom continuity.

Figure 4 shows the geometry of the boom. Were n_i represents a unit vector normal to a generic link, p_i is a unit vector parallel to the link r_i is the position of the link centre of mass and l represents half the length of the link.
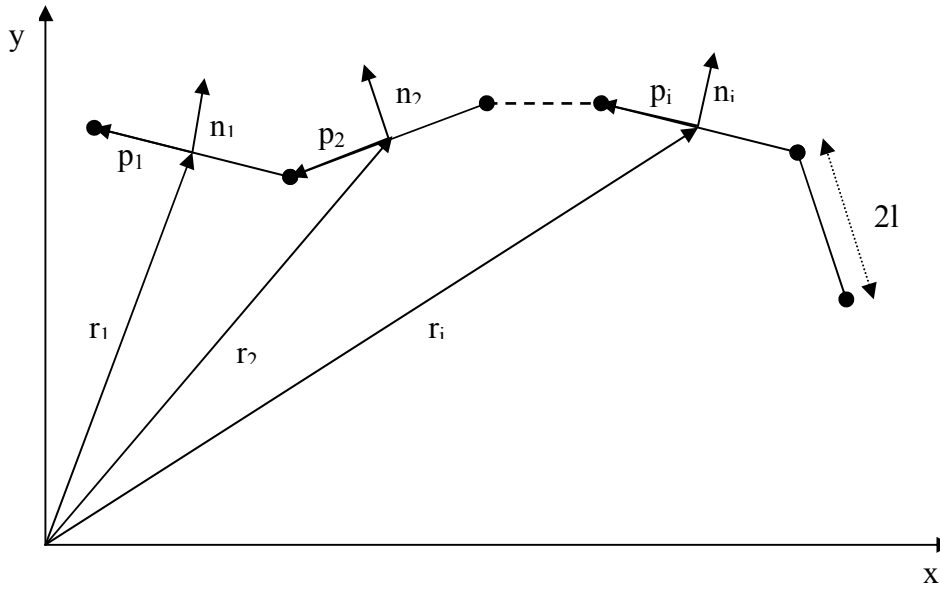
Fig. 4. Geometry of the boom

The motion of a single generic link is given by:

$$\bar{T}_{i,i+1} - \bar{T}_{i-1,i} - \frac{\left(\left|\bar{v}_i \cdot \bar{n}_i\right|s + \left|\bar{v}_i \cdot (-\bar{p}_i)\right|q\right)}{\left|\bar{v}_i\right|}\bar{v}_i = m\bar{a}_i$$

(4)

Were, T represents the strain in a tip of the link, q and s represent longitudinal and perpendicular drag coefficients and m is the mass of the link.

$$\left(\bar{T}_{i,i+1} \cdot \bar{n}_i\right)l + \left(\bar{T}_{i-1,i} \cdot \bar{n}_i\right)l - A\omega_i = I\alpha_i$$

(5)

Were A is a drag coefficient, and I is the moment of inertia.

The closing condition is imposed by means of eq. (6)

$$\vec{r}_i - l\vec{p}_i - l\vec{p}_{i+1} - \vec{r}_{i+1} = 0 \qquad\qquad (6)$$

Were r_i is the position of the link.

The problem to be solved starts from an initial condition, with the boom attached to the ships (they can be considered as links too) and the ships starting to move. The system of equations is solved iteratively along small time intervals.

3 PRELIMINARY COMPUTER EXPERIMENTS

The research begins with the simplest case. Both ships try to go in parallel, along a straight path. Figure 5 shows the result for a boom composed of five elements, the arrows in the extremes represent the successive positions and orientation of both ships. The boom has been represented by lines with a circle in the centre of each element. The boom pulls the stern of the ships, and the ships rotate. Eventually, both ships make a tug of war. The need of a control action on the rudders, to counteract the boom tug, is clear.
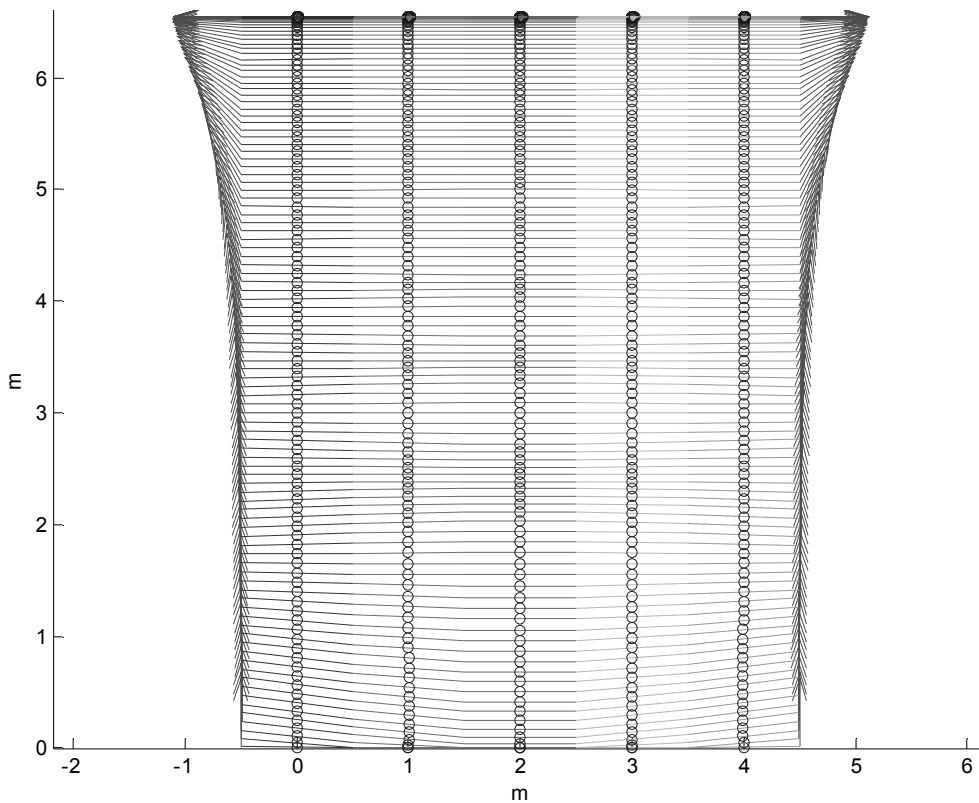
Fig. 5. Motion of the system without control.

It is important to notice that initial conditions have been highly forced. So, ships start their movement forming a square angle with the boom, which has been arranged all its length

extended. This means that slight movements of the ships are going to generate large strains in the boom.

These initial conditions are hardly expectable in the real world, but they have been considered because represent an extreme case in which the ships and boom dynamics are highly interrelated. In this way, the studied case pointed out the problems that rise when both ships move away. The strain generated by the boom in its junctions with the aft of the ships tends to turn these outwards. As far as no effort has been applied by the ships to preserve their course, these begin to shift. This effect still increases more the boom's strain which increases again the rotation of the ships. Eventually, both point to opposite directions.

Now, a simple proportional control, acting over the yaw moment, is put into action to force the ships to follow a straight course. Figure 6 shows the simulated experiment.

A transient appears at the beginning, due to the tightness of the boom and then the ships tend to join smoothly, bending up the boom. A little ripple can also be observed on the ships curse, due to the oscillations of the courses around their set points.
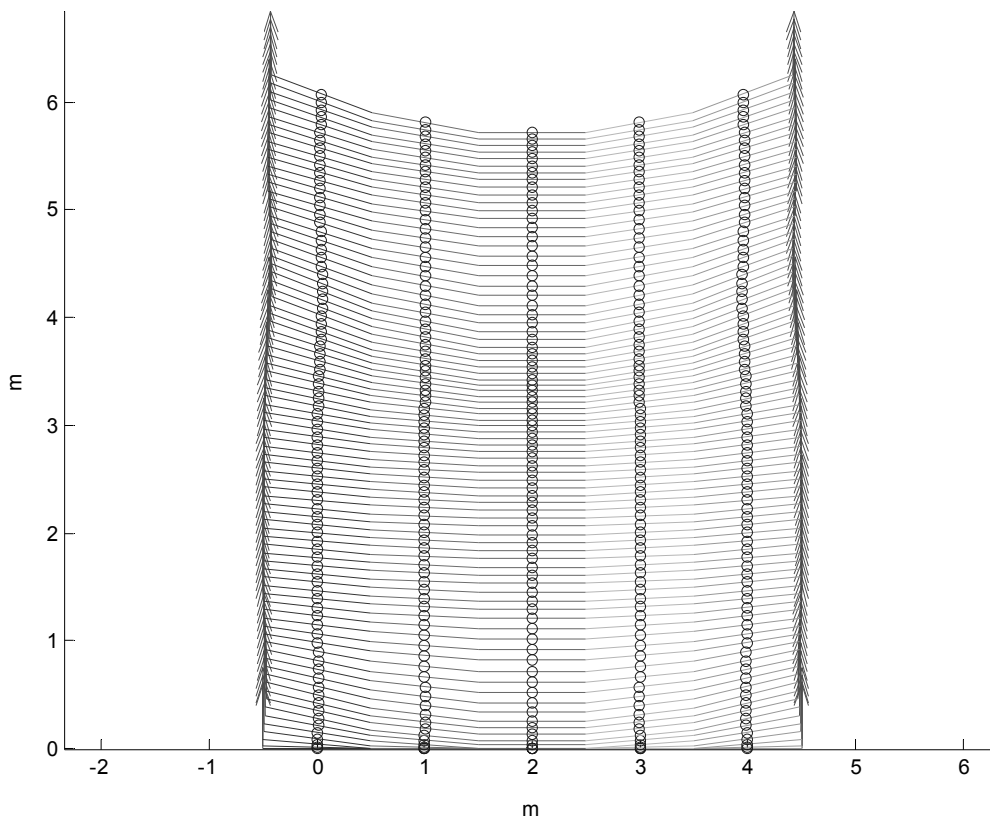
Fig. 6. Motion of the system with individual course control

Even though the course of the ships is now preserved, dragging the boom in such a way imposes the system to take unnecessary strain. To improve the control, a proportional control of the mutual distance has been added to the proportional course control in each ship. Again, the combined action of both controls act over the yaw moment.

The idea is to force both ships to come close, diminishing in this way the strain in the boom. Figure 7 shows the results obtained: both ships approach till they reach the set point distance, which has been established in four meters. Obviously, the system yields a better performance. This can be considered as a coarse mode of coordination control, as far as the course of the ships is now partially determined by a variable that depends on both.

Anyway, this manoeuvre has still important shortcomings. Departing from the initial conditions prescribed for the model, in which the chain is so tight, the effort of both ships to approach one another increases still more the strain in the boom. A more intelligent manoeuvre would be that both ship change its course in the same direction, an after a wile recover the original course. In any case, it is no difficult to realize that better solutions implies different manoeuvres for each ship and therefore the necessity of coordination performed at an upper level to decide how to do these manoeuvres.
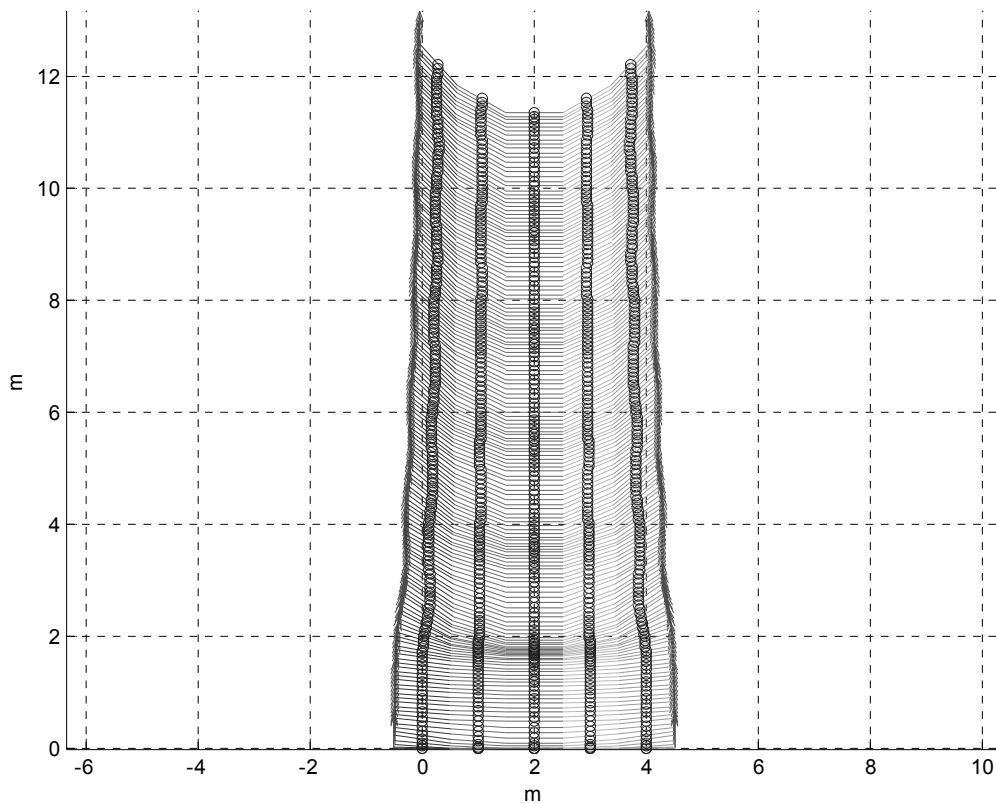
Fig. 7. Motion of the system with coordination control

To complete the discussion, figure 8 compares the values of the horizontal component of the tension between the ship located in the left side and the last link of the boom at which the ship is connected, for the three previously described cases.

For the case on no course control, the tension increases at the same time that the ship rotates counter clockwise. Eventually, this tension will become equal to the force exerted by the ship in the surge direction.

In the case of course control, there are three different phases. First the course of the ships matches it set point. No control action is exerted but after a while ships begin to turn outwards, the control systems reacts and as a consequence the tension begin to rise The combined effect on the tension plus the yaw moment exerted to amend the course causes that the ships were dragged by the boom inwards. The Tension reaches a maximum at some instant between 10 and 15 seconds, after this time, it begins to decrease due to the progressive approach of both ships and the bending of the boom.

The last case, when course and distance between ships is controlled, shows a sharper maximum than the previous one, located between 5 and 10 seconds. The reason is that the yaw moment acts from the beginning; as far as ships try to fulfil the set point impose to their mutual distance. Nevertheless, the tension falls after 15 seconds remaining for the rest of the period showed below the value of the tension for the previous describe case.

It also valuable to notice that there is still a remaining ripple in the last two cases studied, due to the strain exerted by the boom and the control effort that try to counteract this.
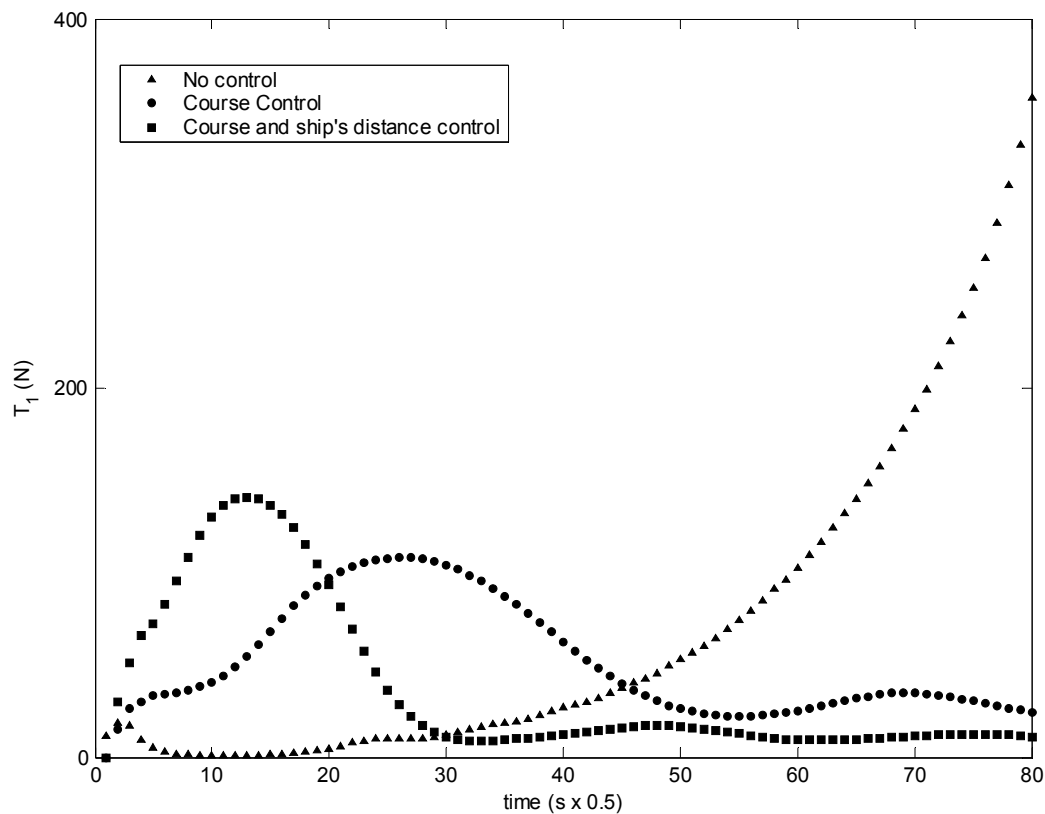
Fig. 8. Comparison among the tensions reached between the left side ship and the first link of the boom for three different cases: No course control is applied, individual course control is applied and course control and mutual distance between both ships is applied.

Tensions applied to the boom should be taking into account also before perform whatever manoeuvre. In the present study no limit has been imposed to these but it is quite obvious that there is a maximum limit for the strain that the boom can bear. After this limit the boom breaks. So, those manoeuvres that exceed this limit should be avoided.

Figure 9 shows also another interesting effect. It represents the angle between the ship direction (from aft to bow) and the ship velocity direction for both ships and for the two last cases discussed previously. In the first case, only course control applied, the left side ship presents always a positive angle and the right side ship presents a symmetrical situation. This means that during the whole period showed both ships are dragged inwards by the boom strain. This effect tends to diminish with time, as the strain of the boom is more and more relaxed.

In the second case, both ships sail nearer and the angle described begins to oscillate around cero. In this case, the reason for the difference of orientation between the ships and their velocities is due to the inertia of the ships; these change their course but the velocity remains still the same for a while, following a little bit delayed the new course of the ships.
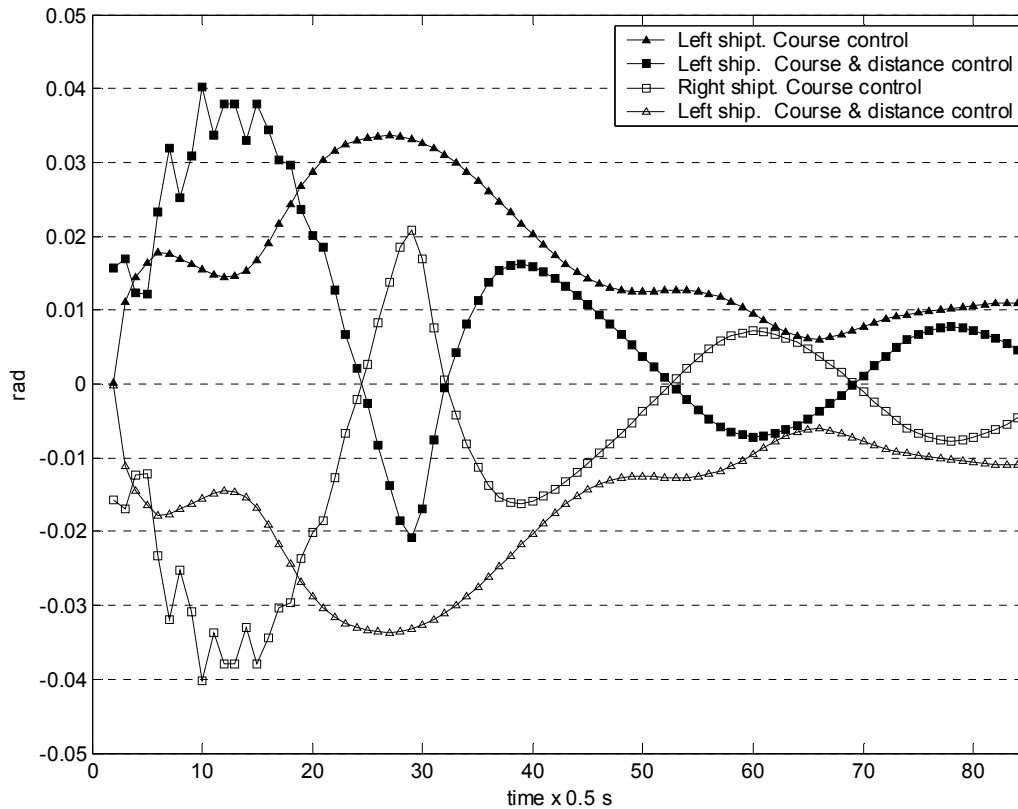
Fig. 9. Angle between ship direction and ship velocity direction.

4 INITIAL MANOEUVRING AND CONTROL EXPERIMENTS

It is clear that for real cases, course changes must be studied. The simplest case is a single turn. Nevertheless this simplest case needs to be performed carefully to avoid problems.

Figure 10 shows a 45º right turn. As can be seen in the figure, the outer ship must cover a longer distance to keep up a synchronous turn, if both ships have the same speed the outer ship delays. When the new course is reached, the outer ship is far the inner one. This lost of synchronicity will be more critical in the case of stronger changes of course, even causing that the outer ship cross over the boom when they turn round large angles.

Indeed the speed of the ship must be adjusted for a correct turn of the system. A speed control is added, with a correction of the speed in function of the angle between the desired course and the line which links both ships. The speed of the ships is increased or decreased until the mentioned line and the desired course forms a 90º angle. Fig. 11 shows the effect of this control action. As can be seen, the outer ship, in this case the left one, describes now a wider curve due to the increasing of its speed, compensating in this way de differences and remaining parallel to the right ship when the turn is finished.
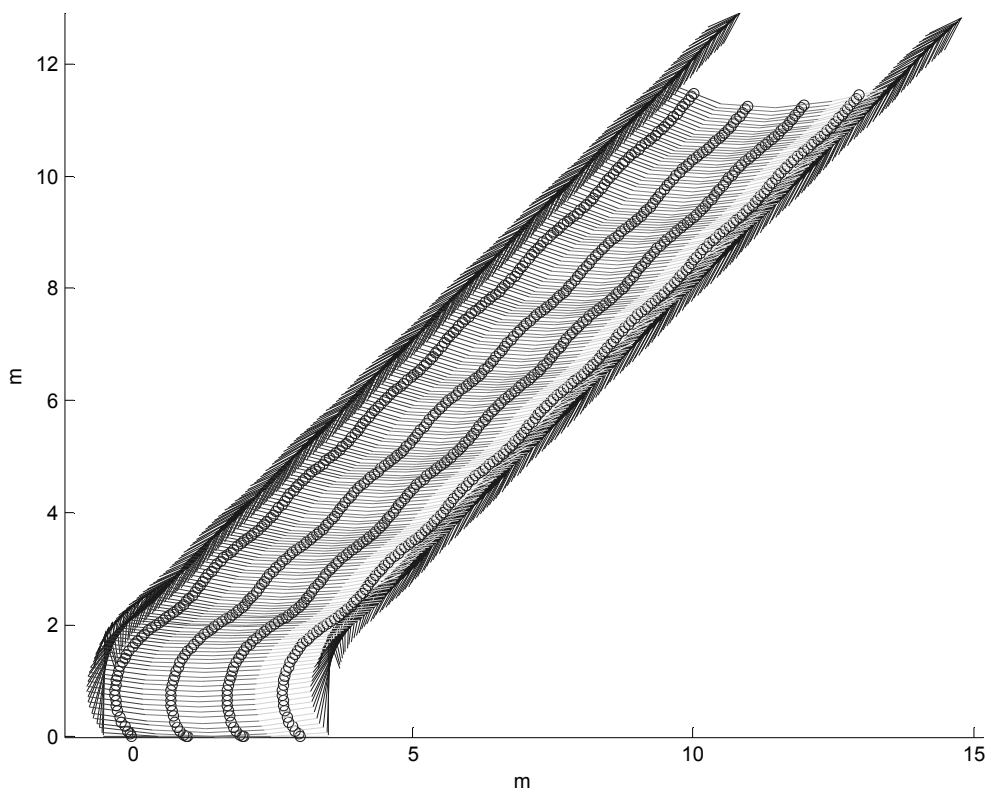
Fig. 10. System turn, ships with same speed.
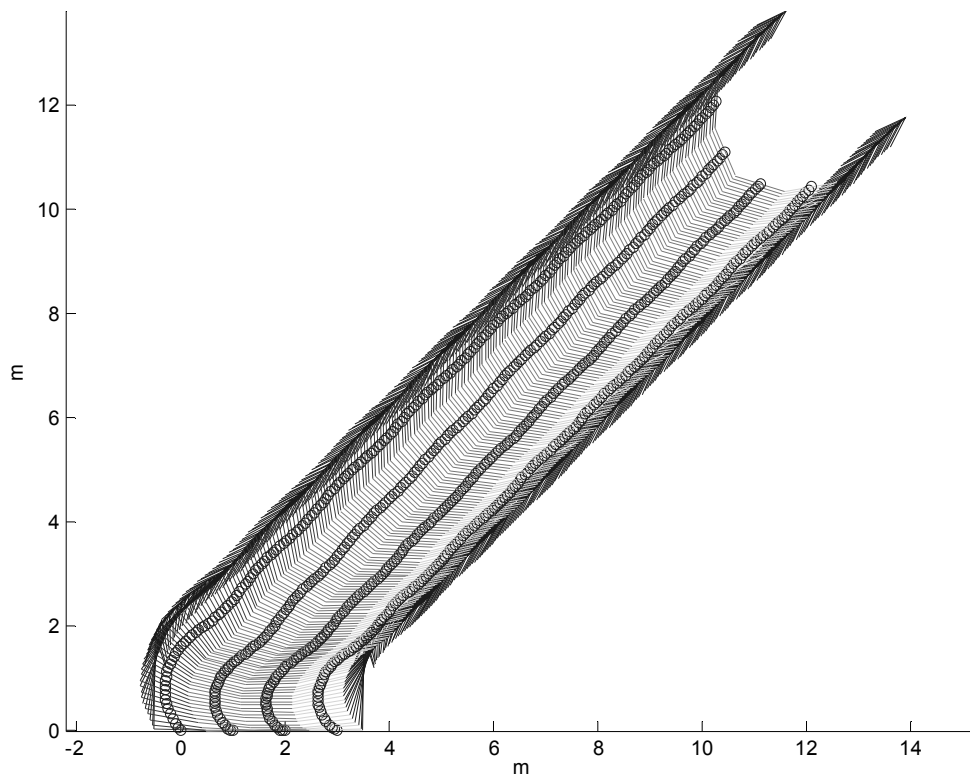
Fig. 11. System turns, with alignment control

5 MORE COMPLEX MANOEUVRES

The final objective o a boom deployment should be the confinement of an oil leakage or other kind of harmful products. This last example considers the pursuit of a movable objective. The desired course for both ships is updated in any iteration according to the new position of the movable objective. Fig 12 shows the results for the case of a hypothetical objective that follows an elliptical trajectory (crossed line in the figure). The computer simulation shows an animated version of the case considered; however the figure may suggest a collision, but this is not the case: the objective and the ships never collide.
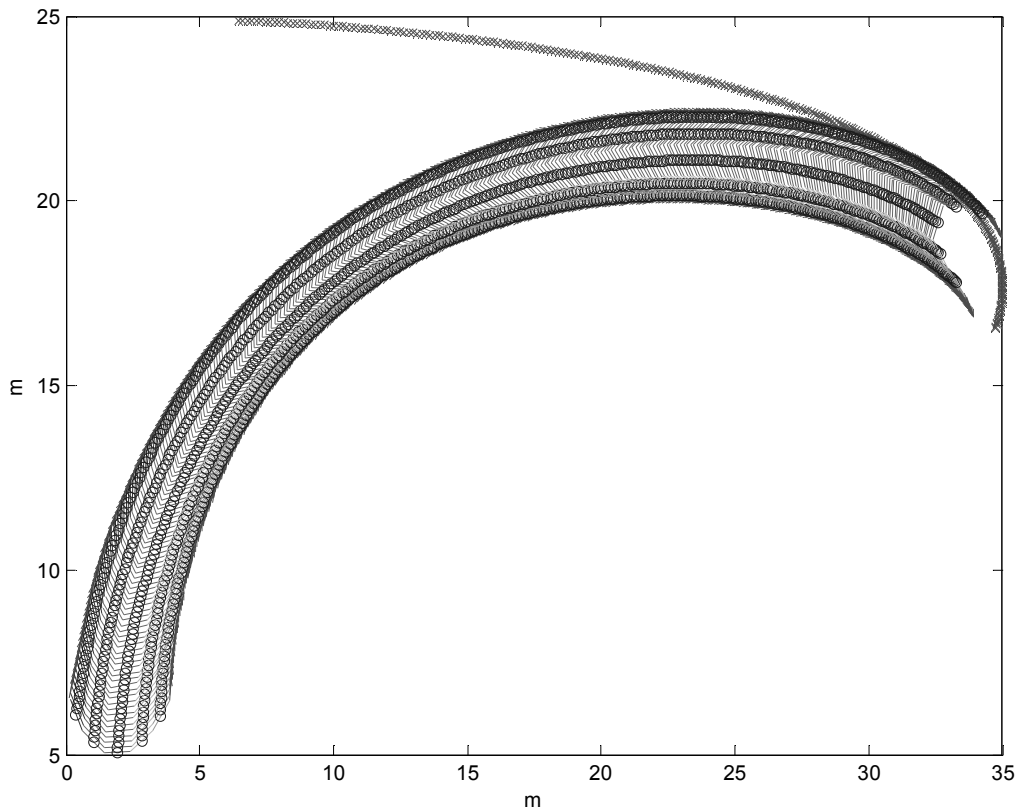
Fig. 12. Movable objective pursuit

For this particular case, every control actions described in previous paragraphs have been employed. Notice how the distance between ships varies along the turn. It seems that this behaviour should be improved by an adequate cooperation strategy on top of control. In particular, an interesting problem would be to decide what to do when the objective has been reached: how to deploy the ships to surround it, etc.

6 CONCLUSIONS

The present paper is devoted to open a new topic in the context of cooperative marine robotics. It has been motivated by a recent spill-over in the Spanish coast. It was observed that the confinement of oil leakage by ships towing booms is a difficult coordination task. Actually, only the simplest team, formed by two ships and one boom, was put on task. It was intriguing to analyse why it is difficult. So a simple scenario, two ships towing a boom, was simulated in order to state a control coordination problem for further studies.

In this paper, the problem was stated in mathematical terms, and a sequence of cases, from the simplest one, was studied. The various needs of control (coordinated) interventions appeared, and, for the moment, were toughly solved. Indeed, a future research will focus on better control.

The scenario is clearly suggestive, not only from the control point of view, but also from the cooperative strategies perspective.

REFERENCES

[1]   Billard, E.A. (2004). Patterns of agent interaction scenarios as use case maps, IEEE Trans. System, Man and Cybernetics, PartB, vol. 34, n4, August, 1933-1939.

[2]   De la Cruz, J.M., J. Aranda, J.M. Giron-Sierra, F. Velasco, S. Esteban, J.M. Diaz, B. De Andres (2004). Improving the comfort of a fast ferry with the control of flaps and T-foil, IEEE Control Systems Magazine, vol. 24, n. 2, April, 47-60.

[3]   Fossen, T.I. (2002). Marine Control Systems, Marine Cybernetics AS, Trondheim..

[4]   Haywood, A.J., A.J. Duncan, K.P. Klaka and J. Bennet (1995). The development of a ride control system for fast ferries, Control Engineering Practice, 695-703.

[5]   Johansen, V., R. Skjetne and A.J. Sorensen (2003). Maneuvering of towed interconnected marine systems, In Proceedings IFAC MCMC 2003, Gerona, Spain, 292-297.

[6]   Kyrkjebo, E. and K.Y. Pettersen (2003). Ship replenishment using synchronization control, In Proceedings IFAC MCMC 2003, Gerona, Spain, 286-291.

[7]   Kyrkjebo, E., M. Wondergem, K.Y. Pettersen and H. Nijmeijer (2004). Experimental results on synchronization control of ship rendezvous operations, In Proceedings IFAC CAMS 2004, Ancona, Italy, 453-458.

[8]   Liu, J. and J. Wu (2001). Multi-Agent Robotic Systems, CRC Press.

[9]   Lloyd, A.R.J.M. (1998). Seakeeping: Ship Behaviour in Rough Weather, A.R.M.J. Lloyd, Gosport, Hampshire, U.K.

[10]   Morishita, H.M., E.A. Tannuri and T.T. Bravin (2004). Methodology for dynamic analysis of offloading operations, In Proceedings IFAC CAMS 2004, Ancona, Italy, 459-464.

[11]   Ryle, M. (1998). Smoothing out the ride, The Motor Ship, January, 23-26.

[12]   Skjetne, R., I.F. Ihle and T.I. Fossen (2003). Formation control by synchronizing multiple maneuvering systems, In Proceedings IFAC MCMC 2003, Gerona, Spain, 280-285.

[13]   Soetanto, D., L. Lapierre and A. Pascoal (2003). Coordinated motion control of marine robots (2003), In Proceedings IFAC MCMC2003, Gerona, Spain, 250-255.

Chapter 6

A Seakeeping Laboratory for Experimental Control Tests

JOSÉ MARÍA RIOLA RODRÍGUEZ
Canal de Experiencias Hidrodinámicas de El Pardo, CEHIPAR

The necessity to know and measure the action of the fluid that surrounds the hull of a ship and the control devices and her consequent response to this interference, precises of the development of mathematical and physical models in a previous known scenario, conditioned by the scale effects. They offer the necessary data for a project optimisation and it introduces us in the hydrodynamic scale research laboratory.

1   INTRODUCTION

From their origins, the hydrodynamics has been focused toward five different areas; the hull resistance, the appendages study, the calm water propulsion, the seakeeping and the maneuverability. The word *"Seakeeping"* defines the study of the marine system motions and efforts due to the waves. The control engineering allows to develop a series of actuators to improve the ship behavior and also operations and work systems in the sea as much as in port. Furthermore the seakeeping performance can have an enormous influence on the choice of competing vessels for a particular route or a warship operating in hostile environments whilst providing a stable platform for crew, weapons and aircraft operations.
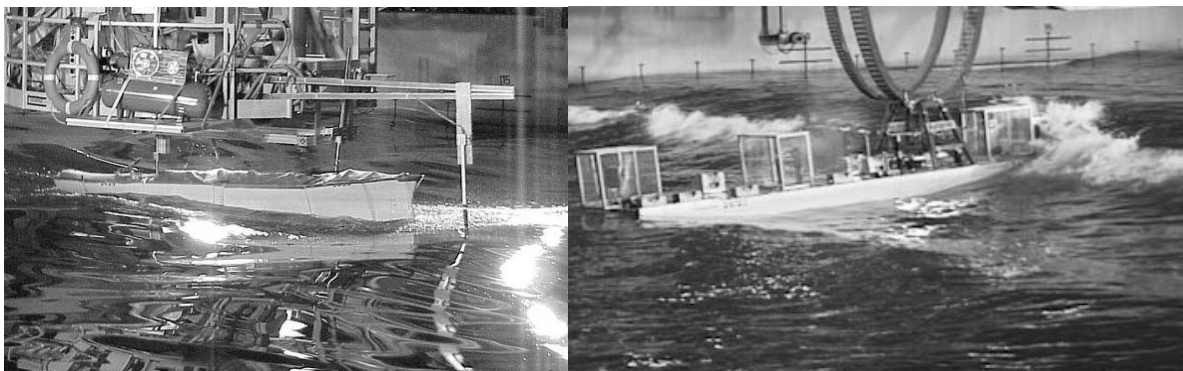
Figure 1. Models in experimentation

Being the general focus of this book, the study of the applied ship control, and in particular, the actuator movements to reduce the vessel motions and accelerations, this chapter is focused toward the knowledge of the *"Laboratorio de Dinámica del Buque"* of the *Canal de Experiencias Hidrodinámicas de El Pardo, CEHIPAR* and its possibilities of testing models for the control development. This knowledge will allow to the researcher in this field to find an excellence instrument to carry out a very wide range of seakeeping and maneuverability control tests with scale models of all types of ships and marine crafts.

The hull resistance and the ship speed are studied in the calm water tanks, and their philosophy consist on towing the model at several speeds to obtaining the resistance-speed curves. The speed and power calculation was studied in this way until middle 50's when some publications established a theoretical calculation of the ship in waves. Weinblum and St. Denis applied Newton laws to solve the ship motion in regular waves, and later on St. Denis and Pierson obtained motion data in irregular seas. It is necessary to highlight the later appearance of the well-known slices theory of Korvin-Kroukovsky. From the widespread acceptance of these theses and pushed by the "off-shore" industry, the seakeeping basins with wave generators were born and developed from the initial regular sinusoidal waves of long crest until the current random seas ones. One of the last pushes to this development has been the electronic that allows the individual control of each flap of the hydraulic or electric plants for a complex sea generation and the control carriage for manoeuvring the model.

Dimensionless parameters may be used to generalize experimental results from the laboratory models and the testing data obtained at a scale are under proper conditions, applicable to a real size vessel confined by geometrically similar boundaries. The only scale that it allows the execution of all the dynamic laws with models is the unit. This is due to the impossibility of completing the Froude law relates the forces and inertia with the Reynolds law relates with the viscosity simultaneously. When forces of inertia dominating on the viscous ones, as in our case, in the main scale factors there is a general acceptance to relate the obtained results with the real ship by means of the equality of the Froude number.

2   SEAKEEPING

High speeds lead to potentially larger relative motions and accelerations which have to be addressed and coped with. This types of vessels are often concerned with the carriage of ships passengers, trucks and cars with all the inherent problems and as a necessary part of their design and operational viability, normally have lightweight structures.

The seakeeping design to quantify the high speed vessels performance, have to be taken into account mainly the following aspects:

-   Safety, speed loss and operational limits
-   Structural loading
-   Passenger comfort and crew workability

The first aspect plays an important role in assessing the overall economic ship viability and the operational limits and hence the availability of the vessel may then be addressed by the probability of these values being exceeded in the expected sea conditions, and hence the

proportion of time the ship is safely available for actual service. Power increase rather than speed loss or delays tends to be a more suitable criterion in the case in high speed ships, particularly ferries because operating speeds tend to be strictly maintained except an insufficient passenger comfort level.

Related structural loading aspects, several design factors need to be addressed which will include pitch, heave and accelerations mainly from the point of view of slamming pressures and green water.

Passenger comfort and crew workability can be related to motion indexes as MII, MIF and MSI in order to know the acceptable operational limit as we can read in this text.

3   TESTING SCENARIO

The laboratory is made up of the three basic facilities:

- The basin itself. Its main dimensions are 150 meters length, 30 meters width and 5 meters depth. The tank has a wave generator along one of its 30 meters side and on the opposite side there is a stainless steel beach that absorbs the waves energy.

- The sixty flaps wave generator pushed by a hydraulic plant is able to generate regular waves with a maximum height of 0.85 meters, random long crested, short crested and episodic waves.
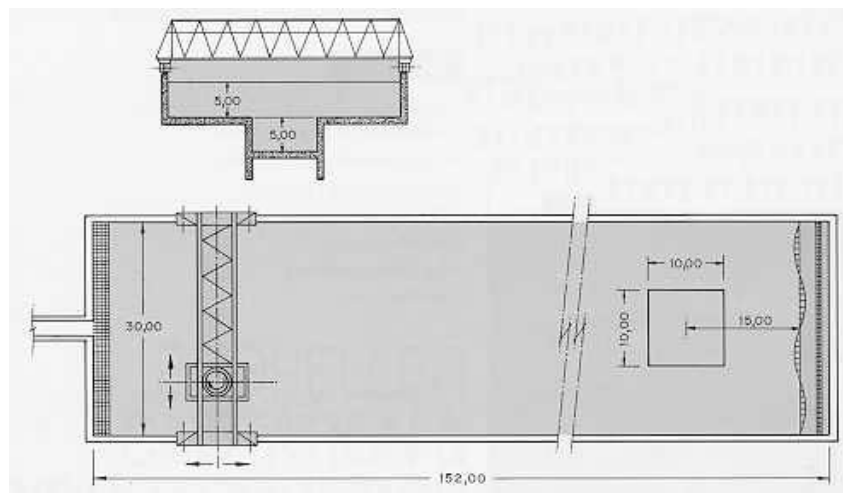
Figure 2. The Computerized Planar Motion Carriage

- The Computerized Planar Motion Carriage C.P.M.C. is able to reproduce any desired horizontal motion or model trajectory on the water. The linear motion of the main carriage is a combination of the three independent sub-carriages with movements in the longitudinal, transversal and rotation senses.

Figure 3. Picture of the Computerized Planar Motion Carriage

The hydrodynamic behaviour of a vessel depends fundamentally of the geometric submerged volume so it is necessary a physical similarity with the real ship as much as possible. The model hull forms elected for the researcher are based on a fast ferry ship or a naval frigate because in both cases the platform stabilization is crucial and the technological added value projects have total interest in the shipyards headquarters in order to maintain their competitiveness into the actual and future market. The first need to sure the passengers comfort and actually the frigates are the workhorses of any Navy, covering nearly everything from high-intensity warfare down to constabulary patrols and their sensors, weapons and crew effectiveness are directly related to the platform motions.

The construction process from the digital body forms is mainly based on the scaled hull characteristics, appendages and detailed maps, the developed instrumentation, sensors and actuators preparation. Also the calibration and generation of waves. As the objective of this research is to demonstrate the behavior of a autonomous fast ship on the sea, the model will be self-propelled to run in longitudinal sense or any other to the wave trains related to the basin.

Figure 4. Ship an actuator models are built with high precision.

The sensors in the majority of control tests are located inside the model, and it is presented and explained in a different chapter, but an external optical tracking system is adequate to obtain and validate the model motions data. This optical system is able to pick up information of several light emitting diodes located on the model. This light emitted enters in the camera lenses and it is picked up in its photosensitive detectors and it is digitized. The system has three cameras mounted in a rigid structure that recognizes the coordinates and the orientation of each one and solves the trigonometrical problem and calculates the ship model six DOF, speed and acceleration. The main components are the LEDs, cameras, data recorder PC and the data flow administration unit.

In order to optimize a fast ship project and in order to compare test results, a standard waves conditions to run the model that define a particular weather scenario are needed. The current wave generators have capacity to generate any long or short, arbitrary or standard type of waves, inside the physical restrictions of the basin and generator. The seakeeping assessment requires a knowledge of the ship RAO's or motion transfer functions together with an assumed wave energy spectrum for the relevant sea area. The statistical parameters habitually used to describe the sea; significant wave height, period, etc., are based on the identification of the individual waves in a recorder of vertical displacements of the sea level. The spectral techniques will have to be employed to provide a statistically meaningful representation of a confused sea.

Spectral calculations can be used to determine the motion energy spectrum and, from it, statistical quantities or attributes such as RMS values of motions exceeding a given value. An ocean wave statistics data base has been built up over many years and it has been published in different forms and sea conditions are represented by wave energy spectra. Among all the sea spectra used in the laboratories, the Pierson-Moskowitz and the JONSWAP (JOint North Sea WAve Observation Project) are the most well known and they are commonly regarded as a good representation of open sea and short crested seas or limited fetch condition, respectively. The JONSWAP spectrum is the most used in Oceanography, Marine Engineering and in the laboratories, so these waves are normally used when the research is focused on the fast ships control.

A wave is represented by the equation: $\zeta(t) = \sum_{j=1}^{N} A_j \cdot \cos\left(\omega_j t - k_j x + \varepsilon_j\right)$

where $\zeta(t)$ is the irregular wave elevation, A_j, ω_j and k_j are the wave amplitudes, frequencies and wave numbers respectively, and ε_j are normally uniformly distributed random phase angles, x and t represent the abscissa of the position considered along the X axis and the time variable, respectively and N is the total number of component waves, An infinite number of component waves: $\zeta(t) = \int_{0}^{\infty} \cos\left(\omega t - k(\omega) x + \varepsilon(\omega)\right) \cdot \sqrt{2\,S(\omega)\,d\omega}$

In which $S(\omega)$ is a wave spectrum. $N = \left(\omega_{max} - \omega_{min}\right)/\Delta\omega$ and then $T_{rep} = 2\pi/\Delta\omega$

T_{rep} is the repeat period, $\Delta\omega$ is the circular frequency interval and ω_{max} and ω_{min} are the boundaries of the frequency range taken into consideration.

The P-M spectrum is given by the expression: $S(\omega) = \dfrac{A}{\omega^5} \cdot \exp\left(-\dfrac{B}{\omega^4}\right)$

Where $A = 8.1 \cdot 10^{-3} \cdot g^2$ and $B = 0.74 \cdot \left(\dfrac{g}{V_{19.5}}\right)^4$ and $V_{19.5}$ is the wind speed at 19.5 m above the still water level in m/sec. Expressions for the significant wave height and the mean zero crossing period are:

$$H_s = 4\,\sigma = 4\,\sqrt{m_0} = 4\,\sqrt{\int_0^\infty S(\omega)\,d\omega} = 4\,\sqrt{\dfrac{\alpha\,g^2}{5\,\omega_0^4}} \cong \dfrac{1.58}{\omega_0^2}$$

$$T_z = \sqrt{\dfrac{m_0}{m_2}} = \sqrt{\dfrac{\displaystyle\int_0^\infty S(\omega)\,d\omega}{\displaystyle\int_0^\infty \omega^2\,S(\omega)\,d\omega}} = \sqrt{\dfrac{\dfrac{\alpha\,g^2}{5\,\omega_0^4}}{\left(\dfrac{4}{5}\pi^5\right)^{\frac{1}{2}} \cdot \dfrac{\alpha\,g^2}{(2\pi\,\omega_0)^2}}} = \dfrac{1}{\omega_0}\sqrt{\dfrac{2}{\sqrt{5\pi}}} \cong \dfrac{0.71}{\omega_0}$$

To obtain the JONSWAP spectrum:

$$S(\omega) = \alpha \cdot \dfrac{g^2}{\omega^5} \cdot \exp\left[-\dfrac{5}{4}\left(\dfrac{\omega_0}{\omega}\right)^4\right] \cdot \gamma^{\exp\left[-\frac{(\omega-\omega_0)^2}{2\cdot\tau^2\cdot\omega_0^2}\right]}$$

In which γ is the peakness parameter, assumed equal to 3.3 for the mean JONSWAP spectrum, although it may vary from 1.0 to 7.0 approximately, γ is defined as the ratio between the height of the spectral peak to that of the corresponding P-M wave spectrum. It is a function of the wind duration and the stage of the growth or decay of the storm. The shape parameter, τ, is the ratio between the area under the spectrum on either side of ω_0 and the maximum spectral ordinate.

Two quantities are needed to specify a JONSWAP spectrum, assuming all other coefficients can be found via the first two. This is the reason why this spectrum is referred to as a two-parameters spectrum. In the formulae above, γ, α and ω_0 can be found either if both wind velocity and fetch are known, or through H_s and T_z. But due to the significant wave height and zero crossing period are related to each other through statistical records, the mean values for a given sea state are accepted. This practically reduces the parameters needed to describe a given JONSWAP spectrum to only one and this is the main reason to its wide use in the research facilities.
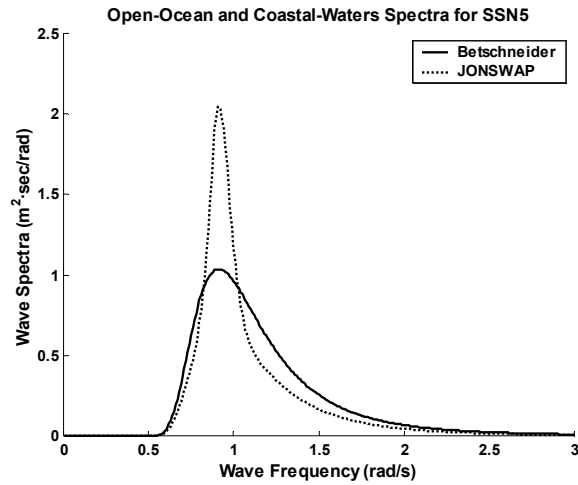
Figure 5. P-M and JONSWAP spectra
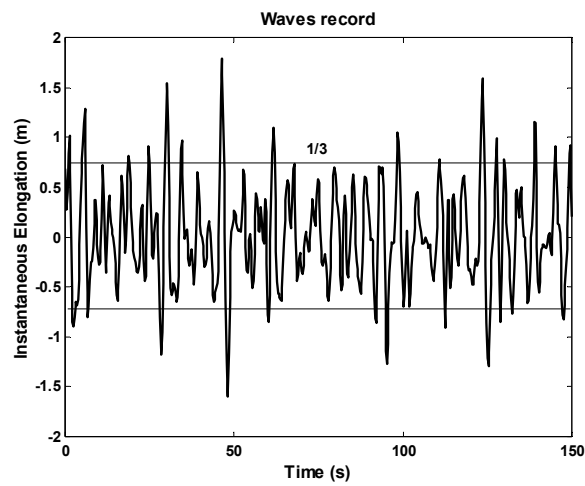
Figure 6. A record of waves encountered by a ship.
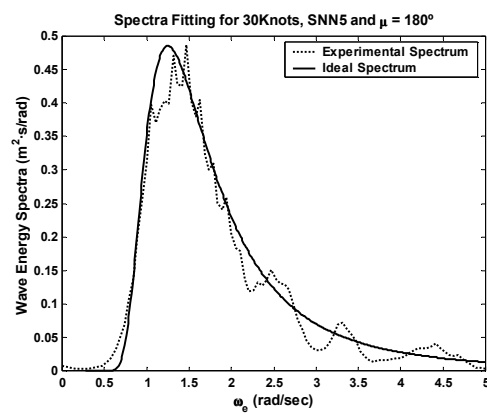
Figure 7. Experimental and ideal spectra for SSN5, 30 Knots and heading seas.

Chapter 7

About Identification of Mathematical Models for High Speed Crafts

ROCIO MUÑOZ MANSILLA, JOAQUÍN ARANDA ALMANSA,
SEBASTIÁN DORMIDO BENCOMO, JOSÉ MANUEL DÍAZ, SEBASTIÁN DORMIDO CANTO
Dept. de Informática y Automática. UNED. Madrid. Spain.

The response of a ship advancing in a seaway is a complicated phenomenon involving the interactions between the vessel dynamics and several distinct hydrodynamic forces. All ship responses are non linear to some extent, but in many cases a linear theory will yield good predictions. Two different approaches of the system identification method have been proposed in order to estimate models for heave, pitch and roll dynamics of a high speed craft. Both of them resolve the identification subject as an optimization problem to fit the best model. The study is focused on a ship advancing at constant mean forward speed with arbitrary heading in a train of regular sinusoidal waves.

1 INTRODUCTION

One of the most important steps in the control of process is the identification of an adequate model of a continuous linear system. The suitability depends strongly on the particular application of the system.

The response of a ship advancing in a seaway is a complicated phenomenon involving the interactions between the vessel dynamics and several distinct hydrodynamic forces. All ship responses are non linear to some extent, but in many cases when nonlinearities are small a linear theory will yield good predictions.

A ship advancing at a steady mean forward speed with arbitrary heading in a train of regular waves will move in six degrees of freedom. That is, the ship's motion can be considered to be made up of three translational components, surge, sway and heave, and three rotational components, roll, pitch and yaw. For the usual case of an unrestrained ship with port/starboard symmetry, the six non-linear equations may be uncoupled into two sets of three linear equations:

    - The vertical–plane or longitudinal motions (surge, heave and pitch)
    - The horizontal-plane or transverse motions (sway, roll and yaw).

The study is focused on a ship advancing at constant mean forward speed with arbitrary heading in a train of regular sinusoidal waves. The linearization of the equations is made on the basis of small motions. The motions will in general be small if the ship is stable and the

incident wave amplitude is relatively small. Experimental and theoretical investigations have shown that a linear analysis of ship motions give excellent results over a wide variety of sea conditions.

In a linear theory, the responses of the vessel will be linear with, ie, directly proportional to wave amplitude and occur at the frequency at which the ship perceives the incident waves, that is known as frequency of encounter.

The past decade has seen a growing interest on high speed crafts for both cargo and passenger transportation. Different designs have been considered, and a significant attention has been focused on fast mono-hull displacement ships. One of the objectives in the design is passenger comfort and vehicle safety. Vertical accelerations associated with roll, pitch and heave motions are the main cause of motion sickness. For that reason, a first goal is to damp these three movements.

Therefore, it is necessary to build a mathematical model of the dynamical system that permits the designing of a controller which achieves the reduction pf the heave, pitch and roll motions, and consequently the reduction of the motion sickness index.

Thus, as an initial study, previous researches of the work group have studied the longitudinal and transversal dynamics separately. Firstly, it has been studied heaving and pitching motion for the case of head seas, (μ=180deg) ([1]), modeled actuators and designed different controllers, ([2], [3]), in order to achieve heave and pitch damping and with successful results. And secondly, it has been analyzed the rolling response for the case of lateral waves (μ=90deg) ([4]) and in the same way, it has been carried out the actuators modeling and controller designing ([5]).

In this work the study has been extended to an analysis of heave, pitch and roll dynamics with different incidence angles between 180 degrees and 90 degrees. Models can be obtained by different techniques. There are many publications related to the ships modelling ([6], [7]).

In this work modeling is obtained from system identification method ([8], [9])., which is based on the observed input output data.

This research presents two approaches for identifying continuous transfer functions of the vertical and transversal dynamics of a high speed craft. In the first one the problem is set out as a nonlinear optimization problem with nonlinear constraints ([1]). There, the proposed solution is described with a hybrid optimization method (genetic algorithm + nonlinear optimization algorithm with constraints from the Matlab toolbox). In the second one a discussion on the first method is made ([10]) and some questions are raised, in order to obtain models more efficiently. There, these new improvements and their application are depicted.

Thus, this chapter is organized as follows. Firstly it is presented the basic steps in systems identification, where the criterion of fitness is developed. Secondly, it is presented the discussion on identification and the new solution of the problem. Finally, an example is shown in order to compare the two approaches.

2 THE STEPS OF SYSTEM IDENTIFICATION

The system identification problem is to estimate a model of a system based on observed input-output data.

The procedure to determine a model of a dynamical system from observed input-output data involves three basic steps:
- the input- output data
- a set of candidate models (the model structure)
- a criterion to select a particular model in the set, based on the information in the data (the identification method).

In general terms, an identification experiment is performed by exciting the system (using some sort of input such a step, a sinusoid or a random signal) and observing its input and output over a time interval. These signals are recorded. Then it is tried to fit a parametric model of the process to the recorded input and output sequences.

The first step is to determine an appropriate form of the model. As a second step some statistically based method is used to estimate the unknown parameters of the model. In practice, the estimations of structure and parameters are often done iteratively. This means that a tentative structure is chosen and the corresponding parameters are estimated. The model obtained is then tested to see whether it is and appropriate representation of the system. If this is not the case, some more complex model structure must be considered, its parameters estimated, the new model validated, and thus repeatedly until the best model is achieved. The procedure is illustrated in Figure 1 ([9]).

2.1. Design the experiment

The system identification method is based on the experimental observation of the system behavior. Therefore, first of all, these set of observed input-output data are required. For that, diverse experiments in CEHIPAR (El Pardo Model Basin, Spain) are made with a scaled down replica (1:25) of the TF120 ferry. Also there is a second self-propelled replica, which is scaled (1:40).

In order to analyze the dynamic of the fast ferry, tests with diverse types of waves, ship speeds (20, 30 and 40 knots) and different angles of incidence have been made. Also CEHIPAR has a program simulation PRECAL, which reproduces specified conditions and uses a geometrical model of the craft to predict its dynamic behavior. PRECAL is based on a CAD description of the hull of the ship to be analyzed. It solves the physical equations of the dynamic of a ship by using the Band Theory ([6], [7], [11]). This theory basically consists of decomposing the ship's volume into narrow transversal bands on which the nonlinear differential equations of the ship's dynamic are solved by numerical integration.

The data given by PRECAL are those that are going to be used in the system modeling. The program gives amplitude and phase data at different frequencies, so identification in the frequency domain is carrying out.

2.2 The input output data

The experimental input- output data are generated by program simulation PRECAL, which models the geometry and behavior of the physical model. Simulations are tried with regular waves, with the following characteristics,

- natural frequency between the rank [0.393,1.147] rad/s
- angles of incidence 90º, 105º, 120º, 135º, 150º, 165º, 180º
- ship speed 20, 30 and 40 knots.

```
┌──────────────────────────┐
│ -design the experiment   │◄──────────────┐
│ -collect input-output    │               │
│  data                    │          3. work further
└──────────────────────────┘          on the input-
             │                        output data
             ▼                             │
┌──────────────────────────┐              │
│ -examine the data        │◄─────────────┘
│ -remove trends and       │
│  outliers                │
│ -filtering               │
│ -select useful portions  │
│  of the original data    │
└──────────────────────────┘
             │
             ▼
┌──────────────────────────┐
│ select and define a      │◄────────┐
│ model structure          │         │
└──────────────────────────┘    1.try another
             │                  model set
             ▼                       │
┌──────────────────────────┐        │
│ compute the best model   │◄───┐   │
│ according to the         │    │   │
│ criterion of fit         │  2.try other
└──────────────────────────┘  criterion of
             │                 fit
             ▼
┌──────────────────────────┐
│ validation of the model  │
└──────────────────────────┘
             │         NO
             ▼
    ( model good enough? )────────────────►
             │
             ▼
           YES
```

Figure 1. Identification procedure

Tests consist of excitation of the ship system by the sea wave (the input is the wave height (m)). For each type of wave, that is, wave frequency and angle of incidence, the ship responses are measured: total forces of heave, surge and sway, total moments of roll, pitch

100

and yaw, and the motion in the six degrees of freedom: heave, surge, sway, roll, pitch and yaw.

In this case, the study is focused on heave, pitch and roll modes. Thus, the given outputs related to these motions are, in the frequency domain, the following ([12]),

- amplitude ([KN/m]) and phase ([deg]) of the total force of excitation heave,
- amplitude ([deg/m]) and phase ([deg]) of the motion response heave,
- amplitude ([KNm/m]) and phase ([deg]) of the total moment of excitation pitch,
- amplitude ([deg/m]) and phase ([deg]) of the motion response pitch,
- amplitude ([KNm/m]) and phase ([deg]) of the total moment of excitation roll,
- amplitude ([deg/m]) and phase ([deg]) of the motion response roll.

2.3. Model of the system
The block diagram of the system to identify is depicted in figure 2.
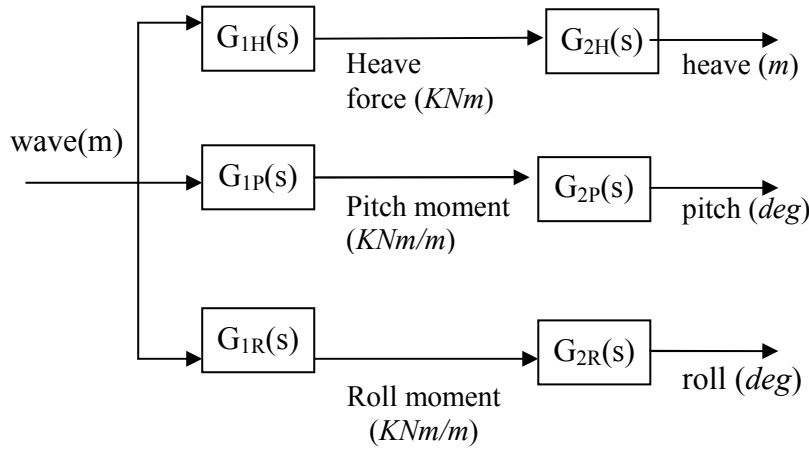
Figure 2. Block diagram of the system

Thus, the transfer functions to be modelled are the following

- $G_{1H}(s)$: from wave height (m) to heave force (kN)
- $G_{2H}(s)$: from heave force (kN) to heave motion (m)
- $G_{1P}(s)$: from wave height (m) a momento pitch (kNm)
- $G_{2P}(s)$: from pitch moment (kNm) to pitch motion (degrees)
- $G_{1R}(s)$: from wave height(m) to roll moment (kNm)
- $G_{2R}(s)$: from roll moment (kNm) to roll motion (degrees)

Based on the principle of linear superposition, it yields that

$$G_Z(s) = G_{1Z}(s) \cdot G_{2Z}(s), \text{ for } Z= H, P, R \tag{1}$$

Therefore, the given input output data are used to identify directly the transfer functions $G_Z(s)$ whose input is the wave height, and the outputs are the heave, pitch or roll motions, and similarly the transfer functions $G_{1Z}(s)$, whose input is the wave height, and the outputs are heave force, pitch moment, or roll moment. The identification of the transfer functions $G_{2Z}(s)$ are made indirectly, by using the relation (1).

2.4 Criterion of fit
Once the experiments with the system to model are designed, and the obtained input output data are examined, next step is to select and define a model structure and give a criterion of fit, so that it can be computed the best model that reproduces the dynamic of the ship system more suitably.

The system identification gives the mathematical model in the form of transfer function. Data given by the simulator PRECAL are in the frequency domain. Therefore, it will be carried out a parametric estimation of the transfer functions in the frequency domain.

In this way, consider the general parameterized transfer function (2). The estimation of the model consists of the fitness of the frequency response or Bode diagram of a transfer function with a fixed number of poles and zeros (model structure) to the actual measured data.

$$G(s,\theta) = \frac{B(s,\theta)}{A(s,\theta)} = \frac{b_{m+1}s^m + b_m s^{m-1} + \ldots + b_1}{s^n + a_n s^{n-1} + \ldots + a_1} \tag{2}$$

For the identification of the model it is employed a parametric method, characterized by the adjustment of the collected data to an estimated parameter vector θ.

$$\theta = (b_{m+1},\ b_m,\ b_{m-1}, \ldots b_1,\ a_n,\ a_{n-1},\ \ldots a_1) \tag{3}$$

The parameter vector θ is determined as the vector that minimizes the sum of squared equation errors. Thus, it is defined the cost function $J(\theta)$:

$$J(\theta) = \sum_{i=1}^{N} \left| G(j\omega_i) - G(j\omega_i, \theta) \right|^2 \tag{4}$$

in this way, the parameter vector is obtained such

$$\hat{\theta} = \arg\min_{\theta} J(\theta) \tag{5}$$

In order to solve the minimization problem and therefore estimate a transfer function model, it must be considered the following factors

1. A physical insight of the dynamic of the system states that at low frequencies roll and pitch responses amplitudes must tend to zero, while the heave response amplitude must tend to one. That is

   - Heave: $G_{1H}(j\omega), G_{2H}(j\omega) \xrightarrow[\omega \to 0]{} 1$

   - Pitch: $G_{1P}(j\omega) \xrightarrow[\omega \to 0]{} 0$ (6)

   - Roll $G_{1R}(j\omega) \xrightarrow[\omega \to 0]{} 0$

   that it is translated for the parameter vector θ

   - $G_{1H}(s)$ y $G_{2H}(s)$ → $|a_1| = |b_1|$
   - $G_{1P}(s)$ → $b_1 = 0$ (7)
   - $G_{1R}(s)$ → $b_1 = 0$

2. The system must be stable. It is translated into the poles of the transfer function must belong to the left plane *s*. Thus, to ensure the stability of the estimated models the transfer functions are reparametrized as

$$G(s,x) = \frac{x_{n+m+1}s^m + x_{n+m}s^{m-1} + ... + x_{n+1}}{\prod_{i=1}^{npc}\left(s^2 + 2x_{2i-1}s + x_{2i-1}^2 + x_{2i}^2\right)\prod_{i=1}^{nps}\left(s + x_{npc+i}\right)} \quad (8)$$

   with n = nps + npc and

$$\begin{cases} x_{2i-1} < -0.005 \text{ for i} = 1, 2,..., \text{npc} \\ x_{npc+i} < -0.005 \text{ for i} = 1, 2,..., \text{nps} \end{cases} \quad (9)$$

Then, the parameters *x* are obtained by minimizing

$$\sum_{i=1}^{N}\left|G(j\omega_i) - G(j\omega_i, x)\right|^2 \text{ subject to (7) and (9)} \quad (10)$$

It is important to note that the constraint $|a_1| = |b_1|$ is a strongly nonlinear function of *x*. This nonlinear minimization problem with nonlinear constraints is solved using the nonlinear optimization toolbox of Matlab.

Starting values are obtained via a genetic algorithm ([13]) or generated at random. The solution of (10) is used as initial guess for a multistep procedure, also called alternating variables method ([14]).

The multistep procedure is motivated by the fact that direct measurements of the heave force to heave motion, pitch moment to pitch motion, and roll moment to roll motion dynamics are not available. Therefore, transfer functions $G_{1Z}(s)$ and $G_Z(s)$ (with Z = H, P or R) are directly

estimated by minimizing (10). The solution given is used to identify the transfer function $G_{2Z}(s)$ (Z = H, P or R) by minimizing

$$\sum_{i=1}^{N} \left| G_Z(j\omega_i) - G_{1Z}(j\omega_i, x_a) G_{2Z}(j\omega_i, x_b) \right|^2 \text{ subject to (7) and (9)} \tag{11}$$

successively x_a is determined for fixed x_b, and x_b is determined for fixed x_a, with $G_Z(j\omega_i)$ the simulated data and Z = H, P or R.

3 DISCUSION ON THE IDENTIFICATION METHOD OF MULTIVARIABLE MODELS

In this section some suggestions are made about the method described in the previous section. The fundamental questions are raised about

- the excitation signal and plant model
- the parametrization of the transfer functions
- the choice of the starting values
- the multistep procedure

3.1 Choice of the excitation signal and the plant model
3.1.1. Excitation signal. Since the heave, pitch and roll dynamics of a ship are described by nonlinear differential equations ([15]), it is important the choice of the excitation signal. It is shown that the frequency response of a system depends on the class of excitation signal used.

It is important that the type and power of the waves used for the linear identification experiment (linear approximation of the true nonlinear behaviour) coincides with the type and the power of the waves that the controller or actuators elements should compensate for in real life.

In this particular case the identification and validation are performed with respectively regular (single sines) and irregular (broadband signal) waves. Regular waves do not exist in nature, however they are very useful for the identification method and obtaining a linear model. The frequency rank and height of the sinusoidal signal used belong to the frequency spectral and amplitudes of the irregular waves, which are those that the real system could find.

3.1.2. Plant model. In system identification the determination of model structure is an important aspect. And overparametrized model structure can lead to unnecessarily complicated computations for finding the parameter estimates and for using the estimated model. And underparametrized models may be very inaccurate. Therefore, it is necessary to employ methods to find an appropriate model structure.

The choice of model structure in practise is influenced greatly by the intended use of the model. For instance, a stabilizing regulator, like it is this case, can often be based on a low-order model, whereas more complex models are necessary if the model is aimed at giving physical insight into the process.

In practise identification often is performed for an increasing set of model orders. Then one must know when the model order is appropriate, i.e, when to stop. Needless to say, any real-life data ser cannot be modelled exactly by a linear finite-order model. However, the methods for finding the 'correct' model order are based on the statistical assumption that the data come from a true system within the model class considered.

Concerning the problem of choosing the model structure, the following question is raised: In the comparison between the frequency response or Bode diagram of the modelled transfer functions and the data ([1]), it is observed that there is a discrepancy in the high frequency range. Thus one can wonder whether these differences are due to the intrinsic nonlinear behaviour of the heave, pitch and roll motions, or to a deliberate simplification of the linear dynamics.

For that reason, it is proposed that one way of guaranteeing that the best (in least square sense) linear approximation has been obtained, and therefore, that all the remaining errors are then due to nonlinear effects, is the utilization of classical model selection criteria such as the Akaike information criterion (AIC), and the whiteness test of the residual applied to the identification data ([8], [9], [16]).

Therefore, in the new approach of the identification method, these criterion are applied in order to ensure the best model structure and thus the best linearization.

3.2 Parameterization issues and starting values

Originally, in order to ensure the system stability, a re-parameterization of the transfer functions is carried out (8). Consequently the constraint (7) results in a cost function (10) that is strongly non-quadratic function of the model parameters.

As a consequence of this parameterization, several disadvantages appear ([10]):

-   Because of the nonlinear minimization and nonlinear constraints, the generation of starting values is non-trivial, especially for high order systems.
-   The selection of the model is more complicated since the number of real *nps* and complex conjugate *npc* poles should be estimated. However, parameterization (2) only needs the number of total poles *n*.
-   The classical derivative based nonlinear optimizers ([14]) will degenerate for multiplicities higher than one. On the other hand, parameterization (2) does not impose nor exclude particular pole positions and pole multiplicities.

These problems can be avoided as follows:

Using parameterization (2), cost function can be written as

$$\sum_{i=1}^{N} \left| G(j\omega_i) - \frac{B(j\omega_i,\theta)}{A(j\omega_i,\theta)} \right|^2 \quad \text{subjetc to (7) and (9)} \qquad (12)$$

Thus, the nonlinear constraint $|a_1| = |b_1|$ can easily be satisfied by minimizing the cost function two times: first subject to $a_1 = b_1$, next subject to $a_1 = -b_1$, and finally selecting the solution with the smallest cost function.

Applying the same trick, high quality starting values for (12) can be obtained via the linear least squares estimate

$$\sum_{i=1}^{N}\left|A(j\omega_i,\theta)G(j\omega_i) - B(j\omega_i,\theta)\right|^2 \quad \text{subjetc to (7)} \tag{13}$$

Concerning the stability constraint, two different approaches are possible for imposing it. Either the constraint is imposed during the minimization as proposed in the previous method and in [17], or first and unconstrained optimal noise removal problem is solved and next a stable approximation is calculated ([18]). In this case the first scheme is applied.

3.3 The Multistep procedure

As it is has been commented in previous sections, the input output data which are obtained from the simulations are the input wave and outputs forces or moments, and the input wave and outputs the movements. These data are used directly for the identification of the transfer functions $G_{1Z}(s)$ and $G_Z(s)$, with $Z = H$, P or R.

The alternating variables method or multistep procedure proposed to minimize (11) is usually inefficient and is not guaranteed to converge to a stationary point of (11).

Hence, another proposed approach is to minimize simultaneously x_a and x_b. If parameterization (2) is used, this scheme will be easier since high quality starting values are available via (13).

Once questions and how to solve them are set out, next section show the definitive approach for the identification problem.

4 RESOLUTION TO THE IDENTIFICATION PROBLEM

In this section it is described the procedure developed for the identification of the models, considering all the suggestions raised in previous sections.

Collecting input-output data. For each particular case of force, moment or motion of heave, pitch and roll responses, initially there are a set of N experimental points of amplitude $|G(j\omega_i)|$ and phase $arg(G(j\omega_i))$, for each type of wave, characterized by the natural frequency ω_{0i}, with $i = 1..N$.

It must be considered that the frequency of oscillation of a ship response when a wave with natural frequency ω_0 reach the ship with an angle μ, is the frequency of encounter ω_e, which is determined by

$$\omega_e = \omega_0 - \frac{\omega_0^2}{g} U_0 \cos \mu \qquad (14)$$

Thus, the frequency of work will be the frequency of encounter.

According to this, the starting point are the experimental data, $G(j\omega_{ei})$, i=1…N, that expressed in binomial form are

$$G(j\omega_{ei}) = |G(j\omega_{ei})| \cos (arg(G(j\omega_{ei}))) + j |G(j\omega_{ei})| \cos (arg(G(j\omega_{ei}))) \qquad (15)$$

Criterion of fit. According to what it has been already commented, the identification problem is solved as an optimization problem. The transfer function to be estimated, with *m* zeros and *n* poles is :

$$G(s,\theta) = \frac{B(s,\theta)}{A(s,\theta)} = \frac{b_{m+1}s^m + b_m s^{m-1} + ... + b_1}{s^n + a_n s^{n-1} + ... + a_1} \qquad (16)$$

where the parameter vector θ is:

$$\theta = (a_1, a_{2...}, a_{n-1}, a_n, b_1, ..., b_{m-1}, b_m, b_{m+1}) \qquad (17)$$

In order to facilitate calculations in the resolution of the optimization problem, the parameter vector is redefined in terms of the *x* variable:

$$x = (x_1, x_{2,...}, x_n, x_{n+1}, ... x_{n+m}) \qquad (18)$$

Thus, the transfer function is:

$$G(s,x) = \frac{B(s,x)}{A(s,x)} = \frac{x_{m+1}s^m + x_m s^{m-1} + ... + x_{n+1}}{s^n + x_n s^{n-1} + ... + x_1} \qquad (19)$$

and then the cost function J(x) is

$$J(x) = \sum_{i=1}^{N} |G(j\omega_i) - G(j\omega_i, x)|^2 \qquad (20)$$

The problem of obtaining the value of the parameters *x* that find the minimum of the multivariable function J(x) is solved with the Matlab optimization toolbox.

Constraints. The constraints of the problem are

i.) $|b_1| = |a_1|$ for $G_{1H}(j\omega_e)$, $G_{2H}(j\omega_e)$

This condition is translated for the parameters vector x into:

$$|x_{n+1}| = |x_1| \tag{21a}$$

ii). $b_1 = 0$ for $G_{1P}(j\omega_e)$

In order to ensure that this constraint is satisfied in the identification of the model wave to pitch moment, it is necessary to impose in the parameter vector x that

$$x_{n+1} = 0 \tag{21b}$$

iii). System stability

This constraint forces the real part of the poles to be negative, that is, to be in the left hand on the *s*-plane.

Starting values. High quality starting values, i.e, near to the global optimum, are basic to reach the convergence point.

In [1], starting values are obtained via a genetic algorithm or generated at random. The trouble met in the identification of new models with different angles of incidence is that in many occasions, due that starting values were not adequate or distant from the minimum, the procedure of minimization was long and costly. This was intensified when genetic algorithms were used, since it is a method based on the heuristic that did not give good results in many cases.

For that reason, it is developed a new method to obtain the starting values x_0. This method consists of a linear least square estimation. From the cost function $J(x)$ expression:

$$J(x) = \sum_{i=1}^{N} \left| G(j\omega_{ei}) - G(j\omega_{ei}, x) \right|^2 = \sum_{i=1}^{N} \left| G(j\omega_{ei}) - \frac{B(j\omega_{ei}, x)}{A(j\omega_{ei}, x)} \right|^2 \tag{22}$$

it yields:

$$\sum_{i=1}^{N} \left| A(j\omega_{ei}, x) G(j\omega_{ei}) - B(j\omega_{ei}, x) \right|^2 \tag{23}$$

Therefore, a problem of least squares is set out. For each frequency value ω_{ei}, the denominator $A(j\omega_{ei}, x)$ and numerator $B(j\omega_{ei}, x)$ are only function of the vector x, and $G(j\omega_{ei})$ is a complex value. Hence, rewriting the above expression leads to an equation of the type $c * x - d = 0$, where x is the parameters vector (the starting values) to estimate.

Next, considering all the points $i = 1..N$, that is, all the frequencies ω_{ei}, one matrix C with N files and $n+m$ columns, and one column vector with $n+m$ size are given. Thus it is raised a least squares problem

$$C\,x - d = 0 \qquad\qquad (24)$$

Multistep procedure. Identification of the transfer functions $G_{2Z}(s)$. In this work, originally it is proposed the multistep procedure, where $G_{2Z}(s,x_b)$ is identified from the previously estimated transfer function $G_{1Z}(s,x_a)$ and the data $G_Z(s)$ (11). As an alternative to this procedure, it is suggested to solve simultaneously both transfer functions and estimate the parameters vector x_a and x_b at the same time.

Another approach for estimating $G_{2Z}(s)$ is to make a previous hypothesis of linearity and determine the points to fit the transfer function from the linear superposition principle. Thus, for each frequency of encounter of wave ω_{ei}, $i = 1..N$:

$$\left| G_{2Z}(j\omega_{ei}) \right| = \frac{\left| G_Z(j\omega_{ei}) \right|}{\left| G_{1Z}(j\omega_{ei}) \right|}; \qquad \arg(G_{2Z}(j\omega_{ei})) = \arg(G_Z(j\omega_{ei})) - \arg(G_{1Z}(j\omega_{ei})) \qquad (25)$$

where $Z = H, P, R$.

Once the implementation of the identification method has been developed and presented, next an example is shown.

5 AN EXAMPLE

The whole work tries to identify a continuous linear model of heaving, pitching and rolling dynamics. Specifically, models of G_{1H}, G_{2H}, G_{1P}, G_{2P}, G_{1R}, and G_{2R} are identified for incidence waves between 90 and 180 degrees. Each plant models set have the same number of poles and zeros.

As in this chapter it has been commented two alternatives for the identification method, in this section it is shown a practical case of application of theses two approaches and a comparison of both of them. Specifically, it is presented the identification of the model corresponding to the wave to heave force plant, for the incident angle 135º and ship speed 40 knots.

Thus, for each case, it is presented the transfer function identified and the Bode diagram, together with another plot in which the Bode diagram of the transfer function and data are compared. Finally, it is shown the temporal response of the final model identified, for the particular case of irregular waves SSN=5.

5.1 Wave to Heave Force $G_{1H}(s)$ Model
First approach. As it has been noted in previous sections, first step is to select a set of candidate model structures. Table 1 shows two of these considered model structures (m,n,nps), and the value of the cost function J for speed 40 knots. Here, m is the number of zeros, n is the total number of poles, and nps is the number of simple poles.

The parameter vector θ and transfer function are determined for each model structure. These all models give very similar Bode plots in the frequency range of interest, so this is a proof

that these must reflect features of the true system. Structure with minimum J is selected as the best model.

Table 1. Model structures, cost function J and AIC

model structure (m,n,nps)	cost function J
(3,4,2)	0.51
(3,3,1)	0.79

Finally, structure (3,4,2) is chosen, and the estimated transfer function is

$$G_{1H}(s) = 9333 \frac{76.56s^3 - 22.21s^2 + 322.5s - 14.92}{s^4 + 21.26s^3 + 154.7s^2 + 289s + 14.92} \quad (26)$$

Figure 3 presents the Bode diagram of $G_{1H}(s)$. Figure 4 shows the Bode plots of the estimated transfer function and the simulated true data. It can be seen that the model is quite capable of describing the system.

Figure 3. Bode plot of the estimated transfer function model $G_{1H}(s)$
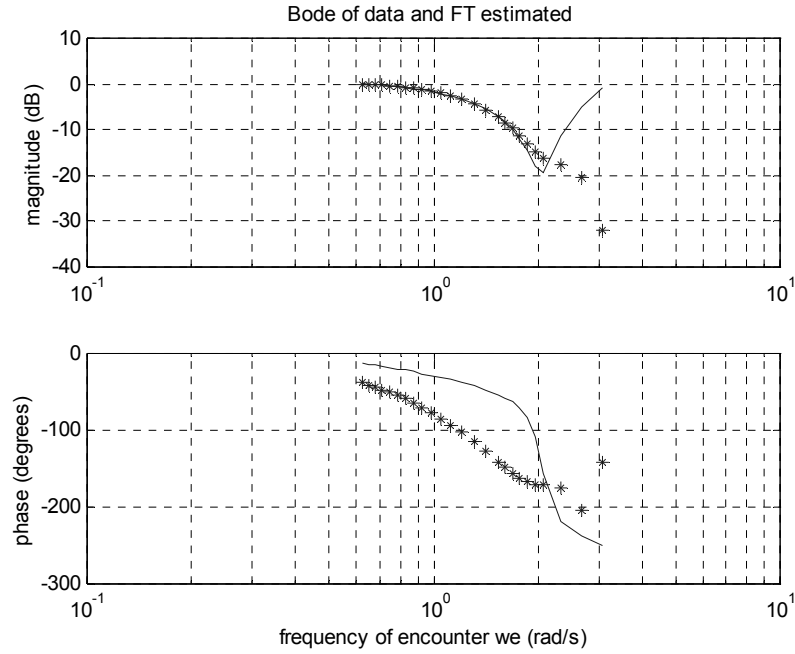
Figure 4. Bode plot of G$_{1H}$(s) and experimental data

Finally, figure 5 shows the response in the temporal domain of the model identified.
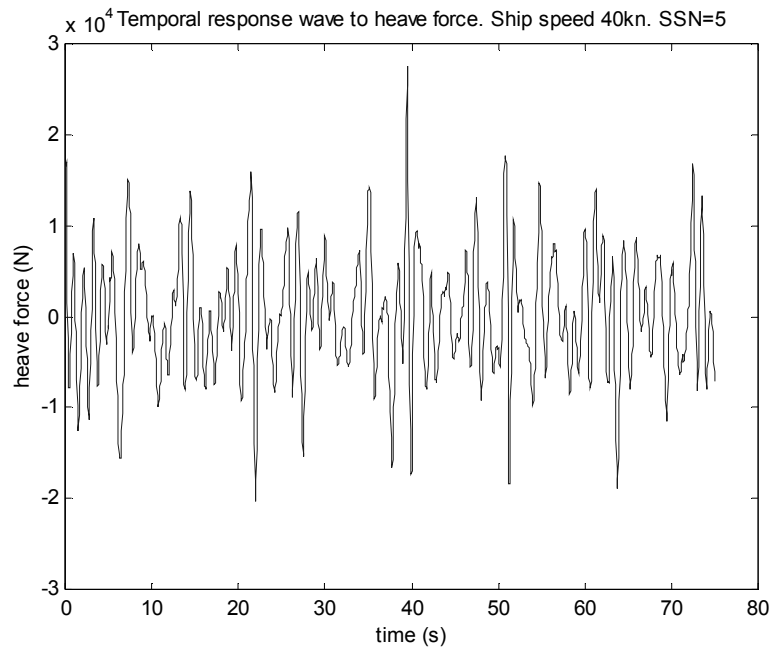
Figure 5. Temporal response G$_{1H}$(s)

Second approach. Table 2 shows two of the model structures (*m* is the number of zeros, and *n* the number of poles) that had been tried, and the respective values of AIC and cost function *J*. According to Akaike's theory, those with the lower value AIC is selected. In this case,

structure (3,4), with $m = 3$ zeros and $n = 4$ poles gives the best result, so this structure is the chosen one.

Table 2. Model structures, cost function *J* and AIC

model structure (m,n)	AIC	cost function J
(3,4)	-63.31	0.0347
(3,3)	-54.71	0.055

Once model structure is fixed, the identification procedure is executed and the following transfer function is estimated:

$$G_{1H}(s) = 9333 \frac{26.02s^3 - 22.13s^2 + 160.9s^1 + 0.9}{s^4 + 125.4s^3 + 149.1s^2 + 181.3s^1 + 0.9}$$ (27)

Figure 6 shows the frequency response of $G_{1H}(s)$, and figure 7 shows the comparison between the Bode diagram of the transfer function identified and the actual data. It is shown that the model fits the data quiet good. Next, figure 8 shows the temporal response of the final estimated model.
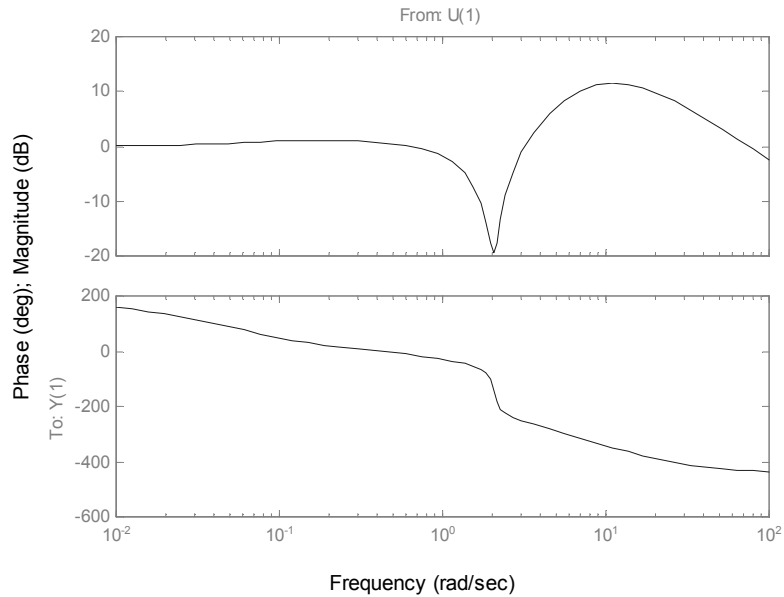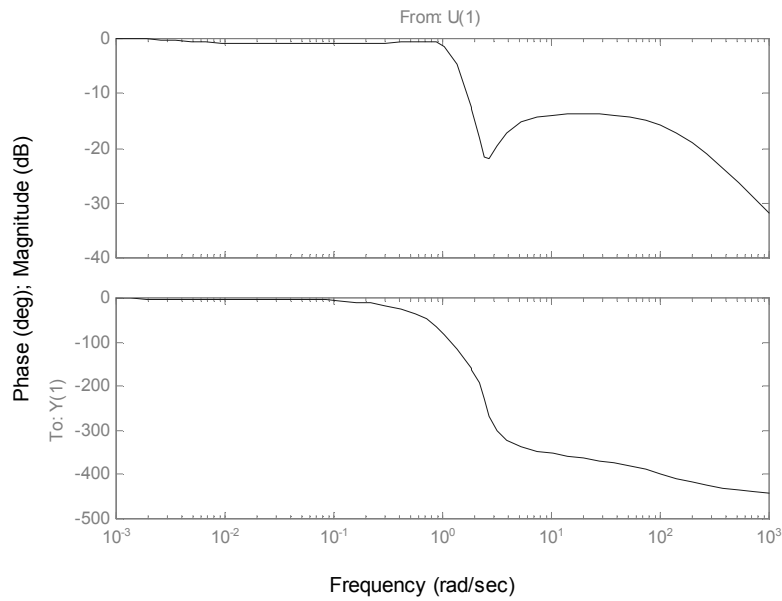

Figure 6. Bode plot of the estimated transfer function model $G_{1H}(s)$
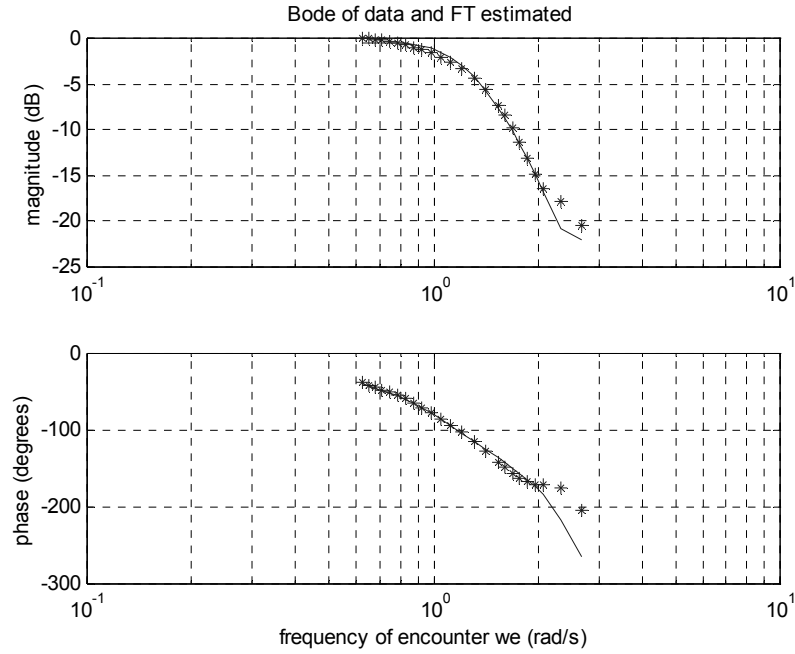
Figure 7. Bode plot of $G_{1H}(s)$ and data
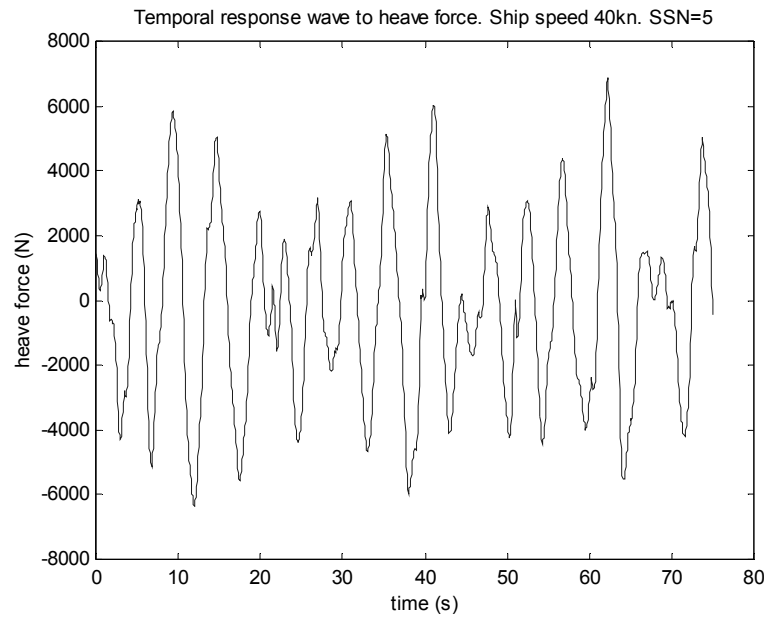
Figure 8.Temporal response $G_{1H}(s)$

Comparison. Evaluating the results of the two implementations, it is seen in numerical results and graphics that the second approach estimates a transfer function model that fits the data more accurately. In addition, in the Bode diagram of the first $G_{1H}(s)$ it is observed that the amplitudes at high frequencies are too much large, which is translated into a very oscillatory and not proper behaviour in the temporal response.

6 CONCLUSIONS

In this chapter two different approaches of the system identification method has been proposed in order to analyse and identify models for the heave, pitch and roll dynamics of a high speed craft.

The first approach uses genetic algorithms and non linear least squares with constraints methods applied in the frequency domain as a criterion of fit to compute the best model. This method has been employed to model the vertical dynamic (heave and pitch modes) for the particular case of waves from directly ahead. However, when the study is extended to the horizontal dynamic (roll mode) and in addition other angles of incidence, it is not obtained such good models. Furthermore, it is observed that the technique does not guarantee the best linear approximation, and involves a lot of computational load due to non quadratic functions.

For that reason it is suggested another procedure. The second approach changes the type of parameterization, in order to facilitate the model selection and avoid non-quadratic functions in the cost function. Moreover and most important, this new parameterization promotes obtaining high quality starting values via a linear least squares estimate.

The chapter is concluded with an example in which the two approximations are applied. The particular case is the wave to heave force plant, with incidence wave 135° and ship speed 40 knots. For each method, obtained model's properties are examined. Bode plots are computed, graphed and compared with experimental data. It is seen that estimated model describes data information. Models which best agree with the experimental data are selected. Temporal response is also depicted. Finally, it is shown that the second approach obtains more accurate models that the first one.

ACKNOLEDGMENTS

REFERENCES

[1] Aranda, J. Cruz, J.M de la, Díaz, J.M. (2004) Identification of Multivariable Models of Fast Ferries. *European Journal of Control.* 10:1-12.
[2] Aranda, J., J.M. Díaz, P. Ruipérez, T.M. Rueda, E. López (2002). Decreasing of the motion sickness incidence by a multivariable classic control for a high speed ferry. *CAMS ProceedingVolume*. Pergamon Press.
[3] Aranda, J., J.M de la Cruz, J.M. Díaz, S. Dormido Canto (2002) .QFT versus classical gain scheduling: study for a fast ferry. *15th IFAC World Congress b'02*.
[4] Aranda, J, R. Muñoz, J.M Díaz. (2003). Roll model for control of a fast ferry. *2nd International Conference on Maritime Transport and Maritime History*.

[5] Aranda, J, R. Muñoz, J.M Díaz. (2004). The problem of the coupling of the vertical movement control with roll movement in fast ferries. In:*CAMS 2004 Proceeding Volume. 239-244.*

[6] Fossen, T.I, (2002). *Marine control systems: guidance, navigation and control of ships, rigs and underwater vehicles*. Marine Cybernetics AS, Trondheim.

[7] Lewis, E.V, (1989), *Principles of Naval Architecture. Volume III*. Society of Naval Architects and Marine Engineers.

[8] Ljung, L., (1999) *System Identification: Theory for the User*. Prentice Hall.

[9] Söderström, T. and P. Stoica.(1989) *System Identification*. Prentice Hall.

[10] Pintelon, R. and Schoukens, J. (2004). Discussion on "Identification of multivariable models of fast ferries"

[11] Lloyd ARJM.(1998) *Seakeeping: ship behaviour in rough water*. Ellis Horwood.

[12] Bazán. National Company (1995). *Sea behaviour tests of the Turbo Ferry TF-120*. OTI-2086-CM-1.

[13] Michalewicz, Z. (1999) *Genetic Algorithms + Data Structure= Evolution Programs*. Third, revised and extender Edition. Springer.

[14] Fletcher, R., (1991) *Practical Methods of Optimization (2nd ed.).*Wiley, New York.

[15] Kenevissi, F., Atlar, M., and Mesbahi, E., (2003) *A new-generation motion-control system for twin-hull vessels using a neural optimal controller*. Marine Technology and Sname News, vol.40. no 3, pp. 168-180.

[16] Pintelon, R. and Schoukens, J., (2001) *System Identification: A Frequency Domain Approach*. Piscataway, USA: IEEE Press.

[17] Van Gestel, T., Suykens, J., Van Doore, P and De Moore, B., (2001) Identification of stable models in subspace identification by using regularization. *IEEE Trans. Autom. Contr.*, vol 46, no 9, pp 1416-1420.

[18] Mari, J. (2000) Modifications of rational transfer matrices to achieve positive realness*, Signal Processing*, vol. 80, pp. 615-635.

Chapter 8

A Research on Predicting and Avoiding Seasickness

S. ESTEBAN, J. RECAS, J.M. GIRON-SIERRA, J.M. DE LA CRUZ
Dep. Arquitectura de Computadores y Automática, UCM, Spain
J.M. RIOLA
Canal de Experiencias Hidrodinámicas de El Pardo, CEHIPAR, Spain

In this paper the coupling between the sea, the ship and humans is studied. In previous researches mathematical models of fast ship's motions have been determined. In the literature there are models of human sickness and models of the sea. This knowledge about seasickness, waves and ship motion has been gathered. Using this information it is possible to extract some criteria for the captain (manoeuvring), for ship designers and for actuators engineering. Taking advantage of the models obtained, a study of seasickness prediction has been done, and some interesting results are presented.

1   INTRODUCTION

Anacharsis, brother of Caduides the king of the Scythians, was a philosopher who traveled around the East Mediterranean and the Black Sea in the 6th century BC. His mother was Grecian woman and the contemporaneous Greeks said him that he exhorted moderation and good criteria in everything he did, for example saying "the vine bears three clusters of grapes: the first wine, pleasure; the second, drunkenness, the third, disgust" [1]. As a seaman, he had to travel in different kinds of sea conditions and he had one of the best references, with the same philosophy, listened about seasickness "people may be divided into three classes; the living, the dead and the seasick".

Seamen know that nothing is better than a sunny day sensation in a quiet sea and a sweet little breeze on the face. Nothing worse under a heavy storm, and between them are the most of the sailing days at sea. Seasickness is a form of motion sickness that is due to erratic stimulation to the brain from sensory receptors and is prompted by constantly changing movements ending with symptoms such as lethargy, nausea, cold sweat, stomach cramps and vomiting.

The sense of spatial orientation sends the brain the information about the space situation and this sense is regulated by the interaction of the body systems to detect motions; the inner ears, eyes, skin pressure receptors, muscles and joint sensory neural receptors. Motion sickness appears when the brain receives conflicting messages from these systems. A simple brain conflict example is when reading a book in a ship, the eyes send similar information to "we observe no motion" but the inner ears send "we feel the ship motion due to the waves".

Ship crew reduce the effectiveness under bad weather, so a better acknowledgement of the ship motions, vertical accelerations, seasickness and stabilizing actuators are really needed.

In previous researches mathematical models of the ship's motions have been determined [2]. Besides this, knowledge about seasickness and waves has been gathered. It is possible to extract some criteria for the captain (manoeuvring), for ship designers (on design time) and for actuators engineering (modifying the ship's performance). Taking advantage of the models obtained, a study of seasickness prediction has been done, and some interesting results have been obtained. Using these results, it is possible to broad the captain's instrument panel, the CFD ship design tools, and the information to design actuators and control systems to improve the ship's behaviour.

The problem of seasickness induced by ship motions is analyzed by using a chain of three filters, figure 1. Each filter is a model: one about excitation due to waves, other about ship motion response, and the third about seasickness effects. The following figure represents this approach:
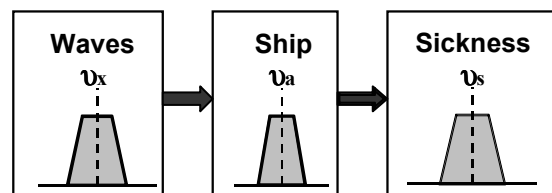
Figure 1. The analogy: A chain of filters.

This analogy will be explored and quantified, obtaining a frequency-domain procedure.

As established by O'Hanlon and McCauley (1974) [3], seasickness (MSI) is a cumulative effect. Each wave induced motion contributes to the MSI increase. More wave amplitude causes more ship motions amplitude and this implies the MSI increases. It is possible calculates the MSI contribution of a wave with a certain amplitude and frequency of encounter. For a given ship's speed and heading, a curve can be plotted relating wave amplitude and frequency of encounter. A wave density of distribution vs. frequency can be found too, this distribution can be obtained from the wave power spectrum. With this distribution, the total MSI can be obtained adding the contribution of each wave to the total MSI.

The paper details the filters and how they change when the sea conditions, ship's speed and heading vary. Several sea states spectra, ship's speeds and heading have been considered. Next section considers the modelling of the three filters, in particular to obtain knowledge of the problem. The third section shows three possible applications of this knowledge to alleviate seasickness on ship.

2   MATHEMATICAL MODELS AND KNOWLEDGE OF THE PROBLEM

2.1   Sea modelling

Wind generated wave start with small ripples which will travel across the surface in more or less the same direction as the wind. If the wind continues to blow for long ripples will advance and grow in length and height. At the same time the wind generate new ripples on the surface of the growing waves and these ripples will grow into waves themselves. There is a mixture of wave lengths and heights superimposed on each other. Lloyd (1998) [4] devotes two chapters of his book to the sea modelling.

The relative importance of each frequency on the waves may be quantified in terms of a wave amplitude energy density spectrum, usually abbreviated as Wave Energy Spectrum. This Wave Energy Spectrum is defined so that the area bounded by a frequency range is proportional to the total energy (per square meter of sea surface) of all components within that range of frequencies. So the spectral ordinate is

$$S_\zeta(\omega_n) = \frac{\zeta_{n0}^2}{2 \cdot \delta\omega} \qquad \left(\frac{m^2}{rad/s}\right) \tag{1}$$

where ζ_{n0} and ω_n are the amplitude and frequency coefficients of the Fourier series fitting.

Generally it is impossible to obtain the same Wave Energy Spectrum twice. But it is a current practice to use idealized wave spectra formulas for open and coastal conditions. Expressions for power spectra of waves can be obtained from literature [4] and [5].

2.1.1   Open ocean spectrum.

The International Towing Tank Conference (ITTC) has adopted the Bretschneider Spectrum (2) as the standard wave energy spectrum to represent the conditions in open ocean, long-crested seas.

$$S_B(\omega) = \frac{4 \cdot \pi^3 \cdot H_{1/3}^2}{\omega^5 \cdot T^4} \cdot \exp\left(\frac{-16 \cdot \pi^3}{\omega^4 \cdot T^4}\right) \qquad \left(\frac{m^2}{rad/s}\right) \tag{2}$$

where $H_{1/3}$ is the Significant Wave Height[1]; T is the Dominant Wave Period, related with the peak period by $T = T_p / 1.408$.

2.1.2   Costal sea spectrum

In coastal waters with limit fetch it is used a variation of the above spectrum. In this case the energy is more concentrated around the peak frequency. The Join North Sea Wave Project spectrum, JONSWAP, represents this situation (3).

$$S_J(\omega) = 0.658 \cdot 3.3^J \cdot S_B(\omega) \tag{3}$$

where

---

[1] The mean value of the highest third of many measurements of mean wave heights.

$$J = e^{-\frac{\left(\frac{\omega \cdot T_0}{2 \cdot \pi} - 1\right)^2}{2 \cdot \gamma^2}} \qquad \text{and} \qquad \gamma = \begin{cases} 0.07 \; \textit{for } \omega < \dfrac{2 \cdot \pi}{T_p} \\[2em] 0.09 \; \textit{for } \omega > \dfrac{2 \cdot \pi}{T_p} \end{cases}$$

The World Meteorological Organization (WMO) has scaled the severity of the sea state using a number for several sea conditions, the Sea State Number (SSN). This SSN represents a sea state conditions defined by several parameters, for example the significant height and the peak period. The parameters define completely the Sea Spectra. Figure 2a compare Bretschneider and JONSWAP spectra for SSN5.

2.1.3   The spectrum observed by a moving ship

As it is well-known, sea spectra suffer changes when it is seen by a moving ship [4]. For instance, the peak of a spectrum will be seen by a moving ship with another frequency, and the frequencies of spectrum will now shifted according (6).

$$\omega_e = \omega - \frac{\omega^2 \cdot U}{g} \cdot \cos(\mu) \tag{6}$$

It is a matter of frequency of encounter with waves, which depends on U, the speed of the ship, and μ, the heading angle (180º for heading seas). To preserve the energy represented by the spectrum the value of the ordinate is modified according to the expression (7).

$$S(\omega_e) = \frac{S(\omega)}{1 - \dfrac{2 \cdot \omega \cdot U \cdot \cos(\mu)}{g}} \tag{7}$$

For instance, for heading waves (μ=180º), SSN 5 and several speeds the shifting and modification of the Bretschneider spectrum is shown in figure 2b.
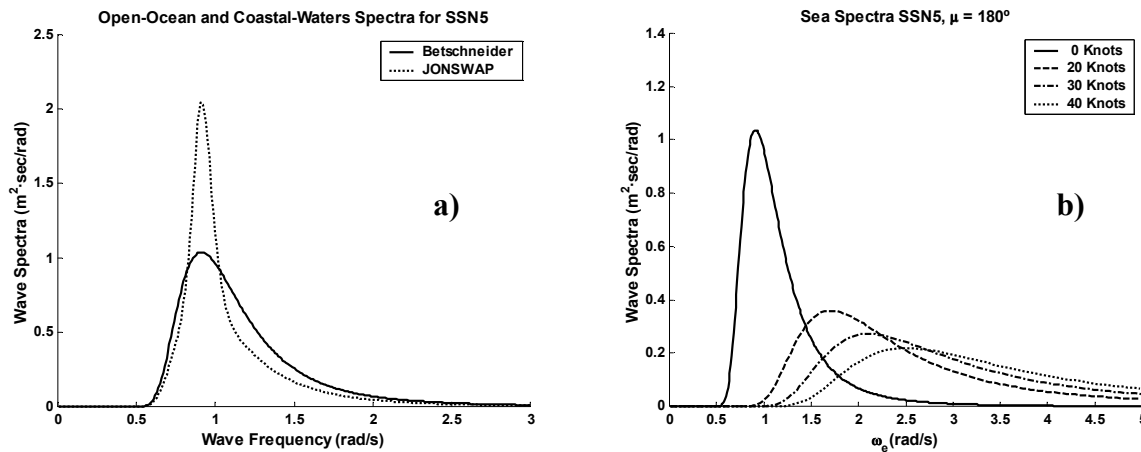

Figure 2. Bretschneider and JONSWAP Spectrum (a). Shifting of Bretschneider Spectrum (b).

2.1.4 *Wave Envelope and Probability Density of Waves*

The wave steepness is defined as H/λ, with H being the wave height (twice the wave amplitude) and λ the wave length. During this research in a seakeeping basin *Canal de Experiencias Hidrodinamicas de El Pardo* (CEHIPAR), Madrid, regular waves with 1/30, 1/40 and 1/50 steepness were used.

Supposing a wave steepness of 1/m, the wave amplitude is related with wave frequency (8).

$$\zeta(\omega) = \frac{H(\omega)}{2} = \frac{\lambda/m}{2} = \frac{\pi \cdot g}{m \cdot \omega^2} \tag{8}$$

The wave amplitude curve is subjected to the shifting of the equation (6) too.

A sort of probability density of waves frequencies is obtained, *f(ω)*, dividing the power spectrum by the energy associated to each frequency (9).

$$f(\omega) = \frac{S(\omega)}{\zeta^2(\omega)/2} = \frac{2 \cdot S(\omega) \cdot m^2 \cdot \omega^4}{\pi^2 \cdot g^2} \tag{9}$$

Using this probability density, the mean amplitude of waves can be easily calculated (10),

$$\overline{\zeta} = \int_0^\infty f(\omega) \cdot \zeta(\omega) \cdot d\omega = \frac{2 \cdot m}{\pi \cdot g} \int_0^\infty S(\omega) \cdot \omega^2 \cdot d\omega \tag{10}$$

Figure 3 shows power spectra, wave amplitude and probability density for SSN5 and ship's speed of 20 and 40 knots. The wave steepness 1/40 is selected.
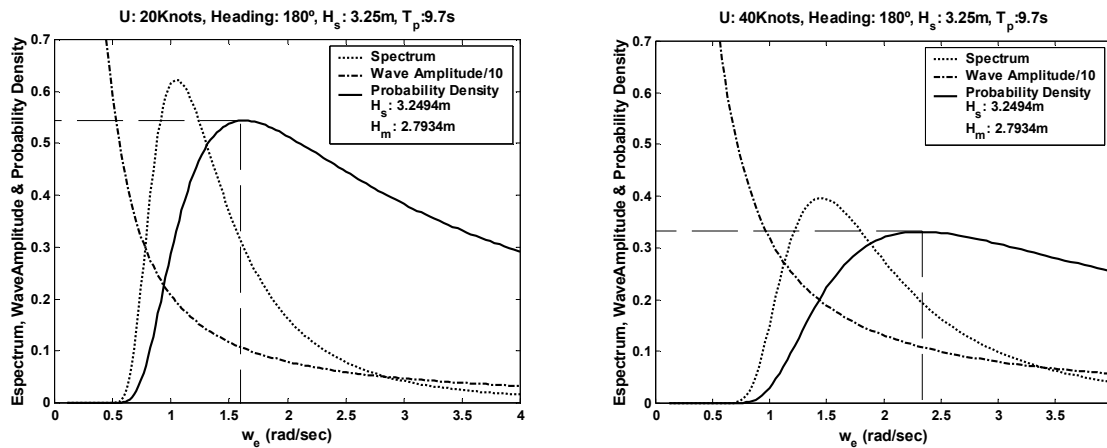
Figure 3. Power spectra, wave amplitude and probability density for SSN5

2.2 Ship Modelling

Usually ship motion is characterized using RAOs (Ratio Amplitude Operators [4]). It is possible to obtain the RAOs of a ship from real measurements, from model scale tests or from CFD (Computer Fluid Dinamic) programs. The degrees of freedom of a ship that contribute to vertical motion are heave, pitch and roll, these motions are the main factors which led to the seasickness. Since seasickness depends on the amplitude and frequency of the vertical

accelerations, it is necessary to obtain the RAO of the place where seasickness will be evaluated. This RAO is obtained operating with heave, pitch and roll in the complex domain, to bear in main the phases. A different RAO is obtained for each particular place of the ship, for example in a lateral near the bow, where passengers can experiment the largest vertical motions (WVM, the worst vertical motions). Vertical accelerations are also measured at the same point where WVM is measured; let us denote this acceleration as WVA. The WVA RAO is the WVM RAO multiplied by the square frequency, result of equation (11). This WVM may be selected for tank sites, weapon, work stations or equipments, etc.

$$WVM(t) = A \cdot \sin(\omega_e \cdot t);$$

$$WVA(t) = \frac{d^2 WVM}{dt^2} = -\omega_e^2 \cdot A \cdot \sin(\omega_e \cdot t); \tag{11}$$

$$|WVA| = \omega_e^2 \cdot |WVM|$$

Figure 4 shows the WVM and the WVA for SSN5 and 20, 30 and 40 knots ship speeds with head seas. The ship can be seen as a band-pass filter. Longer hulls will mean a shift of the frequency band to lower frequencies. In any case, it is important to pay attention to the 1 rad/sec frequency. A ship with a frequency band around 1 rad/sec is prone to causing seasickness.
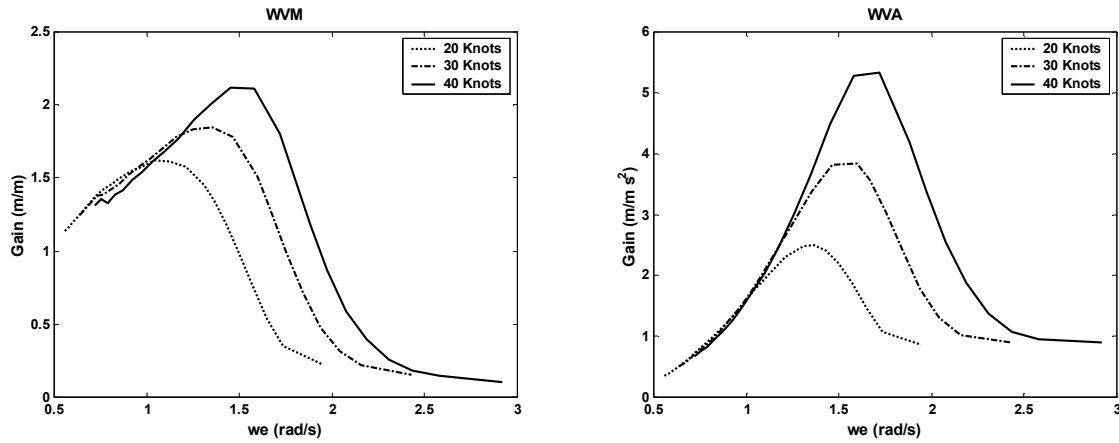
Figure 4. WVM and WVA frequency response for head seas, and 20, 30 , and 40 knots.

2.3 Sickness Modelling

There are several sources of scientific and technical information concerning seasickness. For instance the already cited study of O'Hanlon and McCauley (1974) [3], the base of MIL-STD-1472C defining "vomiting incidence", the standard ISO 2681:1985 and 2631:1990 [6] or the British Standard 6841:1987[7] on whole-body vibrations. These indices are good for short trips. Over longer periods, a few hours to few days, adaptation of the motions occurs, then the sensibility of humans to sickness decay too. There are other indices that do not refer to sickness, for example the Motion Induced Interruptions (MII) [4], which quantify the number of times that the crew must to interrupt a certain task to keep equilibrium.

In this paper the Motion Sickness Incidence index (MSI) proposed by O'Hanlon and McCauley (1974) is used. In a classic experiment O'Hanlon and McCauley measured the

motion sickness response of over 300 American male college student paid volunteers. None of the students had any recent acclimatization to motions. They were tested in pairs in a ship motion simulator which was capable of driving the small enclosed test cabin through a vertical sinusoidal motion with amplitudes up to about ±3.5 m. The cabin had no windows so that the subjects could not receive any visual motion cues and their only task was to monitor their state of nausea by pressing buttons on a control panel. The experiments lasted for up to two hours, or until the subjects vomited. They conclude that sickness is a cumulative effect related to vertical accelerations of certain frequencies. There is a frequency band around 1 rad/s, where the MSI presents a maximum value. In [3] a mathematical model of MSI was found, as expressed in equation (12),

$$MSI = 100 \cdot \left[0.5 \pm erf\left(\frac{\pm \log_{10}(|a_z|/g) \mp \mu_{MSI}}{0.4} \right) \right] \qquad (12)$$

where *erf* is the error function, a_z is the vertical acceleration in a chosen place averaged over a half motion cycle. Supposing sinusoidal motions, a_z can be obtained from the WVA amplitude A_{WVA}, according to (13),

$$|a_z| = \frac{\int_0^{T/2} A_{WVA}(\omega) \cdot \sin(\omega t) dt}{T/2} = \frac{A_{WVA}(\omega)}{\pi/2} \qquad (13)$$

and μ_{MSI} is (14)

$$\mu_{MSI} = -0.819 + 2.32(\log_{10} \omega_e)^2 \qquad (14)$$

where ω_e is the dominant frequency (rad/sec) of encounter with waves. Figure 5a shows that MSI has a main resonance frequency, 1 rad/sec. These formulas show that MSI is a non linear function of the frequency and mean acceleration, but they do not contemplate that a ship crew become habituated with exposure duration. On example of this habituation is shown in figure 5b, that represents a case of the percentage of the crew who vomit versus hours at sea. It is necessary a certain time on initial exposure of about half hour and the MSI rises to maximum which is allocated in a margin of 3 to 5 hours and gradually decreases. In this case in two days all the crew become habituated.
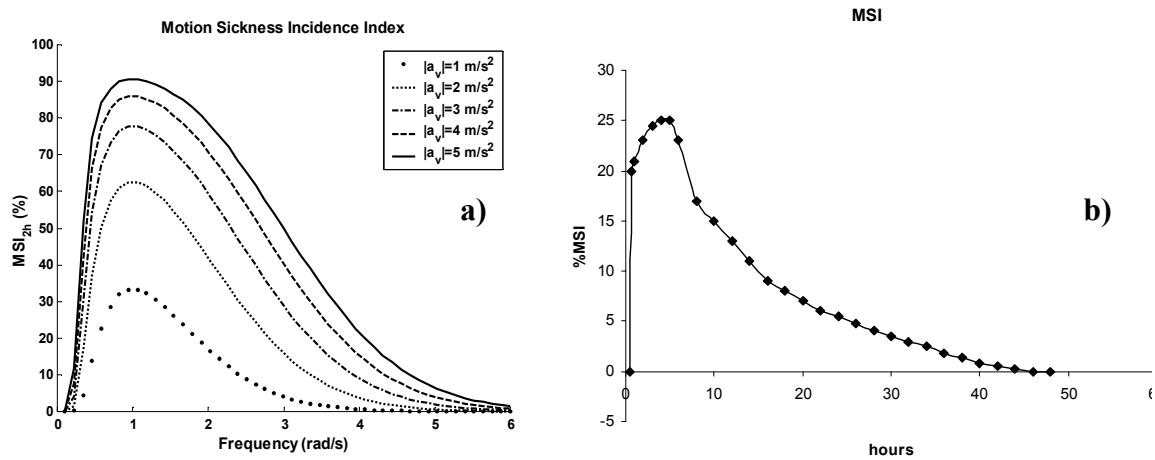
Figure 5. Motion Sickness Incidence index

2.4   Union of Filters

Figure 6 shows the procedure to obtain the MSI for a particular Ship,SSN,speed and heading. The three left blocks calculates the MSI contribution of a wave with a certain amplitude and frequency of encounter for a given ship's speed and heading. Using the Wave Amplitude Envelope (8) as input of the Ship filter (WVA) (11) the WVA amplitude, A_{WVA}, is obtained for each frequency. So it is possible to obtain the contribution of a wave frequency to the MSI using the sickness filter, (12), (13) and (14). Figure 7 shows this contribution.
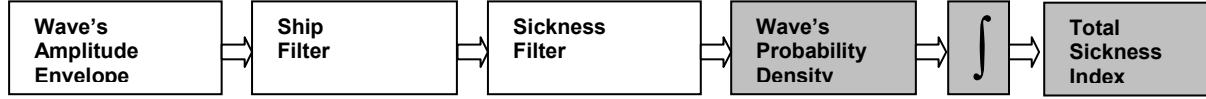
Figure 6. Procedure to evaluate the Sickness.
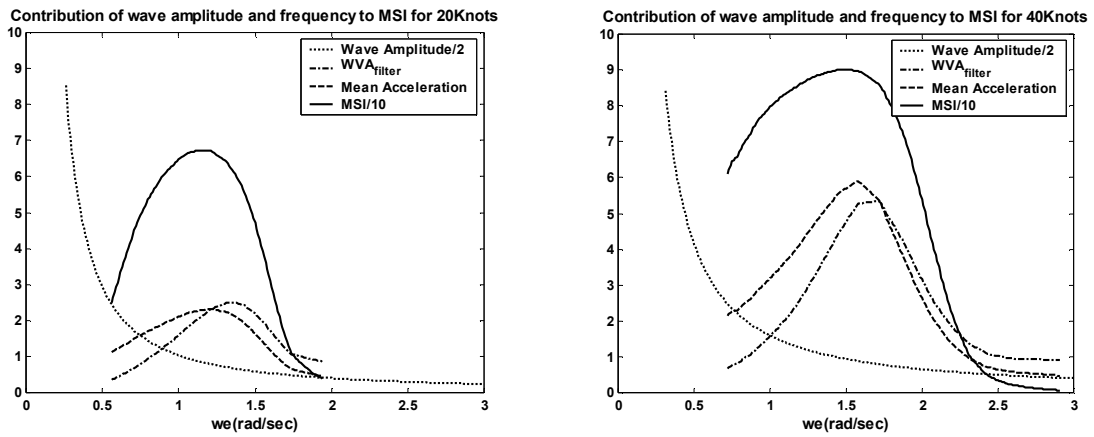
Figure 7. Contribution of waves to MSI in function of wave frequency (20 and 40 Knots)

Finally, carrying out the operations described by the block diagram of figure 6, the total MSI index is obtained integrating the above MSI envelope weighted by the density function associated to particular conditions (SSN, spectrum, speed and heading), figure 8 shows that total MSI can be obtained, in the a frequency-domain, from the area in dark.
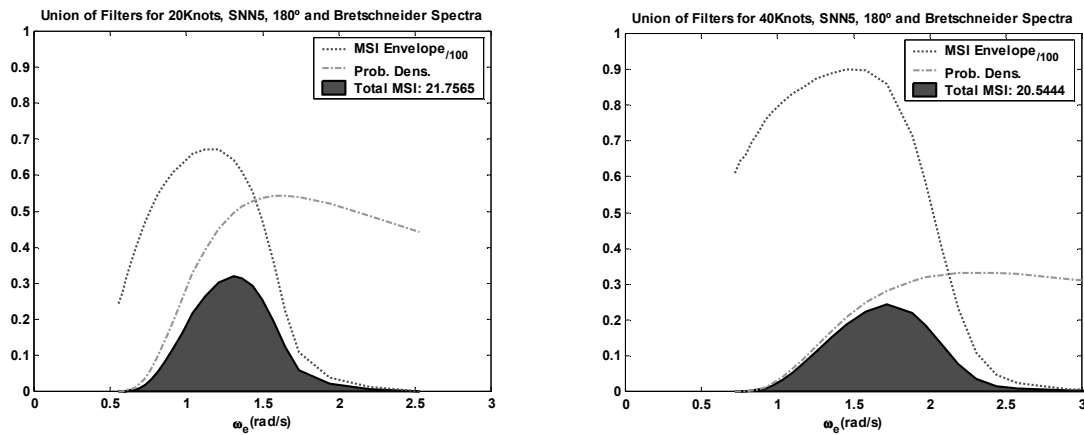
Figure 8. Computation of the total MSI for two different speeds.

3 APPLICATION OF KNOWLEDGE

3.1 Designing the Ship

On ship design time it is possible to obtain the RAO's of the ship using a CFD program. Using the algorithm presented in this paper it is possible to compute the total Sickness index in each place of the ship, for costal or open waters, for a several speeds and headings. Usually ships are designed to be used in some particular trips and the more frequent conditions of sea, speed and heading of this trip are known. It is possible optimize the ship design to work well on this conditions. Figure 9 shows the steps of this process. Figure 10 shows the sickness evaluation for head seas, and a SSN5 JONSWAP spectra.

| CAD Design (Mesh) | ⇒ | CFD Simulation (RAOs) | ⇒ | Sickness Evaluation (MSI) | ⇐ | Trip Requirements (SSN, Spectrum, Speed, Heading) |
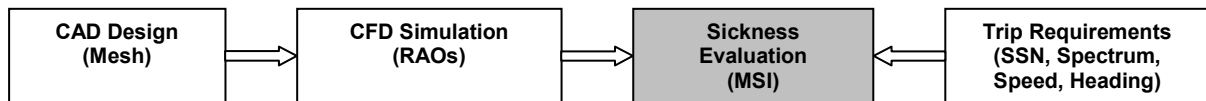
Figure 9. Steps to design a ship bearing in mind the sickness.
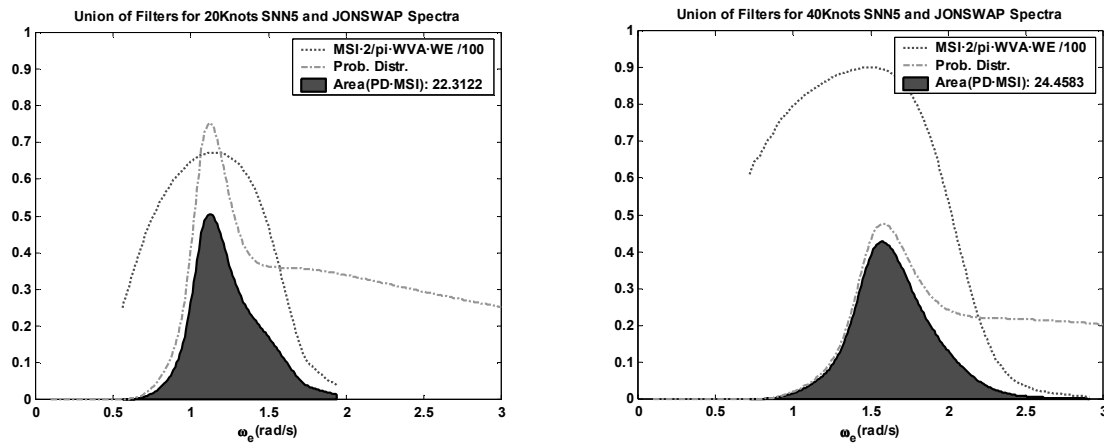
Figure 10. Filters coupling with JONSWAP statistics.

The performance of the ship from the sickness point of view is better if the two filters do not agree in resonance frequency. For example, Bretschneider spectrum, figure 8, generates less MSI than JONSWAP spectrum, figure 10, because the peak of JONSWAP agrees with the peak of the MSI. Ship's design must be optimized with respect to the operational conditions.

3.2 Improving a Built Ship

Sometimes the ship has been built or designed, and its operational range wants to be increased. It may be obtained by applying active control. To do this, it is necessary to use actuators like t-foils, flaps, fins, interceptors, stability tanks, etc. It is very important to optimize the characteristics and locations of the actuators in order to obtain the maximum motion reduction. Figures 8 and 10 show the band width and the main frequency that the actuators must affront. The band width of the problem is important for the control system engineer, because it determines the speed of the actuator and the controller design. Using the mathematical models of the ship [2] and the automatic control algebra, it is possible to close

the control loop, to obtain the ship controlled acceleration response. Using this new acceleration response, the total MSI may be computed to quantify the improvement.

3.3   Sailing the Ship

This knowledge of the sea-sickness can be transferred on sailing time to the master on screen. So, the information may be provided to the captain as figure 11 that shows local sickness indices on each place of the ship for two different headings, a) head seas and b) beam seas.
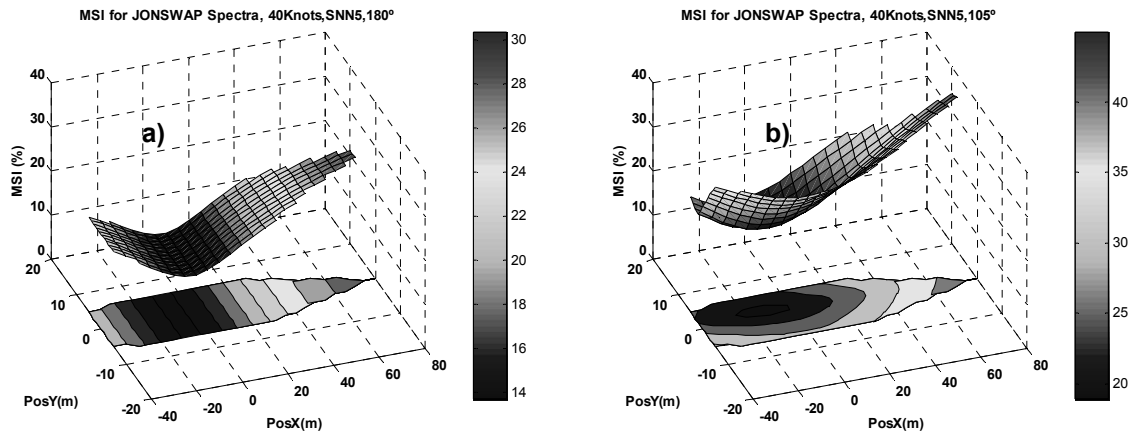
Figure 11. MSI on a desk of the ship, a) heading seas, b) oblique seas.

Figure 12 shows the master how to reduce the sickness index, in a particular place, slightly modifying the speed or heading of the ship. White lines show how the MSI changes when the speed or heading is modified. Of course the results agree with the practice because the heading is very influent on sickness. The figure shows the evolution of sickness for two different places, a) on the side near the bow, and b) on the side near the c.o.g. In case a) it is possible to reduce the sickness increasing the speed, this is not possible in case b).
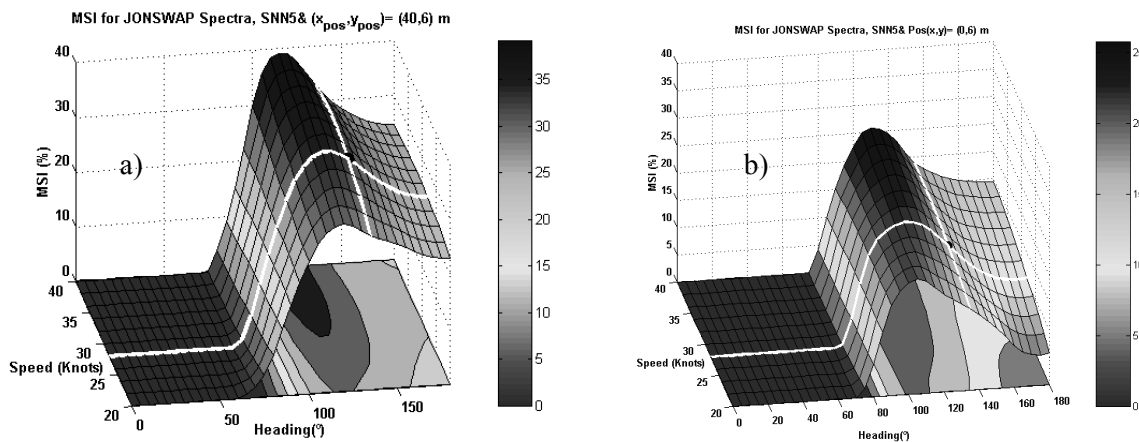
Figure 12. MSI on two lateral places, a) near the bow, b) near the c.o.g.

Mainly, it is important to alert if there is a heave resonance situation for a particular SSN, the peak of the MSI envelope and Wave Probability Density match up.

REFERENCES

[1]   LAERTIUS, D. Live of the Philosophers*, classical.*

[2]   ESTEBAN, S., DE LA CRUZ, J.M., GIRON-SIERRA, J.M. AND DE ANDRES TORO, B. 2000, Frequency-domain model of fast ferry vertical motions, *Proceedings RINA Intl. Conf. Hydrodynamics of High Speed Craft*, London, paper 18, 1-8.

[3]   O'HALON, J.F. and MC CAULEY, M.E. 1974, Motion Sickness Incidence as a Function of Frequency and Acceleration of Vertical Sinusoidal Motion, *Aerospace Medicine*, vol. 45 pp. 366-9.

[4]   LLOYD, A.R.J.M. *Seakeeping: Ship Behaviour in Rough Weather*. Gosport, Hampshire: A.R.M.J. Lloyd, 1998.

[5]   FOSSEN, T.I. *Marine Control Systems*. Trondheim : Marine Cybernetics AS, 2002.

[6]   ISO 8041:1990, Human Response to Vibrations – Measuring instrumentations, *International Organization for Standardization*, Geneve.

[7]   BS 6841:1987, Measurement and evaluation of human exposure to whole-body mechanical vibration and repeated shock. *British Standards Institution,* London

Chapter 9

A Legged Robot for Ship Building Applications

P. GONZALEZ DE SANTOS, E. GARCIA, M. A. ARMADA
Industrial Automation Institute-CSIC, La Poveda, 28500 Arganda del Rey, Madrid, Spain

Legged locomotion has been extensively investigated in the last two decades, during which time many walking machines have been built as test-beds for research purposes. Most of them are laboratory prototypes, but some machines have been tested in outdoors environments and under extreme conditions. Walking machine technology now seems to be ready to accomplish industrial applications. Thus, this chapter presents a legged machine for a real industrial application in naval construction processes. The main task of the walking machine is to provide full motion to a welding manipulator in a very complex scenario, the double hull of a ship. This scenario consists of cells fitted with stiffeners on the top, bottom, and lateral walls to reinforce the ship's structure. The legged machine moves through the cell grasping the top and bottom reinforcements rather than walking on the bottom plane. This improves the machine's stiffness and guarantees its stability. This chapter describes the walking machine's main structure, the leg configuration, and grasping mechanism to accomplish with the industrial working scenario. Features and functionality of the ROWER walking machine are finally reported.

1 INTRODUCTION

Industry is continuously encouraged to improve quality, productivity and labour conditions and, definitely, robotic systems are helping to improve these characteristics. However, traditional robotic systems cannot achieve some industrial applications, especially those involving mobility in complex environments.

In ship building activities, there exists a main stage in the ship erection process, which is the construction and assembly of huge ship blocks. This work is performed in highly automated workshops. Another important stage involves fitting the ship blocks together in the dry-dock after they leave the workshop. Blocks are arc-welded together, and the resulting scenario is so complex that work must be accomplish by operators using manual equipment. That means that the quality of welds, which depends on every operator, becomes quite irregular. In the second stage of the process the operators, handling manual equipment, need to stop frequently and productivity is very low. The weld length in this stage makes up 4 to 6 percent of the total weld length in a ship; however, it requires about 30 to 35 percent of the total weld manpower. Finally, the working conditions are very bad for the operator, who must work in closed cells with very bad ventilation and very thick fumes. These reasons led a team of shipyard companies and researchers to design and build an automatic welding system for ship

erection processes with the main aim of increasing productivity by increasing total arc time, improving weld quality and creating better working conditions for operators.

The overall system consists of a commercial welding system handled by a commercial manipulator. These subsystems are carried on a mobile platform that provides mobility in the working area. A stereo vision system finds the starting and ending points of the welding seam. All four subsystems are remote-controlled by a computer supervised by an operator located off the work site. The supervisor computer also contains a database with the geometric description of each working cell.

The main task of the mobile platform is to provide full motion to a welding manipulator in a very complex scenario, the double hull of a ship. This scenario consists of cells fitted with stiffeners on the top, bottom, and side walls to reinforce the ship's structure.

The complexity of the working scenario and the system mobility requirements made a walking machine the best choice for this application. Legged locomotion has been extensively investigated in the last two decades, during which time many walking machines have been built as testbeds for research purposes. Most of them are laboratory prototypes, but there are machines that have been tested in outdoor environments and under extreme conditions. Some of these prototypes have been mainly focused on space (1) and submarine tasks (2), where machine reliability is of paramount importance for the success of the mission. Such applications do not permit either an easy removal of some parts nor recovery of the machine after a subsystem breakdown. The ongoing applications of walking/climbing machines in industrial processes (3), (4) as well as especial applications on natural terrain (5), (6) demand reliability, speed and accuracy, but also maintainability.

Walking machine technology seemed to be ready to accomplish industrial applications, and with industrial considerations in mind, we investigated different machine configurations for our purpose in light of the end users' strict requirements, such as total weight, dimensions, payload, and assembly/disassembly capabilities. Finally, a four-legged machine able to walk by grasping cell stiffeners was envisaged as the best choice for our application.

Thus, this chapter presents a legged machine for a real industrial application in naval construction processes, and it focuses on presenting the project investigation into the mobile platform's configuration and design rather than presenting the whole project, in which three other companies were involved. The legged machine moves through the cell by grasping the top and bottom reinforcements rather than walking on the bottom plane. This improves the machine's stiffness and assures its stability. This chapter describes the walking machine's main structure, leg configuration, and grasping mechanism and how they cope with the industrial working scenario. Finally, the features and functionality of the ROWER walking machine are reported.

2 PROCESS DESCRIPTION

The ship erection process consists of three main activities: (a) Block construction in the workshop, (b) Block transportation to the dry-dock or slip-way and (c) Block assembly in the dry-dock or slip-way. The first activity consists in the fabrication of big blocks of the ship, as shown in Figure 1. This process is easily automated, and its productivity is relatively high. The third activity consists in connecting consecutive blocks in the dry-dock or slip-way by
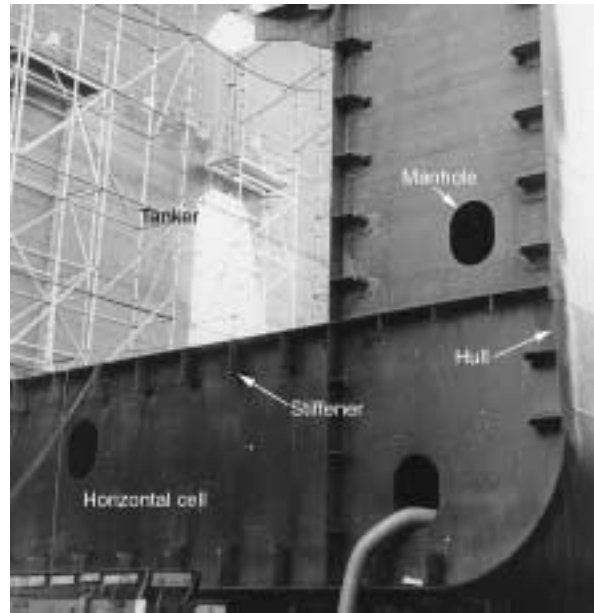
Figure 1. A ship block in the dry-dock

welding together all the longitudinal reinforcements and all the vertical bulkheads. In this way the whole ship is assembled as shown in Figure 2.

   For environmental safety, most ships, especially tankers and bulk carriers, are built with a double bottom and double hull so the cargo will not spill out if the hull is breached. This double structure forms cells all over the ship's hull (See Figure 1). A typical tanker bottom

Figure 2. A ship under construction in the dry-dock

cell (horizontal) can be up to 10 meters long, 4 meters wide and 3 meters high. The welding seams in these cells are mainly located on the walls, bottom, and stiffeners on the section of the junction plane as well as in the ceiling and bottom of a perpendicular plane. Therefore, the welding process can be defined as the welding together of elementary cells, and this can be considered as the working scenario for the mobile platform.

Summarizing, the scenario consists in a cell whose measurements may vary from about 7 to 10 meters long, 2 to 4 meters wide and 1.5 to 3 meters high. Longitudinal stiffeners form part of the ceiling and bottom of the cell to reinforce the hull structure. Stiffener height ranges from about 0.2 meters to 0.7 meters. The mobile platform must bear the welding system along the longitudinal and transversal axes of any cell in the defined range and help the manipulator reach the ceiling and bottom as well. To allow workers inside, the cells have a manhole measuring about 0.8 x 0.6 meters (See Figure 1). This feature is very important in the design of the overall system, because the volume of each subsystem must be constrained to the manhole's dimensions. Another constraint is that the weight of each subsystem (manipulator, welding system, mobile platform, vision system, etc.) must weigh less than 50 kg due to labour regulations on systems carried by operators. This is the reason why the mobile platform must be divided into different parts and assembled inside the cell. For our project's purposes, the reference cell is 10x4x3 meters, the top stiffeners are 0.635 meters tall, and the bottom stiffeners are 0.575 meters tall. In the top and the bottom of the cell, the stiffeners stand 0.88 meters apart. The requirements of mobility in a horizontal plane full of stiffeners make the scenario very hard for a wheeled or tracked vehicle to negotiate. Table 1 summarizes the main requirements for the walking machine.

Legged locomotion seems to be more adequate for mobility in this kind of environment than traditional vehicles. For this particular application, different leg configurations were envisaged as likely candidates for walking on the floor of the cell. The pantographic

Table 1. Main walking machine requirements

Requirement	Value
Dimension of working cells	Length: 7 to 10 m Width: 2 to 4 m Height: 1.5 to 3 m
Type of stiffeners	Bulb, T-stiffener and L-stiffener
Stiffener height	0.2 to 0.7 m
Number of consecutive stiffeners to be welded without moving foot positions	2
Maximum weight of every robot's part	50 kg
Machine assembly/disassembly time	15 minutes
Payload	130 kg

configuration was rejected because the ankle sweeps through a volume when propelling the body forward/backward or up/down (7), (8). This can cause the ankle to collide with a stiffener, and that must be avoided. This feature restricts the foot location area on the bottom of the cell too much. An orthogonal leg was also considered and finally selected. Its main advantage is that its vertical link can be set very close to the stiffeners without sweeping through any volumes when moving the body. Thus, the ankle will not crash into the stiffeners. In this process, the geometry of the cell, defined in the supervisor database, is known *a priori* to an accuracy of about ±20 millimetres. For welding, the manipulator must be placed most accurately by the mobile platform. Therefore, the mobile platform must be accurate enough to accomplish this task. This makes accurate positioning a new feature never before required in walking machines up to this accurate stage.

3 STRUCTURE OF THE ROWER WALKING ROBOT

3.1 Structure of the body

The structure of the body depends on the payload layout and the functionality of the manipulator. In the present case, the manipulator can work in both the up and the upside-down positions. However, it cannot work properly if it is wall-mounted. This feature led us to devise a manipulator mounted on a turntable able to rotate about the longitudinal axis of a U-shaped frame structure body (See Figure 3). Nevertheless, the problems concerning the manipulator and related welding equipment lie outside the scope of this chapter. Thus, a parallelepiped body structure will be assumed in the rest of this chapter. The body structure is made of welded aluminium plates. Every plate has a number of windows; by stripping off needless material, this design makes for a lighter-weight structure.

Although a six-legged machine provides very good stability, especially for industrial
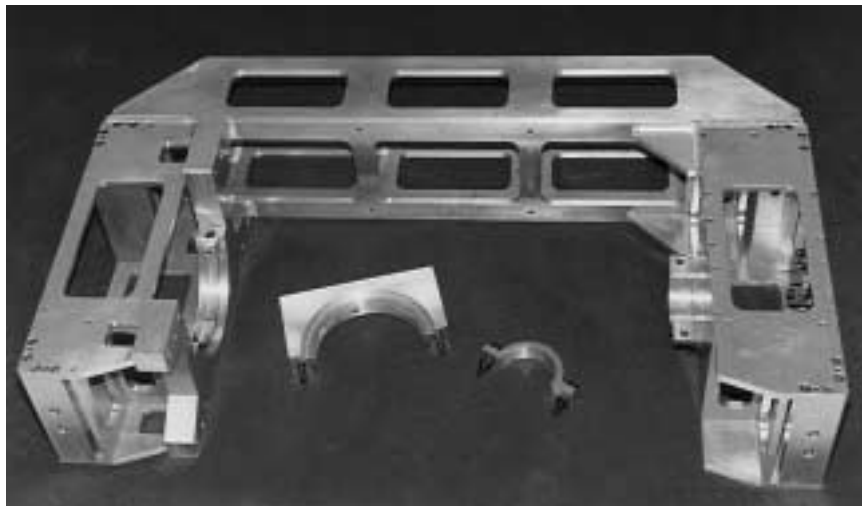
Figure 3. Body of the ROWER walking machine

applications, a four-legged mobile platform was chosen in order to minimize the machine's total weight, which is a top requirement in this application. Also, using four legs drastically reduces the final price, which is normally an important industrial requirement. This initial selection was considered the ideal solution for the final machine's structure, since there are no machine stability problems, as commented later on. The leg and the machine structures are sketched in Figure 4 and Figure 5, respectively, and discussed in the paragraphs below. Figure 5 also shows the working position of the machine with respect to the seam path and surrounding stiffeners (9), (10), (11).

3.2   Structure of legs and grasping device

As mentioned before, the orthogonal leg was considered best for this application. Thus, the
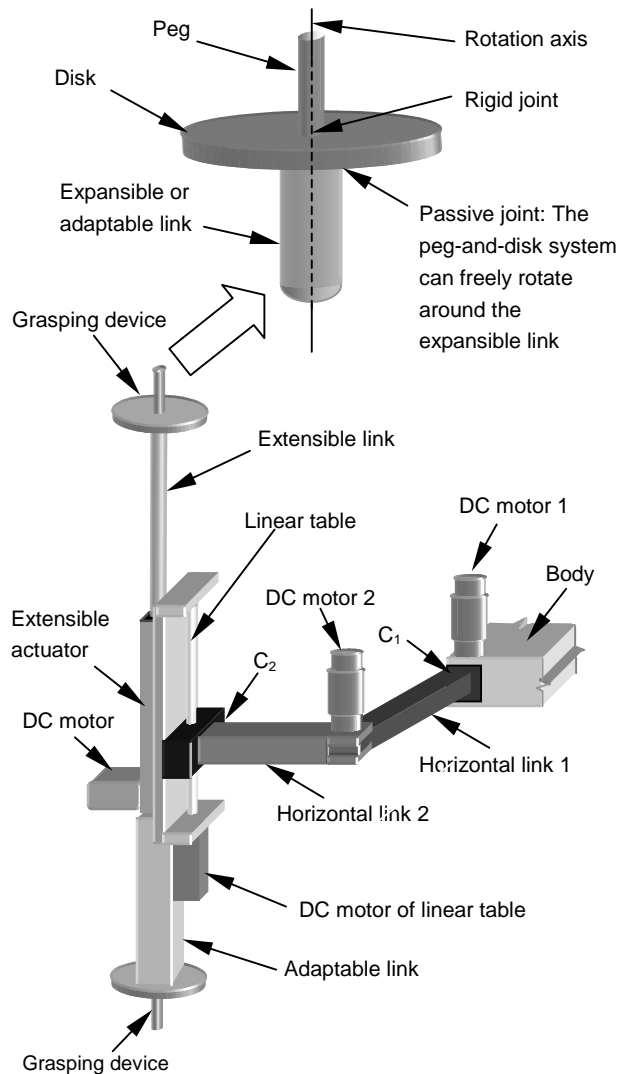
Figure 4. ROWER leg

leg consists of a vertical link actuated by a prismatic joint and two more degrees of freedom to produce horizontal motion. The different combinations of joint types considered --for the first two joints-- included the rotation-translation joint (as in the Ambler walking machine (1)) and the rotation-rotation joint (SCARA-like robot). The latter was finally selected because it provides greater speed than the other, since electric rotary joints are normally faster than electric prismatic joints.

An additional problem with the chosen leg structure was the required size of the vertical link, which had to be two meters high in order to place the manipulator close enough to the ceiling of the cell. This long link and the heavy payload the machine must carry (about 130 kg) make the vertical link very prone to flexion and vibration, especially when the body is located at its highest position. This feature also jeopardizes the machine's static stability. To overcome this problem, an additional structure was proposed, to walk by grasping the stiffeners. The walker structure is basically the same, but a very simple grasping mechanism was added to every vertical link. This grasping mechanism consists of two grasping feet and a prismatic actuator. The grasping foot consists of a disk and a peg that can rotate passively around a vertical axis as shown in Figure 4. A radial symmetrical device is necessary to avoid having to re-orient the device before it grasps the stiffener. These feet are placed at the top and bottom of the vertical link. The prismatic actuator is located at the top of the vertical link, and its function is to press the top foot against the top stiffener as shown in Figure 5. Also, this device can be retracted to let a leg pass between the top and bottom stiffeners. This simple foot design features the advantage of being able to clasp stiffeners of different shapes, such as bulbs, T-stiffeners and L-stiffeners, which are the most common stiffener shapes in ship construction.

Figure 4 identifies the different elements in a leg. The leg was designed to use commercial subsystems as much as possible. The SCARA structure of the leg basically consists of two horizontal links made of commercial aluminium profiles, which are actuated by DC motor and Harmonic-Drive reducers (100 Watts) to eliminate the backlash. The vertical actuator is a DC motor (250 Watts) that rotates the lead-screw of a commercial linear table.   The extensible upper link consists of a commercial electrical cylinder.   Some parts of the transmission mechanisms and the leg attachments to the body are made of steel or special 7075 aluminium to lighten the weight as much as possible.

All four legs grasping the stiffeners on opposite sides, as in Figure 5, accomplish grasping. With this final machine configuration, there are no stability problems because the grasp is firm; however, a stiffener detection problem arises. That means it is necessary either to know very precisely the position of the stiffener where a foot has to be located, or to know the stiffener's approximate position and to detect it accurately using some kind of sensor. As mentioned before, the cell's geometry is known *a priori*, but cell construction accuracy is not good enough for walking in a *blind* mode, and stiffener detection sensors proved absolutely necessary.
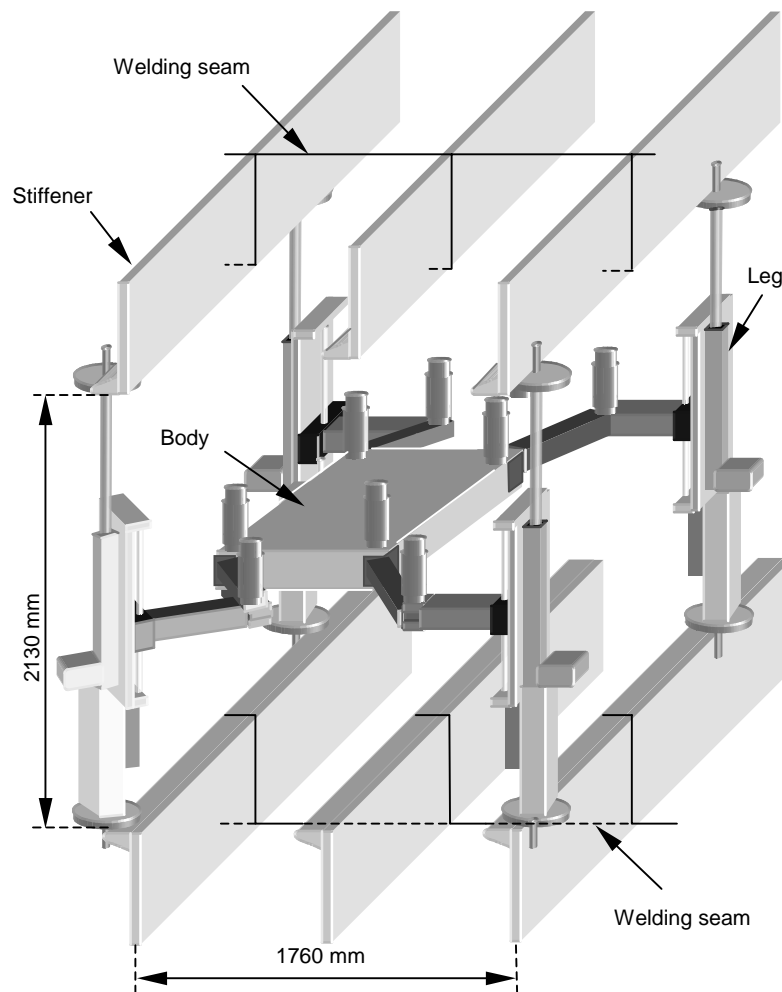

Figure 5. Structure of the ROWER walking machine

3.3 Assembling/disassembling the machine

The maximum operator-carried weight and manhole size requirements are satisfied by all project subsystems except the mobile platform. Thus, the mobile platform must be taken apart so it can fit through the manhole into the cell. The easiest solution seems to be to break the mobile platform down into smaller modules. That means building the machine in modules or series of standardized components which work together in the whole system. The first approach is to divide the machine into body and legs, making it necessary to handle five main pieces. The body has been defined to satisfy weight and dimension requirements (See Figure 3). The leg design satisfies the dimension requirements easily, but not the weight requirements, so one more leg breakdown is required. The final solution is to divide the leg into two parts: vertical link and horizontal links; hence, the walking platform is divided into nine different parts.

The mobile platform is intended to be mounted/dismounted in different cells; therefore an easy mechanism for assembling/disassembling is also required. Two aspects have to be considered. The first is how to break the structure into different pieces. The second is how to break up the power/signal system distributed along the leg structure. These considerations have been taken into account in the design of the ROWER walking machine that is configured to be quickly assembled/disassembled for operational reasons. The solution is simply to provide bolts and guides for mechanical assembly and connectors for electrical connections at points C1 (four bolts and two connectors) and C2 (five bolts and one connector), as indicated in Figure 4. These easy-to-handle elements let a pair of operators fix a leg to the body in less than three minutes. A similar time is required to dismount a leg.

3.4 Dimensions of leg and body

To select the dimensions of every main piece, it was necessary to consider not only the minimum and maximum dimensions of the cell, but also the mobility requirements of the mobile platform's body when the feet are clasped to the stiffeners. The mobile platform's movement through the cell is basically very slow. Hence, in order to optimize process time, the manipulator (i.e. the centre of the body) requires maximum displacement to weld as much as possible without moving the feet. This body movement was stated as ±0.4 meters along the longitudinal axis of the cell, ±0.2 meters along the transversal axis of the cell, and about 0.5 meters along the vertical axis of the cell. The mobile platform's workspace is measured when the right and left legs of the mobile platform are grasping alternating stiffeners (See Figure 5). To find the mobile platform's workspace, the length of the horizontal links has been computed in simulation as about 0.630 meters. The stroke of the extensible link has been selected as 0.5 meters. Thus, the mobile platform can be adapted to work in many different cells. The prismatic joint in the vertical link provides a half-meter run, as required by cell specifications. The dimensions of the body were found using the dimensions of the manhole and the layout of the subsystems on board the body. Finally, the body was defined as a 0.56x1.2x0.25-meter parallelepiped. Table 2 summarizes the dimensions of the ROWER mobile platform. The leg elements in this table are defined in Figure 4.

4   CONTROL SYSTEM

4.1   Hardware/software

The control hardware is envisaged as a traditional robot control system. It is located and distributed on board the body of the machine. The main controller is a PC-based computer that works as a stand-alone system. This controller is connected via a serial line to the supervisor computer. The joint controllers are special tailored cards based on the LM628 micro-controller, which provides a programmable PID control filter and a trajectory tracking command to follow joint trajectories, as specified by the host computer. Drivers, also tailored for this application, are based on the PWM technique. The mobile platform is powered through a tether containing DC power supply, communication with the supervisor controller and welding system power supply. The mobile platform pulls the tether during motion. It is attached to the mobile platform in such a way that it does not interference with the area swept by the feet.

The control software is written in C++ language, and it runs on a real-time multitasking system for the DOS operating system. This system is a library to be linked with the application program. It offers a number of functions for managing tasks, semaphores, mailboxes, interrupts, and so on. The main program may be divided into the following modules: host communications, gait generator, supervisor system, controller communications and sensor system. This last module is mainly in charge of level sensors and positioning sensors.

4.2   Sequence of motions

Table 2. Dimension, weight and payload of the ROWER walking machine

Body	Height	0.25 m
	Length	1.2 m
	Width	0.56 m
	Weight	50 kg
Leg	Vertical Links: Adaptable Displacement of linear table Displacement of extensible link	0.535 m 0.5 m 0.5 m
	Horizontal Links	0.63 m
	Weight	65 kg
Mobile Platform	Total Weight	310 kg
	Payload	130 kg

The gait generator is one of the main modules of the controller. It takes care of the leg and body sequence of motions to propel the mobile platform forward, backward and sideways. When the mobile platform is clasped to stiffeners, no static stability problems appear. The body only moves when all four legs are clasped to stiffeners. The translation of the mobile platform from one pose to the next is achieved by moving legs one at a time. One leg clasping the stiffeners (See Figure 6-1) is released in the recovery of the expansible link. Then, the vertical link is lifted and placed in the middle of the top-bottom stiffener clearance (See Figure 6-2). In this pose, the leg travels at high speed to a location close to the next stiffener. In this location, the extensible link is extended and the vertical link is lowered until the leg cannot pass through the top-bottom stiffener clearance (See Figure 6-4). Now the speed is decreased, and the leg moves forward until the next stiffener is detected (See Figure 6-5). At this stage, the vertical link is lowered until the foot contacts the bottom stiffener, and the extensible link is expanded until the grasping process is completed (See Figure 6-6). With this leg motion algorithm, the full motion of the mobile platform is achieved by first moving in sequence the two front legs, then propelling the body forward, and finally repeating the leg motion procedure with the rear legs. The movement of the mobile platform parallel to the
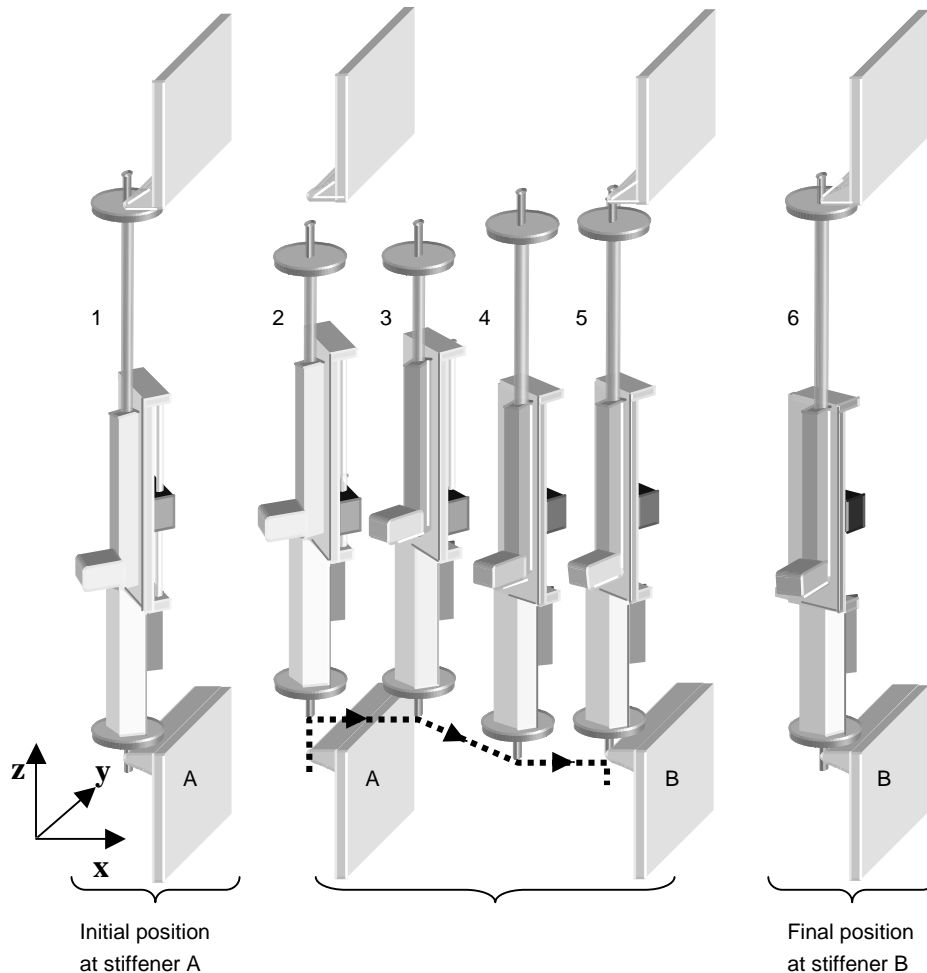

Figure 6. Leg motion sequence for releasing one stiffener and clasping the next

stiffeners is accomplished in a similar manner. Also, this structure allows the body to rotate through about 40 degrees without moving the feet. This motion is sometimes required for the manipulator to get to hard-to-reach areas. Full machine rotation can be accomplished by moving the body and legs in sequence. For a 90-degree turn, the machine must perform 8 leg motions and 3 body rotations. Hence, the machine exhibits high mobility to accomplish the required welding tasks.

4.3   Stiffener detection

It was mentioned before that the ROWER walking machine could move over the stiffener because the cell geometry is *a-priori* given. However, shipbuilding procedures do not guarantee the accuracy required for our purpose; hence the use of sensors to detect stiffeners with precision is essential.

Some problems arise at this point. The first one is that the orientation of the foot and the leg ankle change as the leg reaches the stiffener (See Figure 6); therefore, it is not possible to locate a simple range or contact sensor on the foot/ankle of the leg to detect the stiffener. Many simple sensors in a circular configuration are ruled out because of price and accommodation. Another problem is the installation of electrical cables in a freely rotary foot and the installation of cables from connector C2 to the foot (See Figure 4). Cables on the bottom foot have no special problems, but cables on the top foot need a floating hose to allow the extensible link to change its length, and that will jeopardize functionality.

All these problems can be overcome by using a set of positioning sensors already installed in the machine: the joint encoders. The idea is to monitor the positioning errors of every encoder on a leg to detect the foot/stiffener contact. The advantages of doing so are these:

1. No additional sensors are needed. The encoders are already installed because they are necessary for joint positioning control tasks.

2. No extra electrical cables are needed. Encoders are adequately and securely connected to the controller.

3. The method and the algorithms are useful for detecting stiffeners in the approach phase and securing the grasping as well, i.e. to detect the stiffener in the downward motion of the vertical link and the upward motion of the extensible link. This saves two contact sensors or force sensors as well.

To illustrate this method, an experiment has been conducted which consists in moving a leg against a stiffener as indicated in Figure 6 (See leg positions 4 and 5). The initial foot position is $(x, y) = (890, 1160)$ mm, and the final commanded foot position is $(x, y) = (890, 960)$ mm, where this y component is supposed to be further the stiffener position. The foot is commanded to follow a straight line parallel to the x-axis of the robot's body reference frame (perpendicular to the stiffeners) and the foot position and joint positioning errors are recorded at a given frequency. The controller analyzes the joint positioning errors and stops foot motion when it detects an error greater than a given threshold. In this stiffener detection process only the joints of the horizontal links are involved. Figure 7 shows the joint positioning errors when a leg hits the stiffener at low speed. The joint positioning errors are small at first, but they grow quickly when the leg contacts the stiffener.
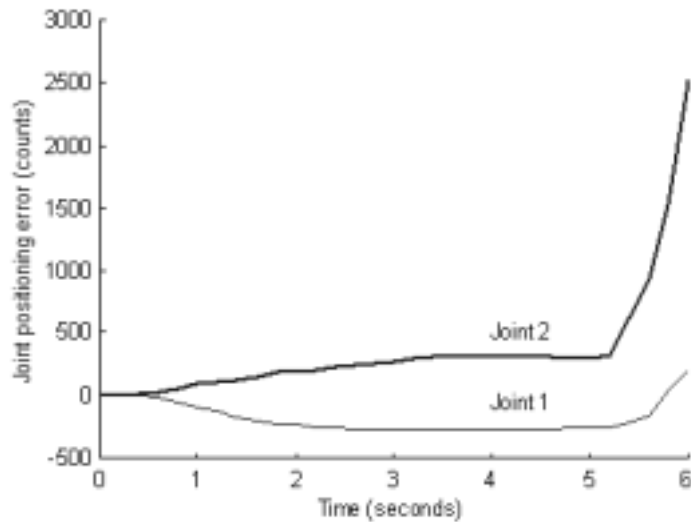
Figure 7. Joint positioning errors during the stiffener detection process

Figure 8 shows foot position along the defined trajectory. The *x* component does not change (foot motion follows a straight line parallel to the *x*-axis of the body) except at the end of the trajectory. At this point the leg exerts force against the stiffener, and the *x* component of the foot re-accommodates because of the flexion and backlash in the walking machine structure. The *y* component of the foot trajectory shows how the leg accelerates, then it moves at a constant speed, and finally it decelerates rapidly when the stiffener is detected. The positioning error still grows, but the final position does not change. At this point it is assumed that the stiffener has been detected, at $foot_y = 961$ mm, and the procedure of locating the lower foot on the stiffener is performed in a similar way. Finally the detection of the upper foot against the top stiffener is accomplished following the same method.

Figure 6 illustrates how a leg grasps the stiffeners when they are perfectly aligned. Normally, stiffeners are neither fully aligned nor the distance between top and bottom stiffeners is constant. In the first case the system still works because the leg is just stopped when one of the two feet contacts a stiffener (top or bottom). In this situation the peg of the
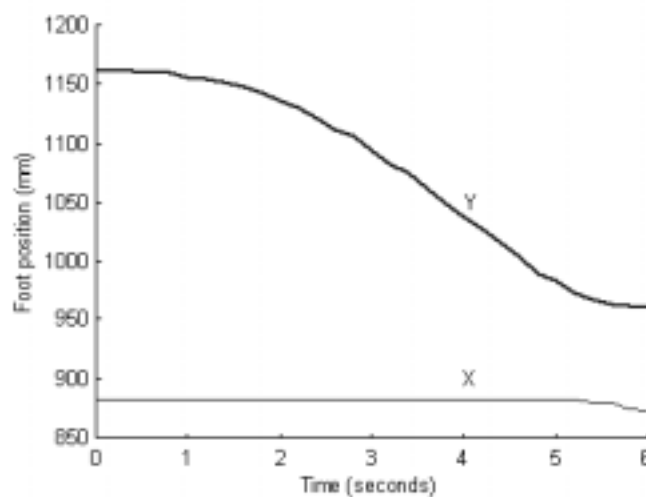
Figure 8. Foot position along the defined trajectory

141

other foot will be a few centimetres away from the stiffener, but the disk of the foot can contact the stiffener and exert the required force due to it has a big radius of about ten centimetres. It is easy to understand from figure 6 that a leg can grasp the stiffeners even if one of them is away from the plane of the other less than the radius of the foot disk.

The second problem is easier to overcome because the extensible link is moved until the foot contacts the stiffener. Therefore, if the distance between top and bottom stiffeners is less than nominal, then the grasp will be achieved earlier than expected. On the other hand if the distance is bigger than nominal, then the grasp will be performed latter than expected, but it will be accomplished because the extensible actuator has a maximum extension that makes the leg bigger than the top-bottom distance. Of course, if either the foot of the extensible actuator reach the commanded final position without detecting any stiffener then the system will be stopped and the operator will be warned.

5   PROTOTYPE AND RESULTS

Figure 9 shows a picture of the ROWER walking machine in a double bottom cell at Fincantieri shipyard facilities, Italy. The machine is carrying the manipulator, welding tools and accessories. The leg, with the dimensions defined in Table 2, can develop a speed of 0.15 to 0.4 meters per second depending on the position of the trajectory in the leg workspace. The speed achieved by its vertical link is about 0.1 meters per second throughout its workspace.

Figure 9. The ROWER walking machine

With this real leg, the task of moving it from one stiffener to the next is accomplished in about 5.5 seconds, while foot grasping and foot release take about 5 and 7 seconds, respectively. Thus the movement from one welding pose to the next is achieved in about 80 seconds. By "welding pose" we mean the pose of the machine on alternating stiffeners, as shown in Figure 9. These speed figures let the machine travel along the cel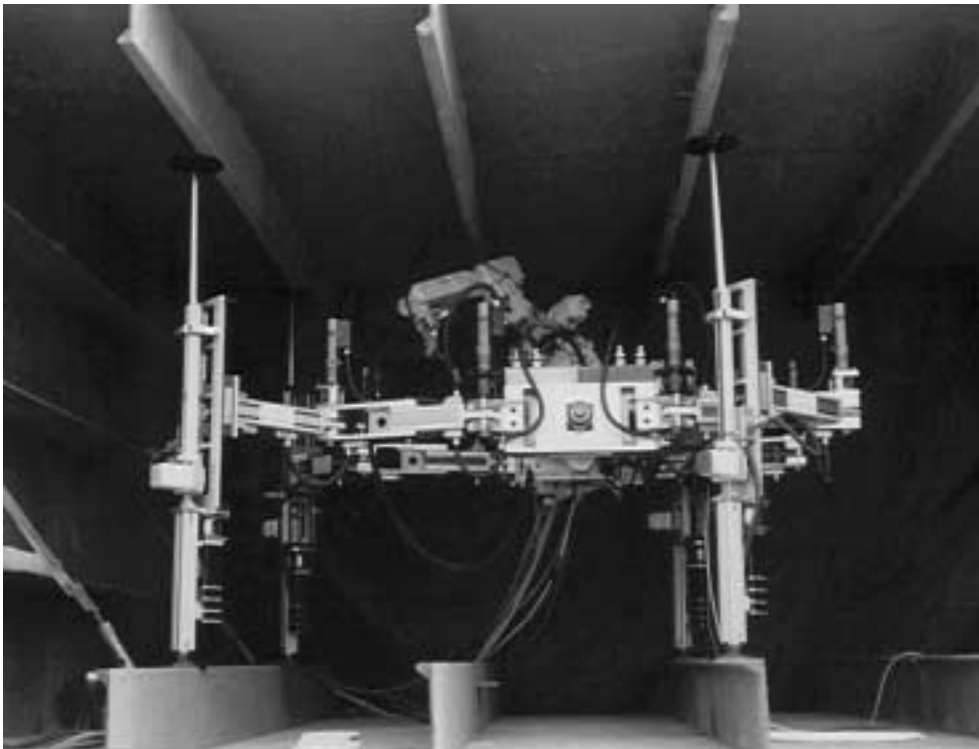l at an average speed of about 13 millimetres per second, which seems slow. The machine's speed is not significant, however, if compared to the speed of the welding process achieved by a human operator. Note that for a single foot pose (the body of the machine can move ±0.4 meters along the y-axis and ±0.2 meters along the x-axis) there are 4 to 5 meters of multi-pass welds that an operator would take a long time to perform. Furthermore, the arc welding time of a robotic system can be half the manual arc welding time. In addition to these features, other important improvements are made in welding quality (much higher with a robotic system than with a human operator), less hazards and better operator's working conditions. These are the

Table 3. Features of the ROWER walking machine

Body mobility	X: ±0.2 m Y: ±0.4 m Z: ±0.25 m
Body speed	0.5 m/sec.
Leg speed	0.7 m/sec.
Foot grasping time	5 sec.
Foot releasing time	7 sec.
Machine average speed	13 mm/sec.

main improvements achieved by this automatic welding system.

Accuracy is paramount in such a big machine, so special attention was paid to the design of links, mechanical transmissions and gears. As a result, the machine displays positioning errors of less than ±10 millimetres, which is good enough to perform motion all over the working cell. The misalignments between theoretical and actual walking machine positions are corrected with the stereo vision system handled by the manipulator and used to detect the starting and ending welding seam points with precision. The main final features of the ROWER walking machine are summarized in Table 3.

6   CONCLUSIONS

Walking machines have been developed for years as test beds for legged locomotion research. Now technology is mature enough to accomplish industrial applications. This chapter proposes a legged machine to provide a mobile welding system in a complex industrial environment, the double bottom of a ship, during the ship erection process. The machine uses the characteristics of the ship's geometry to increase its own stiffness and to guarantee walking stability. This chapter has described how the machine's structure and

dimensions have been tailored to accomplish tasks in the working scenario. Algorithms for gait generation and stiffener detection without using additional sensors have been outlined. The machine has been tested in a shipyard under real working conditions, and the functionality of its working principle has been positively validated. By increasing the welding arc time this system reduces to 1/3 the total working time if compared with the work done by human operators.

Although the general evaluation of the ROWER legged robot has been positive, shipyards have criticised the system as difficult to operate by a non-qualified worker. Therefore, the system needs some further modifications to simplify the man-machine interface as well as provide the global system with the compulsory industrial requirements.

ACKNOWLEDGMENT

REFERENCES

(1)   Bares, J. et al, "Ambler: A walking robot for autonomous planetary exploration," *IEEE Computer*, June 1989, 22(6), pp. 18-26.

(2)   Ishino et al. "Walking robot for underwater construction," *Int. Conference On Advanced Robotics*, 1983.

(3)   Grieco, J.C., Prieto, M., Armada, M.A., and Gonzalez de Santos, P., "A six-legged climbing robot for high payloads," *Proceedings of the 1998 IEEE International Conference on Control Applications*, pp. 446-450, Trieste, Italy, September 1998.

(4)   Byrd, J.S. and DeVries, K.R., "A six-legged telerobot for nuclear application development," *The International Journal of Robotics Research*, Vol. 9, No. 2, pp. 43-52, April 1990.

(5)   Bares, J. and Wettergreen, D., "Dante II: Technical description, results, and lesson learned," *The International Journal of Robotics Research*, Vol. 18, No. 7, pp. 621-649, July 1999.

(6)   Halme, A. and Hartikainen, K, "Designing the Control System of an Advanced Six-Legged Machine," In: Gray, J. O. and Caldwell, D. G.*, Advanced Robotics & Intelligent Machines*, London 1996, The Institution of Electrical Engineers, pp.177-190.

(7)   Hirose, S., "A study of design and control of a quadruped walking vehicle," *The International Journal of Robotics Research*, Vol. 3, No. 2, pp. 113-133, summer 1984.

(8)   Pugh, D.R. et al, "Technical description of the adaptive suspension vehicle," *The International Journal of Robotics Research*, Vol. 9, No. 2, pp. 24-42, April 1990.

(9)   Gonzalez de Santos, P., Armada, M.A. and Jimenez, M.A, "Walking machines: Initial testbeds, first industrial applications and new research," *Computing and Control Engineering Journal*, Vol. 8, No. 5, pp: 233-237, 1997.

(10) Gonzalez de Santos, P., Armada, M.A. and Jimenez, M.A., "An industrial walking machine for naval construction,*" The IEEE International Conference on Robotics and Automation, Albuquerque*, NM, April 1997.

(11) Gonzalez de Santos, P., Armada, M. and Jimenez, M.A., "Ship building with ROWER", *IEEE Robotics and Automation Magazine*, Vol. 7, No. 4, pp. 35-43, December. 2000

Chapter 10

Ship Steering Control

F. J. VELASCO*, E. LÓPEZ**, T. M. RUEDA*, E. MOYANO***
*   Dpto. Tecnología Electrónica e Ing. de Sistemas y Automática. U. Cantabria (Spain)
**   Dpto. Ciencias y Técnicas de la Navegación, Máquinas y Construcciones Navales. UPV/EHU (Spain)
*** Dpto. Matemática Aplicada y C. de la Computación. U. Cantabria (Spain) .

This chapter begins with a historical review of the various control methods used for ship steering. It then goes on to describe briefly the various elements which make up the control system, starting with a general description and moving on to a more detailed description of the elements and objectives of the steering control. Next, the mathematical model of a ship is presented, including the description of both the linear and the non-linear models most widely used in ship steering. Finally, the course-changing manoeuvre control for two ships is presented, developed by the authors as part of the research projects of the CICYT of Spain. In the first case, three different control techniques are applied: Classical controllers tuned using Genetic Algorithms (GAs), Quantitative Feedback Theory (QFT) and Internal Model Control (IMC), and a comparison is made of the results obtained with each system. In the second case, the design of classical controllers is described, tuned using GAs for the course-changing manoeuvre for a container ship. To describe the dynamics of the ship, a mathematical model of 4 degrees of freedom is used, and the same model is also used both for the simulation and for the design of the controllers.

1 INTRODUCTION

The manual steering of ships, especially on long-distance trips and under adverse meteorological conditions can be tedious and tiring. The application of a certain degree of automation is thus desirable, as has been acknowledged for a number of years now. Automatic ship steering control dates from the early nineteen hundreds, as a continuation of the invention of the gyrocompass. Fossen, in (1), describes the development of the gyrocompass and its influence on the evolution of autopilots. Allensworth (2) points out that the first electrically driven gyroscope is normally accredited to C. À. Bohnenberger in 1810 although the first one tested by G. M. Hopkins was in 1890. The development of the electrically driven gyroscope was motivated by the need for more reliable navigation systems for the new steel ships and battle submarines. A magnetic compass, as opposed to a gyroscopic compass, is extremely sensitive to the magnetic disturbances which commonly arise in submarines equipped with electrical devices. At the same time, Dr. H. Anschutz in Germany and Elmer Sperry in The USA worked on a practical application of the gyroscope. In 1908, H. Anschutz patented the first gyroscope, while three years later, Elmer Sperry

created a patent for his ballistic compass which included vertical damping. In 1911, Elmer Sperry built the first automatic mechanism as an application of the gyrocompass to ship steering and to the closed loop control (2), (3). This device, named "Metal Mike" or metal helm, was an autopilot guided by a gyrocompass. "Metal Mike" emulated well the behaviour of an experienced helmsman, and included a compensation for variable sea conditions using feedback control and automatic gain adjustments.

The work presented by Minorsky (4) in 1922 on automatic ship control was another of the important contributions of the emerging literature on the general subject of ship steering. In the same year, Sperry (5) presented an automatic ship steering control system. These first autopilots were of a completely mechanical construction and supplied a corrector signal to the rudder which was proportional to the heading error. In order to prevent oscillatory behaviour, a low gain was selected so that the device could only be used for course-keeping, for which there was no need for a great accuracy in the response. The next improvements were the inclusion first of a derivative term for the heading error and then another integral term which led to the proportional-integral-derivative (PID) controller.

The commercial development of the PID algorithm significantly improved the capacity of the controller and almost all of the autopilots in service up to the decade of the eighties were based on this control algorithm (6). These classical autopilots were basically PID controllers whose adjustment was described in terms familiar to the seaman. In this way, any adjustment required in the parameters of the autopilot could be carried out by users who did not have any in-depth knowledge of the principles of automatic control. For example, as well as the proportional action "rudder·", the derivative action "counter rudder" and the integral action "automatic permanent helm", adjustments called "rudder-limit" and "weather" often appeared on the autopilot console. "Rudder limit" is a control which restricts the maximum rudder applied and is used mainly in course-changing situations in order to limit the induced roll angle. The "weather" adjustment determines the dead bandwidth deliberately introduced into the telemotor system in order to suppress the high-frequency movements of the rudder caused by the waves. Through the manual adjustment of the PID parameters, different sailing conditions can be taken into account (the various load situations, speed and atmospheric conditions).

Although the use of an appropriate nomenclature made the manual adjustment of the autopilot parameters simple for crew members who were not experts on control techniques, these parameters were often, in practice, left fixed. This led to a deficient behaviour when, on varying the operating conditions, the ship dynamics changed. Moreover, most of these autopilots could only be used for course-keeping at the ship's normal cruise speed. More important still, the relation between the controller parameters and the criteria adopted as the measurement of the ship's behaviour in course-keeping mode. For example, the selection of the best relation between accuracy (which will minimise the distance sailed) and the control effort (movement of the rudder which will produce an additional dragging force and the consequent loss of speed). However, this consideration is not always the same and is very difficult to deduce for the crew members. In different sailing conditions, different priorities can be designated between accuracy and control effort. When the ship is sailing in restricted waters, accuracy must be the main objective, while on the open sea, the minimisation of fuel consumption may be considered more important. Also, some of the controller parameters,

146

when combined with others, may produce effects which worsen the behaviour of the ship course-keeping. For example, the adjustment of the dead band "weather" was designed to suppress small amplitudes of high frequency of the rudder movements produced by disturbances in the sea state. However, low-frequency or low amplitude heading errors are also suppressed by generating a low accuracy in the course-keeping.

It is obvious therefore that the behaviour of the classical autopilots is far from optimum even for fulfilling the relatively simple demand for maintaining a fixed course in open sea conditions. These limitations are far greater when a course-changing manoeuvre or other manoeuvring situations are performed. This meant that in the nineteen-sixties, the demand arose for a more sophisticated autopilot.

The most popular approach in response to the above demands was the Linear Quadratic (LQ) controller, in which the controller parameters are selected to satisfy certain optimal criteria expressed as a cost function. For example, in (7) to (10) several different cost functions are proposed in which the deviations in the rudder and the yaw, fuel consumption, etc, are taken into account. Although the LQ technique fits in very well with the formulation of the course-keeping control problem and would seem more robust for changes in the parameters, the nineteen seventies saw the introduction of adaptive control techniques such as the reference model controller (11) and (12) or the auto-tuned controller (13) and (14), which are more appropriate for the formulation of the course-changing problem. These algorithms proved attractive because of such important advantages as the improvement in fuel consumption, the increase in the ship's speed and the reduction in the manual adjustments for compensating for operating changes and environmental conditions. At present, adaptive autopilots combined with other control techniques are still an important area of research (15) a (20).

Parallel to the adaptive approach where the controller parameters are constantly adjusted to acquire the optimum cost function, robust LQG and H-infinity techniques are applied in order to find the control parameters capable of guaranteeing an acceptable behaviour in a wide range of operating conditions (21)to (23).

As well as LQG and H-infinity techniques, other techniques have been applied since the nineties, such as the non-linear control technique (1). Also, encouraged by the advances in computer technology, more sophisticated algorithms have begun to be applied based on neural networks and fuzzy logic techniques. In (24) a thorough review of the development and use of these autopilots is presented. Similarly, new optimisation methods are being used now such as GAs for the optimal tuning of controllers (25) and (26) and new control methods such as QFT (27), IMC(28), or Predictive Control (29) applied to steering control and the stabilisation of ships.

2 SHIP STEERING CONTROL

The control of the course of a ship is essential for reaching a specific geographical point, for following a planned trajectory or for making any course change. Ship steering control is performed by acting on the rudder and/or any other devices which allow the desired trajectory to be obtained. This action varies according to the type of ship (petrol tankers, container ships,

ferries, warships), the sailing conditions (ship speed, loaded or ballast, through restricted zones etc.) and the environmental conditions (wind, waves and currents).
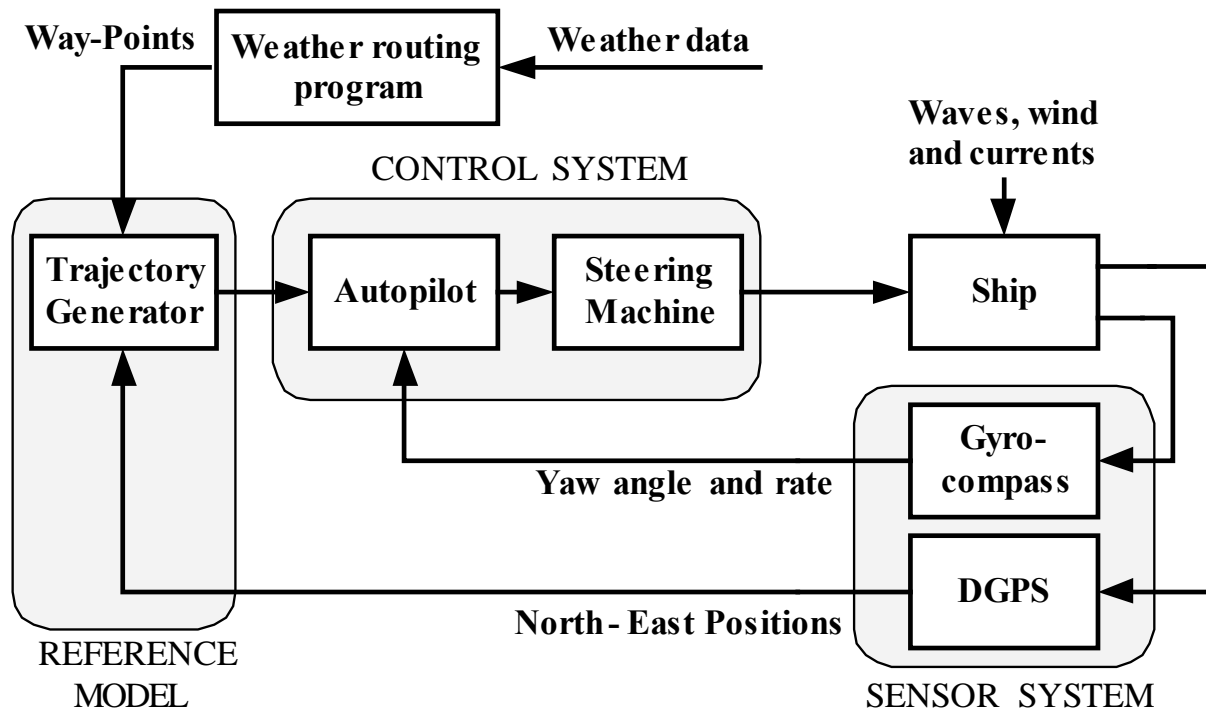

Figure 1. Ship steering control system

Figure 1 shows a general block diagram of a ship steering control system made up of a reference model, a sensor system and a feedback control system. The reference model receives the data on the position and speed of the ship from the DGPS (Differential Global Position System) and also receives external data provided by an operator (Deck Officer) and other data concerning the environmental conditions (height and slope of the waves and speed and direction of the wind and currents). The reference model computer processes the information and supplies the results as the reference input (desired course) for the ship steering control system. The control system also receives information supplied by the measurement system and determines the forces and moments which are to be supplied to the ship in accordance with the established control objective, in most cases together with the reference model system.

In ship steering control, we should distinguish between two main control objectives: the constant maintenance of a previously determined course to navigate between two points or 'course-keeping', and the undertaking of a change of course, or 'course-changing manoeuvres) as a specific case of the more general 'trajectory tracking control' in which the position and speed of the ship must perform the monitoring of reference signals which vary in time.

2.1 Course control

This chapter focuses exclusively on the ship steering control system considering it as a single input – single output (SISO) control system. Thus, the ship steering system in Figure 1 can be presented in the more simplified form shown in Figure 2. The command applied is ψ_r, which

represents the reference heading, ψ_d is the desired heading and ψ_e is the heading error. The control signal of the controller which acts as a command to the steering gear is δ_c and represents the rudder angle required to correct the deviation from the heading. The actual value of the rudder angle is δ and ψ is the actual ship's heading angle (all in degrees). A description is made below of the three blocks of the control system, leaving the description of the mathematical models for the following section.
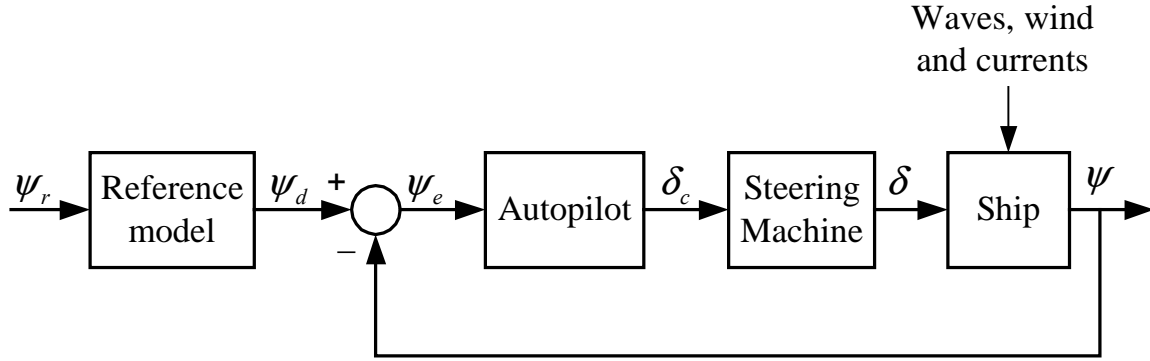

Figure 2. Block Diagram of the ship steering system

2.1.1 Ship autopilot

An autopilot is a ship steering controller, which acts within the control loop to handle the rudder in order to reduce the error between the desired heading angle ψ_d and the actual heading angle ψ. Autopilots must be designed to perform two different functions: *course keeping* and *course changing*. In the first case, the control objective is to maintain the ship's heading following the desired course (ψ *(t)* = constant). In the second case, the purpose of the control system is to alter the course of the ship by changing the heading angle ψ through manipulation of the rudder. The aim is to implement the course change without oscillations and in the shortest time possible. In both situations, the operability of the system must be independent of the disturbances produced by the wind, the waves and the currents. One simple way to do this is by using a reference model.

2.1.2 Reference model

A reference model may be regarded as a pre-filter which ensures that the numerical difficulties associated with large step inputs are avoided (31). The dynamics of the reference model must be equal to the dynamics of the ship, irrespective of the magnitude of the course change demanded by the reference signal. Generally, the course followed by a vessel can be specified by means of a second order reference model. In (32), van Amerongen proposes the following model:

$$T_m \ddot{\psi}_d + \dot{\psi}_d + K_m \psi_d = K_m \psi_r \tag{1}$$

where T_m is the time constant and K_m is the gain factor of the model. Equation 1 can be expressed (31) as:

$$\ddot{\psi}(t) + 2\zeta\omega_n\dot{\psi}(t) + \omega_n^2\psi(t) = \omega_n^2\psi_r \tag{2}$$

where ω_n is the natural frequency and ζ ($0,8 \leq \zeta \leq 1$) is the desired damping coefficient of the closed loop system.

If a more realistic model is required allowing smooth accelerations to be generated, a third order model can be used, such as the following (33):

$$\frac{\psi_d(s)}{\psi_r(s)} = \frac{\omega_n^3}{(s+\omega_n)(s^2 + 2\zeta\omega_n s + \omega_n^2)} \tag{3}$$

It can be seen that $\dot{\psi}_d$ and $\ddot{\psi}_d$ are smooth and bounded for in-step reference inputs ψ_r.

2.1.3 Steering machine

The function of a steering machine is to move the rudder to a desired angle when demanded by the control system or by the helmsman. A simplified model of the steering machine, proposed by Van Amerongen (16) is shown in Figure 3 where δ_c is the commanded rudder angle and δ is the actual rudder angle. The rudder angle and rudder rate limiters will typically be in the ranges of $-35^\circ \leq \delta_{max} \leq 35^\circ$ and $2.5^\circ/\sec \leq \dot{\delta}_{max} \leq 7^\circ/\sec$.
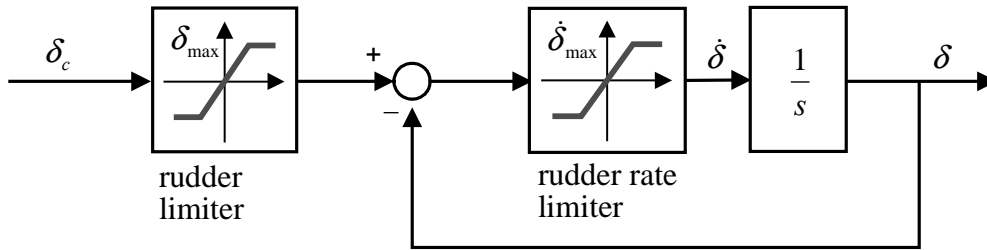
Figure 3 Simplified diagram of the Steering machine

3 SHIP MATHEMATICAL MODEL

3.1 Degrees of Freedom and Notations

The movement of a ship, considered as a rigid solid, has six degrees of freedom (DOF) which means that six independent coordinates are required to determine its position and orientation. Table 1 shows the description of each DOF and the corresponding nomenclature used to describe the ship's forces and motions. This is the standard notation recommended in SNAME, (34) for use in ship manoeuvring and control applications.

Table 1: Notation and DOF description

DOF	Translation	Forces	Linear velocity	Position
1	surge	X	u	x
2	sway	Y	v	y
3	heave	Z	w	z
	Rotations	**Moments**	**Angular velocity**	**Angles**
4	roll	K	p	ϕ
5	pitch	M	q	θ
6	yaw	N	r	ψ

The first three coordinates and their derivatives are used to describe the position and translation movements on the axes x_B, y_B and z_B , while the other three coordinates and their derivatives are used to describe the orientation and rotation movements. For sea vessels, the six different motion components are defined as surge, sway and heave for translation motions in the three directions and roll, pitch and yaw for rotation motions around the three axes.

Using the above notation, the motion of a ship with six DOF can be described by means of the following vectors:

– The speed vector which is normally defined in relation to the ship's coordinates system:

$$\mathbf{v} = \left[\mathbf{v}_1^T , \, \mathbf{v}_2^T \right]^T , \; \mathbf{v}_1 = \left[u, \, v, \, w \right]^T , \; \mathbf{v}_2 = \left[p, \, q, \, r \right]^T \tag{4}$$

– The external forces and motion vector which is also defined in relation to the ship's coordinates system:

$$\boldsymbol{\tau} = \left[\boldsymbol{\tau}_1^T , \, \boldsymbol{\tau}_2^T \right]^T , \; \boldsymbol{\tau}_1 = \left[X, \, Y, \, Z \right]^T , \; \boldsymbol{\tau}_2 = \left[K, \, M, \, N \right]^T \tag{5}$$

– The position and orientation vector defined with respect to the inertial reference system:

$$\boldsymbol{\eta} = \left[\boldsymbol{\eta}_1^T , \, \boldsymbol{\eta}_2^T \right]^T , \; \boldsymbol{\eta}_1 = \left[x, \, y, \, z \right]^T , \; \boldsymbol{\eta}_2 = \left[\phi, \, \theta, \, \psi \right]^T \tag{6}$$

3.2 Coordinate frames

In order to analyse the ship's motion at sea in six DOF, two coordinate frames are used, as shown in Figure 4.
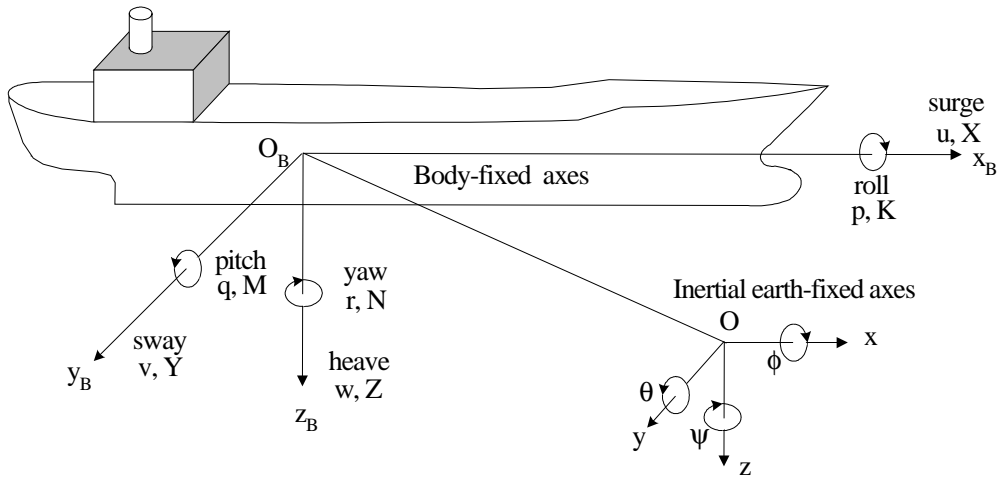
Figure 4 Coordinate Systems with definition of angles, velocities, forces and moments

The moving coordinate frame x_B, y_B, z_B is fixed to the ship and is called the body-fixed reference frame. The origin O_B of the ship's coordinate system can be selected to coincide with the Centre of Gravity (CG) if the CG is situated on the main plane of symmetry. Generally, however, this is not a good choice, since the CG is not located at any fixed point as the load conditions of the ship change constantly. The most widely used option, allowing a

reduction in the complexity of the equation (31), consists in selecting an orthogonal coordinate system parallel to the main axes of inertia in order to eliminate the products of inertia in the motion equations. These requirements are satisfied in practically all sea vessels, the origin being located at the intersection of the two planes of symmetry. The motion of the body-fixed frame is described in relation to an inertial reference axis xyz, and it is normally assumed that the acceleration of one point of the surface of the Earth will have little effect on the slow motion of sea vessels. As a result, it can be considered that a reference system located on Earth O_{xyz} is an inertial system. Thus, the position and orientation of the ship is described in relation to the inertial reference system and its linear and angular velocities in the ship's mobile coordinate systems.

3.3 Ship Motion Equations

Representing the motion equations in the body-fixed reference frame, with the origin of the coordinates located at the intersection of the planes of symmetry, the motion equations of a ship, starting from Newton's equations, can be expressed (35), (36) or (31) as follows:

$$m\left(\dot{u} - rv + qw - (q^2 + r^2)x_G + (pq - \dot{r})y_G + (rp + \dot{q})z_G\right) \quad = X$$
$$m\left(\dot{v} - pw + ru - (r^2 + p^2)y_G + (qr - \dot{p})z_G + (pq + \dot{r})x_G\right) \quad = Y \qquad (7)$$
$$m\left(\dot{w} - qu + pv - (p^2 + q^2)z_G + (rp - \dot{q})x_G + (qr + \dot{p})y_G\right) \quad = Z$$

$$I_x\dot{p} + (I_z - I_y)rq + m\left(y_G(\dot{w} + pv - qu) - z_G(\dot{v} + ru - pw)\right) \quad = K$$
$$I_y\dot{q} + (I_x - I_z)rp + m\left(z_G(\dot{u} + qw - rv) - x_G(\dot{w} + pv - qu)\right) \quad = M \qquad (8)$$
$$I_z\dot{r} + (I_y - I_x)pq + m\left(x_G(\dot{v} + ru - pw) - y_G(\dot{u} + qw - rv)\right) \quad = N$$

where (x_G, y_G, z_G) is the position of the ship's CG; m is the mass of the ship; u, v, w, $\dot{u}$, $\dot{v}$, $\dot{w}$ represent the linear velocities and accelerations in the x_B, y_B and z_B directions; r, q, p, $\dot{r}$, $\dot{q}$, $\dot{p}$ represent the angular velocities and accelerations related to the axes x_B, y_B and z_B. I_x, I_y and I_z are the moments of inertia of the ship with respect to the same axes of the body-fixed frame. The forces and moments *X, Y, Z, K, M* and *N* represent the results of all external actions on the ship's body.

These equations can be expressed more concisely in vectorial form by the equation:

$$\boldsymbol{M}_{RB}\,\dot{\boldsymbol{v}} + \boldsymbol{C}_{RB}(\boldsymbol{v})\,\boldsymbol{v} = \boldsymbol{\tau}_{RB} \qquad (9)$$

where $\boldsymbol{M}_{RB}$ is the inertial matrix, and $\boldsymbol{C}_{RB}(\boldsymbol{v})$ is the matrix of Coriolis and centripetal terms, both caused by the dynamics of the rigid solid. $\boldsymbol{\tau}_{RB}$ is a generalised vector of the external motions and forces. These forces and motions can be broken down into several components according to their origin (37), (38):

$$\boldsymbol{\tau}_{RB} = \boldsymbol{\tau}_H + \boldsymbol{\tau}_{CS} + \boldsymbol{\tau}_P + \boldsymbol{\tau}_E \qquad (10)$$

τ_H : hydrodynamic forces and motions produced by the movements of the hull in the water, normally separated according to their origin into several groups using the equation $\tau_H = -\tau_A - \tau_D - \tau_R$ (added mass, hydrodynamic damping and restoring forces).

τ_{CS} : forces and motions caused by the control surfaces (rudders, blades etc.).

τ_P : forces and moments generated by the propulsion systems (forces produced by the propellers and thrusters).

τ_E : forces and motions which act on the hull due to environmental disturbances (waves, winds and currents).

Moreover, if the kinematics of the ship is to be included, the following equations are normally used as the vectorial expression of the 6-DOF motion equations:

$$M\dot{v} + C(v)v + D(v)v + g(\eta) = \tau \tag{11}$$

$$\dot{\eta} = J(\eta)v \tag{12}$$

where $M = M_{RB} + M_A$ is the inertial matrix (including added mass matrix M_A), $C(v) = C_{RB}(v) + C_A(v)$ is the matrix of Coriolis and centripetal terms (including added mass matrix $C_A(v)$), $D(v)$ is the damping matrix, $g(\eta)$ is the vector of gravitational forces and moments and $\tau = \tau_{CS} + \tau_P + \tau_E$ is the vector of the propulsion forces and moments, control surfaces and environmental disturbances.

The concept of added mass is usually misunderstood to be a finite amount of water connected to the vehicle such that the vehicle and the fluid represent a new system with mass larger than the original system. Added (virtual) mass should be understood as pressure-induced forces and moments due to a forced harmonic motion of the body, which is proportional to the acceleration of the body (31).

The term $J(\eta)$ of equation 12 is the transformation matrix used to represent the position and orientation vector η in the Earth-fixed frame. Equation 12 can be expressed by:

$$\begin{bmatrix} \dot{x} \\ \dot{y} \\ \dot{z} \\ \dot{\phi} \\ \dot{\theta} \\ \dot{\psi} \end{bmatrix} = \begin{bmatrix} c(\psi)c(\theta) & -s(\psi)c(\phi)+c(\psi)s(\theta)s(\phi) & s(\psi)s(\phi)+c(\psi)c(\phi)s(\theta) \\ s(\psi)c(\theta) & c(\psi)c(\phi)+s(\phi)s(\theta)s(\psi) & -c(\psi)s(\phi)+s(\theta)s(\psi)c(\phi) \\ -s(\theta) & c(\theta)s(\phi) & c(\theta)c(\phi) \\ & & \\ & \mathbf{0}_{3\times3} & \end{bmatrix}$$

$$\begin{bmatrix} & & \\ & \mathbf{0}_{3\times3} & \\ & & \\ 1 & s(\phi)\,t(\theta) & c(\phi)\,t(\theta) \\ 0 & c(\phi) & -s(\phi) \\ 0 & s(\phi)/c(\theta) & c(\phi)/c(\theta) \end{bmatrix} \begin{bmatrix} u \\ v \\ w \\ p \\ q \\ r \end{bmatrix} \tag{13}$$

where $s(\cdot) = \sin(\cdot)$, $c(\cdot) = \cos(\cdot)$, $t(\cdot) = \tan(\cdot)$.

3.4 Hydrodynamic forces and motions

An important step in the development of maneuvering models is to expand the forces and moments in Taylor's series. In this way, the hydrodynamic forces and motions are normally represented as a non-linear function of the accelerations $\dot{\mathbf{v}}$, velocities $\mathbf{v}$, and Euler angles included in $\boldsymbol{\eta}$:

$$\boldsymbol{\tau}_{\mathrm{H}} = \mathbf{f}(\dot{\mathbf{v}},\, \mathbf{v},\, \boldsymbol{\eta}) \tag{14}$$

where the function $\mathbf{f}$ is calculated through the development in Taylor series of the functions X, Y, Z, K, M and N as, for example, for force X:

$$\frac{dX}{dt} = \frac{\partial X}{\partial u}u + \frac{\partial X}{\partial v}v + \ldots + \frac{\partial X}{\partial \dot{u}}\dot{u} + \frac{\partial X}{\partial \dot{v}}\dot{v} + \ldots \tfrac{1}{2}\frac{\partial^2 X}{\partial u^2}u^2 + \ldots \tfrac{1}{6}\frac{\partial^3 X}{\partial u^3}u^3 + \ldots \tag{15}$$

and the partial derivatives of the development, termed *hydrodynamic derivatives* or *hydrodynamic coefficients*, are represented by terms such as:

$$X_{\dot{u}} = \frac{\partial X}{\partial \dot{u}}, \quad X_{uu} = \tfrac{1}{2}\frac{\partial^2 X}{\partial u^2}, \quad Y_{vv} = \tfrac{1}{2}\frac{\partial^2 Y}{\partial \delta^2}, \quad N_{v|r|} = \frac{\partial^2 N}{\partial v \partial |r|} \ \ \mathrm{y} \ \ K_{ppp} = \tfrac{1}{6}\frac{\partial^3 K}{\partial p^3} \ \ldots \tag{16}$$

evaluated at equilibrium conditions. The initial condition of motion equilibrium is chosen as straight ahead motion at constant speed (39).

If the ship has lateral symmetry (37) an approximation to the equation 14, in stationary state, can be obtained using the Taylor development around the state of equilibrium $u = u_0$ and $\mathbf{v} = \dot{\mathbf{v}} = \mathbf{0}_{6\times1}$, obtaining a polynomial of the fourth order or lower(40).In (39) and (37) it is proposed that up to the third order of development should be taken. No terms higher than the third order are included since experience has shown that their inclusion does not significantly increase accuracy. Moreover, several terms can be discarded due to the lateral symmetry of ships and by taking into account only terms with acceleration of the first order.

The hydrodynamic derivatives can be determined approximately from the hydrodynamics theory (strip theory) (37), by experiments using scale models (37), (41) and (42) or by system identification methods carrying out experiments on the ships (43) and (44). However, it is

difficult to determine all of the hydrodynamic coefficients of a ship. To obtain a good model of the vessel, these coefficients need to be determined reasonably accurately.

4 MATHEMATICAL MODELS FOR STEERING CONTROL

In general, for surface ships, roll, pitch and heave movements can be discarded in the description of course-changing or course-keeping, since these have only a minor influence with respect to the other movements. Thus, the ship's model is represented by the surge, sway and yaw, and the movement of the ship with three degrees of freedom can be represented, making the roll, pitch and heave terms zero ($\dot{p} = \dot{q} = \dot{w} = p = q = w = 0$) in equations 7 and 8, with the set of Newton equations indicated below:

$$
\begin{aligned}
\text{surge:} \quad & X = m(\dot{u} - v\,r - x_G r^2) \\
\text{sway:} \quad & Y = m(\dot{v} + u\,r + x_G \dot{r}) \\
\text{yaw:} \quad & N = I_z \dot{r} + m x_G (\dot{v} + u\,r)
\end{aligned}
\tag{17}
$$

where I_Z is the moment of inertia of the ship with respect to the axis *z*, *m* is the mass of the ship and the centre of gravity is assumed to be in the position (x_G, 0, 0), The linear surge and sway velocities are represented by *u* and *v* and the angular yaw velocity by *r*.

Figure 5 shows the variables used to represent the movement on the horizontal plane:
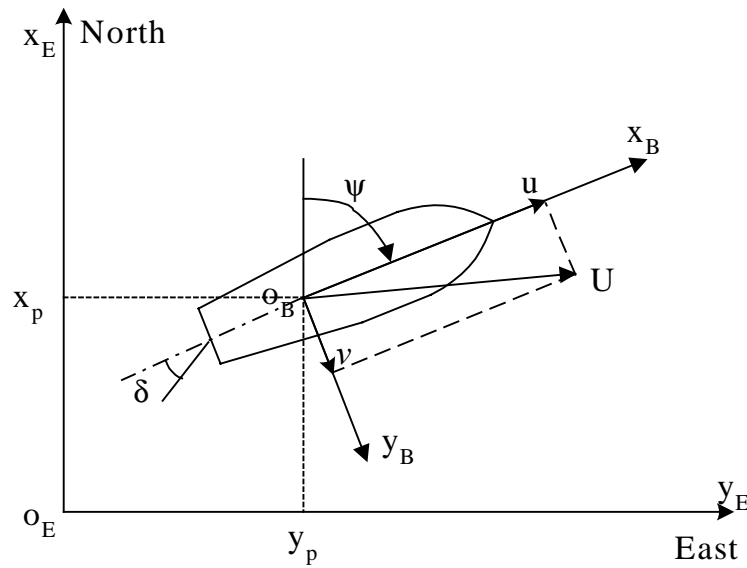
Figure 5: Ship position coordinates

Using the movement equations, the basic dynamics of a ship's steering control system in the horizontal plane can be described, by means of linear and non-linear modelling techniques. In order to facilitate the design of the ship steering control algorithms and their implementation in the autopilots, linear models with added non-linearities are also used. A review of these techniques can be found in (45) and (46).

4.1 Non-linear models

There are different approaches to the modelling of non-linear equations of movement. The basic difference between one and another lies in the expression of the hydrodynamic forces *X* and *Y*, and in the hydrodynamic moments *N*, which are complex functions of the ship's movement.

Abkowitz (39) proposes taking up to the third order of development in the Taylor series of the functions *X, Y* and *N* around the state of balance $u = u_0$ and $v = r = \dot{u} = \dot{v} = \dot{r} = 0$. Experience has shown that the inclusion of terms higher than the third order does not significantly increase the accuracy of the model. Moreover, Abkowitz (39) also points out that several terms can be discarded due to the lateral symmetry of ships, and that only terms with first order acceleration need to be taken into account.

4.2 Linear Models

In order to obtain the linear equations of movement, equation 17 is taken as a starting point and it is assumed (31) that the sway velocity *v*, the yaw rate *r* and the rudder angle δ are small. Then, assuming that the ship's speed u_0 does not vary and the thrust remains constant, the first equation (surge) can be separated from the other two (sway and yaw). It is also considered that the sway velocity and yaw rate are $v_0 = r_0 = 0$. thus, for small disturbances around the nominal values u_0, v_0 and r_0, equation 17 can be written as:

$$\text{surge:} \quad X = m\dot{u}$$
$$\text{sway:} \quad Y = m(\dot{v} + u_0\, r + x_G\dot{r}) \tag{18}$$
$$\text{yaw:} \quad N = I_z\, \dot{r} + mx_G(\dot{v} + u_0\, r)$$

The first equation (surge) relates the thrust of the propeller with the speed of the ship. This relation is non-linear but, when studying ship steering using linear models, it is assumed that the speed is kept constant and only steering control equations (sway and yaw) are considered. Fossen (31) presents a non-linear expression of the surge equation, together with a linearised approach.

4.2.1 Transfer function models

The transfer function which relates the yaw rate *r* with the rudder angle δ can also be obtained:

$$\frac{r}{\delta}(s) = \frac{b_1 s + b_2}{(s^2 + a_1 s + a_2)} = \frac{K'(1 + sT_3')}{(1 + sT_1')(1 + sT_2')} \tag{19}$$

and the function which relates the sway speed *v* with the rudder angle δ is given by:

$$\frac{v}{\delta}(s) = \frac{c_1 s + c_2}{(s^2 + a_1 s + a_2)} = \frac{K_v'(1 + sT_v')}{(1 + sT_1')(1 + sT_2')} \tag{20}$$

where:

$$a_1 = -a_{11} - a_{22} \qquad b_1 = b_{21} \qquad c_1 = b_{11}$$
$$a_2 = a_{11}a_{22} - a_{12}a_{21} \quad b_2 = a_{21}b_{11} - a_{11}b_{21} \quad c_2 = a_{12}b_{21} - a_{22}b_{11} \tag{21}$$

and where $K_v{}'$ y $T_v{}'$ are the gain and the time constant which describe the sway motion.

Taking into account that for movements restricted to the horizontal plane, $\dot{\psi} \equiv r$, equation 19 can be rewritten as:

$$\frac{\psi}{\delta}(s) = \frac{K'(1 + sT_3')}{s(1 + sT_1')(1 + sT_2')} \tag{22}$$

The differential equation in the time domain associated to this transfer function can be expressed as:

$$T_1'T_2'\dddot{\psi} + (T_1' + T_2')\ddot{\psi} + \dot{\psi} = K'(\delta + T_3'\dot{\delta}) \tag{23}$$

where K', T_1', T_2' and T_3' are the parameters which represent the ship's dynamics. These parameters are determined mainly by the dimensions and shape of the ship, but depend also on operating conditions such as speed, load or ballast situation, draught, trim and depth of water.
These models, first proposed by Nomoto and others (47), are those which are generally used in the analysis of ship stability and in the design of automatic pilots. Nomoto and others (47) also proposed the following approximate first order model:

$$\frac{\psi}{\delta}(s) = \frac{K'}{s(1 + sT')} \tag{24}$$

with $T' = T_1' + T_2' - T_3'$ an effective time constant. The differential equation in the time domain in this case is:

$$T'\ddot{\psi} + \dot{\psi} = K'\delta \tag{25}$$

and in dimensional form:

$$T\ddot{\psi} + \dot{\psi} = K\delta \tag{26}$$

where the adimensional parameters T' and K' are related to the dimensional parameters T and K through $T' = T(V/L)$ and $K' = K(L/V)$

4.3 Linear models with added non-linearities
The linear models outlined above can only be used for small deviations from the point of equilibrium $v = r = \delta = 0$, or to adequately describe the movement of a ship following a straight trajectory. However, if it is the rotation characteristics of a ship that are to be studied, linear equations can only be used in the linear interval for ships with directional stability. In

order to increase the range of validity of these linear models, Kallström and Aström (44) propose the addition of a non-linear term to the linear model. The equation is then:

$$T_1 T_2 \ddot{\psi} + (T_1 + T_2)\ddot{\psi} + KH(\dot{\psi}) = K(\delta + T_3 \dot{\delta}) \tag{27}$$

where $H(\psi)$ is a non-linear function of $\dot{\psi}$, which can be obtained from the relation between $\dot{\psi}$ and δ in the state of equilibrium by means of the spiral test, and which can be approximated (12) by:

$$H(\dot{\psi}) = a\dot{\psi}^3 + b\dot{\psi} \tag{28}$$

In the approximate first order model, this non-linearity would give:

$$T\ddot{\psi} + H_N(\dot{\psi}) = K\delta \tag{29}$$

where:

$$H_N(\dot{\psi}) = n_3 \dot{\psi}^3 + n_1 \dot{\psi} \tag{30}$$

5 APPLICATIONS TO COURSE CHANGING CONTROL.

This section describes several examples of course-changing control applied to two ships.

5.1 R. O. V. Zeefakkel
The ship 'R. O. V. Zeefakkel' of 45 m length can be represented by the non-linear mathematical model given by equation 29, the model parameters for a ship speed of 10 knots being (48):

$$K = 0.5 \text{ s}^{-1}, \ T = 31 \text{ s}, \ n_1 = 1, \ n_3 = 0.4 \text{ s}^2$$

The nonlinearity of the model is seen in the considerable variation in both the parameters of its rudder course-changing commands and in the saturation of its rudder angle and speed.

For the control of the course-changing manoeuvre of a ship, this non-linear behaviour causes great difficulty in the adjustment of the parameters of a single controller for the full range of possible changes in course. Three different control techniques will be applied: Classical controllers tuned using GAs (26), QFT (27) and IMC (29) and a comparison will be made of the results obtained.

For the adjustment of the parameters of the classical controllers, the non-linear model of the ship is used. However, for the design of QFT and IMC controllers, a linearised model is used, the first order Nomoto model (47), which relates the heading angle with the rudder angle. The possible effects of rudder saturation and rudder rate limits have been taken into account in the design.

The simulation of various course-changing manoeuvres with the different control structures obtained is performed using a Simulink model of the closed loop for the non-linear ship model (12).

As shall be verified below, this comparative study shows that the course-change manoeuvre is satisfactorily achieved without overdamping with the three algorithms applied. Moreover, the responses obtained with the QFT and classical controllers are faster than those of the IMC controller.

5.1.1 Classical controllers tuned with Genetic Algorithms

This section describes the most widely used classical control structures: PID controllers with approximate derivative action in the standard forms, in series and parallel, a first order controller and a second order controller. GAs have been used for the optimum design of the controller. These algorithms form an optimisation technique that acts on a population of defined individuals through a chromosome formed by binary genes. The GA's act on the chromosomes using selection, crossover and mutation operators for a specific number of generations. In order to quantify the aptitude of the individuals, an objective function is maximised Φ. The starting point is an initial population $P(0)$, formed by p individuals. Some genetic operators are applied to this population to modify it probabilistically to create a new population $P(1)$. The process is repeated over a given number of generations T, the successive generations, $P(t)$ being obtained. The solution is obtained among individuals of the last generation $P(T)$. Figure 6 shows a flow diagram of a simple GA.
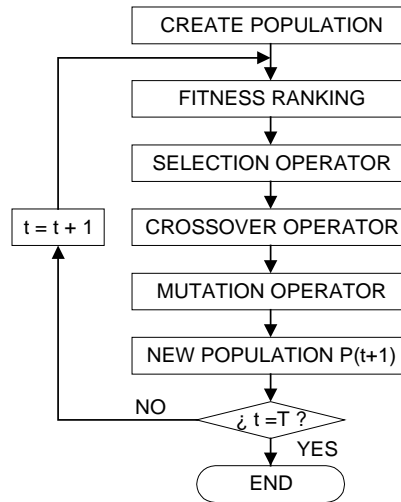

Figure 6. Basic genetic algorithm

The cost function selected was:

$$J(\theta) = \sum_{i=1}^{n} \left| \Delta \psi_i \right| \tag{31}$$

159

where θ is the vector of the controller parameters, n is the total number of dots in the response curve determined in each simulation and $\Delta\psi_i$ the ith heading angle error between the desired and obtained heading.

5.1.1.1 Simulations
The simulation was performed with the Matlab Toolbox, SIMULINK. The genetic algorithm evaluates the cost function (31) in each iteration after performing the simulation of the model with the corresponding controller.

Table 2 shows a summary of the results obtained with the controllers studied. The values indicated in the table represent for each case the cost function obtained with the optimal values of the controller parameters for each course-change manoeuvre.

Table 2. Cost functions

Cost function (rad)	Heading angle (deg)			
	10	20	30	40
Standard PID	-0.81713	-1.2376	-7.2708	-20.5162
Parallel PID	-16.5396	-16.3993	-16.320	-17.39103
Series PID	-0.6499	-1.15744	-5.7518	-16.59227
1st order controller	-0.0065	-0.01301	-0.0195	-0.026071
2nd order controller	-0.04139	-0.0827	-0.1238	-0.16483

It can be appreciated that the best results are achieved with the first order controller. Good results are also obtained with the second order controller. The PID controller with the best results is the in-series structure one. An acceptable behaviour can be obtained with this controller for course-changing manoeuvres of 10º and 20º but for manoeuvres of 30º and 40º, a significant degree of error is produced.

First, the parameter value that led to the best behaviour was determined for each controller in all the cases studied. The results are shown in table 3. With these parameters the response to course-changing manoeuvres of 10º, 20º, 30º and 40 º were obtained, as shown in Figure 7.

Table 3. Controller parameters

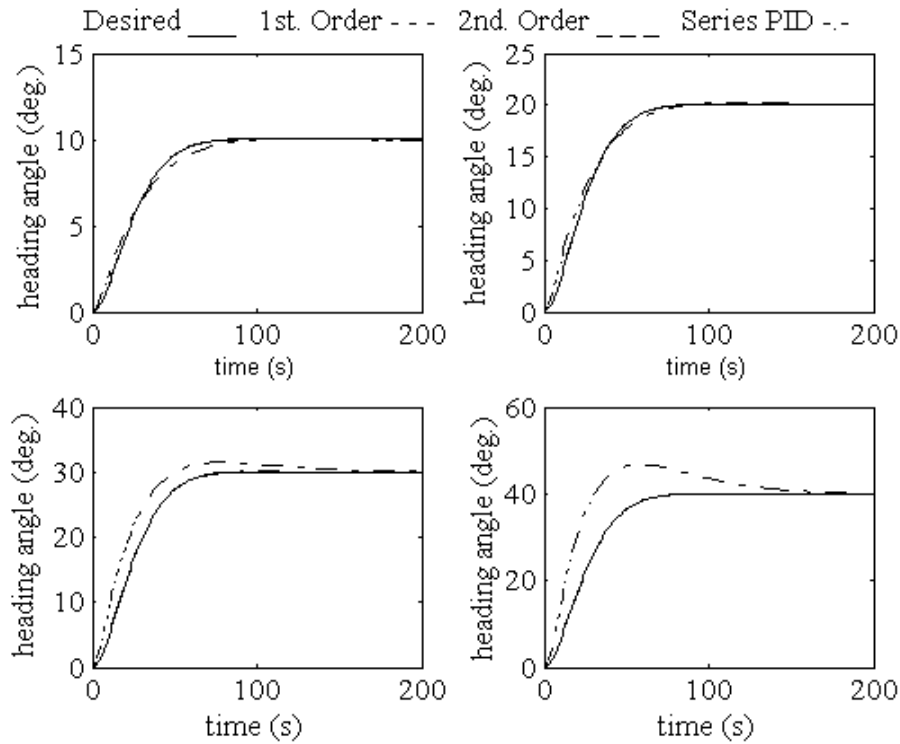| Controllers	Gain (k)	Zeros	Poles
1st. Order Controller	0.301746	-0.032197	-0.125038
2nd. Order Controller	0.300891	-0.032501 -4.376560	-0.124082 -4.422973
PID Serie	0.75766	-0.03761 -0.00004	-0.03761 0

Figure. 7. Course-change manoeuvres

5.1.2 Quantitative Feedback Theory

QFT is a robust control design technique in the frequency domain through which a satisfactory balance is achieved between the degree of uncertainty in the system and the complexity of the mathematical process involved.

In the case of a set of linear SISO plants, QFT proposes a control structure with two degrees of freedom (shown in figure 8). This includes a cascade compensator, $G(s)$, and a prefilter $F(s)$ (both LTI) in order to reduce the variations in the output of the system caused by the uncertainties in the plant parameters and disturbances.

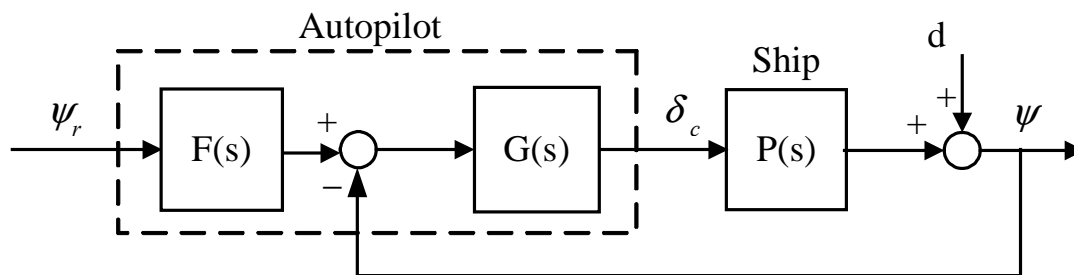**Figure. 8 Block diagram of the two degree-of-freedom control system**

The Nichols Chart is used to obtain the desired robust design by representing the uncertainty of the plant by means of frequency dependent regions (templates) and the design restrictions by means of the bounds of regions that combine those of uncertainty and the design specifications for each frequency. A nominal plant is selected for the QFT design process

within the uncertainty range. A suitable, finite set of frequencies must be selected to carry out the design, which will be determined by the bandwidth and by the desired frequencies given by the required behaviour specifications.

Once the bounds have been calculated, the next step is to obtain an adjustment in the loop function $L_0(j\omega)$ that manages to satisfy the restrictions and, at the same time, minimises the control effort. The problem of obtaining a good adjustment of the function $L_0(j\omega) = G(j\omega)P_0(j\omega)$, ($P_0$ being the nominal plant function) can be considered as a problem of optimisation. After that, the prefilter $F(s)$ is adjusted. With the MATLAB QFT Toolbox (49), the results of each adjustment can be observed.

5.1.2.1 Simulations
The non-linearities in the ship model mean that the performance in response to changes in course may vary. The prior study of this effect has led the authors to consider for the model design the vessel given by equation (26) with the following uncertainty in the K and T parameters (at a speed of 10 knots): $K \in [0.21, 0.5]$ and $T \in [29.5, 31]$

The system must fulfill robust stability and robust tracking specifications. For the robust stability margins, the phase margin angle should be at least 45º and the gain margin 2 dB. For the robust tracking, the change of course must be defined within an acceptable range of variation:

$$T_{RL}\left(j\omega\right) \le T_R\left(j\omega\right) \le T_{RU}\left(j\omega\right) \tag{32}$$

where $T_R(s)$ represents the closed loop transfer function and $T_{RL}(s)$ and $T_{RU}(s)$ the equivalent transfer functions of the lower and upper tracking bounds. In this case:

$$T_{RL}\left(s\right) = \frac{269.5 * 10^{-6}}{s^3 + 181 * 10^{-3}s^2 + 118.3 * 10^{-4}s + 269.5 * 10^{-6}} \tag{33}$$

$$T_{RU}\left(s\right) = \frac{195 * 10^{-4}s + 49 * 10^{-4}}{s^2 + 112 * 10^{-3}s + 49 * 10^{-4}} \tag{34}$$

for $\omega \le 0.4$ rad/s.

The following nominal plant has been chosen for the design:

$$P(s) = \frac{0.5}{s(31s+1)} \tag{35}$$

and the following set of frequencies for the design has been established:

$$\Omega = \{0.03, \ 0.07, \ 0.1, \ 0.2, \ 0.4, \ 1, \ 1.2\} \tag{36}$$

Adjusting the nominal open-loop transfer function the controller obtained is:

$$G(s) = \frac{180.45*10^{-3}s^3 + 625.38*10^{-3}s^2 + 16.57*10^{-3}s + 36.92*10^{-7}}{s^4 + 168.53*10^{-2}s^3 + 203.23*10^{-2}s^2 + 18.73*10^{-2}s} \tag{37}$$

With this controller, the robust stability specification is fulfilled but not the robust tracking specification. By adjusting the prefilter:

$$F(s) = \frac{128.89*10^{-3}}{s+128.89*10^{-3}} \tag{38}$$

a restriction on the frequency response of the system is obtained such that it is maintained within the limits imposed in the design.
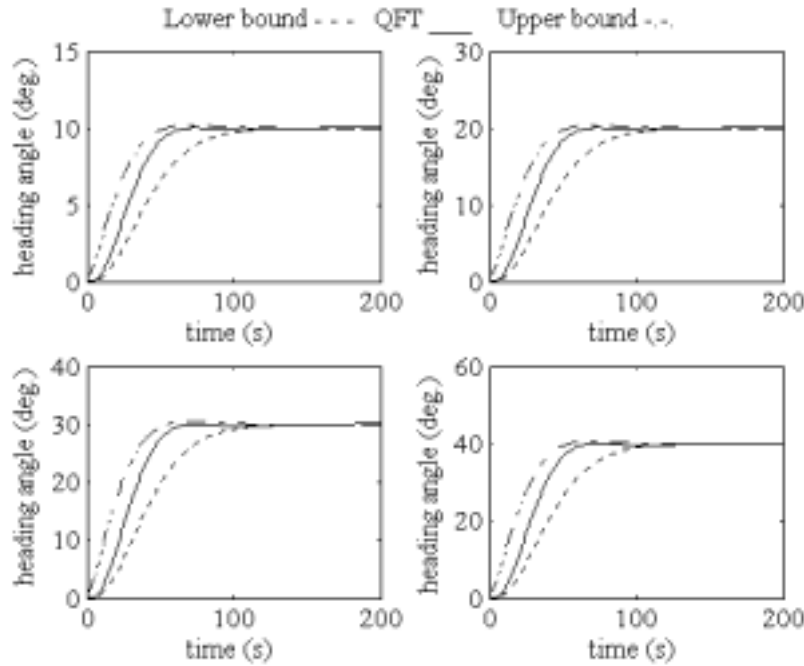
Figure 9. Course-changing manoeuvres

Figure 9 shows the response to course-changing manoeuvres from 10° to 40°. The response is observed to be kept within the established bounds.

5.1.3 Internal Model Control

Figure 10 shows a block diagram of a control structure with IMC structure. G(s) represents the process to be controlled, $\tilde{G}(s)$ is the mathematical model of the process used for the controller design, and $Q(s)$ is the IMC controller whose transfer function must be determined. Here, r represents the reference input, y the output, u the control signal and d the effect of the disturbances on the output.

Figure 10. IMC structure

The IMC structure offers several advantages over the traditional feedback structure (50): it is a structure with which an inherently stable control system is obtained, it explicitly takes into account the uncertainties of the model and it allows a 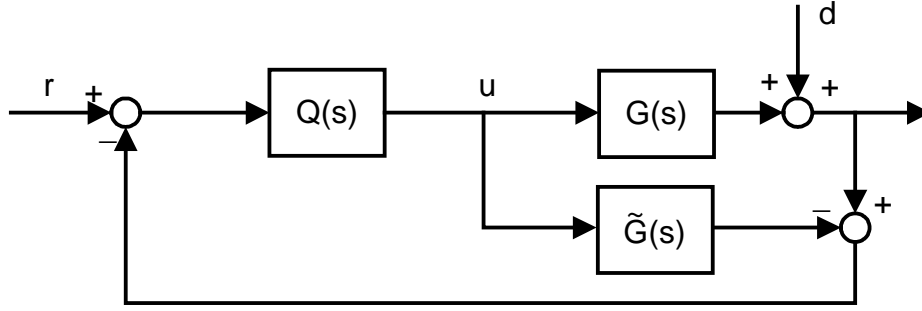robust behaviour to be obtained towards changes in the process and modelling errors. Moreover, if the control signal u is subjected to saturation type limits on the actuator, these can even be included in the implementation of the structure.

The IMC controller design is carried out in two steps:

1. The model is factorised into:

$$\tilde{G}(s) = \tilde{G}_+(s)\tilde{G}_-(s) \tag{39}$$

where $\tilde{G}_+(s)$ contains all the time delays and the zeros in the right-half plane. $\tilde{G}_+(s)$ is specified such that the open loop steady-state gain is the unit. $\tilde{G}_-(s)$ is stable and minimum phase. In the case where G(s) is minimum phase $\tilde{G}_+(s) = 1$ and $\tilde{G}(s) = \tilde{G}_-(s)$

2. The controller is specified as:

$$Q(s) = \tilde{G}_-(s)^{-1}F(s) \tag{40}$$

where *F(s)* is a low-pass filter of the form:

$$F(s) = \frac{1}{(\lambda s + 1)^n} \tag{41}$$

where λ is the desired time constant of the system and *n* is a positive integer number selected to make $Q(s)$ be a suitable transfer function.

One of the main advantages of IMC structures is that they guarantee stability in closed loop when a stable IMC controller is selected. The IMC structure allows the effects of the restrictions on the actuator to be compensated, simply through the implementation of this structure. To take into account the effect of the rudder saturation and the rudder rate limits, these are included in the model shown in Figure 11.
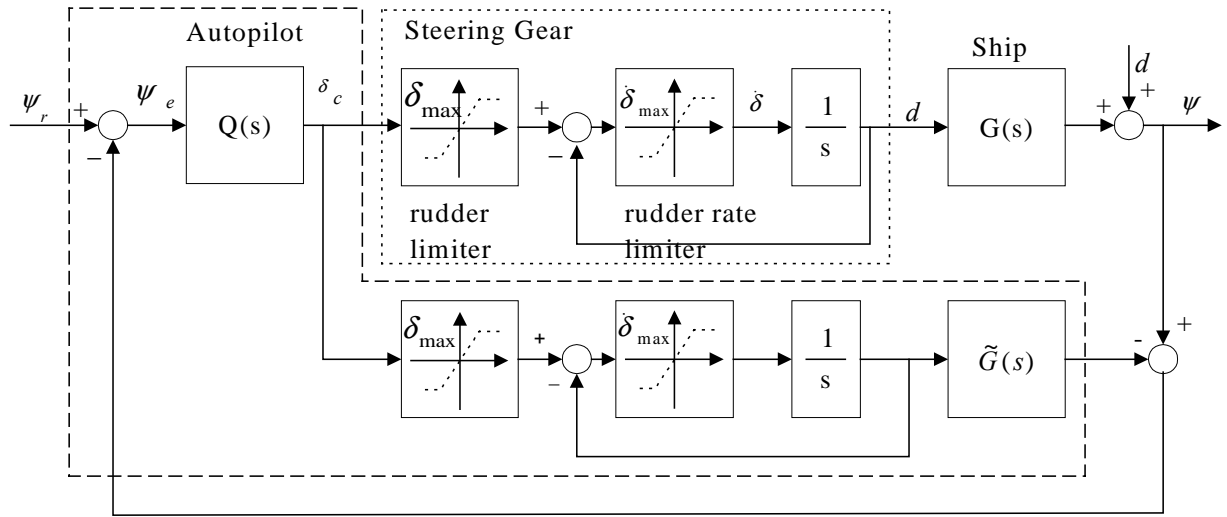
Figure 11. Implementation of the IMC controller

Applied to the study case using equation (26) as the ship's dynamics model:

$$\tilde{G}(s) = \frac{K}{s(1+Ts)} \tag{42}$$

with $K = 0.5$ s^{-1}, $T = 31$ s. And the controller is given by:

$$Q(s) = \frac{s(1+Ts)}{K(1+\lambda s)^2} \tag{43}$$

with $\lambda = 25$.

5.1.3.1 Simulations
Figure 12 shows the response to course-change manoeuvres from 10º to 40º.

Figure 12. Course-change manoeuvres

5.1.4 Comparison

The heading followed in response to various changes in the commands was simulated, subjecting the vessel to the effect of bow waves in the order of 1m in significant height.

Figure 13. Course-changing manoeuvres

Figures 13 and 14 show a comparison of the paths followed in response to changes in the ship's course with a first order controller, with the one designed with the IMC structure and with QFT, and the required variations in the rudder angle signal control.

Figure 14. Rudder Angle

5.2 The container ship

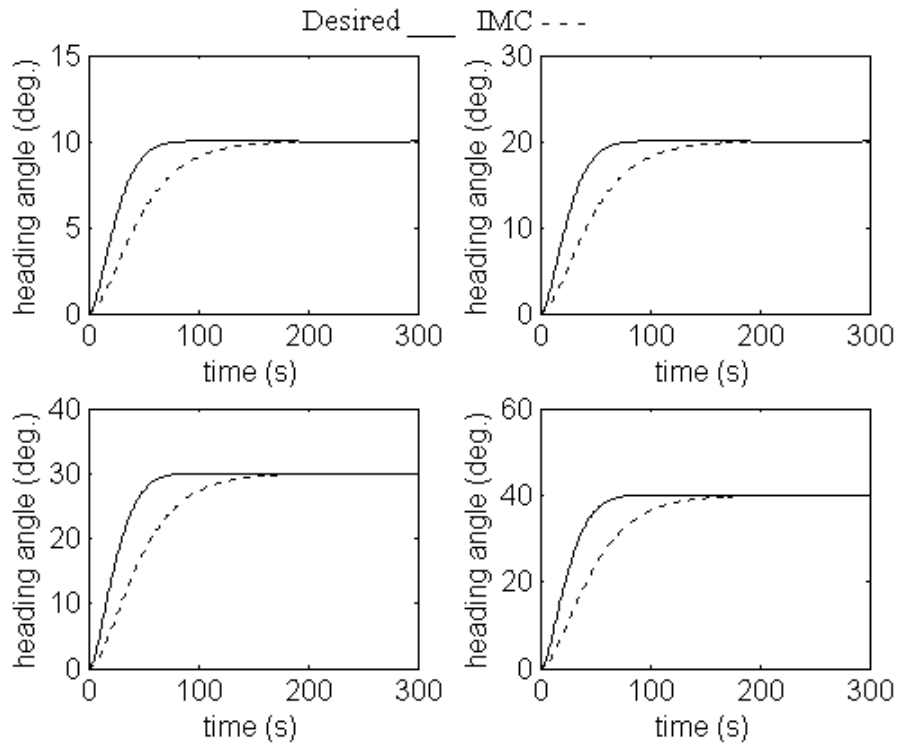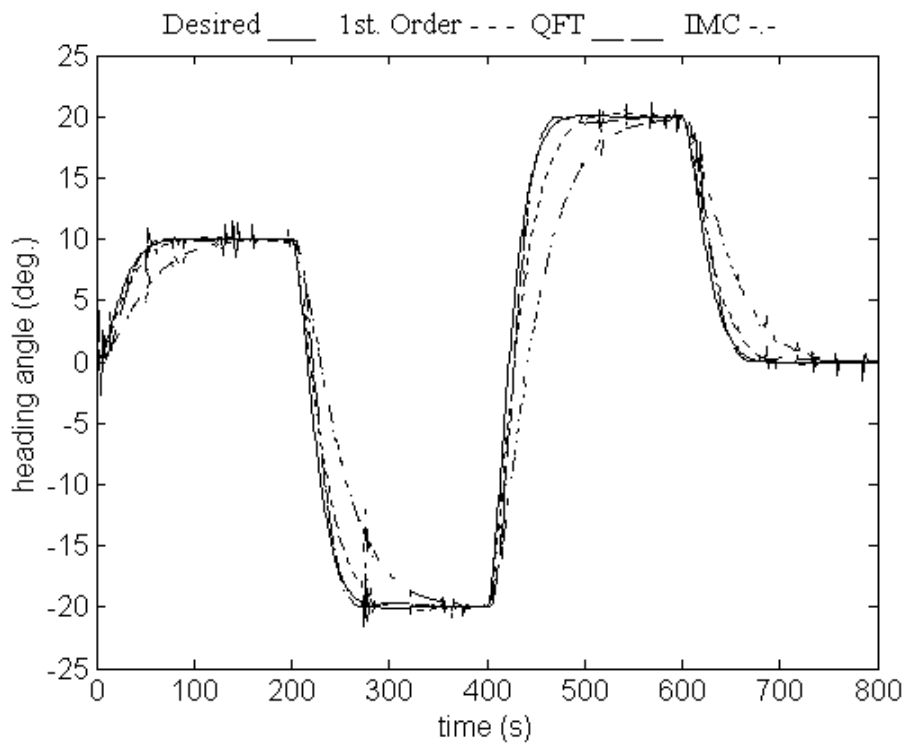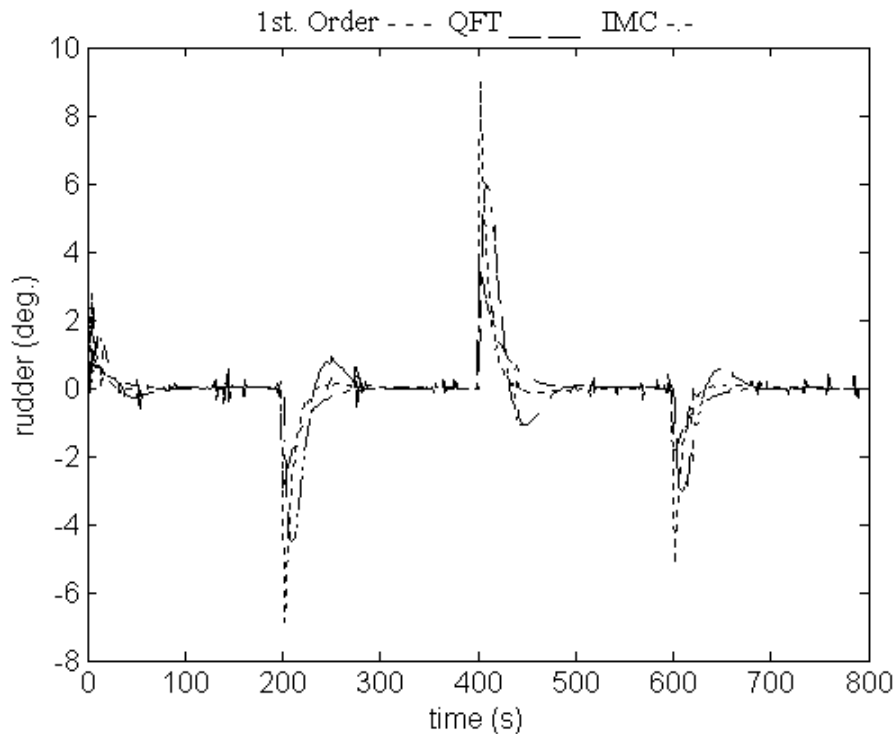This section outlines the design of classical controlers for the control of a course-changing manoeuvre of a container ship. Both for the design of the controllers and for the subsequent simulation of various course-changing manoeuvres, a non-linear ship model is used (45). The characteristics of this type of ship mean that the mathematical model for ship steering requires 4 degrees of freedom, since the movement of the balance is not insignificant. The model uses cross coupling movement equations of surge, sway, roll and yaw to take into account the effects of rolling during the changes of heading which these ships usually undergo due to their low metacentric height. It also includes the effects of rudder saturation.

It is difficult to procure a good behaviour from the adjustment of the controller parameters in all situations if the mathematical model used in the design of the controller is not precise, or if there are external disturbances. This is why adaptive or robust control techniques are usually used in the design of the controller. Genetic algorithms have been used to solve the problem optimisation in the calculations for several classic controller parameters.

As shall be shown below, the optimisation by means of GAs (51) to (53) of the controller parameters provides completely satisfactory results for the behaviour of the simulation of the non-linear model of the ship for different situations of change of course, particularly when using a second order controller.

For the container ship contemplated in this study we will consider course-keeping or course-changing and roll dampening, while the pitch and heave movements can be ignored due to their low values in comparison with other movements. Thus, the mathematical model of the ship is considered in surge, sway, yaw and roll motions and the movement of the ship can be represented using Newton equations with four degrees of freedom (42), by the following equations:

$$
\begin{aligned}
\text{surge:} \quad & m(\dot{u} - vr - x_G\, r^2 + z_G\, pr\cos\phi) = X \\
\text{sway:} \quad & m(\dot{v} - ur - z_G\, \dot{p}\cos\phi + x_G\dot{r}) = Y \\
\text{yaw:} \quad & I_{zz}\dot{r} + m\, x_G\,(ur + \dot{v}) = N \\
\text{roll:} \quad & I_{xx}\dot{p} - mz_G\,(ur + \dot{v})\cos\phi = K - \rho g\nabla G_z(\phi)
\end{aligned}
\tag{44}
$$

where ∇ indicates the ship displacement, g the gravity constant, ρ the water density, I_{XX} and I_{ZZ} are the inertial moments of the ship about x_B and z_B axes respectively, m is the mass of the ship and the centre of gravity is assumed to be in the position $(x_G, 0, z_G)$. The linear surge and sway velocities are represented by u and v, the angular yaw and roll ones by r and p, and the corresponding yaw and roll angles are ψ and ϕ measured in the inertial frame. The righting arm function $G_z(\phi)$ can be approximated using (37):

$$
G_z(\phi) = (GM + \tfrac{1}{2} BM \tan^2\phi)\, \sin\phi
\tag{45}
$$

where GM is the nominal ship metacentric height and BM is the distance from the centre of buoyancy to the metacentre. For small roll angles, equation 45 is usually approximated by $GM \sin\phi$ or simply $GM\, \phi$.

The terms X, Y, N and K denote the hydrodynamic forces acting along the axes x_B and y_B, and the hydrodynamic moments around the z_B and y_B axes respectively. These quantities take into account the hydrodynamic effects of the movements of the hull, the forces and moments exercised on the ship by the propeller and the rudder and the influence of the wind, waves and currents.

In (45), a detailed presentation is made of the container-ship model used in this paper. As well as the ship's hydrodynamics, the saturations in the rudder mechanics have also been included. This is easily achieved by limiting the maximum amplitude and velocity of the rudder movement (12). The rate limit is taken as 4.6 degrees/second and the maximum rudder deflection is 30 degrees (42). These limitations on the rudder performance contribute to the diminished controllability of the ship.

The aim of the design of this work is that the ship should make a fast course change following, without oscillations, the course determined by the values $\zeta = 0.9$ and $\omega_n = 0.06$ rad/sec.

The ship data and the hydrodynamic coefficients used in the mathematical model (45), correspond to a container ship from the late nineteen-seventies whose main characteristics are outlined in Table 4.

Due to the non-linearity of the model and to the fact that its behaviour in response to a course change shows substantial variations, the non-linear model is used to perform an optimal tuning of the controller parameters using GAs.

Table 4: Main data for the container ship

Quantity	Symbol	Measure	Unit
Length between perpendiculars	L_{pp}	230	m
Beam	B	32	m
Draft	D	10.7	m
Displacement	∇	46,000	m^3
Nominal speed	U_0	12.7	m/s
Rudder speed	$\dot{\delta}_{max}$	4.6	deg/sec
Nominal X_B coordinate of GC	x_G	-0.5	m
Nominal Z_B coordinate of GC	z_G	-3.5	m
Nominal metacentric heigth	GM	55 - 90	cm

This paper uses the most widely used classical control structures: PID controllers with approximate derivative action in its standard and series forms, a first order controller and a second order controller.

5.2.1 Classical controllers tuned with Genetic Algorithms
GAs have been used for the optimal tuning of the controllers (52). The cost function selected was:

$$J(\theta) = \sum_{i=1}^{n} \left| \Delta \psi_i + \lambda \delta_i \right| \qquad (46)$$

where θ is the vector of the controller parameters, n is the total number of iterations in the control system simulations, $\Delta \psi_i$ the ith heading angle error between the desired and obtained heading, λ is a scaling factor ($\lambda = 0,05$ in this case) and δ_i the ith rudder angle deflection. The term δ_i has been included in order to take into account also the minimisation of the control effort. A simulation time of 200 sec. has been used.

A population of 25 individuals over 300 generations has been used, with a probability of crossover of 60% and of mutation of 10%. The genetic algorithm evaluates the cost function (equation 46) in each iteration after performing the simulation of the model with the corresponding controller. The growth rate and mutation values affect the method's convergence characteristics, depending on the problem and the algorithm in question. The mutation is introduced in order to attempt to guarantee that any point in the search space can be reached and to prevent the GA from being blocked in a local optimum.

Table 5. Cost functions and heading errors

Heading angle (deg)	Standard PID	Series PID	1st. order controller	2nd. order controller
	Cost function (rad)			
10	1.494878	1.537111	1.180951	0.832180
20	1.767833	1.791547	1.700806	0.925994
30	2.155522	2.158248	2.145421	1.949617
	Heading error (rad)			
10	1.073519	1.112889	0.819301	0.421504
20	1.033627	1.048331	0.995293	0.296864
30	0.912204	0.913328	0.905311	0.761659

Table 5 shows a summary of the results obtained with the controllers studied. The values indicated in the table represent for each case the cost function and the heading error obtained with the optimal values of the controller parameters for each course-change manoeuvre.

It can be appreciated that the best results are achieved with the second order controller. Satisfactory results are also obtained with the first order controller and with the two PID controllers, being the standard slightly better than series one.

With the results obtained, a set of specific controllers can be implemented for each of the situations studied (course changes of 10, 20 and 30 degrees), with a scheduling control. Moreover, the set of controllers could be extended to take in course changes of 0 to 30 degrees with a lower interval.

The option presented here consists in determining a single controller with which the best behaviour is achieved for all of the cases studied. The results are shown in Table 6.

Table 6. Controller parameters.

Controller	Gain (k)	Zeros		Poles	
		z_1	z_2	p_1	p_2
2nd. Order Controller	108.4685	- 0.05825 + 0.02834j	- 0.05825 - 0.02834j	- 0.6197	- 0.1137
1st. Order Controller	147.411	-0.0481	0	-1.0484	0
PIDMixto	67.6173	- 0.04934	- 0.00001	- 0.5429	0

5.2.1 Simulations
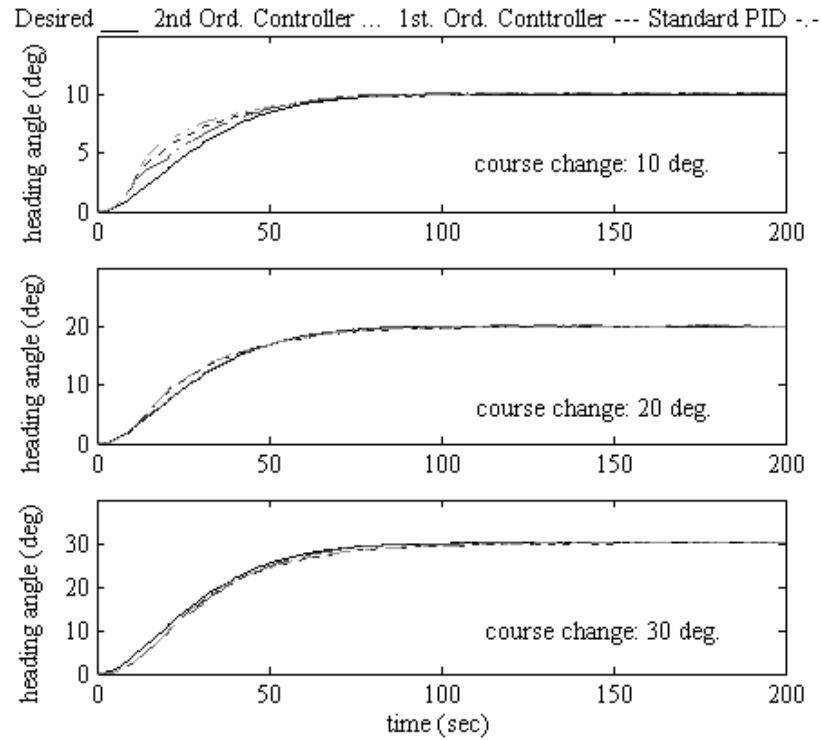
Figure 15. Course-changing manoeuvres: heading responses

Figure 15 shows the course-change manoeuvres of 10, 20 and 30 degrees with the controllers from Table 6.

Figure 16 shows the heading angle errors between the desired and obtained heading responses. It can be observed that the second order controller obtains a good performance for the three course change manoeuvres studied. The first order controller produces also a good behaviour with errors below 2 degrees for all cases. With the PID controllers, the errors are greater, especially for course changes of 10 degrees
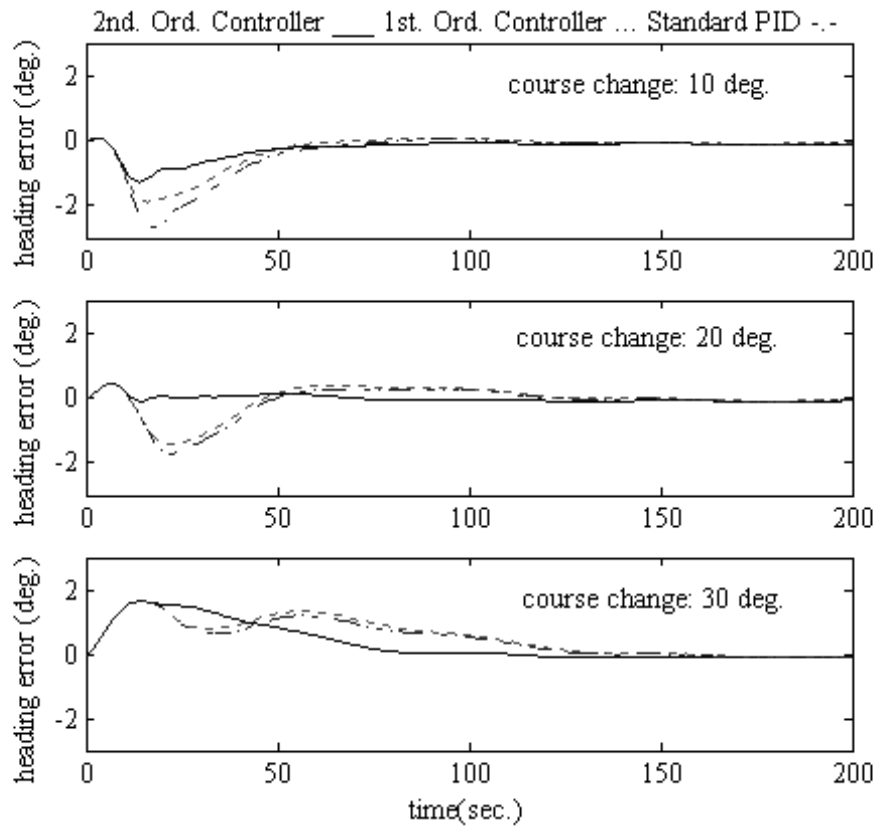
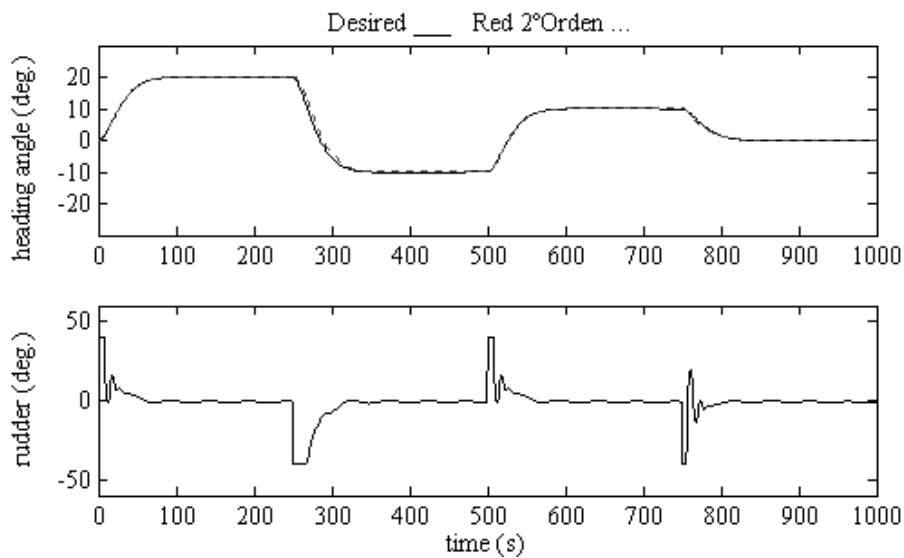**Figure 16. Course-changing manoeuvres: heading error**

Figure 17. Course-changing manoeuvres: heading and rudder responses.

Figure 17 shows the results of the simulation of several course changes with the second order system. It can be observed that the desired course is followed accurately.

REFERENCES
(1)   Fossen T.I., "A survey on nonlinear ship control: From theory to practice". *Proceedings of the 5th IFAC Conference on Manoeuvring and Control of Marine Craft.* Aalborg, Denmark, 2000, 1-16.
(2)   Allensworth T., A short history of Sperry Marine, 1999. http://ww.sperry-marine.com/pages/history.html.
(3)   Bennet A., "A history of control engineering 1800–1930". Peter Peregrinus Ltd; 1997.
(4)   Minorsky N., "Directional stability of automatically steered bodies", J. *Naval Eng., XXXIV, 280-309 (1922).*
(5)   Sperry E., "Automatic steering". *Trans. SNAME, 53-57 (1922).*
(6)   Mort N., "Autopilot design for surface ship steering using self-tuning controller algorithms". *PhD Thesis*, University of Sheffield, 1983
(7)   Koyama T., "On the optimum automatic steering systems of ships at sea". *J. Soc. Naval Archit. Japan*, 122, 1967
(8)   Norrbin N.H., "On the added resistance due to steering on a straight course". *Proceedings of the 13th International Towing Tank*, vol. 1. Berlin, 1972; 282-408.
(9)   Broome D.R., Keane A.J. and Marshall L., "The effect of variations in ship operations on an adaptive autopilot". *Proceedings of the Ship Steering and Automatic Control*, Genova, 1980; 77-95.
(10)   Amerongen J van and Nauta Lemke H.R., "Optimun steering of ships with an adaptive autopilot". *Proceedings of the 5th Int. Ship Control Systems Symposium*, Annapolis, 1978.
(11)   Honderd G. and Winkelman J.E., "An adaptive autopilot for ships". *Proceedings of the Third Ship Control Systems Symposium*, vol. 2, *Bath*, 1972.
(12)   Amerongen J. van and Udink Ten Cate A.J., Model reference adaptive autopilots for ships. *Automatica*, vol. 11, 1975, 441-449.
(13)   Kallström C.G., Astrom K.J., Thorell N.E., Eriksson J. and Sten L., "Adaptive autopilots for tankers". Automatica, vol.15, 1979 254-284.
(14)   Brink A.W., Baas G.E., Tiano A., Volta E., "Adaptive automatic course-keeping control of a supertanker and a container ship: a simulation study". *Proceedings of the 5th Int. Ship Control Systems Symposium*, Annapolis, vol 4, 1978.
(15)   Astrom, K.J., "Why use adaptive techniques for steering large tankers", *Int. J. Control*, vol.32(4), 1980, 689-708.
(16)   Amerongen J. van., *Adaptive steering of ships: a model-reference approach to improved manoeuvering and economical course keeping*. PhD Thesis, Delft University of Technology, 1982.
(17)   Arie, T., Itoh M., Senoh A., Takahashi N., Fujii S. and Mizurio N., "An adaptive steering system for a ship", *IEEE Control Systems Mag.*, 1986, 3-7 N..
(18)   Katebi, M.R. and Byrne J.C., "LQG adaptive ship autopilot", *Trans. Inst. MC*, vol. 10(4), 1988, 187-197.

(19)   Fossen, T.I., and Paulsen M. J., "Adaptive feedback linearization applied to steering of ships", *Modelling, Identification and Control*, vol. 14(4), 1993.

(20)   Zirilli A, Roberts G.N., Tiano A., and Sutton R., "Adaptive steering of a containership based on neural networks", *Int. J. of Adaptive Control and Signal Processing*, vol.14(8), 2000, 849-873.

(21)   Reid R.E., and Mears B.C., "Design of the steering controller of a supertanker using LQG control theory: A feasibility study". *IEEE Trans. Automat. Contr.* vol. AC-27, 1982.

(22)   Roberts G.N., *Ship motion control using a multivariable approach*. PhD Thesis, University of Wales, 1989.

(23)   Grimble MJ, Zhang Y, Katebi MR., "H-infinity based ship autopilot design". *Proceedings of the 10th Ship Control Systems Symposium*, Canada, 1993.

(24)   Roberts G.N., Sutton R., Zirilli A and Tiano A., "Intelligent ship autopilots – A historical perspective". *Mechatronics*. Vol 13, 2003, 1091-1103.

(25)   Alfaro-Cid E. and MºGookin E.W., "Genetic algorithm optimisation of oil tanker control systems". *IFAC Conference on Control Applications in Marine Systems*, Glasgow, 2001.

(26)   López, E., Rueda, T., Velasco, F.J., Moyano, E., Nanclares, J.L. "The Tuning Of Classical Controllers For Course-Changing Manoeuvres Using Genetic Algorithms". *1ˢᵗ International Congress on Maritime Transport*, Barcelona. Spain. 2001, 145-154.

(27)   Rueda, T., Velasco, F.J., Moyano, E., López, E., "Robust QFT Controller for Marine Course-Changing Control". *5th International Symposium on Quantitative Feedback Theory and Robust Frequency Domain Methods,* vol. 1. Pamplona. Spain, 2001.

(28)   Tzeng C.Y., Goodwin G.C. and Crisafulli S., "Internal model control autopilot design with saturating and slew rate limiting actuator", *Int. Shipbuilding Progress*, vol. 46,1999, 401-420.

(29)   Velasco, F.J., López, E., "Predictive Control of Ship Steering Autopilots". *2nd International Congress on Maritime Technological Innovations and Research*, vol.1, Cádiz. Spain, 2000, 89-98.

(30)   Wahl A. and Gilles E.D., "Track-keeping on waterways using model predictive control". *IFAC Conference on Control Applications in Marine Systems*. Fukuoka, Japan,

(31)   Fossen, T. I., *Guidance and Control of Ocean Vehicles*. John Wiley and Sons Ltd., England. 1994.

(32)   Amerongen J. van, "Adaptive steering of ships - A model reference approach", *Automatica*, vol. 20(1), 1984, 3-14.

(33)   Fossen T.I., "Marine Control Systems: Guidance, Navigation, and Control of Ships Rigs and Underwater Vehicles". *Marine Cybernetics*. Trondheim, Norway. 2002.

(34)   SNAME. (The Society of Naval Architects and marine Engineers). "Nomenclature for Treating the Motion of a Submerged Body Through a Fluid". *Technical and Research Bulletin*, Nº 1-5. 1950.

(35)   Norrbin, N.H., "Theory and observation on the use of a mathematical model for ship maneuvering in deep and confined waters". *8th Symposium on Naval Hydrodynamics*. 1970.

(36)   Blanke M., *Ship propulsion losses related to automatic steering and prime mover control*. PhD Thesis. Servolaboratory. Technical University of Denmark. Lyngby. Denmark. 1981.

(37)   Lewis E.V. *Principles of Naval Architecture*. (2nd ed.), Vol. 3. The Society of Naval Architects and Marine Engineers. 1989.

(38)   Faltisen, O.M., *Sea Loads on Ships and Offshore Structures*. Cambridge University Press. 1990.

(39)   Abkowitz M.A., "Lectures on Ship Hydrodynamics, Steering and Manoeuvrability". *Technical Report Hy-5 Hydrodynamics Department*. Hydro and Aerodynamics Laboratory, Lyngby, Denmark. 1964.

(40)   Kallström C., *Identification and adaptive control applied to ship steering*. PhD Thesis. Lund Institute of Technology. 1982.

(41)   Son, K.H. and Nomoto K., "On The Coupled Motion of Steering and Rolling of a High-speed Container Ship". *Journal of Naval Architecture and Ocean Engineering*. Vol. 20. Japan. 1981.

(42)   Blanke M. and Jansen A.G., "Dynamic properties of a container vessel with low metacentric height". *Trans Inst MC*. Vol. 19(2). 1997.

(43)   Aström K.J. and Kallström C.G., "Identification of Ship Steering Dynamics". *Automatica*. Vol. 12(9). 1976.

(44)   Kallström C.G. and Aström K.J., "Experiences of System Identification Applied to Ship Steering". *Automatica*. Vol.17(1). 1981.

(45)   López E., Velasco F.J., Moyano E., Rueda T. M., Bravo L., and Nanclares J.L., "Use of Mathematical Models of Ship to simulate sea Trials". *3rd International Congress on Maritime Tecnological Innovations and Research*. Bilbao. Spain. 2002.

(46)   López E., Velasco F.J., Moyano E., Rueda T. M., "Mathematical Models of Ships for Manoeuvering Simulation and Control", *Journal of Maritime Research.* 2004. To appear.

(47)   Nomoto, K., Taguchi, T., Honda, K., Hirano S., "On the steering qualities of Ships". *International Shipbuilding. Progress*. Vol. 4. 1957.

(48)   Fossen T.I. and Paulsen M.A., "Adaptive Feedback Linearization Applied to Steering of Ships". *1st IEEE Conference on Control Applications*. 1992.

(49)   Borguesani, C., Chait, Y., Yaniv, O., "Quantitative Feedback Theory Toolbox – For use with MATLAB". *The MathWorks Inc*. 1995.

(50)   Morari M. and Zafiriou, *Robust Process Control*. New Jersey. Prentice Hall. 1989.

(51)   Goldberg, D., *Genetic Algorithms in searching optimisation and machine learning.* Addison Wesley, Reading, MA, 1989.

(52)   Fleming P.J. and Purshouse R.C., "Evolutionary algorithms in control systems engineering: a survey". *Control Engineering Practice*. Vol.10. 2002.

(53)   Michalewicz Z., *Genetic Algorithms + Data structures = Evolution Programs.* Springer Verlag.1994

Chapter 11

URIS: Underwater Robotic Intelligent System

J. BATLLE, P. RIDAO, R. GARCIA, M. CARRERAS, X. CUFÍ, A. EL-FAKDI, D. RIBAS,
T. NICOSEVICI, E. BATLLE
Computer Vision and Robotics Group, University of Girona, Spain
G. OLIVER, A. ORTIZ AND J. ANTICH
Systems Robotics and Vision Group, University of the Balearic Islands, Spain

Oceans play an important role in human existence. They are a huge source of natural resources (oil, food, minerals, etc.). Nevertheless, humans are not adapted to the underwater environment. Hence, technology developments have been traditionally used to carry out underwater exploration. First manned submersibles were used mainly for scientific campaigns. Nowadays, ROVs are the workhorses being used for scientific and industrial applications. Although several successful applications have been reported for research AUVs, very few of them are commercially available. When it comes to low cost small size AUVs, it is even more difficult to find available systems. The Computer Vision and Robotics research group of the University of Girona is interested in the research and development of low-cost small-size AUVs. In this context, the URIS project represents the first work of our team to prove the viability of this kind of robot as a research test bed, but also as a useful platform for shallow water applications. This paper presents the main developments carried out within this project.

1 INTRODUCTION

The Ocean, a huge mass of water with an extension of 361 million km^2, covers 71% of the earth's surface (1). About 37% of the world's population lives within 100 Km of the sea. These data gives us an idea of the importance of oceans for human existence. They are a source of food, minerals and oil, and exert enormous influence on our climate. Historically, oceans have been natural borders between countries, and have delimited for centuries the frontier between the known and the unknown. Since time immemorial, inherent human curiosity and its fascination for exploring new environments together with the need for new resources compelled people to invent machines and engineer vehicles with which to travel over the seas, and then to dive under them. In this context, underwater robotics is a basic tool for ocean exploration, both from a scientific and industrial viewpoint.

Unmanned Underwater Vehicles (UUVs) are distinguished from conventional submarines by the absence of a crew. The self-propelled torpedo, perfected in 1868 by Whitehead could be

considered a precedent for UUVs (2). With the development of the technology, the first Remotely Operated Vehicles (ROV) appeared. A ROV can be defined as a UUV requiring instruction from an operator via a tethered cable or an acoustic link. The cable-controlled underwater recovery vehicle designed and constructed by the US Navy in 1958 could probably be considered the first true ROV. It was used in 1963 in the search for the ill-fated USS *Thresher* and again in 1966 when it helped to recover the hydrogen bomb lost by the US Navy off the coast of Palomares in Spain. During the late 70s and 80s many different ROVs were built. In 1985 Dr. Ballard's team at the Woods Hole Oceanographic Institution used JASON Jr ROV to discover *The Titanic* sitting on the ocean floor at a depth of 3798 m. Ten years later, in 1995, the ROV *Kaiko* navigated the deepest rift in the ocean, the Mariana Trough (10.058 meters). Such vehicles began to be and are still used in the offshore industry and for scientific oceanographic studies. ROVs have come to be considered the workhorses for commercial use and over 100 different varieties are commercially available world wide. Nevertheless, extensive use of ROVs is currently limited to only a few applications because of their prohibitively high operational costs, operator fatigue and safety issues (3). The natural evolution of such vehicles goes towards providing the vehicle with more autonomy. An Autonomous Underwater Vehicle (AUV) is an untethered UUV which carries its own power source and has intelligent software permitting it to execute a mission. This mission would consist of a sequence of pre-programmed instructions potentially modifiable on-line as depending on the data gathered by the on-board sensors. The *SPURV1,* developed in 1963 by the Applied Physics Lab of the University of Washington, was one of the first AUVs (4) able to reach 3658 m depth used to carry out measurement in the water column. During the 90s, about 30 AUV vehicles were developed, although only a few have been transferred for commercial use. From this group, two kinds of vehicles have been developed: (a) Cruising type vehicles, and (b) hover vehicles. The first are used in fly-by type missions during which the main goal consists of gathering information using on-board sensors. These are long range vehicles and used to have a torpedo or flat fish type hull, optimised for long displacements. On the other hand, hover type vehicles are commonly used for intervention missions. These vehicles are frequently provided with one or more robotic arms in order to interact with the environment. With a short or middle range, a variety of different shapes have been chosen by their developers.

The missions which require the use of underwater vehicles range from remote observation of the relatively unknown realm of deep-seafloor processes to the inspection of man-made structures in the oil industry. Table 1 presents a classification of potential applications for underwater robotics. Underwater vehicles have greatly advanced as a tool for undersea exploration and navigation in the last few years. In particular, autonomous navigation, localization and mapping have become topics of increasing interest both for researchers in underwater robotics and marine scientists. From a control viewpoint, the non-linear, time-varying nature of the underwater robot, together with uncertainties in the hydrodynamic coefficients, makes the underwater vehicle a challenging system to be controlled. Vehicle control, coordinated motion control (vehicle and arm) and fault tolerance control systems have great importance for robots moving through an unknown, unstructured, and probably hazardous environment. Sensors have enormous importance in reaching full autonomy. Three types of sensors can be found in an underwater robot: (*i*) Navigation sensors, used for estimating the motion of the vehicle; (*ii*) mission sensors, providing information about the

environment; and finally, (*iii*) system sensors, providing information about the vehicle itself and heavily relied on for self diagnostics and safety. On the other hand, mechanical manipulators are needed for intervention missions. Although most ROVs are endowed with one or more arms, most AUVs do not have any arms and are restricted to survey-type missions. Communication is not considered a big problem in AUVs if we expect them to do their work autonomously. Communication, however, is much more important when we work with ROVs. Most possess an umbilical with coaxial or optical fiber. For untethered vehicles, such as semi-autonomous UUVs, acoustical modems are used at very low speeds.

TABLE 1. Potential application of underwater robots

Field	Applications
Science	- Seafloor mapping - Rapid response to oceanographic and geothermal events - Geological sampling - Study of marine biology
Environment	- Long term monitoring - Environmental remediation
Industrial	- Inspection of underwater structures: - Pipelines - Dams - Harbours - Ship hull and internal tank inspection - Underwater communication & power cables installation and inspection - Nuclear power plant inspection - Construction and maintenance of undersea structures - Fisheries underwater ranger - Ocean survey and resource assessment
Civil	- Rescue - Entertainment tours - Underwater Archaeology
Military	- Shallow water mine laying and/or disposal - Submarine off-board sensors - Clandestine missions

The research work carried out at the Computer Vision and Robotics Research group of the University of Girona has the aim of contributing to the development of Autonomous Underwater Vehicles (AUV). In the experimental work of the laboratory, two underwater robots have been developed. The first one, GARBI, was first conceived as a Remotely Operated Vehicle (ROV) for inspection purposes. Then, the effort was centered in building a control architecture for achieving the missions with autonomy, converting GARBI to an AUV. The second prototype, URIS, was directly designed as an AUV. This robot has very small dimensions allowing the experimentation in small water tanks, and therefore, allows a fast testing of any control system. These two platforms are used to investigate in several research lines related to underwater robotics: control architectures for autonomous and teleoperated robots; artificial intelligence techniques applied to robot control; robot dynamics and identification; real-time 3D hardware in the loop simulation; simultaneous localization and map building; mission control; image mosaicking and vision-based guidance.

The goal of this paper is to present the URIS project. The paper is organized as follows. Section 2 presents the robot design as well as the setup used for the experimentation. In section 3 the behavioural control architecture for the real time control is reported. Section 4, describes the software architecture and section 5 explains the navigation system used for water tank experimentation as well as the navigation system used for real missions. Section 6 presents real applications which have been carried out in the context of the URIS project and the paper comes to an end with the conclusions in section 7.

2. THE URIS PROJECT

The URIS robot is the result of a project started in 2000 at the University of Girona. The main purpose of this project was to develop a small-sized underwater robot with which easily experiment in different research areas such as control architectures, dynamics modelling and underwater imaging. Another goal of the project was to develop an Autonomous Underwater Vehicle (AUV) with the required hardware and software systems as the word "autonomous" implies. Other principles are flexibility in the tasks to be accomplished and generalization in the developed systems.

2.1 Robot Description

The design of this vehicle was clearly influenced by its predecessor GARBI ROV (5), although some mechanical features were redesigned. The shape of the vehicle is defined by a spherical hull surrounded by various external elements (the thrusters, sonar and camera sensors). The hull is made of stainless steel with a diameter of 350 mm, designed to withstand pressures of 3 atmospheres (30 meters depth). On the outside of the sphere there are two video cameras (forward and down-looking) and 4 thrusters (2 in X direction and 2 in Z direction). All these components were designed to be water-proof, with all electrical connections made with protected cables and hermetic systems. Figure 1 shows a picture of URIS and its body fixed coordinate frame. Referred to this frame, the 6 degrees of freedom (DOFs) in which a UUV can be moved are: *surge*, *sway* and *heave* for the motions in X, Y and Z directions respectively; and *roll*, *pitch* and *yaw* for the rotations about X, Y and Z axis respectively.

URIS weighs 30 Kg., which is approximately equal to the mass of the water displaced and, therefore, the buoyancy of the vehicle is almost neutral. Its gravity centre is in the Z axis, at some distance from below the geometrical centre. The reason for this is the distribution of the weight inside the sphere. The heavier components are placed at the bottom. This difference between the two centres entails stability in both pitch and roll DOFs. The further down the gravity centre is, the higher the torque which has to be applied in the X or Y axis to tilt the robot a certain value in roll or pitch, respectively.

The motion of the robot is accomplished through its 4 thrusters. Two of them, labelled X1 and X2 in Figure 1, exert a force in X axis and a torque in Z axis. The resultant force of both thrusters is responsible for the surge movement of the vehicle, and the resultant torque is responsible for the yaw movement. Similarly, the other two thrusters, Z1 and Z2, exert a force in Z axis and a torque in Y axis. The resultant force is responsible for the heave movement of the vehicle, and the resultant torque is responsible for the pitch movement. In this case, the

pitch movement is limited to only a few degrees around the stable position, since the gravity and buoyancy forces cause a high stabilization torque compared to that of the thruster. Therefore, only 4 DOFs can be actuated leaving the sway and roll movements without control. Like the pitch DOF, the roll DOF is stabilized by the gravity and buoyancy forces. The sway movement is neither controlled nor stabilized by any force, which makes it sensitive to perturbations like water currents or the force exerted by the umbilical cable. Hence, URIS is a nonholonomic vehicle.
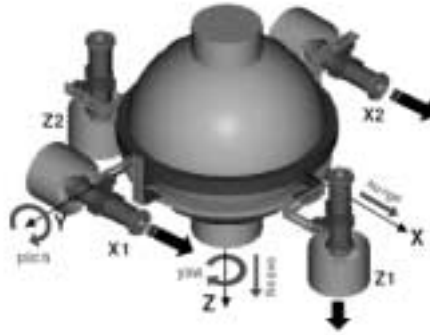

FIGURE 1. Scheme of URIS' AUV.

The inside of the hull was arranged to contain all the necessary equipment for an autonomous system. First of all, the lower part of the sphere contains various battery packages designed to power the vehicle for a period of one hour. A second level, above the batteries, contains the drivers of the 4 thrusters. Some electronic boards, mainly sensor interfaces, are also included in this level. In the third level, all the hardware components and electrical connections among all systems is found. The hardware architecture is compounded of two embedded computers. One computer is mainly in charge of the control of the robot and the other is used for image processing and other special sensors. The communication between computers is done through an Ethernet network and the communication between these computers and sensors/actuators is done through other interfaces: serial lines, analogue and digital inputs and outputs, and video frame grabbers. All these devices, except the thruster drivers, are powered by a DC-DC converter which supplies different voltages. The thruster drivers are directly powered by some battery packages specifically used for that purpose.

Besides the systems located in the robot, URIS' experimental set-up is also compounded of external systems, making some kind of connection indispensable. For this purpose, an underwater umbilical cable is used. Three different types of signals are sent through this cable. First, two power signals are sent to the robot to supply the power for the thrusters and the power for all the electronics independently. The second type of signal is an Ethernet connection, connecting the on-board and off board computers. Finally, two video signals from the two on board cameras are also transmitted. Different reasons justify the use of this umbilical cable. First, the use of external batteries increases the operation time of the robot up to the whole journey. The second reason is to help in the understanding of the experiments, allowing a real-time supervision of them through data and video monitoring.

2.2 Actuators

As described on above, URIS has four actuators to move the vehicle in four DOFs. Each actuator or thruster is equipped with a DC motor, encapsulated in a waterproof hull and connected, through a gear, to an external propeller. Around the propeller, a cylinder is used to improve the efficiency of the water jet. The power of each thruster is 20 Watts carrying out a maximum thrust of 10 Newton at 1500 rpms. The control of the DC motor is accomplished by a servo amplifier unit. This unit measures the motor speed with a taco-dynamo and executes the speed control according to an external set-point. The unit also monitors the values of the motor speed and electric current. Communication between the onboard computer and each motor control unit is done through analogue signals.

2.3 Sensors

The sensory system is one of the most important parts in an autonomous robot. The correct detection of the environment and the knowledge of the robot state, are very important factors in deciding how to act. URIS has a diverse set of sensors. Some of them are used to measure the state of the robot and others to detect the environment. Hereafter the main characteristics and utility of each sensor are commented upon.

- **Water Leakage Detection**. In order to detect any water leakage, there are several sensors which use the electric conductivity of the water to detect its presence. These sensors are located inside each thruster case as well as inside the lower part of the hull. Any presence of water is immediately sited before valuable systems can be damaged. The interface of the sensors is through digital signals.
- **Thruster monitors**. As commented above, each thruster is controlled by a control unit which monitors the thruster's rotational speed and its electric current. These two analogue measures can be used to detect faults. For instance, if the current is much higher or much lower than in normal conditions, it may mean that the helix has been blocked or has been lost. In addition, knowledge of the thruster speeds can be used to calculate the thrust and, using the dynamics model of the vehicle, to estimate the acceleration, velocity and position of the vehicle. Obviously, the inaccuracies of the model, the external perturbations and drift of the estimations would entail to a rough prediction, but combining it with another navigation sensor, a more realistic estimation can be obtained.
- **Inertial Navigation System**. An inertial unit (model MT9 from Xsens) is also placed inside the robot. This small unit contains a 3D accelerometer, a 3D rate-of-turn sensor and a 3D earth-magnetic field sensor. The main use of this sensor is to provide accurate real-time orientation data taken from the rate-of-turn sensor. The accelerometers and the earth-magnetic field sensors provide an absolute orientation reference and are used to completely eliminate the drift from the integration of rate-of-turn data. From this sensor then, the roll, pitch and yaw angles can be obtained. The interface with the sensor is through the serial line.
- **Pressure sensor**. This sensor measures the state of the robot. In this case, the pressure detected by the sensor provides an accurate measurement of the depth of the robot. Due to the electromagnetic noise, the sensor signal needs hardware and software filtering and also data calibration.
- **Forward and down-looking video cameras**. Unlike previous sensors, the video cameras provide detection of the environment. URIS has two water-proof cameras

outside the hull. One of them is a color camera looking along the positive X axis, see Figure 1. The use of this camera is to detect targets. Another use is for teleoperation tasks. The second camera is a black&white camera looking along the positive Z axis. The main utility of this camera is the estimation of the position and velocity of the vehicle. For this purpose, two different approaches have been considered. In the first approach, the motion estimation is performed from images of the real underwater bottom using visual mosaicking techniques. This localization system is one of the research lines of the underwater robotics group (6). The second approach was inspired by the first and was developed to work specifically in the URIS experimental set-up. It is a localization system for structured environments based on an external coded pattern.

- **Sonar transducer**. This sensor is used to detect obstacles in the environment. The sonar transducer (Smart sensor from AIRMAR) calculates the distance to the nearest object located in the sonar beam. The transducer is placed outside the hull looking in the direction in which objects have to be detected. A typical application is to point the beam at the bottom to detect the altitude of the vehicle. The interface of this sensor is through a serial line.

(a)
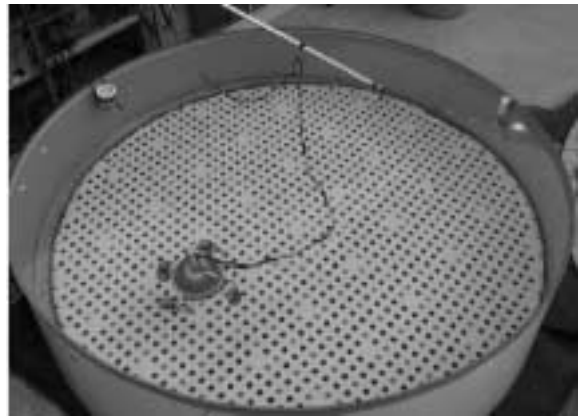
(b)

(c)

(d)

FIGURE 2. (a) Underwater Robotics Research Facility at the University of Girona; (b) Water Tank for URIS experimentation; (c) URIS AUV; (d) GARBI III AUV.

2.4 Robot setup

The Computer Vision and Robotics Group of the University of Girona (UdG) has an Underwater Robotics Research Facility (see Figure 2a) financed by the Spanish Ministry of Science and Technology, the Catalan Government and FEDER funds. The facility consists of a testing pool (18 x 8 x 5 meters), an underwater control room, a robot hangar and several labs. The bottom of the pool is covered with a digital poster of a real underwater scene allowing then to test computer vision algorithms like image mosaicking, pipe tracking, and so on. The underwater room, allows a direct view of the robot during its operation, helping then in the development process. It is worth noting that this centre is available for industries interested in the research and development of underwater robotic technology.

A second facility consisting of a small water tank (see Figure 2b) of 4.5 m of diameter and 1 m. depth is available for experimentation with URIS. This pool is equipped with a very accurate vision-based navigation system, able to provide the robot position, attitude and velocity in real time. Although the water tank is mainly used for thruster and robot dynamics identification, it can also be used for simple control experiments with small robot prototypes. Besides URIS (see Figure 2c), a second prototype has been designed and developed by our team: the GARBI III AUV, which will be available for training and experimentation (see Figure 2d).

3 CONTROL ARCHITECTURE

Different control architectures can be used to help increase the autonomy of AUVs (7). They could be categorized into three groups: deliberative, behaviour-based, and hybrid architectures. Deliberative architectures are based on planning using a world model (8). A mission is specified to achieve a set of goals and each goal is executed by a control system. They allow reasoning and making predictions concerning the environment. Data flows from sensors to the world model, which is used to plan new actions to be undertaken by the actuator. When dealing with a highly dynamic environment, the delay in the response time is the main drawback. Behavioural architectures are also known as *reactive* architectures (9). The decomposition is based on the desired behaviours for the vehicle and missions are normally described as a sequence of phases with a set of active behaviours. The behaviours continuously react to the situation sensed by the perception system. The vehicle's global behaviour emerges from the combination of the elemental active behaviours. The real world acts as a model to which the vehicle reacts, based on the active behaviours. As active behaviours are based on the sense-react principle, they are suitable for dynamic environments. However, since each behaviour pursues its own goal, reaction actions issued by one behaviour may cause another behaviour to deviate from its respective goal. As a result, the vehicle behaviour is, at times, unpredictable. Hybrid architectures take advantage of the two previous architectures while minimizing their limitations (10,11). They usually consist of three layers: the deliberative layer, the behaviour-based layer, and the control execution layer. On the other hand, the deliberative layer has the goal of breaking down the mission to be accomplished into a set of tasks. The behaviour-based layer has the goal of carrying out each task. The deliberative layer also acts over the behaviour-based layer by configuring the particular set of behaviours and the priorities among the behaviours. Finally, the control execution layer

determines if the task is being accomplished properly by monitoring sensor information and the output of the behaviour-based layer.

3.1 Hybrid control architecture

The control architecture, or high-level controller, used in URIS AUV is a hybrid control architecture. As explained above, the main advantages of hybrid architectures are reactive and fast responses due to a behaviour-based layer, and mission planning due to a deliberative layer. In this case, the deliberative layer has the goal of breaking down the mission to be accomplished into a set of tasks. The behaviour-based layer has the goal of carrying out each one of these tasks and is formed by of a set of behaviours and a coordinator. The deliberative layer acts over the behaviour-based layer by configuring the particular set of behaviours and the priorities existing among them. It activates the best behaviour configuration for the current task. To decide if the task is being accomplished properly, it supervises what the robot is perceiving and also the actions that the behaviour-based layer is proposing. The behaviour-based layer acts over the low-level controller generating the actions to be followed. These actions depend directly on the current perception of the robot since behaviours are very reactive. Finally, the low-level controller acts over the actuators to accomplish these robot actions. The whole control system of the robot just described is depicted in Figure 3. In this paper, the behaviour-based layer is only described since the experiments presented below required just this part of the control architecture.
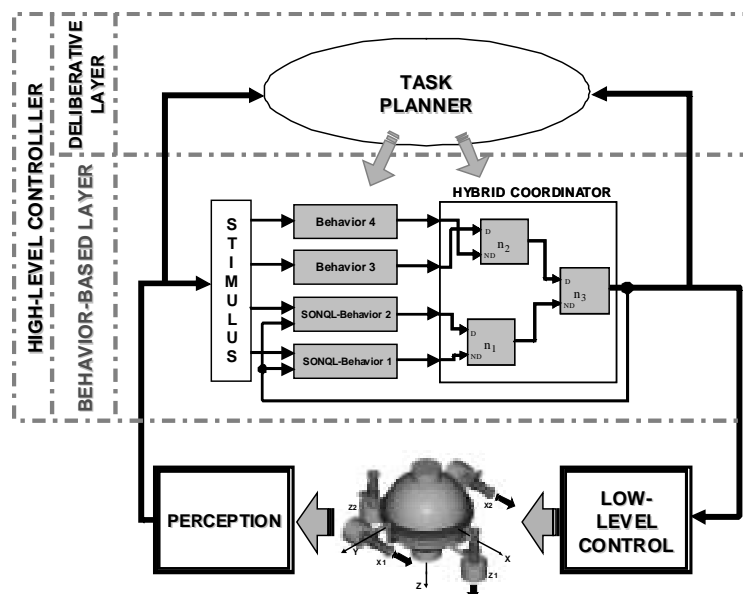

FIGURE 3. General schema of the control system conceived to control URIS' autonomous robot.

3.2 Behaviour-based layer

The behaviour-based layer (11) has been designed using the principles which behaviour-based control architectures propose. Therefore, the layer is compounded of a set of behaviours and a coordinator, see Figure 4. The most distinctive aspect of the layer is the coordination methodology. The coordinators can be classified as competitive or cooperative. Competition

methods (see Figure 4a) choose only one behaviour at each time-step to control the robot. In such methods, the priorities among the behaviours have to be established so that the highest priority behaviour becomes activated and will control the robot. Competitive coordinators are very robust in the sense that the highest priority active behaviour will always control the robot, and not allow less priority active behaviours to influence in the final performed action. Cooperative methods (see Figure 4b) offer other advantages. Usually these coordinators are very simple and the obtained trajectory can be optimal. The term optimal is here understood as a smooth, short and safe trajectory. The reason is that not only one behaviour action is taken by the coordinator, but a merging of all behaviour responses. Although high priority behaviours influence the trajectory to a large degree, the control actions of the non-priority behaviours also have an influence on the final trajectory. If the parameters required by the coordinator are properly given, the trajectory can be optimal. However, a small variation in these parameters, or a small change in the environment, can generate a wrong control action.
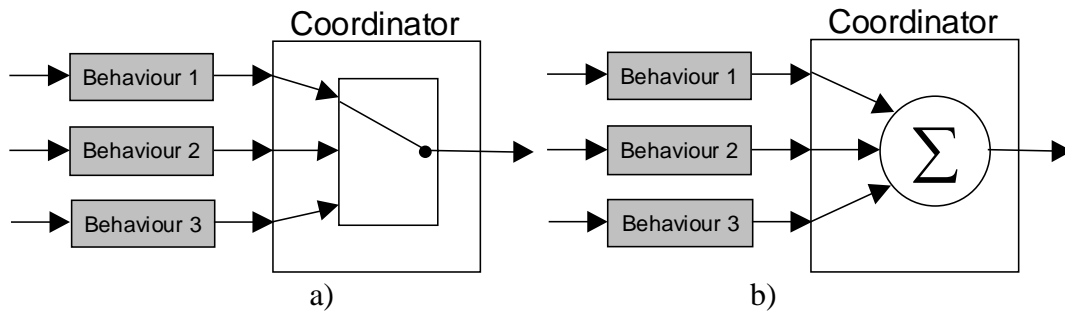

FIGURE 4. Coordination methodologies: a) competition b) cooperation.

The coordination methodology used in this behaviour-based layer is a hybrid coordination methodology, between competition and cooperation, which tries to benefit from the advantages of both. The coordination is done through a hierarchy among all the behaviours and an activation level. If higher priority behaviours are fully activated, the coordinator will act as competitive. On the other hand, if higher priority behaviours are partially activated, a merged control action will be generated. The methodology allows the coordination of a large number of behaviours without the need of a complex designing phase or tuning phase. The addition of a new behaviour only implies the assignment of its priority with reference to other behaviours. The hybrid coordinator uses this priority and a behaviour activation level to calculate the resultant control action. Therefore, the response r_i of each behaviour is composed of the activation level a_i and the desired robot control action v_i, as illustrated in Figure 5. The activation level indicates the degree to which the behaviour wants to control the robot. This degree is expressed by a numerical value from 0 to 1.
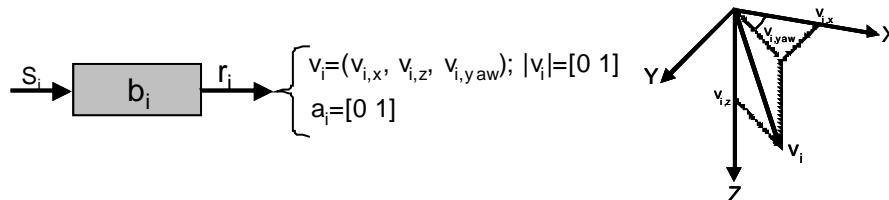

FIGURE 5. The normalized robot control action vi and the behaviour activation level ai constitute the behaviour response ri.

The robot control action is the movement to be followed by the robot. There is a different movement for each degree of freedom (DOF). By movement, we mean the velocity the robot will achieve for a particular DOF. In the case of the underwater robot URIS, which has 3 controllable DOFs, the control action is a vector with three components. This vector is normalized and its magnitude cannot be greater than 1. Therefore, the units of the vector v_i do not correspond to any real units. After the coordination phase, this normalized vector will be re-escalated to the velocities of the vehicle.

The hybrid coordinator uses the behaviour responses to compose a final control action. This process is executed at each sample time of the high-level controller. The coordination system is composed of a set of nodes n_i. Each node has two inputs, the dominant and the non-dominant, and generates a response which also has an activation level and a control action. The response connected to the dominant input will have a higher priority than the one connected to the non-dominant. When the dominant behaviour is completely activated, $a_d = 1$, the response of the node will be equal to the dominant behaviour. Therefore, in this case, the coordination node will behave competitively. However, if the dominant behaviour is partially activated, $0 < a_d < 1$, the two responses will be combined, in which case the coordination is cooperative. The response of a node cannot be discerned from one of a behaviour. By using these nodes, the whole coordination process is accomplished. After connecting all the behaviour and node responses with other nodes, a final response will be generated to control the robot.

3.3 Automatic learning of reactive behaviours

Another distinctive aspect can be found in the proposed behaviour-based layer. Due to the difficulty of manually tuning or designing each behaviour, some learning capabilities have been included to learn its internal structure. Reinforcement Learning (13) is a suitable technique to online learning when no information about the environment is available. This technique has been used to learn the internal state/action mapping of a reactive behaviour. The Semi-Online Neural-Q_learning algorithm (SONQL) was developed (14) to this end. This algorithm combines the classical Q_learning (15) algorithm together with a feed-forward NN and a database of visited states/action pairs. The main feature of the SONQL algorithm is the capability of using continuous variables, instead of discrete spaces in Q_learning. Therefore, the information coming from the sensors can be directly linked to the SONQL algorithm, which will point out, after the learning process, the action to be performed for the current perceived situation.

3.4 Example of behaviour-based layer

Figure 6 shows an example of behaviour-based control layer to accomplish a target following task on the URIS water tank. In this case, a set of 4 behaviours were coordinated with three coordination nodes. The wall avoidance behaviour had the highest priority and prevented the vehicle to collide with the walls of the water tank. The teleoperation behaviour was used to move the robot according with the commands of a human operator. The target following behaviour had the goal of generating the control actions to follow the robot at a certain distance. This behaviour was learnt with the SONQL algorithm. And finally, the target recovery behaviour spun the robot in order to find the lost target.

4 SOFTWARE ARCHITECTURE

In this section, the software architecture used to control URIS AUV is detailed. As will be described, a software framework was developed as a tool to easily implement the architecture needed to carry out a mission.

4.1 Distributed Object Oriented Framework

When working with physical systems such as an underwater robot, a real-time Operating System (OS) is usually required. The main advantage is better control of the CPU work. In a real-time OS, the scheduling of the processes to be executed by the CPU is done according to pre-emptive priorities. More priority processes will be first executed and will also advance processes which are already in execution. Using a correct priority policy it is possible to guarantee the frequency in which the control architecture has to be executed, which is very important to assure the controllability of the robot.
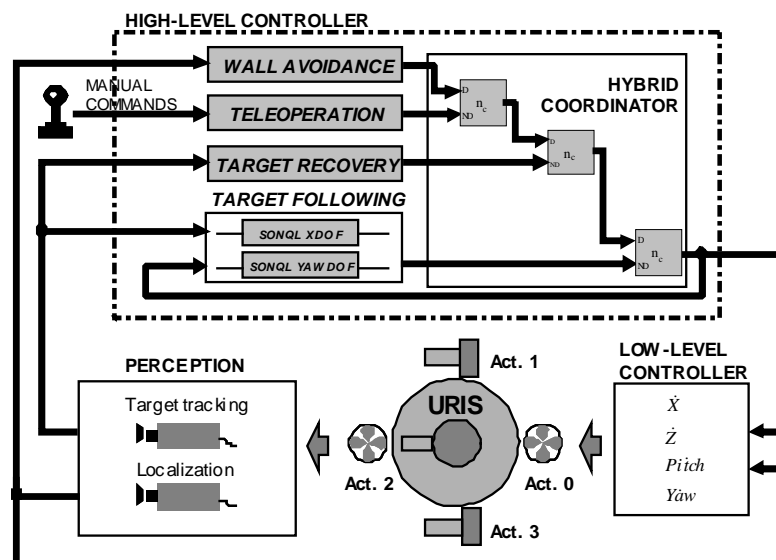

FIGURE 6. Control system architecture used in the target following task.

A software framework, based on a real-time operating system was specially designed for URIS AUV. In particular, QNX OS was used. This framework is intended to assist the architecture designers to build the software architecture required to carry out a particular mission with URIS AUV. The framework proposes the use of a set of distributed objects which represent the architecture. Each object represents a component of the robot (sensors or actuators), or a component of the control system (low-level or high-level controllers). An Interface Definition Language (IDL) is used to define the services which the object supports. From the information contained in the IDL, the object skeleton is automatically generated. Each object has usually two threads of execution. One of them, the periodic thread, is executed at a fixed sample time and is used to perform internal calculations. The other thread, the requests thread, is used to answer requests from clients.

The priority of each object thread is set independently and, depending on that, the objects will be executed. If a sample time is not accomplished, a notification is produced. These notifications are used to redesign the architecture in order to accomplish the desired times. The software framework allows the execution of the objects in different computers without any additional work for the architecture designer. A server name is used in order to find the location of all the objects. Evidently, objects that are referred to as physical devices, such as sensors or actuators, have to be executed in the computer which has the interfaces for them. Communication between objects is performed in different ways depending on whether they are executed sharing the same logical space and if they are executed in the same computer. However, these variations are hidden by the framework, which only shows a single communication system to the architecture designer.

Although this software framework was developed to work under a real-time operating system, the execution of objects under other conventional OS is also supported. The main reason for that is the lack of software drivers of some devices for the QNX OS.

4.2 Example of Architecture

The software architecture used for the example shown in Section 3.4 can be represented as a set of components or objects which interact among them. The objects which appear in the architecture can be grouped in three categories: actuators, sensors and controllers. A scheme of all the objects, with the connections between them, can be seen in Figure 7. The actuators' category contains the four actuators objects. The sensor category contains the water detection, target tracking and localization objects and, the controllers category contains the low-level, high-level and the two SONQL behaviours. It is important to remark on the difference between low and high-level controllers. The low-level controller is in charge of directly actuating on the actuators of the robot to follow the movement set-points which the high-level controller generates. On the other hand, the high-level controller is responsible for the mission accomplishment and generates the set-points which the low-level controller has to reach.

All these objects are mainly executed in the on board embedded computer, but two external computers have also been used. The on-board computer contains the actuators, controllers and sensory objects. One of the external computers, which has been called the vision computer, contains the two vision-based sensory systems, which are the target tracking and the localization system. The other external computer, which has been called the supervision computer, is only used as a client of the previous objects. Its main goal is to control the operation of the objects and to monitor them. It has also the task of sending commands for robot teleoperation.
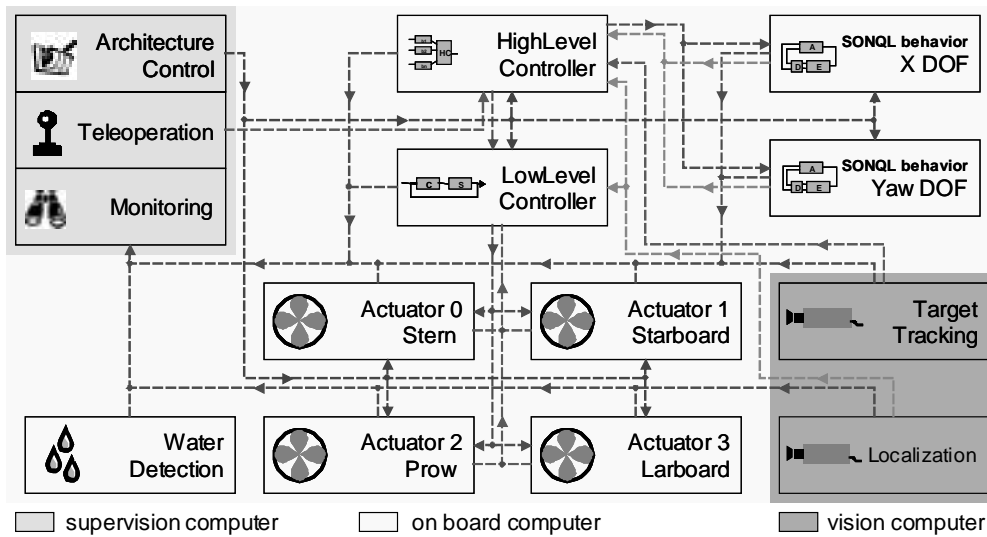
FIGURE 7. Objects which appear in the software architecture.

5 NAVIGATION

The pose (position and orientation) of an underwater robot can be calculated by integrating the apparent motion between consecutive images acquired by a down-looking camera carried by the vehicle. Knowledge of the pose at image acquisition instances can also be used to align consecutive frames to form a mosaic, a composite image which covers the entire scene imaged by the submersible. Several strategies have been presented in the literature to recover the vehicle motion by means of visual mosaics. These visual positioning systems allow the vehicle to localize itself on the mosaic map as it is being constructed (known as Simultaneous Localization and Mapping - SLAM). Once the map has been constructed, the mosaic serves for several purposes: (*i*) map-based navigation, planning the path of the vehicle during the execution of the mission; (*ii*) the generated mosaic can be used as a high-quality image to perform some further processing; and (*iii*) localization of interest areas, enabling detection of temporal changes in the morphology of biodiversity of the underwater terrain.

The characteristics of the underwater environment offer many special challenges for image mosaicking: significant attenuation and scattering of visible light, lack of image contrast and blurring of some parts of the image. The need of artificial illumination causes shadows that move with the motion of the camera. Moreover, light attenuation does not allow images to be taken from a large distance, thus to gain global perspective of the surveyed area mosaicking techniques are needed.

We conceive the navigation system for a small-class UUV as a system composed by an image mosaicking module, a low-cost INS (for attitude estimation) and a sonar altimeter (for altitude estimation). All these sensors are integrated by means of an Extended Kalman Filter (EKF). Our proposal consists of using a vision-based sensor (mosaicking) together with the hydrodynamic model of the UUV and integrated through an EKF. The filter provides position and velocity estimates reducing the noise, having also the role of estimating the motion of the vehicle along

"blind" regions (occlusions). In the following subsections we describe both the indoor and outdoor navigation system.

5.1 Down-Looking Camera Model

The camera used by the localization system is an analogue B/W camera. It provides a large underwater field of view (about 57º in width by 43º in height). The camera model that has been used is the (16) algorithm in which we include a first order radial distortion term. This model is based on the projective geometry and relates a three-dimensional position in the space with a two-dimensional position in the image plane, see Figure 8.
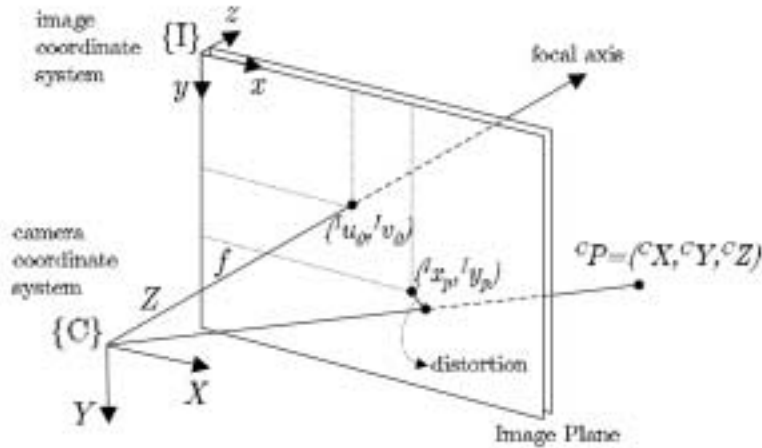

FIGURE 8: Camera projective geometry.

The calibration of the intrinsic parameters of the camera was done off-line using several representative images and applying an optimization algorithm, which by iteration, estimated the optimal parameters.

5.2 Indoor Vision-based navigation

An accurate computer vision-based navigation system has been designed and implemented to be used in the water tank. The system is based on a down-looking camera attached to the robot and a coded pattern placed on the bottom. The main goal of the pattern is to provide a set of known global positions to estimate, by solving the projective geometry, the position and orientation of the underwater robot. The pattern is based on grey level colours and only round shapes appear on it to simplify the landmark detection (see Figure 9). Only three colours appear on the pattern, white as background and grey or black in the dots. Again, the reduction of the colour space was done to simplify the dots detection and to improve the robustness. The dots have been distributed among the pattern following the "main lines" (X and Y directions), see Figure 9. The absence of a dot identifies a global mark. The pattern contains some global marks, which encode a unique global position. These marks are recognized by the absence of one dot surrounded by eight dots (see Figure 9). From the eight dots that surround the missing one, three are used to find the orientation of the pattern and five to encode the global position. The three dots which mark the orientation (marked with a circle in Figure 9) appear in all the global marks in the same position and with the same colours. The global position is encoded in the binary colour (grey or black) of the five remainder dots. The maximum number of

positions is 32. These global marks have been uniformly distributed on the pattern.

A total number of 37 global marks have been used, repeating five codes in opposite positions on the pattern. The zones of the pattern that do not contain a global mark have been fulfilled with alternately black and grey dots, which help the tracking algorithm. The navigation algorithm is based in eight sequential phases as shown in Figure 10. First, 1) an image is grabbed by the down-looking camera. Then 2), after correcting for the non-uniform sensitivity of the camera using the illumination-reflectance model, the image is binarized. In the next phase 3), the dots are detected and labelled as grey, black and unknown. In phase 4) the radial distortion on the camera is compensated (the camera was previously calibrated using Faugeras-Toscani algorithm where only the first-order radial distortion was taken into account). Once the position of the gravity centre of the dots is known, the main lines of the pattern (X and Y directions) are detected (phase 5)). These main lines allows for the detection of the dots neighbourhood. This means that is possible, after phase 6), to know for each dot every one of its eight neighbours. Once in that point, two alternatives arise. In case a global mark is visible, the global positions of its dots with respect to the frame {T} are known. Moreover, using the neighbourhood computed in phase 6), to extend the global position to all the visible dots. If no global mark is available, then the dots that were visible in the previous image are tracked. If the global position of the dots was known in the previous image, a matching algorithm is used to identify the global position of the dots visible in the current image. Hence, after phase 7) the global position of all the visible dots is known. Finally in phase 8), the projective geometry is used to solve for the 3D position. Refer to (17) for details.
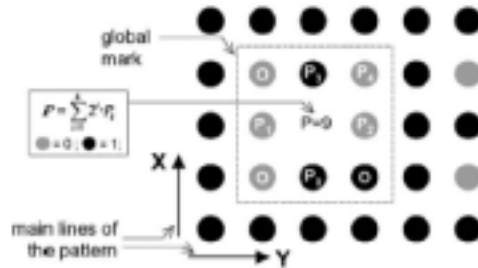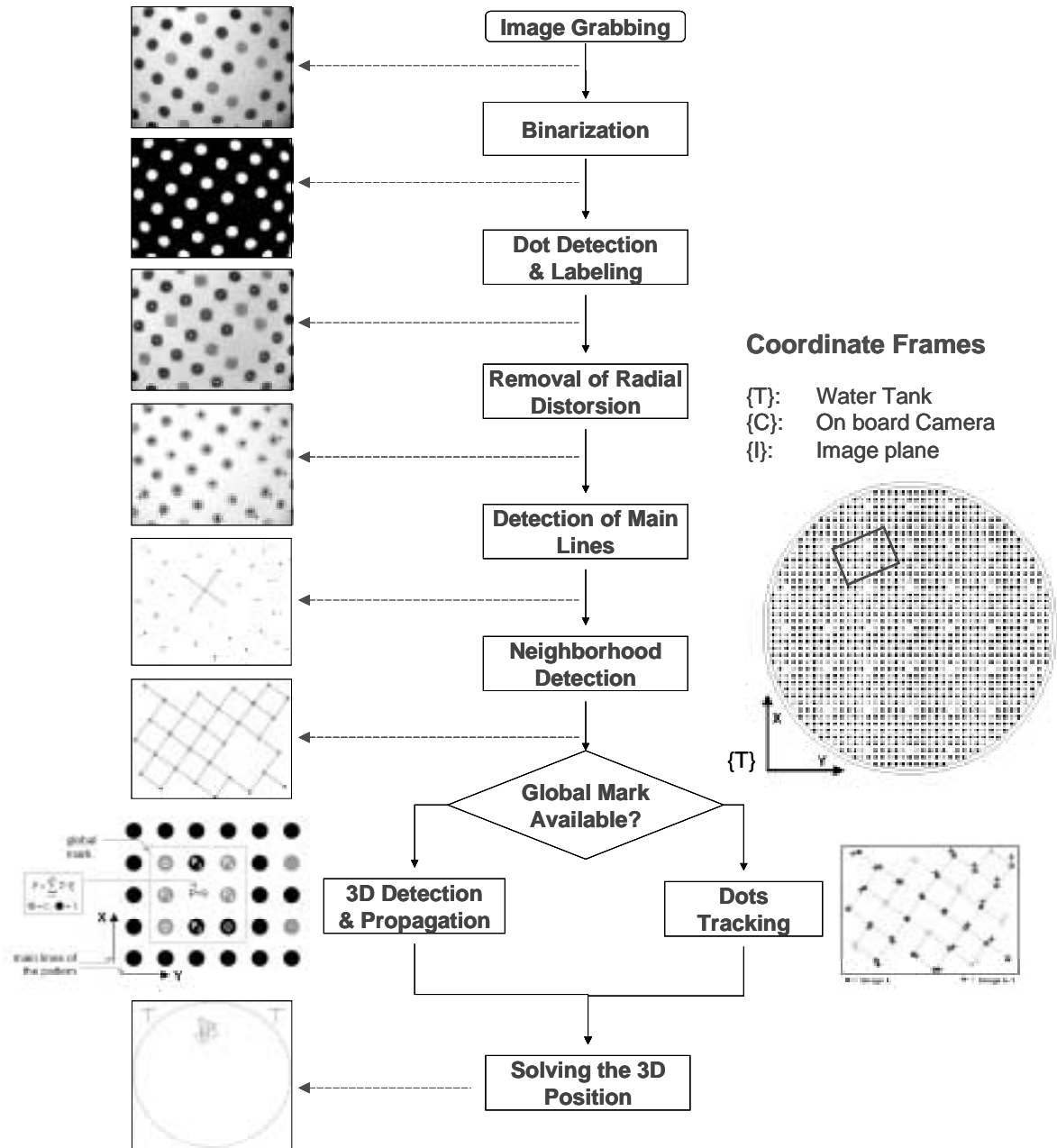

FIGURE 9. Coded pattern used for navigation.

FIGURE 10. Navigation algorithm.

5.3 Mosaic-based navigation

A composite image constructed by aligning and combining a set of smaller images is known as a mosaic (18). In most cases the construction of a mosaic involves recovering the relative motion between the camera (and therefore the robot) and the scene. Our mosaicking system is divided into two main blocks, namely: *mosaic controller* and *mosaic engine*. The mosaic controller keeps the state of the mosaicking system and takes decisions according to this state. It is responsible of the mosaic data structure, *i.e.*, updating the mosaic image (I_m) according to the estimated motion. On the other hand, the motion is estimated by the mosaic engine. It considers the current image (I_c) and a reference image (I_r) and computes a planar transformation matrix which describes the motion between both. Selection of the reference image is performed by the mosaic controller. Figure 11 illustrates the relationship between both modules.
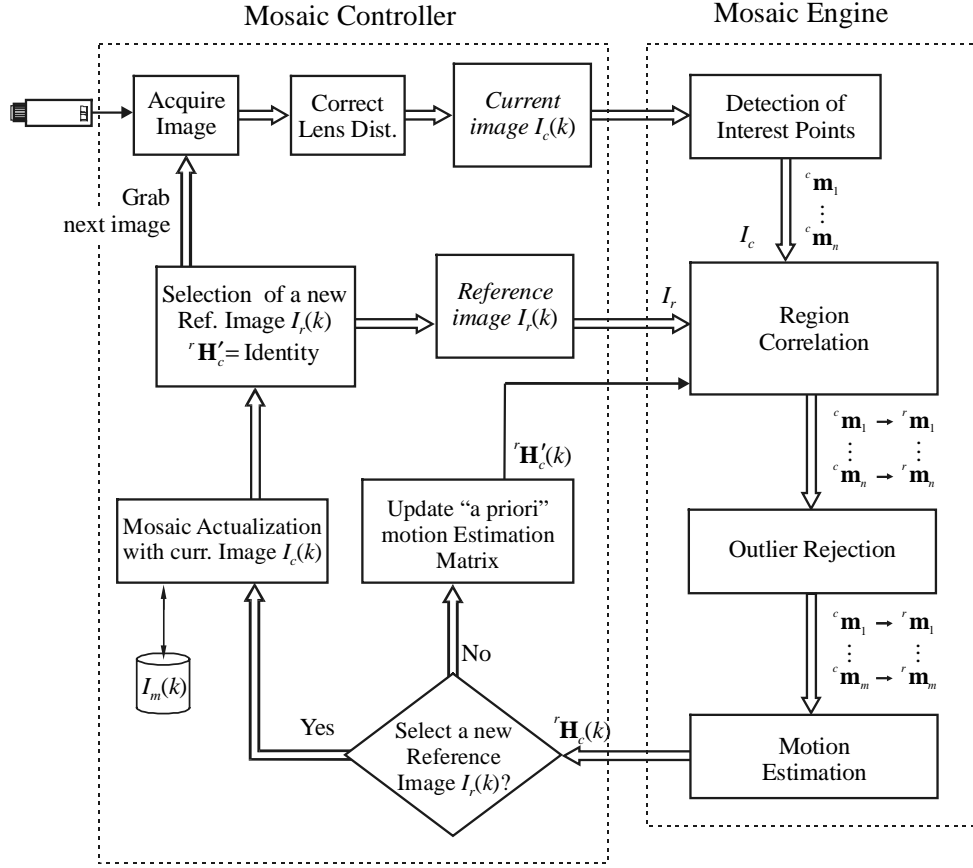
FIGURE 11. Bloc diagram illustrating the relationship between the *mosaic controller* and the *mosaic engine*.

5.3.1 Mosaic Controller

This module aims to analyze how the vehicle is moving and generates the pertinent commands to control the mosaic engine. The mosaic controller provides the engine module with the images which will be used to estimate the motion of the vehicle. One of these images is the current frame acquired by the camera (I_c) The second one is a reference image (I_r), extracted from the mosaic image I_m by the controller.

Every iteration of the algorithm starts when current image I_c is acquired. Then, the geometric distortion caused by the lens (and the water-glass-air interface of the camera housing) is corrected through a simplification of the Faugeras-Toscani algorithm (19) to correct uniquely radial distortion, instead of performing full camera calibration (16). Once lens distortion has been corrected, the current image at time instant k, denoted $I_c(k)$, is rotated and scaled so that its orientation and scale matches that of the reference image $I_r(k)$.

Consider a 3×3 matrix ${}^{r}\mathbf{H}_{c}(k)$ as the planar transformation (known as *homography*), which transforms the coordinates of a point in image $I_c(k)$ into its corresponding coordinates in the

reference image $I_r(k)$. The motion estimated at the previous time instant $^r\mathbf{H}_c(k-1)$ is assumed to be valid as an "a priori" motion estimation for instant k, since motion between two consecutive images is rather small due to the high frame-rate of the sequence. Then, images $I_r(k)$ and $I_c(k)$, together with "a priori" motion estimation matrix $^r\mathbf{H}_c(k-1)$ are passed to the mosaic engine, and it is told to execute. The output of the mosaic engine is the homography matrix $^r\mathbf{H}_c(k)$, which estimates the motion between $I_c(k)$ and $I_r(k)$ at time instant k. It should be noted that the engine is executed only when the controller requires it.

Once the engine has finished its execution, the controller decides if the mosaic image (I_m), should be updated. The controller can be configured to actualize the mosaic every α images, with $\alpha \in [1,100]$. It uses $^r\mathbf{H}_c(k)$ to update the mosaic image with the current image.

The next step consists of deciding whether a new reference image I_r has to be selected for the next iteration. The controller uses matrix $^r\mathbf{H}_c(k)$ to check if the overlapping between the reference image $I_r(k)$ and current image $I_c(k)$ is below a given threshold (*e.g.* 40% of the size of the image). In this case, it has to select a new reference image $I_r(k+1)$ for the next iteration of the algorithm. Following this methodology, drift in the estimation of the trajectory of the vehicle increases more slowly than registering every pair of consecutive images.

On the other hand, if the overlap between images $I_c(k)$ and $I_r(k)$ is bigger than the threshold, the reference image will not change, *i.e.* $I_r(k+1) = I_r(k)$.

5.3.2 Mosaic Engine

The engine begins its execution by detecting interest points in the current image. The goal of the interest point detector is to find scene features which can be reliably detected and matched when the camera moves from one location to another. Moreover, these features should be stable when lighting conditions of the scene change somewhat. A slightly modified version of the Harris corner detector (20) is used to detect the interest points. Once the relevant features of image I_c have been detected, the next step consists of finding their correspondences in the reference image I_r. Before searching for correspondences, both images are smoothed with a 3×3 Gaussian mask. Given an interest point in the current image, we predict the position of its correspondence in the reference image, based on the previous estimation. Then, a search window is selected in this predicted position, and a similarity function looks for the feature in the search window of I_r which is more similar to the selected interest point of I_c. This similarity is computed as a correlation of texture vectors (21).

In order to provide more robustness to the system, the incorrect correspondences (known as *outliers*) are detected through the Least Median of Squares (LMedS) algorithm, which removes points describing non-dominant motion (22). These "bad" correspondences may be in fact correctly matched points that do not describe the real motion of the ROV, belonging to some moving object of the scene, such as a moving fish, algae, etc.

Finally, the motion estimation $^r\mathbf{H}_c(k)$ between current and reference images is computed from the remaining pairs of points. When the engine completes its execution, it gives back the control to the mosaic controller.

6 APPLICATIONS

Although the URIS robot was conceived as a test bed for research purposes, during these years it has also been used as a test bed for real applications including visual guided dam inspection, seafloor mapping and cable/pipe tracking. These applications constitute our first steps in real applications of industrial interest. The following subsections describe a set of applications carried out using URIS AUV.

6.1 Dam inspection
The experiments reported here were carried out in the context of a bilateral program between University of Girona and IPA CIFATT of Cluj (Romania). The goal of the two-days trials was to evaluate the possibility of using a small ROV for dam inspection missions (see Figure 12).
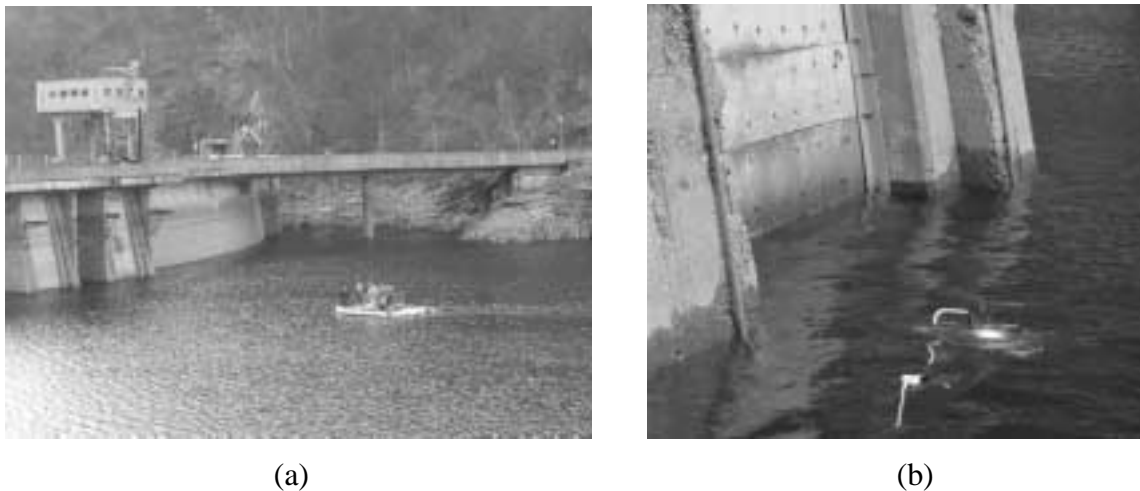

(a)   (b)

FIGURE 12. (a) Tartina Dam in Cluj (Rumania). (b) URIS in front of the dam wall.

The experiments took place at the Tartina hydro dam, located near Cluj, Romania on November 2002. The trials of the first day were concentrated on the state-analysis of the outlet located downstream the dam. The maximal depth of the experiment reached 10 m. The vehicle proved to be very useful in accessing difficult places. The ROV gave the inspectors the possibility to visualize different aspects of the area (state of the concrete and metal installation, obstruction of pipes, etc.).

The second day experiments took place downstream of the dam. The maximal depth was 20 m. As in the first day, one of the main goals was the real-time inspection of the wall and installations. In addition, video sequences of the wall were recorded for off-line mosaicking.

Once in the lab, the video sequences were processed and used to create video mosaics. It should be noted that the conditions of the experiment were not ideal for the mosaicking system. In order to achieve best mosaicking results, it is needed to move the robot parallel to the wall while keeping a constant distance to the wall. Due to the actual configuration of URIS (the *sway* degree of freedom is not actuated) the distance to the wall could not be kept constant without turning the robot (yaw movement). For this reason, in order to describe a typical survey trajectory, the ROV could not always keep the camera parallel to the wall, sometimes even loosing the view of the wall.

Figure 13 shows a mosaic of the wall dam in which the vehicle performs a downward motion. This mosaic covers a vertical area of 14 m while the vehicle moves 4 m in the horizontal axis.

FIGURE 13. Mosaic image of the upstream dam wall

6.2 Exploration and mapping of unknown environments

Several sea trials have been performed in the last few years in the coastal waters of Costa Brava. To perform each experimental run, the pilot teleoperates the vehicle positioning it at suitable range above the seabed. Then, as the vehicle moves, the acquired images are sent to

the surface through the umbilical tether, where they are either stored to a tape or processed in real time.

Figure 14 shows the mosaic constructed while the vehicle was following a submersed chain at the harbour of Platja d'Aro. At the beginning of the sequence (right) the chain is at the range of the sea bed, but, as the image sequence progresses towards the left, it goes up from the floor. It is possible to see how the underlying assumption of flat scene is violated. However, the vehicle path can be reconstructed from the mosaic without a major problem. Although point correspondences detected in the chain are correctly established, the points detected in the chain undergo a different apparent motion than the background sea floor points, due to differences in range. For this reason the LMedS algorithm detects them as outliers.
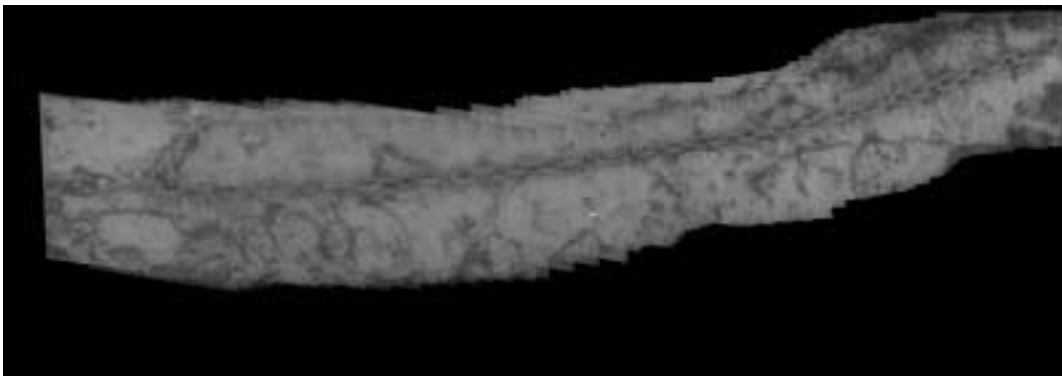

FIGURE 14. Transect of a sample trajectory followed by the submersible during a sea trial at the harbour of Platja d'Aro.

The sea trial reported Figure 15 shows a trajectory performed by the vehicle in an area of the sea floor formed by rocks and algae. The original trajectory is formed by 4.380 images acquired at a frame rate of 25 i.p.s. The sequence has been sub-sampled, taking only one image of every five, thus the mosaicking system has processed 876 images. It can be observed in this Figure that image alignment is quite good, although the underwater terrain is not flat.
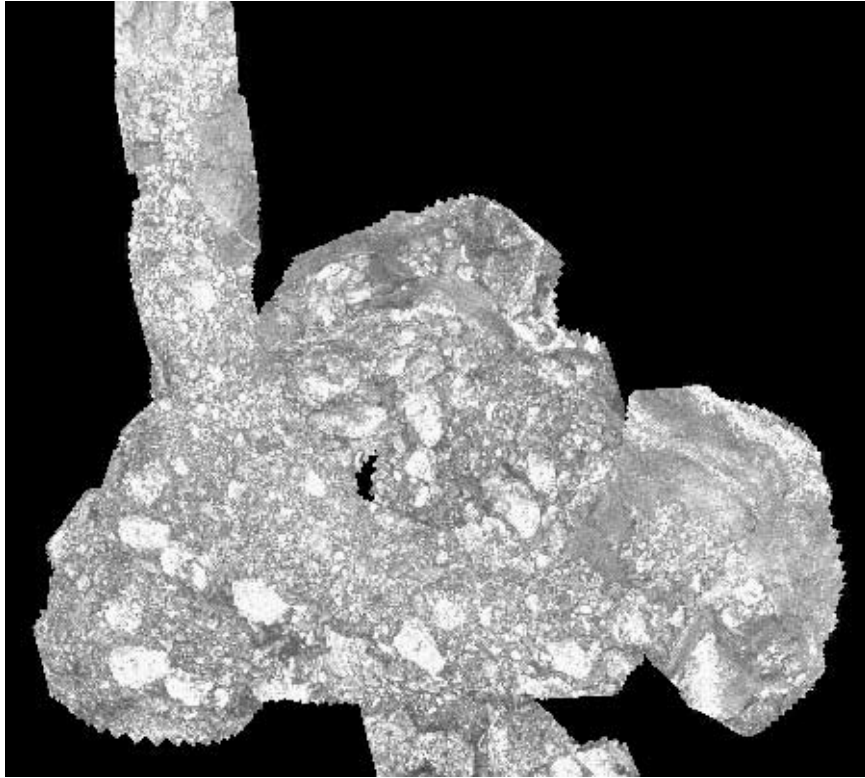
FIGURE 15. Part of a surveillance trajectory described by URIS at Cala Margarida (Palamós-Girona).

6.3 Cable Tracking

During summer 2003, the vision-based cable tracking (see Figure 16) algorithm, developed by research team of the University of the Balearic Islands (23), was interfaced with the URIS control architecture and tested the UdG water tank (24). A new behaviour was developed to configure the URIS control architecture for a cable tracking application (see Figure 17). The cable detection and tracking behaviour moves the robot through the water tank in a random way looking for the cable/hosepipe. Note that, considering the small dimensions of the water tank used for the experiments, more sophisticated searching strategies will not significantly reduce the average time required to detect the cable. Once the cable has been detected, the tracking stage starts. At this point, the AUV can be oriented in any one of the two possible and opposite directions to start tracking the cable. The particular choice is based on a predefined parameter which establishes a certain range of preferred orientations. Along the tracking, two different tasks are sequentially executed: the first one tries to keep the cable oriented vertically in the captured images, while the second task intends to maintain the cable in the central area of the images. In this way, improvements in both the cable visual detection and the longitude and smoothness of the vehicle's path are expected. As it can be anticipated in a real application, anomalous situations can arise. In particular, the cable can disappear from the images because the AUV's course has drifted apart from the actual cable location. In such cases, a suitable recovery mechanism is activated, consisting in making the behaviour return to its internal search state, where the vehicle acquires the aforementioned wander movement.
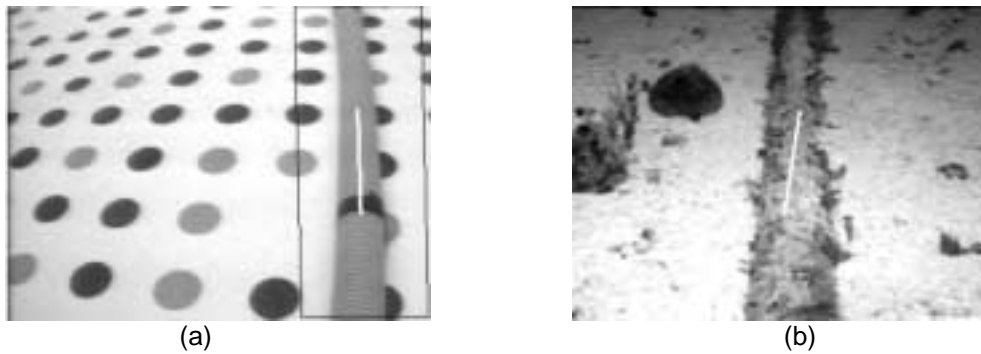
(a)   (b)

FIGURE 16. Output of the vision-based cable tracking. (a) Cable tracked in the water tank. (b) Real scenario image processed with the vision-based cable tracker.

During this research three different missions were carried out. As it can be observed in Figure 18, the main difference among them was the curvature of the cable/hospepipe placed at the bottom of the testing pool. Figures 19 to 21 show the results of the missions 1 to 3 respectively. For each mission, the XY trajectory followed by the robot, the cable position and the time variation of the robot heading are reported. A shown in these figures, the results are promising and further experiments in real environment will be performed in the near future.
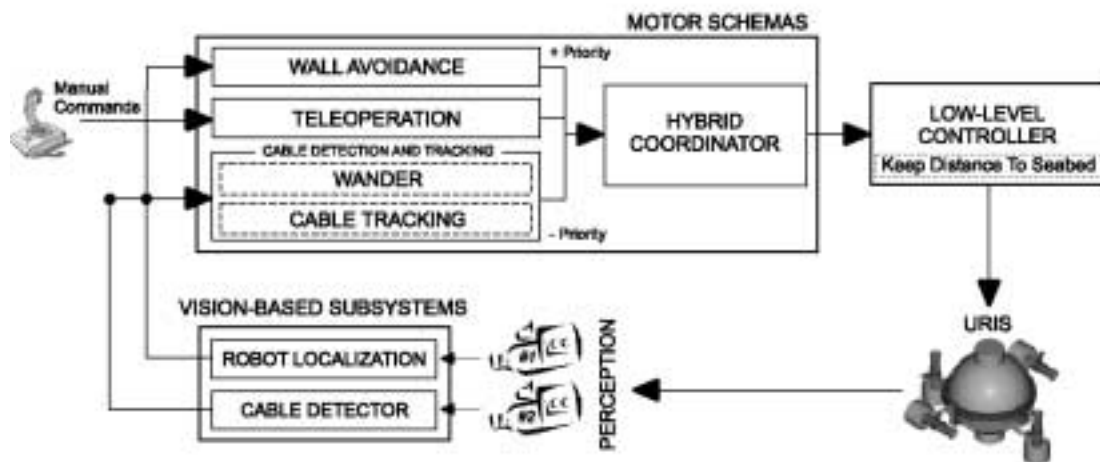

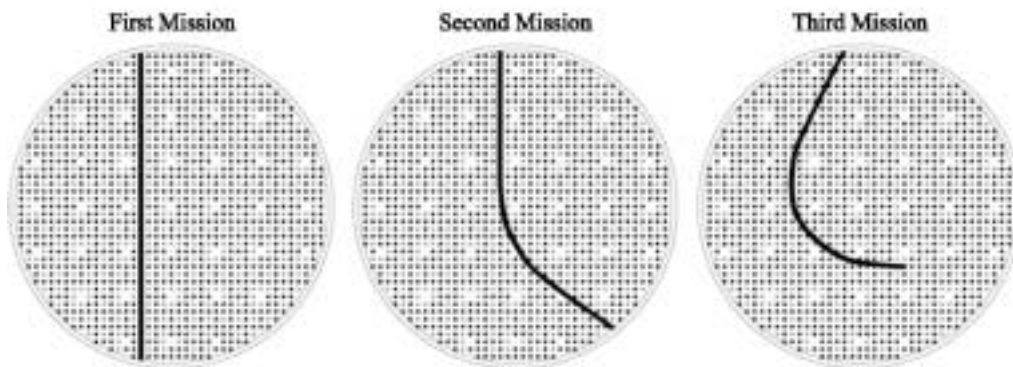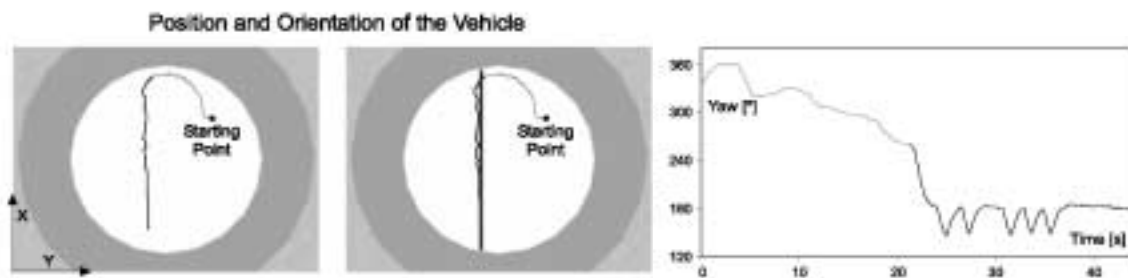**FIGURE 17. Control Architecture for Cable Tracking.**

FIGURE 18. Tested Missions
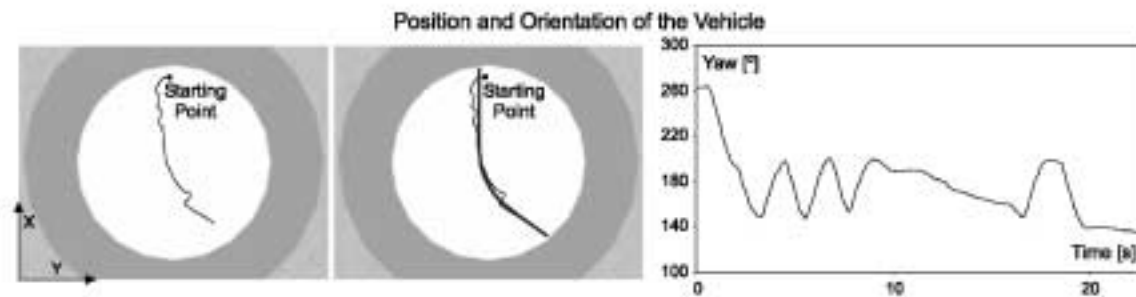

FIGURE 19. Results of Mission 1.

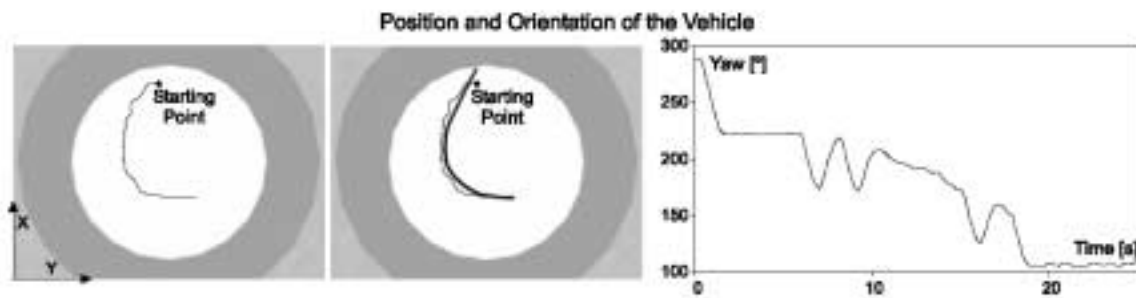**FIGURE 20. Results of Mission 2.**

FIGURE 21. Results of Mission 3.

7 CONCLUSIONS

URIS AUV is a small-size, low-cost AUV to be used as a testbed for the research in the fields of intelligent control architectures for autonomous robots, robot dynamics and underwater computer vision systems. It has a hybrid control architecture that allows reactive and fast responses provided by its behavioural layer, and mission sequencing thanks to its deliberative layer. Action selection is carried out by means of a hybrid cooperative/competitive coordinator. An interesting feature of our system is its capability to learn by itself robot behaviours using a new algorithm called semi-online neural Q-learning.

URIS software runs on a distributed hardware architecture composed by 3 computers, used for: (1) control and sensors interfacing, (2) image processing and (3) remote supervision. A set of distributed objects are used for implementing the control architecture. There are objects for the main components: sensors, actuators, controllers, behaviours and so on. This framework, which is in charge of the real time performance, is intended to assist the robot designer to build the architecture required for a particular mission.

The navigation systems of URIS are based on computer vision techniques. Two different systems have been developed. The first one is intended for structured environments. It is a very accurate absolute positioning system which makes use of a coded pattern placed on the bottom of the water tank. The second is based on image mosaicking techniques and sensor fusion and is intended for natural underwater environments. The system allows the vehicle to build a visual map and self localize within it, solving the SLAM problem.

In this paper, we have reported successful results in the use of a small-sized, low-cost underwater robot for challenging applications including visual dam inspection, seafloor imaging and cable tracking. Hence, it is our belief that low cost AUVs will play an important role in the context of shallow water applications, where the cost of the underwater technological components can be moderately bounded.

REFERENCES

(1)   Yuh, J. and Ura, T. Guest Editor's Introduction, *Autonomous Robots*, vol. 3, pp. 75-77. (1996).
(2)   Sutton, R., Roberts, G.N. Unmanned Underwater Vehicles, *Int. Journal of Systems Science*, vol. 30, pp. 899-900. (1999).
(3)   Yuh, J. Underwater Robotics, *In: Proceedings of the IEEE Int. Conf. on Robotics and Automation*, vol. 1, pp. 932-937. (2000).
(4)   Yuh, J. Introduction, *Underwater Robotic Vehicles, TSI Press,* New Mexico. (1995).
(5)   Amat, J., Batlle, J., Casals, A., and Forest, J. GARBI: a low cost ROV, constrains and solutions. *In 6eme Seminaire. IARP en robotique sous-marine,* pages 1–22, Toulon-La Seyne, France. (1996).
(6)   Garcia, R., Batlle, J., Cufí, X., and Amat, J. Positioning an underwater vehicle through image mosaicking. *In IEEE International Conference on Robotics and Automation, ICRA'02*, pages 2779–2784, South Korea. (2001).

(7) Ridao, P., J. Batlle, J. Amat and G.N. Roberts. Recent trends in control architectures for autonomous underwater vehicles. *In: International Journal of Systems Science,* 30 (9),pp. 1033-1056, (1999).

(8) Meystel, A. M. and Albus, J. S.. Intelligent Systems, Architecture, Design and Control. John Wiley & Sons, (2002).

(9) Arkin, R. Behavior-based Robotics. MIT Press, (1998).

(10) Arkin, R.C. Path planning for a vision-based autonomous robot. In *Proceedings of the SPIE Conference on Mobile Robots*, pages 240-249, Cambridge, MA, (1986).

(11) Gat, E. Reliable Goal-directed Reactive Control for Real-World Autonomous Mobile Robots. PhD thesis, Virginia Polytechnic and State University, Blacksburg, Virginia, (1991).

(12) Marc Carreras, Joan Batlle and Pere Ridao. Hybrid Coordination of Reinforcement Learning-based Behaviors for AUV Control. *IROS 2001, International Conference on Intelligent Robots and Systems*. Maui, Hawaii, USA, October, (2001).

(13) Sutton, R. and Barto, A. Reinforcement Learning, an introduction. MIT Press. (1998).

(14) Marc Carreras, Pere Ridao and Andres El-Fakdi, Semi-Online Neural-Q- learning for Real-time Robot Learning, *IEEE-RSJ International Conference on Intelligent Robots and Systems*, Las Vegas, USA, October 27 - 31, (2003).

(15) Watkins, C. and Dayan, P. Q-learning. *Machine Learning*, 8:279-292. (1992).

(16) O. Faugeras, G. Toscani, The calibration problem for stereo, in: *IEEE Conference on Computer Vision and Pattern Recognition*, pp. 15–20. (1986).

(17) Carreras, M., Ridao, P., García, R., & Nicosevici, T. Vision-based localization of an underwater robot in a structured environment. In *IEEE International Conference on Robotics and Automation, ICRA'03*, Taipei, Taiwan. (2003).

(18) R. Szeliski, Image mosaicing for tele-reality applications, in: *IEEE Workshop on Applications of Computer Vision*, pp. 44–53. (1994).

(19) R. Garcia, J. Batlle, X. Cufí, A system to evaluate the accuracy of a visual mosaicking methodology, in *MTS/IEEE OCEANS Conference*, Vol. 4, Honolulu, Hawaii, pp. 2570–2576. (2001).

(20) C. Harris, M. Stephens, A combined corner and edge detector, in: *Alvey Vision Conference*, Manchester, U.K., pp. 147-151. (1988).

(21) R. Garcia, X. Cufí, J. Batlle, Detection of matchings in a sequence of underwater images through texture analysis, in: *IEEE International Conference on Image Processing*, Vol. 1, Thessaloniki, Greece, pp. 361–364. (2001).

(22) P. J. Rousseeuw, A. M. Leroy, Robust Regression and Outlier Detection, John Wiley and Sons, New York, (1987).

(23) Miquel Simó, Alberto Ortiz, Gabriel Oliver. Optimized Image Sequence Analysis for Real-Time Underwater Cable Tracking. *Proceedings of the MTS/IEEE Oceans*, Providence, Rhode Island, USA, 11-14 September, (2000).

(24) J. Antich, A. Ortiz, M. Carreras and P. Ridao, Testing the Control Architecture of a Visually Guided Underwater Cable Tracker by using a UUV Prototype, *5th IFAC/EURON Symposium on Intelligent Autonomous Vehicles. IAV'04*, Lisbon, Portugal. (2004).

Chapter 12

Research in Underwater Robotics in the Automatic Control Department at the Technical University of Catalonia

JOSEP AMAT, ALÍCIA CASALS, ALEXANDRE MONFERRER, LUIS M. MUÑOZ
MANEL FRIGOLA, JOSEP FERNANDEZ, ORIOL ESCOTÉ, XAVIER GIRALT
Dep. Automatic Control and Coputer Engineering, Technical University of Catalonia (UPC) – Barcelona, Spain

1. INTRODUCTION

The Robotics group of the Automatic Control Department at UPC started its research in Underwater Robotics in 1991, under a request of professor Margalef (1927-2004), a well recognized ecologist. The aim of the first project was to provide biologists with a low cost underwater vehicle able to operate off shore, for underwater exploration and observation. The project Garbí was born from the first workshops, where the two teams studied and evaluated the needs and technological possibilities. The project started in 1992.

The conjunction of twofold objectives, the design and construction of a low cost platform and the will to not renounce to high levels of efficiency, forced us to limit the operability of the system to depths of 200 meters. This relatively short range makes possible the use of a conventional umbilical cable for the transmission of information between the vehicle in immersion and the external control unit, and for the external feeding of the robot from the support vessel as well. The constrain to operate up to 200 meters depth is not really quite restrictive since for applications in marine biological research, the interest is mainly centred over the marine platform that does not surpass this depth. Furthermore, the potential industrial interest, as for instance the inspection of ships, harbours, damps or marine platforms, takes place at depths lower than 200 meters.

Since the vehicle has been provided with a high vertical stability, it has been possible to reduce to four the number of degrees of freedom. For simplicity of the structure the two robotic arms have only three degrees of freedom each. The compensation of such limitation passes through the use of a double parallelogram structure that enables the arms to decouple the two rotation movements of the arm joints, keeping constant the orientation of the hand.

One of the main goals of the project is to facilitate the task of the human operator for teleoperation tasks to be performed with the two robotic arms, (1). This is achieved, even

having only three degrees of freedom for each arm and very low loading capability, thanks to the fact that the underwater robot control system is endowed with a stereoscopic vision system, accumulating the experience of the research group in this field. From the 3D vision information it is possible to stabilize dynamically the robot, automatically, in front of an object, as for instance, a rope.

2. THE DESIGN OF THE UNDERWATER ROBOT GARBI

The achievement of the goal of designing a low cost underwater vehicle has been possible using the rarely used technique of servopressurizing the inside of the capsule with pressurized air, using a standard diver air bottle. This technical solution has enabled us to null the difference in pressure, internal-external, and thus to build a capsule with the most adequate shape for navigation and accommodation of all the required elements inside, without the restrictions of shape that would be needed to resist pressures of up to 20 atmospheres, fig. 1.

Fig. 1 The underwater robot Garbí

In what refers to the arms, the positioning of the robot hands in any position and orientation would require to have available at least 6 degrees of freedom. A great number of underwater robots are provided with 7 DoF to achieve more accessibility. These arms frequently use hydraulic technology, their cost is high, they are complex and require a lot of space inside the vehicle for their power system, and their consumption is high. The design of the Garbi arms, provided with only 3 DoF, has considered the minimal requirements for an effective operability. For this reason, one of the hands has been mounted in the vertical plane and the other in the horizontal plane, thus enabling the robot to collect samples and manipulate small objects with the most adequate hand, each with the help of the other.

The first prototype was endowed with a local control system, with reactive control capabilities, based both, the own navigation sensors, depth sensors, speed log, US sensors, frontal presence and see bottom detection, and the stereoscopic vision system.

The robot is controlled from the surface by means of the remote control unit, shown in fig. 2, enabling the displacement and control of the robot towards the working area. The two teleoperated arms are guided from outside by means of an exoskeleton, as shown in fig. 3.

This underwater vehicle did its first immersion mission in the UPC channel in 1994, (2) and the first immersion at open sea in 1995. From the experience obtained with the first works, the research of the team was oriented to achieve a higher dexterity that enable to compensate the constrains in degrees of freedom, both of the vehicle and its arms.
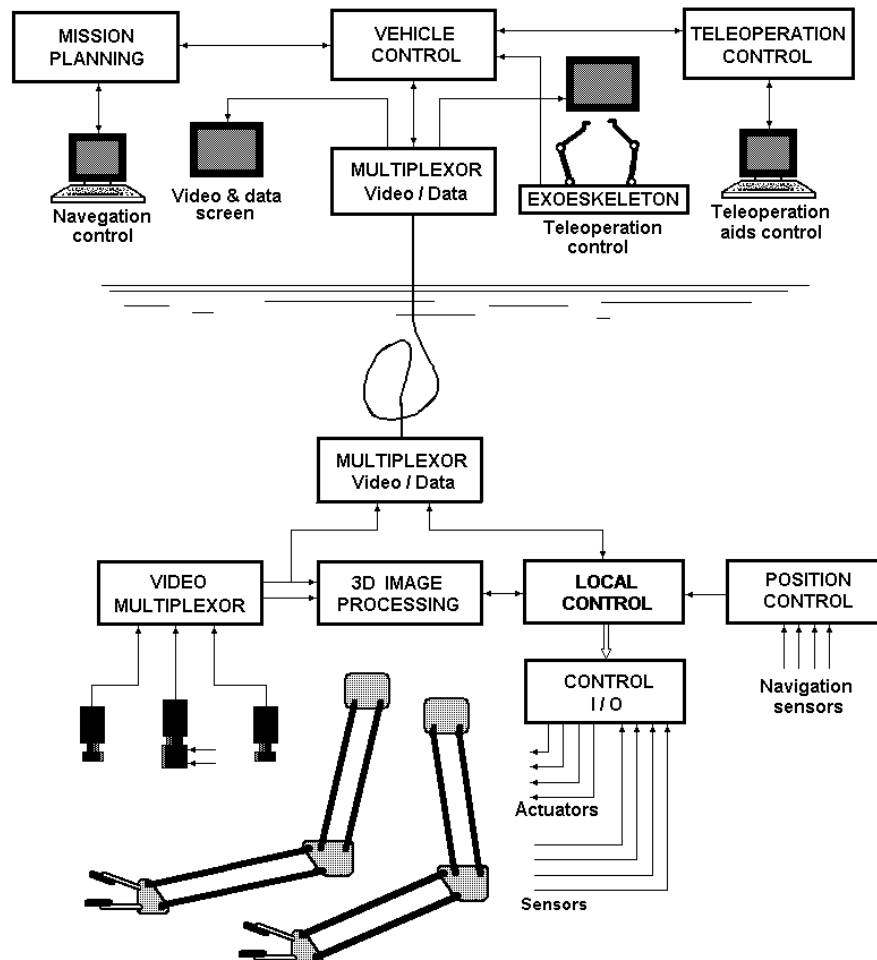

Fig. 2 Control architecture of Garbí

Fig. 3 The exoskeleton for the two arms control

3. DEXTEREOUS TELEOPERATION AIDS

A goal of the work developed within the frame of the research project Garbí, is to endow the robot with some teleoperation aids that enable the user to mitigate the constraints of operating by means of two arms having only three degrees of freedom each.

Its aims is to provide the master-slave control unit with a vision system that provides the data necessary to generate attraction forces towards the more relevant objects of the scene. In this way, when the master-slave position error is small, the robot arm tends to approach the object located in the proximity of the fingers. Thus, although the users don't have excessive ability in steering the arms with high precision towards the samples they desire to collect, the arms can stop precisely at the desired position, without surpassing the detected objects. Additionally, in the case that the base of the vehicle is not stable, the attraction forces would make possible to maintain the arms close to the target, as well as to track it.

Attraction and repulsive forces generated from sensing the environment or from data coming from environment models are used in different kind of applications, both for autonomous robots or teleoperated manipulators. Several methods based on potential functions can be found in the literature (3, 4). The generation of the attraction forces is based on the shape of the visible objects. The objects having shapes adequate to be grasped or tighten, according to the phase of the manipulation process, are those that produce these attraction forces.

3.1 Objects characterization

With the aim of providing the user with some support in the execution of manipulation tasks a first aid consists in the determination of the objects position. A vision system is used to detect

the desired object, generating from the image segmentation a potential well, which is placed in the centre of gravity of the object that is located closer to the point where the teleoperated arm stops.

Looking deeper at the process of manipulation and grasping, we have studied a procedure to determine, depending on the object's shape, the points more adequate for the object to be grasped, as well as those inadequate. From this principle, three kind of potentials are defined: positive, negative and neutral. To illustrate the process we could define the positive potentials as those corresponding to punctual or circular objects, the negative ones are those corresponding to the robot hand approaching the scene elements, and the neutral correspond to big objects, objects with undefined shapes or part of them. The positive - negative attraction can be assimilated to the peg in a hole problem, one acting as the peg (the negative) and the other as the hole (the positive), attracting one to each other to execute an insertion task.

The classification of points in favourable or unfavourable, or even indifferent, for grasping requires an analysis of the image and the verification of the achievement of the "grasping" criterion. These criteria have been defined from the curvature radii of the detected objects. Fig. 4 shows a straight object, like a rope or a peg, being attracted towards the centre of a circle, or a hole, while in fig. 5 different straight and curved objects are tighten together.
Since the manipulation operation will be carried out in a 3D environment, the visual analysis of the curvatures and typology of the different elements in a scene is performed by means of a stereovision system.
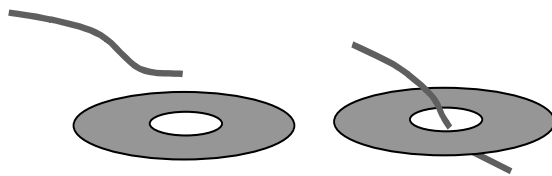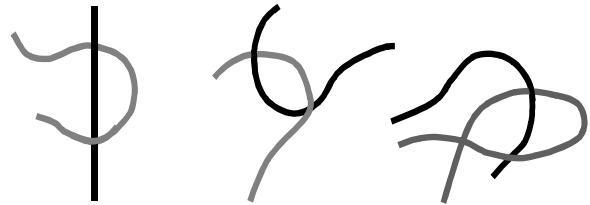
Fig. 4 Examples of object shapes   *Fig. 5   Different straight and curved objects are tighten together.*

3. 2 Image segmentation

The characterisation of the objects that appear on the image of the working scene starts with an image segmentation step. This image processing is carried out from the images acquired by the same cameras used by the vehicle for the visualisation of the working space. The goal of the image segmentation process is the determination of the position in space of the objects present in the scene, and from their shape the attraction forces are computed.

Classical segmentation methods are usually based on colour, movement, or texture. Due to the lack of contrast in underwater environments, movement information can improve the segmentation process when applicable. From the segmented image, the next step is to extract some features for stereo matching. Common methods for features extraction are based on local features, local correlation or colour boundaries. Working with underwater images, the method that has given better results is based on the matching of contour segments, that are considered the most contrasted features of the image. The algorithm for contours extraction

uses a variable threshold. The criterion for threshold computing is the maximisation of the correlation function between homologue contour segments in the two stereo images, with the aim of making the stereoscopic matching process easier. The matching carried out by means of contour segments, or micro-matching, has become highly robust and provides a precision higher than that obtained from the methods based on point to point correlation. Image segmentation in real time makes possible the use of the obtained data in the control loop.

3.3 Generation of attraction forces

Based on the principle that the operations to be carried out are the manipulation of ropes, or hook like shapes, to tighten or hook the objects to be hoisted or manipulated from the support ship, the teleoperated robotic arms actions will be simple hooking actions or ropes tightening. Consequently, the problem to be solved is to operate with enough precision so as to be able to join adequately the two parts to be tightened.

Knowing the underwater visibility problems and the low dexterity with which the simple three d.o.f. arms used can be operated, the attraction forces are generated to compensate this operating limitations. Therefore, we need that the robot hand is attracted by the target object. For that reason, we will give the hand a neutral potential and the target object will have a positive or neutral potential, depending on its shape. Let's consider the task of taking a rope and then fit it in a link or hook. The first action to perform is to give the hand a negative potential and the rope (straight or slightly curved object) due to its shape will have a neutral potential. Operating this way, the hand will be slightly attracted by the rope when the operator moves the arm close to it. Once the rope has been grasped, the operator moves the hand towards the hoop (circular or highly curved object, the shapes to which the rope can be tighten somehow). Such objects constitute the new targets, that in this case offer a positive potential, while other straight like shapes around the robot have a much smaller effect. The smaller curvature the object has, the higher is the attraction force. Thus, the stronger forces coincide with the parts more difficult to point out and to reach successfully.

In each step of the process the user guides the teleoperated arms towards the target, and when the slave approaches the desired visualised object, an increasing attraction forces reinforces the operator desired action.

The attraction law is a function of the distance, but in spite of using the common Newtonian or electrostatic functions, which value increase with the square of the distance, we use a linear law. This is due to the fact that a too high force would not allow the user to interact adequately when there are different options to choose.

The attraction function is: $F_X = d \cdot K$, for $d \le a$, otherwise $F_X = 0$, being a the variable defining the action range of the attraction force, K the gain, d the Euclidean distance, and P_0 represents the point $(x_0 \, y_0 \, z_0)$. fig. 6.
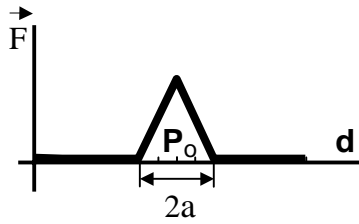
Fig. 6 Attraction force function

Fig. 7 Laboratory scenario

This method, (5, 6) that has been tested in a laboratory scenario, has resulted to be highly efficient in collecting samples semi-automatically, on the "sea bottom". The laboratory scenario, fig.6, has enabled us to define the attraction function both working in static conditions, with the robot laying on the floor, as well as dynamically, since the robot support has been designed in such a way that the vehicle can be provided with pendular movements. Therefore, tasks such as passing a hook through a ring have given satisfactory results. Figure 8 shows the potential points on the objects in the scene, obtained as a function of their shape. The assigned values are: K = 1 for closed elements with area < U_0, and K = 0,5 for open lines.
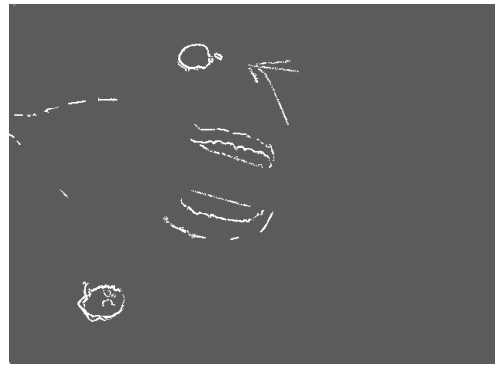

Fig. 8 View of the zones with attraction potential derived from their shape

This kind of operations make possible to hook an object by means of ropes, using simple and low force arms, and hoisting or manipulating them from a crane on a ship (6). The improvement on the operation dexterity has been achieved by associating the potential forces to attract the arms, to the scene elements to be manipulated. The potential wells are computed from the relevant segments of these objects, such as holes or end of prominent areas, thus facilitating teleoperation.

4. AUGMENTED REALITY FOR UNDERWATER OPERATION

The execution of underwater tasks by teleoperation is based on the visualisation of the scene through the vehicle onboard TV cameras. The visibility of the scene depends greatly on the water transparency. This water conditions is not always achievable since in many ports or working areas the water turbulence does not permit to guarantee visibility at distances greater than 20 or 40 cm. On the other hand, the shaking provoked by the vehicle thrusters and the vehicle own movements makes the water muddy, even in quiet waters that are usually transparent. This lack of transparency makes difficult to carry out any telemanipulated work with the minimal acceptable conditions. This fact is aggravated by the spotlights used, that produce light reflections which also contribute to reduce the clarity of the obtained TV images.

The use of acoustic images facilitates the vision in turbid waters but presents the difficulties derived from the long scanning time required to acquire images at a given resolution level. This drawback makes acoustic images useless when dealing with real time applications. With the aim to partially overcome the low resolution problem, 3D acoustical images segmentation operating from sparse data is described. The implemented algorithm is oriented to generate an augmented or virtual representation of the obtained images in order to assist a human operator for the navigation and inspection of underwater environments containing objects or structures, such as pipes.

In the same way, image augmentation, but working with TV images, the proposed solution in this work is the superposition of a synthetic image over the unclear optical image acquired from the scene (7, 8, 9). With this aim a vision based system designed for the identification and 3D location of the objects in the working environment has been developed. A synthetic image, generated from a simplified model of the arms and the acquired objects, is superposed to the real video images to make up for the lack of visibility when necessary. The new augmented image enables the operator to carry out the teleoperated tasks by means of the visual feedback of the arms position when the arms are not visible due to water turbidness. This system is also useful in cases in which although the clarity of water is good, some occlusions are produced by the working elements themselves. In this line, a previous work dealing with telemanipulation with ropes in environments with occlusions is described in (10).

The modelling of the robot own elements is possible since their CAD models are usually available. But, since the modelling of the elements on the working environment is very complex, the risk of obtaining models with not enough quality could provide erroneous synthetic information that could disturb rather than improve the visual feedback. Thus, to get the required information, it is necessary to have available 3D perception systems able to obtain images with enough quality. The 3D objects augmentation is necessary since the visual conditions decreases along the execution of a task, and thus, the visual perception becomes very difficult when time goes. This need is specially true when the robot arm moves, changing the point of view of the scene and the manipulated objects, as seen by the operator.

212

4. 1 The visibility problem in underwater teleoperation

In teleoperation tasks, the visual feedback of the scene through TV images constitutes the means that enables the control of the teleoperated arms, using any device such as joysticks, exoskeletons, gloves or so. The problems that appear in teleoperation are mainly due to both, the reduced visibility (as it usually happens in underwater robotics) or the delay in receiving the video signal (this is specially critical in space exploration).

The help usually provided to the user to improve visual feedback is the superposition, over the real images, of synthetic data or images. Augmented reality techniques are becoming more and more used to compensate these problems, but the merging of real and virtual data, to enrich the available images, is not still well solved for every possible situation, since the superposition of a synthetic image over a real one, produces at the same time some loose of real data, those that become occluded by the synthetic image. The situations considered are mainly those produced when the water gets muddy, either due to water dirtiness, as it can happen in areas such as ports, or due to water turbulence produced by the work carried out in areas with mud laying in the sea bottom.

The designed procedure starts with the segmentation process, being the segmented image the base for the volumetric objects representation. From this information, the generation of the synthetic image and its progressive superposition over the real one to form the augmented reality image constitute the following steps.

4. 2 Gradual augmented reality as a function of the visibility

The above considerations dealing with data acquisition and mixing of real and synthetic images, have motivated a study on the necessary aspects to be taken into account to achieve a good compromise between the level of synthetic information to superpose over the real image to augment it, and the loose of useful direct visual information that results when the synthetic image occupies a significant part of the real image.

With the aim of improving this compromise, a system for mixing the video and the synthetic images has been developed. The system does not operate in a fixed form, switching from the real image to synthetic data, but changing in a progressive way, a gradual mixing that superposes the synthetic image over the real one operating according to two criteria:

- At local level in the image, to make the synthetic image grow progressively over the zones with low visibility.
- At model level, solidifying the modelled object bodies, in accordance with the level of visibility, from wire-frame type minimally invasive models up to solid models.

The achievement of this progressive image superposition has required the use of a local visibility measure function, based on the local gradient histogram. The objective is to progressively superpose the synthetic video over the real images acquired from the scene in real time, from the measurement of $C(x,y)$, the local clarity, or image visibility function.

Consequently, the progressive appearance of the synthetic image over the real one is not binary, but progressive, as a function of the clarity or water transparency. This gradual change,

thus affects both, the spatial image, that is, the boundaries from the real to the mixed area move progressively as a function of water transparency, as well as the weight with which the synthetic image appears over the real one in the mixed area.

4. 3 Measure of the image clarity

The visualisation of the synthetic images in the scene background is highly useful in environments with reduced visibility. On the contrary, it results bothering when operating in transparent waters. For this reason a window of variable size, that adapts itself quickly to the water turbidness, is used. The resulting augmented images improve the operator environment perception.

The gradual appearance of the synthetic image over the real one is carried out by extracting the gradients of the available residual image, the current blurred image, and performing the matching with the synthesised image, so as to minimise the positioning errors.

Therefore, the first step to follow in the gradual augmented reality process is the appreciation of the transparency of the milieu that conditions the working visibility. This step is based on the analysis of the gradient image, from its histogram. The histogram of gradient images from blur or unclear scenes show a high density of pixels in the very low range of the grey scale, while clear, or more contrasted scenes, produce higher values on the gradient image histogram. To appreciate this effect, fig. 9 shows two images of the same scene with different levels of simulated turbid ness, and their corresponding histograms. In this later case, the distribution of pixels in the grey level axis of the histogram depends not only on the water transparency and image clarity, but also greatly on the scene characteristics. Consequently, the achievement of a progressive superposition of the synthetic image pass through the definition of a clarity function, C(x,y), in order to decide which are the areas of the scene with low visibility and to what extend they are unclear. This function has to provide a measure of transparency, independently of the kind of visualised image. Obviously, scenes with many structures tend to give a greater amount of gradients, while clear and contrasted images give more density in the high range of the histogram grey level axis.

The superposition function, x, is thus defined locally according to the clarity or water visibility measured, C(x,y), and their parameters can be adjusted by the user according to their preferences.
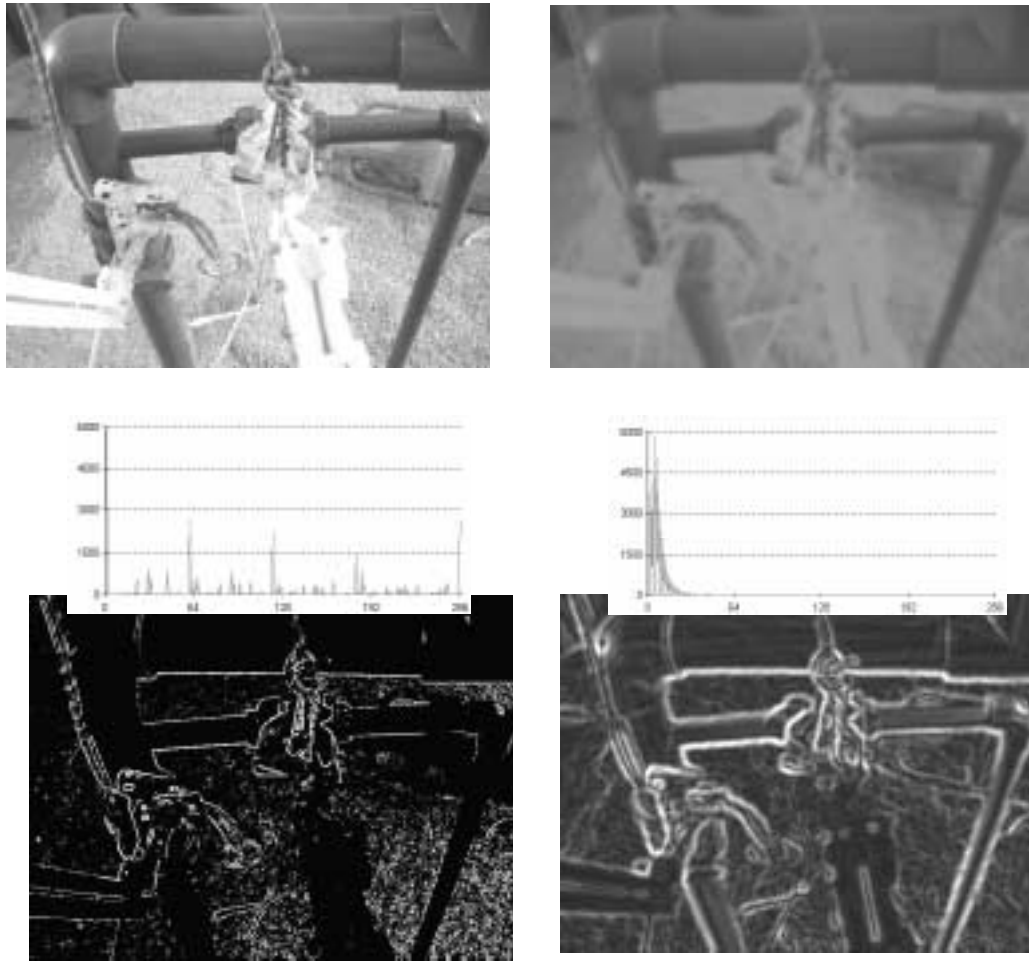
***Fig. 9. Histogram differences of clear and blurred images   a) Clear original image
and its histogram and gradient   b) the same for a blurred image***

ξ can be expressed as $\xi = f(x,y,C)$. ξ is a fuzzy function that will be used to determine for every area of the augmented image if it must be purely real, or to what extend the synthetic image is superposed over the real one. It is a three steps function in which there will be two zones defined for 0 % synthetic image superposition, that's pure real, or 100% synthetic data superposed over the real (blurred area), and in the middle the transition zone, fuzzy, for the transition from 0 to 100% superposition.

The formal expression of the merging function used is:

$$\xi \begin{cases} = 1 & \text{for} \quad \mathbf{C}(x,y) < Th_1 \\ = 1 - K \cdot \mathbf{C}, & \text{for} \quad Th_1 \le \mathbf{C}(x,y) \le Th_2 \\ = 0, & \text{otherwise} \end{cases}$$

The clarity function C, that has provided better results in what refers to the independence of the kind of scene and the topology of the contained objects has been the one obtained from the distance Dc, that correspond to the gradient values containing the 95% of the gradient histogram, computed in every region of the image. Fig. 10 shows the value of Dc, as the measure of the image clarity, within the considered region, computed from the gradients histogram. This valued Dc results to be independent of the kind of objects and their characteristics, since blurred images present very low gradient values.
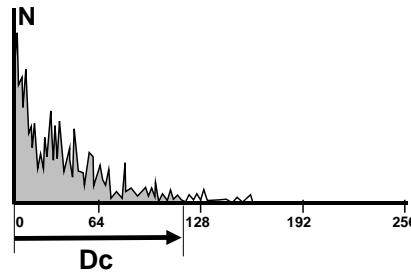

Fig. 10 Representation of the Dc value to evaluate the clarity of a region of the image

The classification of the different clarity areas of the image are obtained from local histograms, within the corresponding window, which size is not fixed.

The values of Δx, Δy, the length of the window sides, where the local histogram is calculated can be adjusted, so as the boundaries of the mask, or superposed image can have different resolution levels. Thus, the window size depends on the desired resolution degree in the gradual expanding area of the synthetic image, ranging from 16 x 16 pixels up to 128 x 128.

The degree of the desired virtual information when working with low quality scenes can be adjusted by the user. Both the threshold values and the gain of the transition zone can be customised, thus controlling the synthetic superposition image law.

4. 4 Synthetic images superposition process

Previous to the superposition process the procedure for the generation of the synthetic images must be established. There are two kind of elements to be synthetically generated, the grasped objects, or those in the working environment, and the robot arms and hands. In the former case, the system developed enables us to acquire and memorise the manipulated objects in the area of good visibility, close to the cameras, before the water gets muddy. The robot arms approach the objects being held towards the cameras so as the system can acquire the required images. In this phase, the process for objects segmentation can be improved considering the movement. Thus, an aiding option, when the image is not contrasted enough for obtaining a good segmentation, is to move the handled object back and forth, or left to right, in front of the cameras.

Since the user does not need a very detailed image, but to perceive the volume occupied by the objects and the relative position of the arms and grasped objects with respect to the workspace, the synthetic image consists of a 3D volume of the arms, as well as the 3D wire-

frame representation of the objects, which is circumscribed on the 3D contours of the scene elements (11).

The vision system designed for the construction of the visualised objects 3D model, starting from the segmented images, fig. 11, consists of the following steps:
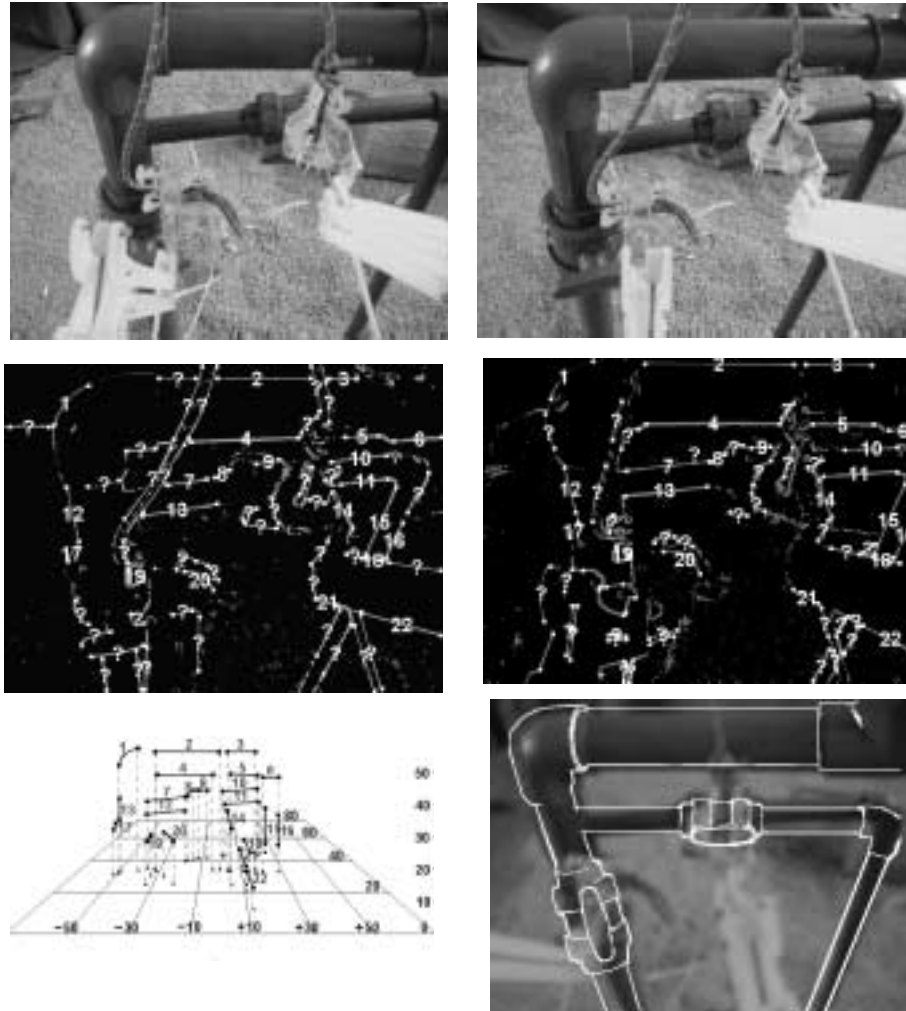

Fig 11 Two stereo images (a) and the matching of homologue segments (b).
c) shows the depth reconstruction for the CAD model positioning.
d) Synthetic image superposed

1st Step: After image segmentation some object contour fragments are extracted applying a low threshold. Obtaining such "bad quality contours" enable us to extract the most significant contour pieces, which are used as image features. These contour fragments are thin, constituting good feature points for matching.

2nd Step: The homologue contour fragments in the two stereo images are matched to compute their depth, providing the required 3D information

3rd Step: Such disconnected contour fragments located in the 3D space are interpolated by means of straight lines and circular arcs to build longer models

4th Step: A wire-frame representation of the scene elements circumscribed contours is superposed to the image of the working area.

Once the 3D modelling of the objects is done, the volumetric occupation of the arms and their handled objects are added to the video image available. This augmented image enables the operator to keep seeing the arms, even when they are occluded by the scene elements or due to water turbulence, thus making the teleoperation process based on visual feedback possible.

5. COOPERATIVE CONTROL OF TWO UNDERWATER VEHICLES

Manual teleoperation solves the problem of having to provide the vehicle with intelligence enough so as to be able to operate autonomously.

ROVs, although being teleoperated to be easily governable, require to have available some reactive control capabilities. Therefore, in the development of relatively complex tasks, the human operator can obviate some simpler problems, such as to maintain a distance to an object constant, to maintain a position, and consequently he or she can concentrate on the development of the main task, for instance an inspection task or a given manipulation operation.

Some automatic behaviors are, for instance, the self-positioning of the robot in front of a pipe or even the navigation of the robot following such a pipe. In the context of ROVs, a global task such as object manipulation can be split into three phases. First, the robot has to approach to the point where the task has to be carried out, the navigation phase. The absolute localization of the robot can only be achieved when the robot navigates in a well-known environment using in most cases external absolute positioning systems, for instance transponders. Second, the robot has to be self-positioned in front of the work-space. This step involves the use of dead-reckoning techniques and the knowledge of the object over which the task has to be carried out. The robot locates the object and has to keep the same orientation and distance with respect to it and, at the same time, to minimize the effect of environmental disturbances, using vision systems or high precision US scanners. Finally, the third step corresponds to the development of the task.

In some cases, however, it is possible that the task can not be completed by a single ROV, i.e. the recovery of large objects, undertaking simultaneous repair of underwater structures at different positions or the delivery of a number of payloads to a single location. Under such circumstances different procedures can be followed. First, the task can be achieved using uncoupled vehicles where each ROV is teleoperated by a different operator, that is, each ROV carries out a subtask without interacting with the other ROVs. In a second procedure, the ROVs are teleoperated by the same operator, in a way that each ROV works with some level of cooperation with the others, in order to undertake the task. Cooperation means that each

218

ROV has to modify its behavior related to the behavior of the other ROVs. Some tasks can be considered such as the transportation of a large object, which has to be grasped by more than a single ROV (Fig. 12), or the manipulation of underwater pipes.

A third procedure would include an automatic assistance. For instance, in the global behavior of a task of transporting a large object to a fixed position, each robot would have to readjust its behavior not only to maintain the grasping, but also to implement some reactive automatic assistance actions. These actions would be oriented towards the goal of moving the object to a desired location. In this work, a vision-based control system allows two ROVs to work in a co-operative manner, a master-slave configuration. The operator controls the two robots, the master and the slave. In this case the master will operate as a ROV and the slave, also a ROV, operates with some autonomous capabilities.
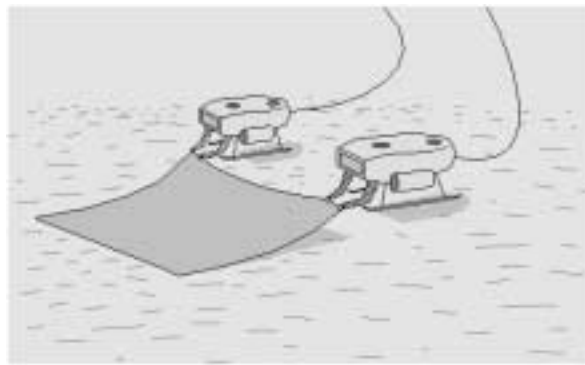

Fig. 12 Example of two robots working in cooperation

5. 1 The slave automatic assistance capabilities

The slave robot has to know with enough accuracy the position and orientation of the master robot in order to follow it and to maintain the desired distance between them, while they are performing a task. This is achieved using a vision-based system required to obtain the position and orientation of the master, assuming that the model of the master is known. The vision system endowed with three cameras is located on the slave. Two cameras have been placed in both sides of the robot and the third one in the front, to attain in a static way a wide visibility field.

The frontal camera is used for navigation and teleoperation of the robot. The frontal camera has an aperture of 50º. Both lateral cameras have an aperture of 70º and they have been placed in those positions with the aim that both image fields are draped with the image field of the frontal camera. The acquired images have a size of 640x480 pixels. Then, due to the digitalization of the image, both lateral cameras give the worse resolution, which is about 4 cm when the master is place at 2 m. and decreases to 10 cm. when the master is placed at 5 m.

The three video signals are multiplexed and sent to the operator located on the harbor, near the sea or in the mother-ship. The user teleoperates the robots using these images. On the other hand, these images are processed in order the robot can follow an alternative run at the

operator's will. The operator has available a mission-planning module to facilitate the navigation towards the working area, as well as a mechanical exoskeleton to teleoperate both robot arms to perform the desired ask.

To supervise the mission and the task to be performed, the user needs different types of information that should be put in an interface. A user-friendly interface has been developed taken into account the typology of users and their abilities (biologists, geologists or engineers).

5.1.1 Vision-based virtual link

The three cameras placed in the slave robot obtain two-dimensional images of the scene continuously. The images can be used in conjunction with the known dynamics of the slave and the model of the master to compute the orientation and position of the viewed master. The following steps define the operation of the vision-based link:

1) Initially, an image of the scene is taken and processed in order to segment the master from the rest of the scene.
2) Once the master vehicle is located in the image plane, the general contour of the master is extracted using edge detection, image filtering and enhancement techniques.
3) Linear prediction of the model view point. A first order function has been used to predict the position and orientation of the master in order to reduce the searching in the model.
4) Matching of the contours image with the model 2D projection, taken from the estimated position.
5) Application of the function that permits to obtain the distance from size analysis.
6) Obtaining the matching function and searching of the global maximum coincidence.

Some of the main difficulties about the stabilization of the robot are solved with the visual link system. The main objective is to obtain the position and orientation of the master. Then, the computing time to process the images and the total time needed to obtain the position and orientation of the master robot is highly constrained, to facilitate the stability of the position control. The image has to be processed in order to obtain the main contours of the master. Afterwards, the obtained image is matched with the 2D projection, from each view point tested, of the 3D simplified model available of the master vehicle, without the arms. Each matching of one position and four shifts is completed in 280 ms., that means to operate at a frequency of 3.5 Hz. With the aim of minimizing the computing time the position and orientation of the robot is predicted using a first order function. Then, the matching is started from the predicted solution of the model, obtaining that the function (that relates the processed image to the model) converges to a global maximum faster. Obviously, the frequency is highly constrained on the accuracy of the prediction.

The vision-link system has been developed for distances up to 10 m. The Mediterranean sea is quite clear without a lot of scattering allowing to obtain, in most cases, images accurate enough.

The system has been tested in the Polytechnic University of Catalonia experimental channel that is 100 m. long, 5 m. wide and 5 m. depth. The experimental test consists in the verification of the position stabilization of the slave robot with respect to the master by using the vision-link system. The image is processed by using image analysis techniques with the aim to obtain the main contours of the robot. On the other hand, the simplified 3D CAD model of the robot is available (Fig. 13). The model has been done without arms to avoid matching uncertainness. The contour image is used, for each point of view of the model, to obtain the best matching. Once the matching is obtained, it is easy to obtain the distance and the orientation of the master.

Fig. 13 The simplified CAD model of the Garbí, used for matching with the real image

6. DESIGN OF A TELECONTROLABLE APPENDIX

The difficulties for the vehicle in accessing the working zone and getting a good image of this area, the best point of view, has motivated the design of a multiarticulated sensorial appendix, with a TV camera as the terminal element, adapted for underwater work. So as to make this experimental appendix telepositionable and of the least possible dimensions, its mobility has been accomplished by means of water jets, fed from the host. Therefore avoiding the need of using motors, drivers and other control elements.

The sensorial appendix is composed of a base which connects it to the host, its body, totally flexible, and the terminal element which is an hermetic container for the TV camera, lights, and the ducts for propulsion, fig.14.

6. 1 Capsule design

The mobility of the terminal element, the sensors capsule, is provided by six water jets at 45º off the z-axis and in planes 120º apart, as seen in fig.15.
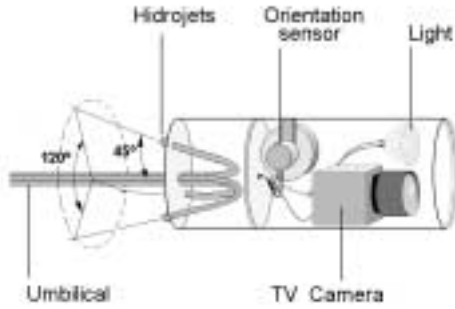
Fig. 14 The hidrojet explorer

Fig. 15 The propulsive jets

Modulation of the strength of each of the three water jets provides the means of orienting the resultant force and also of varying its strength. To obtain an static equilibrium the resultant of the three jet forces $F_a + F_b + F_c = F_r$ must equal the reaction of the umbilical F_t.

In a first experimentation phase, it has been operated with uniquely the three jets on the capsule, In this case, to get a resultant force F_r not axial, a differential modification of the three jet rates is done. This force produces an acceleration a of the capsule, and now the dynamical equilibrium of the capsule is given by $F_a + F_b + F_c + F_t + ma + kv = 0$ being m the mass of the capsule, v its velocity and k the friction coefficient of the capsule against the medium.

As the viscosity of the medium produces also a resisting force along all the umbilical, a deviation of the resulting force F_r produces also a displacement of the capsule as shown in fig. 16a, and a curving of the umbilical as shown in fig. 16b.

The architecture of the sensor appendix is equivalent to a polyarticulated chain in which the angle between each element Δl_i and Δl_{i+1} is given by the direction of the propulsive vector at each instant, $F_p(t)$ and the dynamics of the capsule and umbilical.
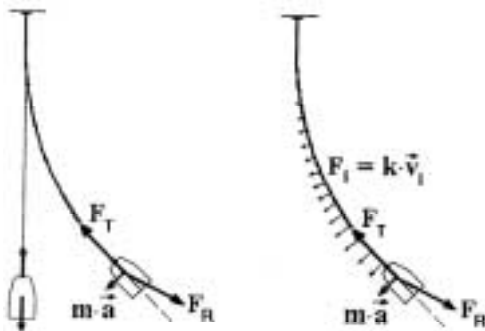

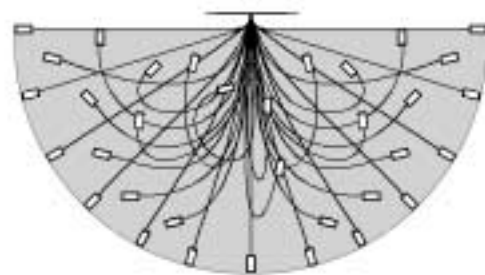*Fig. 16 Forces that produce the movement*

Fig. 17 Space accessible modifying Fr(t)

To study the accessible space of this appendix a simulation was done with an approximate model. In it the capsule moves in the plane of F_t and the instantaneous z-axis of the capsule.

Velocity is proportional to $F_t \sin \theta$ being θ the angle between F_t and the z axis. The time of acceleration to the equilibrium velocity, a few seconds in reality, is taken as zero.

The angle between consecutive elements Δl_i and Δl_{i+1} is $\beta_I (k) = c\, \beta_I (k-1)$. In this way it can be seen that the volume accessible by the appendix, by a judicious modulation of the jet rates, q_a, q_b, q_c has the shape shown in fig. 17

## 6. 2 Control of the polyarticulated sensing appendix.

The sensing capsule is balanced in mass/volume to make its density as similar to the medium as possible. It has 6 degrees of freedom. The capsule position control in an weightless environment, with propulsion by liquid jets, has been experimented (12). In underwater applications and with a feeder umbilical, this system presents some mobility restrictions, due specially to the length of the umbilical. When this length is fixed so as to have the capsule just at the desired distance of the working zone, its local mobility is restricted to an spherical surface with radius the length of the umbilical. In this case there are only 2 degrees of freedom, and with unidirectional jets, the minimum number necessary to move along this surface is 3.

So as to miniaturize the capsule and minimize its cost, only three jets are used. This implies that the capsule can't be oriented in stable equilibrium. Stable equilibrium means that the tension of the umbilical equals the resulting force of the jets, which must be along the z-axis and grater than zero, $F_a = F_b = F_c > 0$.

On the other hand, the volume of space accessible (i.e. not only the surface of the sphere) can be reached, and with a given orientation, following some trajectory. But in this case equilibrium is unstable, as it means $F_a = F_b = F_c = 0$ and this equality can (and will) be broken by any perturbation.

6. 3 2D position control

There are cases when it is sufficient to keep the capsule position in front of a given point, with no need of keeping its orientation. In these cases, the control of the capsule is done (fig. 18) by playing out a length of umbilical l=R and controlling F_a, F_b and F_c in function of the observed position error.

Fig. 18
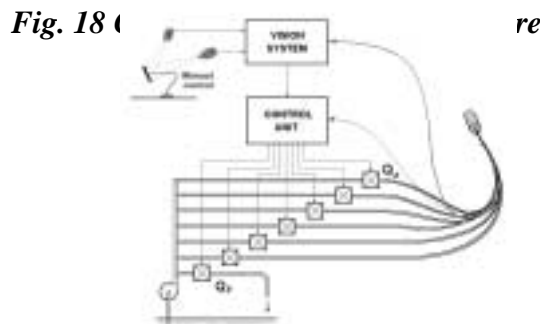
The position error can be measured manually or automatically. Manual control using the images obtained by the camera is adequate for exploring and locating uses, when an autonomous control strategy would defeat the low cost objective. Once the object is located and the camera is in place, keeping it in place manually would be expensive in man-hours.

This can be done by the automatic analysis of the visualized image and tracking of some relevant object in the scene, or it can be done via position sensors in the capsule.

In the experimental system developed, the two methods have been simultaneously used. The tracking system has not mean an overcost, as the host in which this appendix has been mounted is a ROV, GARBI, with a real time tracking system on board. As position sensor, a bidimensional angular sensor has been used. The clinometers used, one each in the X- and Y-axis of the capsule, move a 270° potentiometer through a 3:2 reduction. This allows pitch and yaw of up to ±200° This angular limitation has been introduced so as to reduce the possibility of self-strangulating loops in the umbilical, which would cut the feeding of the jets, with the result of a capsule out of control. The station keeping of the capsule in front of a point can be done using the known angles of pitch and yaw, as the torsion of the umbilical in a limited environment is minimal. The low resolution of those measures give a great uncertainty zone, but it is of great help as an incremental measure to help in stabilizing the capsule by visual tracking.

The control mission is essentially one of transforming the errors (ε_x and ε_y are angular errors in the x and y directions, ε_z is the relative variation of distance along the z-axis) into the forces along the three jet axes, and to adjust the parameters of the control action to compensate the variations due to the differences between the valves.

6. 4 Experimental results

The positionable sensor appendix studied has been tested with an experimental prototype with 3 jets. Fig. 19. Mobility has resulted very similar to the one obtained by simulation.

Fig. 19 The Fura, the experimental hydrojet appendix

The pump is a centrifugal one, half an HP of power, giving a flow of 100 *l/min* and a mean propulsive force of about 2+2+2 *kg*. Proportional valves for the flow control have the

handicap of their hysteresis and dead zone, greatly hindering the control at low speeds. To solve this problem servovalves would be indicated, but their high price defeat the objectives of low cost. Instead, a fourth proportional valve with its flow connected directly to the return, has been used to move the working point of the valves well out of the dead zone. This means working with higher control inputs, not only for position changes but also for low correcting flows.

This appendix can be very useful as a complement for a ROV, or directly as a tool for inspecting very restricted spaces, where conventional ROV's can't go, or to search point of views that enable the operator to get images more adequate for teleoperation.

All these works are oriented to the improve dexterity in underwater manipulation.

REFERENCES

(1) J. Amat, A. Casals, An overview on the main issues dealing with Underwater Robotics *Int. Workshop on Underwater Vehicles*. IROS'98. Pp. 1- 8. Octubre 1998. Victoria, (Canada)

(2) Amat, J., J. Codina, X. Cufi and J. Puigmal (1995) Vision Based Control of Underwater Vehicle for Long Duration Observations. *Int. Conf. on Autonomous Robots 1*, 273-277.

(3) P. Vadakkepat, K C.Tan, W. Ming-Liang, Evolutionary Artificial Potential Fields an Their Application in Real Time Robot Path Planning. Department of Electrical Engineering, The National University of Singapore, 2000, Singapore

(4) N. Y. Chong, T. Kotoku, K. Ohba and K. Tanie, Virtual Repulsive Force Field Guided Coordination for Multi-Telerobot Collaboration, *Int. Conference on Robotics and Automation*, Seoul, Korea, May 2001

(5) J. Amat, A. Casals, J. Fernandez, Vision Based Assisted Operations in Underwater Environments Using Ropes. *IEEE International Conference on Robotics and Automation.* May 1999, Detroit, (USA)

(**6**) J. Amat, L. Muñoz, M. las Heras, P. Ridao, Dextereous Teleoperation with few degrees of freedom arms, *Iarp International Workshop on Underwater Robotics*, Pp 186-190. October 2001, Rio de Janeiro (Brasil)

(7) R. Giannitrapani A. Trucco and V. Murino, Segmentation of underwater 3D acoustical images for augmented and virtual reality applications *OCEANS '99 MTS/IEEE.*, Volume: 1 , 1999

(8) Q. Lin, C. Kuo, Virtual tele-operation of underwater robots, *IEEE International Conference on Robotics and Automation*, 1997

(9) D. Ernadotte, P. Fuchs and C.Laurgeau. Teleoperation and augmented reality. *ICAR '97. 8th International Conference on Advanced Robotics*, 1997

(10) J. Amat, A. Casals, J. Fernandez, Vision Based Assisted Operations in Underwater Environments Using Ropes. *IEEE International Conference on Robotics and Automation. May 1999, Detroit*, (USA)

(11) Casals, J. Fernandez, J. Amat, J. Batlle, Augmented Reality for Teleoperation *Iarp International Workshop on Underwater Robotics,* Pp 191-196. October 2001, Rio de Janeiro (Brasil)

(12) J. Amat An experimental Underwater Hidrojet Explorer Camera, *Int. Workshop on Underwater Vehicles. IROS'98*. Pp. 67-76.Octubre 1998. Victoria, (Canada)

Chapter 13

Underwater robot of variable geometry based on the Stewart-Gough parallel platform: Conception and hydrodynamic modeling

ROQUE J. SALTARÉN, RAFAEL ARACIL, VÍCTOR M. GARCÍA
Universidad Politécnica de Madrid, ETSII-DISAM

The use of the parallel robots as underwater robots is novel and promising. But the development of these types of robotics application required an important effort to develop its hydrodynamic model. The dynamic models for a conventional underwater vehicle are based on a series of differential hydrodynamics equations develop for vessels of fixed geometry. An underwater parallel robot (UPR), changes its geometry configuration to navigation, orientating one of its two rings. Those geometric changes are made necessary develop new methods to calculate the hydrodynamics parameters, such as the inertial matrix, the damping matrix, etc. The damping hydrodynamics coefficients are the most important hydrodynamics parameters that are needed to be calculated. This paper suggests a methodology to calculate these coefficients in function of the geometric of the UPR robot.

1 INTRODUCTION

This article propose the application of the of Stewart-Gough parallel platform (11), (12), as underwater robot, UPR (Underwater-Parallel-Robot). The Stewart-Gough (S-G) platform is a parallel mechanism of six DOF, based on two rings that are connected by six linear actuators through spherical and universal joints. The result of this kinematics configuration is that this mechanism has numerous advantages in comparison with the serial mechanisms. The first of them is a very simple mechanism with high rigidity, thanks to its linear actuators which is part of its mechanical structure. Also, the parallel assembled of the linear actuators on the end-effector, gives place to increase the payload capacity. Finally thanks to its reduced inertia, a S-G platform can reach high speeds and accelerations.

The use of a S-G parallel platform for underwater applications allows to solve two important aspects with the same device in the robotization of submarine works. These aspects are related to the functioning of both the underwater vehicle and the carry out robotics works. In a detailed way we are discussing these two possible applications:

227

a. The platform of S-G, with the appropriate mechanical adaptations (11), can become a versatile underwater parallel vehicle (UPR). An UPR can behave in the submarine depths as a surprising performance. The platform of S-G used as UPR, it permits to have a variable geometry vehicle that needs a minimum number of thrusters. In an UPR robot, the linear actuators are joined to the rings that can be oriented in the three Euler angles: Roll, Pith and Yaw. This allows The UPR vehicle to have the capacity of making a trajectory in any address, simply changing the orientation of its rings. On the other hand, thanks to the geometry adaptability, an UPR robot can pass through holes or intricate spaces, turns and displaces its rings, as if it was a contortionist.

b. When a UPR robot arrives to its workplace and one of its rings can be held, it is possible that the device works as a parallel robot of 6DOF, to carry out robotics tasks such as the inspection or welding of submarine pipes, repair of ships´ helmets or marine rescues.

In figure-1, are shown two types of UPR robots. An UPR robot can be designed to different applications, for example, to navigation purposes. In the figure-1 (a), a UPR robot is designed to transport loads or to carry out recognition tasks. In this case, the conception of the UPR robot results in the design of incorporated fins to the rings to increase the forces of sustentation of the vehicle. We can observe that the later ring is used as helm with fins. The navigation is allowed to orientate the later ring to guide the displacement of the UPR robot. See also, that the thrusters are located in the head of the UPR robot as well as the on board electronics control.

In the case of the oceanic currents, a UPR robot is capable of modifying its geometry to have a better dynamics performance. The possibility of modifying the geometry surfaces of the robot, allows the navigation with "six degree of freedom" due to the oceanic currents and the allowance of having an enormous maneuverability capacity and control of the attitude.
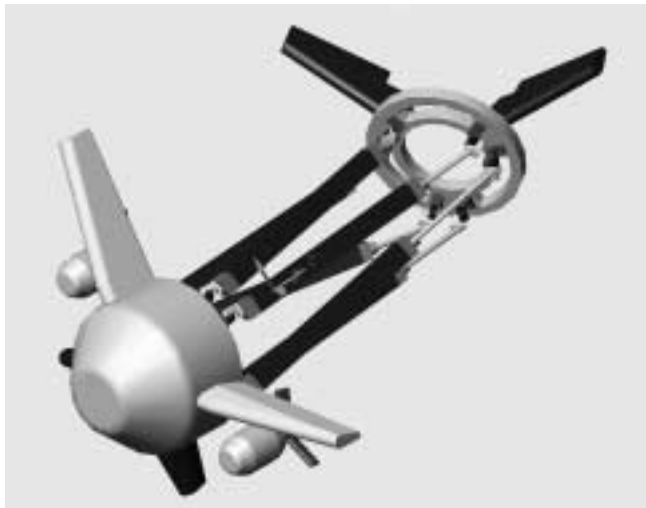
a) UPR for navigation applications   b) UPR for underwater manipulations
works.

Figure 1: Conception of two types of UPR robots

In figure-1 (b), the design of the UPR robot is developed for submarine works that involve manipulations tasks. In this type of design, the thrusters are centering on each ring. The robot's sailing is controlled by the rings turning to allow that the sum of forces generated by the thrusters motors to go in the required path. In this case, are less important the surfaces of sustentation and the sailing which depend on the vector forces of the thrusters, that take place to a concept of "vectorial navigation". The concept of "vectorial navigation" allows solving the holonomic restrictions that affect the underwater robots. The centering on the rings of the thrusters also allows carrying out works with precision more easily. For example, in the case that is necessary to pass through labyrinths or holes of shipwrecks or to work in rescues or manipulations. The possibilities of this robot's maneuver are enormous, for example this device can operates a helicopter from a similar way guiding its rings and its thrusters to counteract the oceanic currents and to stay on a fixed work position.

The first objective of this paper is to propose a methodology to study the characterization of a hydrodynamic pattern of a UPR robot with variable geometry, like type shown in figure-1 (a). Particularly we proposed a method for the computational estimation of the forces and hydrodynamic coefficients. These parameters are necessaries to solve the differential equation of the dynamics of the UPR robot. To carry out this hydrodynamic study, we first created a FEM surface model of the robot. Based on the FEM pattern of the robot, we modeled the hydrodynamic of the robot using the concept of digital physics (6) using the package CFD PowerFLOW.

2 THEORETICAL FRAMEWORK FOR THE DYNAMICS MODELING

This section presented the theoretical framework for the dynamics modeling of an UPR robot. The goal is to study the dynamics mathematical models more used for the modeling of underwater vehicles of rigid body and to make the convenient modifications to adapt those to an UPR robot with variable geometry.
The kinematics equations are obtained through transformations of the lineal and angular speeds from the fixed frame on the body {B} and the reference system attach to the earth {N}, where: NED (X-north), (Y-east), (Z-down).

In general, the dynamics equations are obtained writing the Newton-Euler equations referred to the reference system attach to the robot body and adding the effect of the hydrodynamic forces, the flotation forces and the effects of the waves and marine currents. The result is a compact dynamic model, in which the properties of the system can be exploited (symmetries, lineal properties, etc.) to simplify the calculation of the hydrodynamic coefficients.

2.1 Reference frames

In navigation and guidance of underwater vehicles, usually are used the ZYX rotation sequences (321), therefore the rotation matrix is equal to:

$$\mathbf{R}_b^n(\mathbf{\Theta}) = \mathbf{R}_{z,\psi}\mathbf{R}_{y,\theta}\mathbf{R}_{x,\phi} \tag{1}$$

The kinematics variables (position, velocities, etc.) for a marine vehicle are defined according to the international notation SNAME (1950), (7), (8),

For modeling the kinematics and dynamics of a UPR robot, is convenient to define several reference systems. If a vehicle operates in a reduced area without traveling big distances a good approximation will model the kinematics for a latitude and longitude constants. This circumstance t is known as flat earth navigation, and we only need two reference systems: a bound system to the vehicle {B} and another attach to earth (N) (north (X), East (AND), Down (Z)). This approximation allows the use of an inertial frame and the Newton-Euler laws.
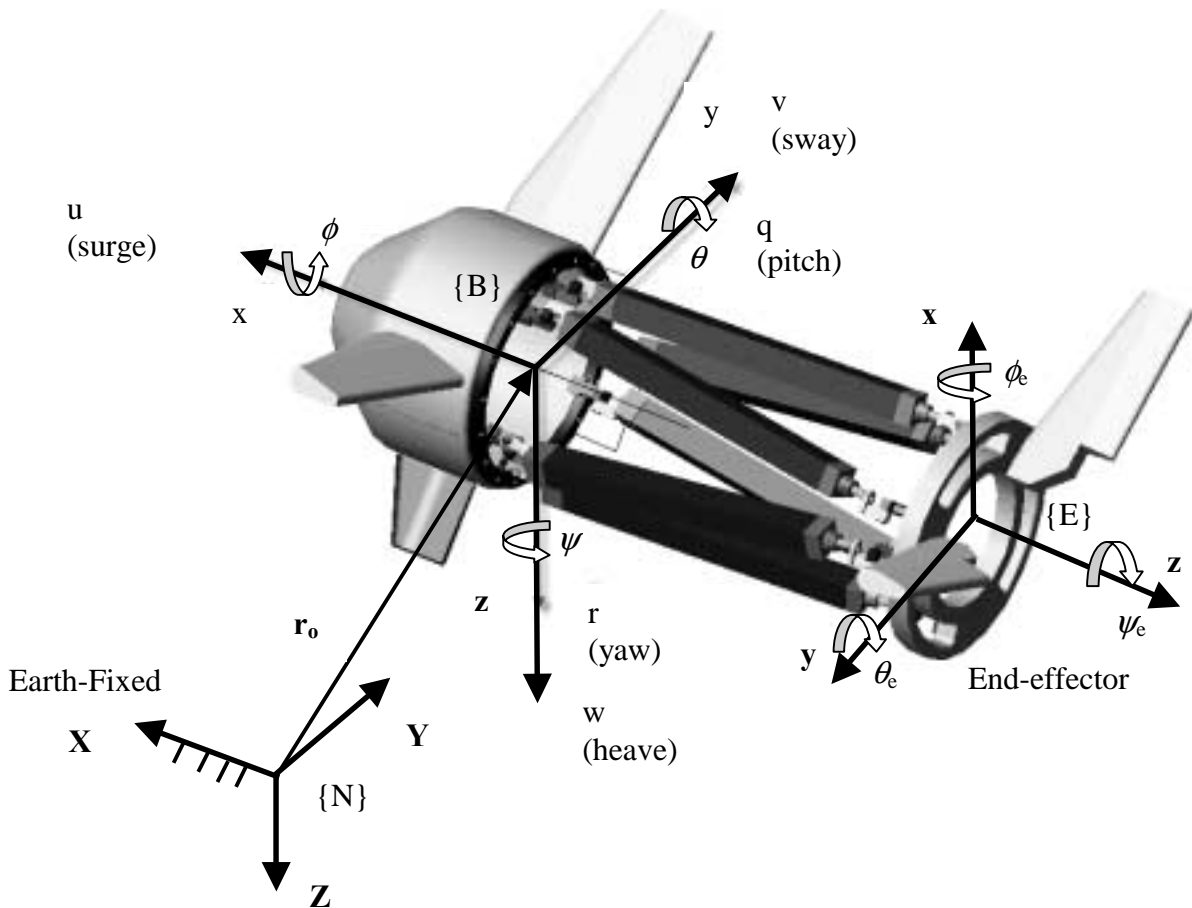
Figure 2 Reference frames for the UPR robot

The reference system attach to the body {B}, has its origin in the centre of gravity of the vehicle, and its axes are chosen such as they coincide with the main axes of inertia of the UPR robot. This vectorial notation will be used to develop the kinematics and dynamics model of the UPR robot

$\mathbf{v}_o^n$ = Is the linear velocity of the point O discomposed on the frame {N}.

$\mathbf{w}_{eb}^n$ = Is the angular speed of the reference system {B} respect of the system {E} decomposed on the frame {N}.

In accordance with the previous notation the following vectors are defined:

$$\mathbf{p}^n = \begin{bmatrix} n \\ e \\ d \end{bmatrix} \in \mathbb{R}^3 \text{ , Position on the frame \{N\}.}$$

$$\mathbf{\Theta} = \begin{bmatrix} \phi \\ \theta \\ \psi \end{bmatrix} \in S^3 \quad \text{Euler angles.}$$

$$\mathbf{\eta} = \begin{bmatrix} \mathbf{p}^n \\ \mathbf{\Theta} \end{bmatrix}, \mathbf{v} = \begin{bmatrix} \mathbf{v}_o^b \\ \mathbf{w}_{nb}^b \end{bmatrix}, \mathbf{\tau} = \begin{bmatrix} \mathbf{f}_o^b \\ \mathbf{m}_o^b \end{bmatrix} \tag{2}$$

The vector $\mathbf{\eta}$ defines the position and orientation of the vehicle in the reference system {N}, supposing flat earth navigation.

In the following sections the kinematics equations that relate the reference frame systems {B} and {N}, will be deduced.

2.2 Motion equations

The dynamic equations are represented   to the following expressions, (8) and are deduced in based of the kinematics equations that relate the reference systems {B} and {N}.

$$\mathbf{v}_o^b = \begin{bmatrix} u \\ v \\ w \end{bmatrix} \in \mathbb{R}^3 \text{ Linear velocity of point O decomposed in frame \{B\}.}$$

$$\mathbf{w}_{nb}^b = \begin{bmatrix} p \\ q \\ r \end{bmatrix} \in \mathbb{R}^3 \text{ Angular velocity of the system \{B\} respect to the system \{N\} decomposed on}$$
the system {B}.

$$\mathbf{f}_o^b = \begin{bmatrix} X \\ Y \\ Z \end{bmatrix} \in \mathbb{R}^3 \text{ Forces on the reference system \{B\}}$$

$$\mathbf{m}_o^b = \begin{bmatrix} K \\ M \\ N \end{bmatrix} \in \mathbb{R}^3 \text{ Body-fixed moment of point O decomposed in frame \{B\}.}$$

$\mathbf{r}_g^b = \begin{bmatrix} x_g, y_g, z_g \end{bmatrix}$ Vector from O until the center of gravity decomposed in frame {B}.

The hydrodynamics model for rigid-body is:

$$\mathbf{M}_{RB}\dot{\mathbf{v}} + \mathbf{C}_{RB}(\mathbf{v})\mathbf{v} = \boldsymbol{\tau}_{RB} \tag{3}$$

Where:

$\mathbf{M}_{RB}$ is the inertia matrix of the body, $\mathbf{C}_{RB}$ is the Coriolis-centripetal matrix, . On the other hand, exists various representations $\mathbf{C}_{RB}$ matrix, and the vector τ_{RB} represents the propulsion forces and moments.

In an underwater vehicle the equation (3) is completed by the radiation-induced forces or hydrodynamics forces.

The phenomena that give place to those forces and moments are the following ones:

- The added mass $\mathbf{M}_A$ matrix, due to the inertia of the fluid that surrounds the UPR robot.
- The coriolis-centripetal matrix $C_A(V)$.
- The vector of restitution forces $\mathbf{g}(\boldsymbol{\eta}) + \mathbf{g}_0$, due to the dead weight and flotation forces.

$\mathbf{D}(\mathbf{v})$ Is the damping matrix that includes dissipative effect, such as:

- The effect of the radiation-induced potential damping due to the energy carried by the generated surface waves
- The effects of the superficial friction
- The effects of the vortex shedding
- The effects of the wave drift.

The total hydrodynamic damping matrix (8), can be modeled as :

$$\mathbf{D}(\mathbf{v}) = \mathbf{D}_P(\mathbf{v}) + \mathbf{D}_S(\mathbf{v}) + \mathbf{D}_W(\mathbf{v}) + \mathbf{D}_M(\mathbf{v}) \tag{4}$$

2.3 Resulting model.

The resulting hydrodynamics model can be written as the sum of the two dynamics: The dynamics due to the rigid body and the dynamics due to the environment forces and moments (radiation-induced forces) (1), (2), (3), (4), (5), (8), (10), (13), (14).

$$\underbrace{\mathbf{M}_{RB}\dot{\mathbf{v}} + \mathbf{C}_{RB}(\mathbf{v})\mathbf{v} + \mathbf{g}(\boldsymbol{\eta})}_{\text{Part of Rigid Body Dynamics}} + \underbrace{\mathbf{M}_A\dot{\mathbf{v}} + \mathbf{C}_A(\mathbf{v}_r)\mathbf{v}_r + \mathbf{D}(\mathbf{v}_r)\mathbf{v}_r}_{\text{Part of Hydrodynamics}} = \mathbf{g}_0 + \mathbf{w} + \boldsymbol{\tau} \tag{5}$$

$$\mathbf{M}\dot{\mathbf{v}} + \mathbf{C}(\mathbf{v})\mathbf{v} + \mathbf{D}(\mathbf{v})\mathbf{v} + \mathbf{g}(\boldsymbol{\eta}) = \mathbf{g}_0 + \mathbf{w} + \boldsymbol{\tau} \tag{6}$$

Where

$$\begin{aligned} \mathbf{M} &= \mathbf{M}_{RB} + \mathbf{M}_A \\ \mathbf{C}(\mathbf{v}) &= \mathbf{C}_{RB}(\mathbf{v}) + \mathbf{C}_A(\mathbf{v}) \end{aligned} \tag{7}$$

2.4 Mathematical model of the damping matrix

The hydrodynamic damping force can be model as:

$$f(U) = -\frac{1}{2}\rho C_D(R_n)A|U|U \tag{8}$$

Where U is the velocity of the robot, A is the projected area under water, C_D is the drag-coefficient based on the representative area (this coefficient, depend of the Reynolds number, Rn) ρ is the density of the water. When a body moves with a speed in a certain address, it experiences a force due to the reduction in the address of the speed that it can be modeled with the equation. However it could also appear other forces in other addresses due to the hydrodynamic sustentation. Moments can appear as well. To be able to contemplate all these cases the following equations are used:

A more comfortable matricial representation could be used:

$$\boldsymbol{\tau}_D = \mathbf{D}(\mathbf{v})\mathbf{v} = \begin{bmatrix} |\mathbf{v}|^T \mathbf{D}_1 \mathbf{v} \\ |\mathbf{v}|^T \mathbf{D}_2 \mathbf{v} \\ |\mathbf{v}|^T \mathbf{D}_3 \mathbf{v} \\ |\mathbf{v}|^T \mathbf{D}_4 \mathbf{v} \\ |\mathbf{v}|^T \mathbf{D}_5 \mathbf{v} \\ |\mathbf{v}|^T \mathbf{D}_6 \mathbf{v} \end{bmatrix} \tag{9}$$

We can used the next matrix equation

$$\boldsymbol{\tau}_D = \mathbf{D}(\mathbf{v})\mathbf{v} = \begin{bmatrix} |\mathbf{v}|^T \mathbf{D}_1 \mathbf{v} \\ |\mathbf{v}|^T \mathbf{D}_2 \mathbf{v} \\ |\mathbf{v}|^T \mathbf{D}_3 \mathbf{v} \\ |\mathbf{v}|^T \mathbf{D}_4 \mathbf{v} \\ |\mathbf{v}|^T \mathbf{D}_5 \mathbf{v} \\ |\mathbf{v}|^T \mathbf{D}_6 \mathbf{v} \end{bmatrix} \tag{10}$$

Where:

$|\mathbf{v}| = \left[|u|,|v|,|w|,|p|,|q|,|r|\right]^T$, and $\mathbf{D}_i$ $(i=1,...,6)$ are diagonal matrices of 6×6, with:

$$\mathbf{D}_i = \frac{1}{2}\rho \begin{pmatrix} C_{iu}A_f & 0 & 0 & 0 & 0 & 0 \\ 0 & C_{iv}A_f & 0 & 0 & 0 & 0 \\ 0 & 0 & C_{iw}A_f & 0 & 0 & 0 \\ 0 & 0 & 0 & Cm_{ip}A_f & 0 & 0 \\ 0 & 0 & 0 & 0 & Cm_{iq}A_f & 0 \\ 0 & 0 & 0 & 0 & 0 & Cm_{ir}A_f \end{pmatrix} \tag{11}$$

4 STRATEGY FOR THE MODELING OF AN UPR ROBOT

The use of the parallel robots as underwater robots is innovative and promising. But the development of this type of the parallel robots' application outlines an important problem from the point of view of the dynamic model. The dynamic models used for underwater robots, are based on a series of equations developed for vehicles of fixed geometry (7). Such as is shown in the figure-1, the navigation of a UPR robot can be controlled turning its later ring (helm-ring) in a similar way to a flight control of a small airplane. In consequence, it is necessary to make some mechanical modifications on the parallel platform, adding surfaces (fins) for the navigation control. The possibility of controlling the guidance and the attitude robot varying its geometry opens numerous advantages, for example: The reduction of the quantity of thrusters' necessaries to navigate in any direction, and the possibility that the underwater robot can be controlled in a better way in front of the currents marine merely changing the orientation of its navigation surfaces, or the possibility to vary the robot's geometry such that the UPR robot could pass through holes, or move for rough areas.

Figure 3 Different geometric configuration of the UPR robot

4.1 Develop of a solution for the hydrodynamics model of a UPR robot

The problem of the hydrodynamics modeling of a UPR robot can be seen from two points of view:

- Once reached a fixed configuration, the robot behaves as a rigid body. In that case, the dynamics equations can be applied such as we have seen up to now. The biggest difficulty rests in estimation of the $\mathbf{D}_i$ damping matrix of coefficients because this matrix depends fundamentally on the robot geometry, because the UPR can get different geometric configurations, for each configuration we should know the mass parameters (matrix of inertia, M_{RB}), and the hydrodynamic apparent mass properties (matrices of added mass M_A and damping $D(v)$). With the geometric configurations changes of the UPR robot, the position of the mass centre ($\mathbf{r}_g^b$) and the flotation centre ($\mathbf{r}_b^b$) varies sensibly, this effects will affect to the vector of forces and restitution moments ($\mathbf{g(\eta)}$).

- While the robot is changing its configuration, the hydrodynamics equation (6), cannot be applied, since these equations have been developed for a rigid solid. In the most general case this problem can be solved by applying the multibody dynamics that is based on treating the body like a mechanical system formed by diverse connected links and related to each other by a series of movement restrictions. This solution requires a different mathematical formulation of the dynamics model, and also a procedure of resolution of the most complex equations. But, in any case, the calculation of the main inertia matrix M_{RB} is unavoidable and the matrix of added mass M_A of each one of the elements of the system. It will be also necessary to know the damping matrix $D(v)$ for each element of the UPR robot, in function of its orientation.

To solve the problem we suggested an approach to modeling a UPR robot and this can based on the following reasons:

a. In the navigation process is not usual that an UPR robot changes continuously its configuration, to carry out different maneuvers, it is better that the robot makes a slowly change on its geometric configurations. Therefore, most of the time, the robot configuration will be fixed and they will be been able to apply the hydrodynamics equations seen up to now.
b. If the change of a configuration to another is slow, we can simulate the process by means of a finite number of intermediate positions in those that the vehicle behaves as rigid solid.
c. If the configuration change is very fast one can simulate the process by means of two extreme positions (initial and final) including the differential model as initial conditions, a vector of forces and moments (in function of the damping matrix).

The procedure explained previously is an approach that allows to apply a simpler and quicker dynamic model when carrying out simulations.

The simplification that is carried out has two aspects that we should analyze:

1. It is supposed that the velocity of the robot doesn't vary in an interval of time, in which modifies the robot's configuration.
2. A series of moments forces appear due to the movement of the helm ring, we discard this because it forces and moments are small, of course whenever the helm ring turn slowly.

The point-1 depends fundamentally on the size of the interval. As much as the size of this interval there are bigger errors. Therefore, it is necessary to keep in mind that if there is acceleration the velocity also should vary. Therefore, another form of acting would be not to reject the variation of those derived of grade 2 (acceleration), and in that case the velocity would vary. This form of acting would consider a constant acceleration. Depending on the precision that is wanted to be achieved it should be cut starting from those derived of certain order.

As in point 2, thanks to the path planning it would be possible to calculate the reaction forces that could generate the movement of the helm ring and that affects the rest of the robot. Also,

other forces could be produced by the movement of the effectors that pushes the water in its movement. These forces could be modeled starting from the acceleration and speed of the effector it could be calculated with the path planning, using the direct an inverse kinematics calculations.

$$\boldsymbol{\tau}_{efector} = \mathbf{M}_{efector} \dot{\mathbf{v}} + \mathbf{D}_{efector}(\mathbf{v})\mathbf{v} \qquad (12)$$

These terms should be added to the propulsion forces, but it won't usually be necessary, because the movement of the final effector is quite slow, which would give us some small reaction forces in comparison with the forces of the propellers.

4.2 Determination of the hydrodynamics matrix parameters for the UPR robot

In this section we discussed a methodology that we will be used to calculate the inertia matrix of rigid-body, added mass and damping coefficients matrix. Although, we expected to center our attention in the calculation of the dimensionless coefficients for the damping matrix, because this is the more complex aspect in develop of a hydrodynamic model for a UPR robot.

The calculation of the added mass can be approach using different procedures (8). The classic method is based on the application of the theory of ideal fluid, but this numeric determination of the coefficients is only possible in very simple cases. To solve this problem, it has been developed the strip theory (10) that it is also based on the theory of ideal fluid, but it allows the numeric calculation of more complicated cases. Starting from the strip theory, there have been developed several software packages that allow the calculation of the hydrodynamic parameters based on the geometry of the submarine body.

The calculation of the damping matrix is more complicated, and it usually requires the use of a CFD (Computational Flows Dynamics) software packages. Only in very simple cases we can appeal to tabulated values of the coefficients of reduction.

4.2.1 Determination of the damping matrix

For the determination of the damping matrix we decided to use a commercial program CFD PowerFlow. By means of this program forces and moments of damping can be calculated for each component of a underwater vehicle. In the case of the UPR robot, the variation of its projected underwater area necessarily go to the calculation of several damping coefficients for many geometric configurations and its interpolation when change its configuration. For the interpolated estimation of the hydrodynamics coefficients, an important problem resides in dividing the robot in simple parts, and calculated the hydrodynamics parameters for each part (for example for the linear actuators, the helm ring, etc.) The results could be transformed to the {B} frame system of the robot.

The hydrodynamic simulations can be divided in three groups:

The hydrodynamics CFD simulations has been made for each part of the UPR robot (head of the robot, linear actuators, and helm ring), in base to this simulation we can obtain the damping hydrodynamics coefficients: $\mathbf{D}_i(1,1) = C_{iu}A_f$, with $C_{xu}, C_{yu}, C_{zu}, Cm_{xu}, Cm_{yu}, Cm_{zu}$.

    1. Simulations for a velocity profile in the *X* axis for $u = 2$ m/sec., to calculate:

$$C_{xu}(\phi_e,\theta_e),C_{yu}(\phi_e,\theta_e),C_{zu}(\phi_e,\theta_e),Cm_{xu}(\phi_e,\theta_e),Cm_{yu}(\phi_e,\theta_e),Cm_{zu}(\phi_e,\theta_e)$$

2. Simulations for a velocity profile in the *Y* axis for *v* = 2 m/sec., to calculate:
$$C_{xv}(\phi_e,\theta_e),C_{yv}(\phi_e,\theta_e),C_{zv}(\phi_e,\theta_e),Cm_{xv}(\phi_e,\theta_e),Cm_{yv}(\phi_e,\theta_e),Cm_{zv}(\phi_e,\theta_e).$$

3. Simulations for a velocity profile in the *Z* axis for *w* = 2 m/sec., to calculate:
$$C_{xw}(\phi_e,\theta_e),C_{yw}(\phi_e,\theta_e),C_{zw}(\phi_e,\theta_e),Cm_{xw}(\phi_e,\theta_e),Cm_{yw}(\phi_e,\theta_e),Cm_{zw}(\phi_e,\theta_e).$$

With the previous simulation it is possible to obtain 18 of the 36 damping coefficients that are necessaries for the $\mathbf{D}_i(1,1)=C_{iu}A_f$, damping matrix. To obtain the remaining parameters, we can operate from a similar way for what was explained up to now, that is to say, carrying out several simulations. However, an approximate method that allows to already taking advantage of the coefficients calculated deriving the remaining ones exists. The application of this procedure has already been used in less complicated cases, to see (13), with good results. This owes you without a doubt that this type of vehicles moves with very low speeds (4 Knots), and that the rotation speeds are very small, what causes that the forces and subduing moments that you/they appear are also very small. The saving of time in simulations added so that he/she doesn't loose a lot of outstanding information makes him to be an appropriate method to the case of an UPR robot.

4.2.2 Stable state verification for simulations with a profile of velocity of V_x=2m/s:

They have been carried out several simulations, with the robot's different configurations. Each configuration comes defined by the orientation of the end-effector with regard to the base, by means of the angles of Euler (ϕ_e, θ_e, ψ_e).

The results are only represented obtained in a couple of simulations in each case of speed, since the results are very similar in all the cases.

4.3 Hydrodynamics simulations for a configuration of the helm-ring (end-effector):
$$\phi_e=0,\theta_e=0,\psi_e=0$$

The evolution of the force on the base and of the density in an aleatory point of the measure volume contributes the following results. It can be proven that after an initial oscillation the value spreads to be stabilized.
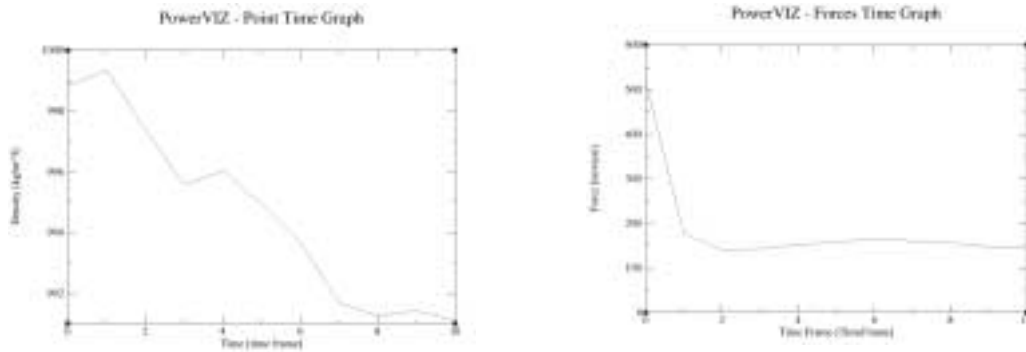
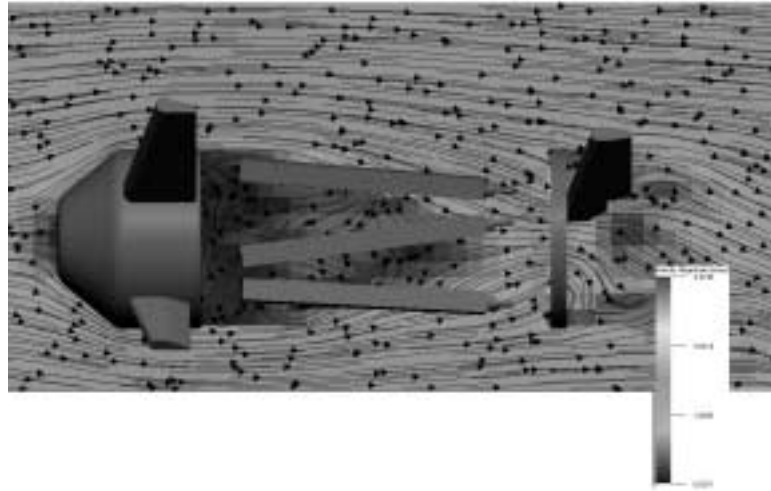**Figure 5. Evolution to stable state of the density and force in a hydrodynamic simulation**

Figure 6 Field of velocities for V$_x$ = 2.0 m/sec

In the figure 6, it can be observed the field of velocities on the half plane of the submarine. The color bar in this figure 6 indicates the magnitude of the total velocity. It is possible to observe that the highest speeds are reached inside of the helm ring. It is also necessary to highlight the whirls formed in the later part of the base, where due suction processes take place due to the abrupt disappearance of the rigid surface of the robot. It is in these later areas to the effector and mainly in their bases that most losses take place. Next they are carried out courts for different planes, which can be appreciated in a global way which is the velocity field.

Figure 7 Slice planes for the hydrodynamics analysis
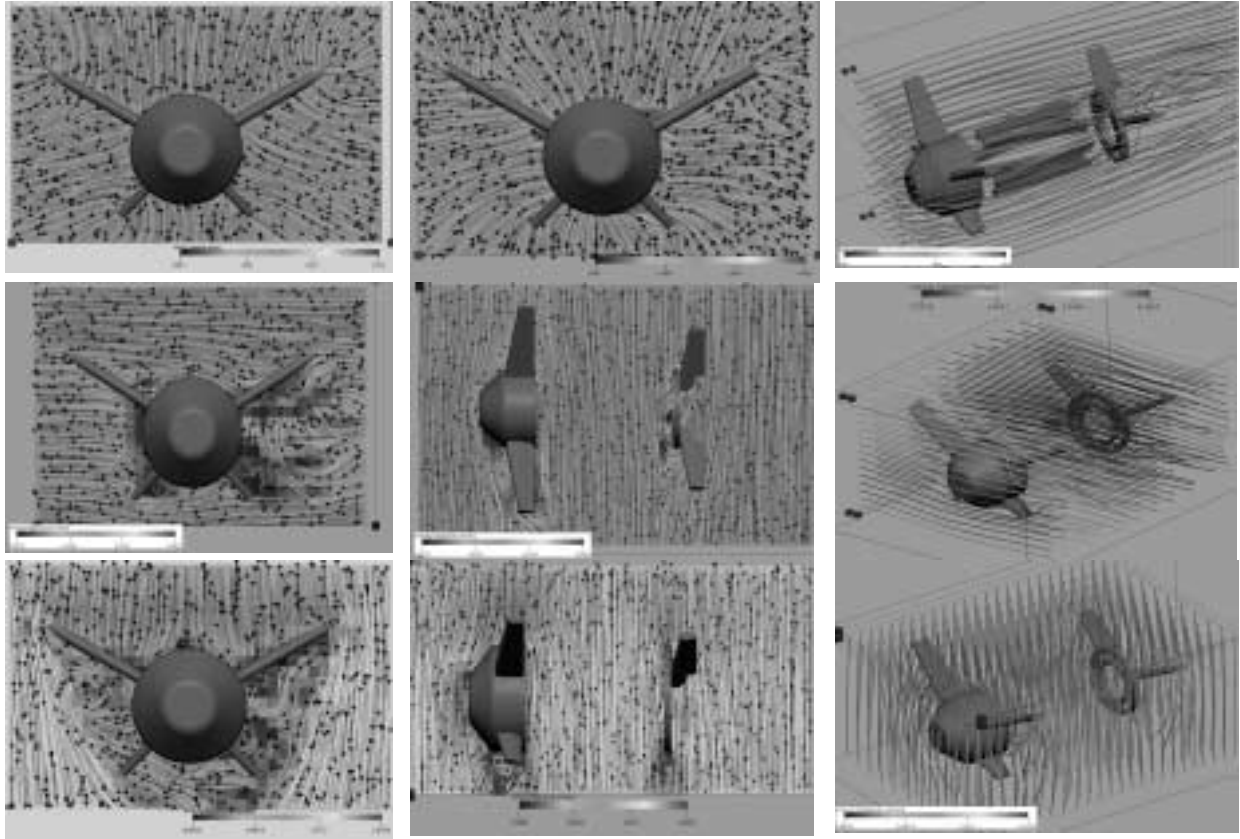
Figure 8. Velocities fields for the study of the hydrodynamics performance of the UPR robot

It is observed clearly how the flow of water spreads to separate the vehicle in the head of the robot, but in the half area appears a suction effect. The profiles of speeds are shown in even different planes to have an idea of the field of speeds that takes place when the vehicle suffers a speed of lateral slip. These situations usually take place in the event of carrying out address changes or with oceanic currents

Where P_c is the characteristic static pressure, P is the total pressure, ρ is the characteristic density and vc is the characteristic velocity. They are usually chosen like characteristic values those of the free flow and the equation (13) can be as:

$$C_P = \frac{P - P_\infty}{\frac{1}{2}\rho_\infty v_\infty^2} \tag{13}$$

The coefficient of pressure can give us information about the losses of suction processes that are taking place. A value of $C_P = 0$ can be interpreted as that the total pressure that is similar to the static pressure of the free flow, what means that the fluid in that point has stopped. When $C_p < 0$, suction processes are happening in this point, and the rising losses increase.

Another form of analyzing the losses that take place is to use the coefficient of speed. This coefficient can be defined as:

$$C_{vi} = \frac{v_i}{v_c}$$
$$i = (x, y, z)$$

(14)

Where v_i is the i-nth component of the lineal speed and v_c is the characteristic speed (that usually correspond with the free flow). If it is considered the coefficient of speed in the axis x $C_{vx} = \frac{v_x}{v_c}$, a value of $C_{vx} = 0$ indicates that the component x of the velocity in that point is null, that is to say, the flow has been stopped in that address. If $C_w = 0$, it indicates that the fluid has a component x of the negative velocity, namely, the flow is reverse, and it is producing whirls, with the rising losses.

As it will be observed both coefficients are much related to each other, giving very similar results.

The form of analyzing these coefficients can be carried out in several ways:

- A form is to analyze the value of the coefficients in courts carried out by a plane. This is usually to make analysis of the hydrodynamic profiles around of the fins, in function of the pressure coefficient.

- The other form is to represent surfaces that have a certain value of the coefficients (isosurfaces). In this case, inside the obtained surface values will be smaller than the coefficients (bigger losses), and in the external part to the surface the values of the coefficients will be bigger.

In figure 10, other results are presented which allow analyzing the isosuperficies that reflect the variation of the coefficient of pressure. In the first line and first column one has results for the coefficient $C_P = -1.0$. The color of the surface represents the module of the total speed of the fluid, and these results can be interpreted with the map of colours that it is included.
For example, in the first line and second column of the figure… appears the results with iso-surfaces that corresponds to the value of Cp = -0.5, we can see how the surfaces concentrate around these areas of the UPR robot go to develop of whirls, because in these areas are where the suction phenomena take place.

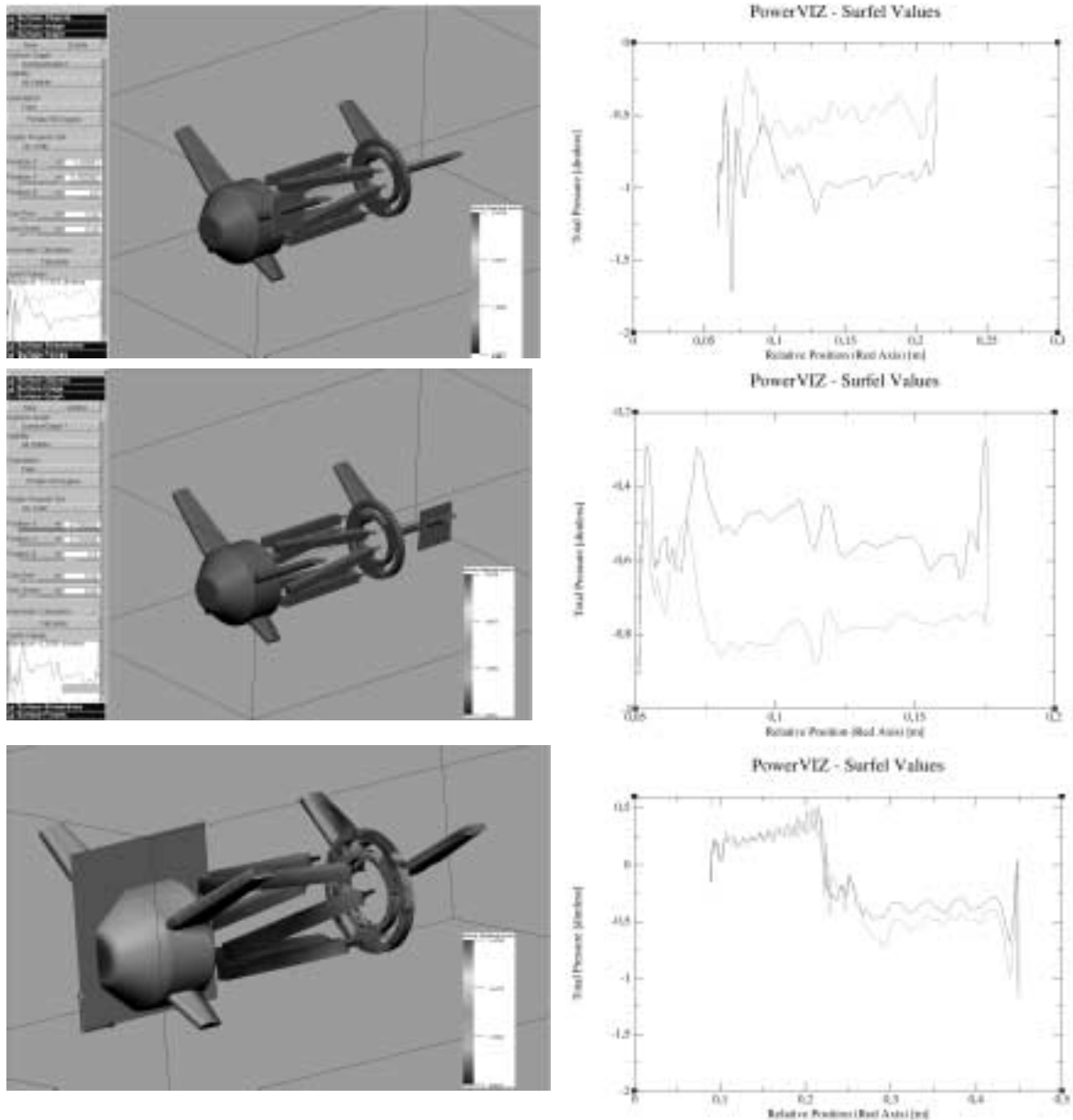**Figure 9 Hydrodynamics simulation test of the lift forces on the fins**

Simulations of the hydrodynamic performance of the UPR robot for Vx=2m/s.

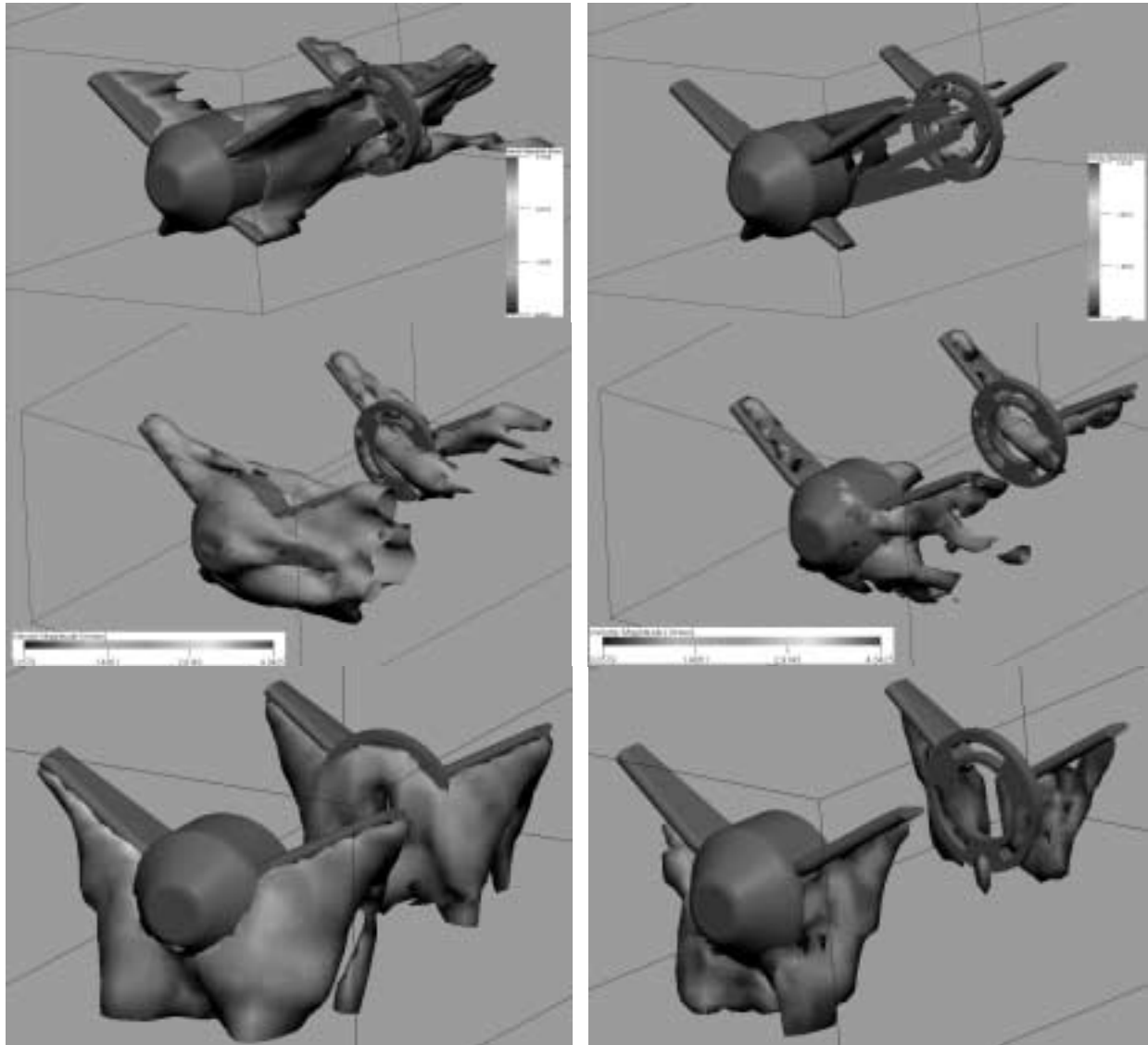**Figure10 Simulations results that show the hydrodynamic performance of the UPR robot for a profile of velocity of V=2m/s in each one of the principal axis.**

5 HYDRODYNAMICS FORCES

This section obtained the resultant forces and moments of damping that affects the UPR robot when these are moving in the water. These data are the most important, and they are the ones that will be used to make the damping coefficients matrix necessary for the hydrodynamic model. To carry out these calculations, we suppose that the helm ring (end-effector) and linear actuators could be displaced and oriented with respect to the head of the robot, therefore the head of the robot is the reference frame.

In the first place summarizing the data of forces and moments obtained in the simulations of the robot's head (CFD-PowerFLOW), and the base of these forces the damping coefficients are calculated. The values of forces and moments that act on the base can be summarized in the following chart. The values vary depending on the speed of the simulation:

Table 1 Forces on the Head of the UPR robot

	Fx (N)	Fy (N)	Fz (N)
Vx = 2 m/s	-120	-1.2	-21.27
Vy = 2 m/s	137.301	-200.65	-12.801
Vz = 2 m/s	123.48	6.96	400.9

Table 2 Moments on the head of the UPR robot.

	Fx (Nm)	Fy (Nm)	Fz (Nm)
Vx = 2 m/s	1.25	-1.482	3.2
Vy = 2 m/s	-23.45	-9.234	6.07
Vz = 2 m/s	-2.35	-32.55	2.25

5.1 Hydrodynamics forces on the helm ring and linear actuators.

The hydrodynamics forces calculate for the helm ring and linear actuators for some angle orientation of the helm ring are presented below.

5.1.1 The simulations have been made for a velocity of Vx=2m/s.

Table 3 Resulting forces for Vx=2m/s

Phi	Theta	Fx	Fy	Fz
0	0	130,259	-3,70917	40,7886
0	30	148,279	1,76265	-11,0299
30	0	109,364	-29,6695	34,9915
30	30	37,3453	-4,05358	-52,9691
0	60	169,207	9,12384	-32,9473
60	0	114	-28,3788	-24
60	60	102,22	-17,5182	10,9345

Table 4 Resulting moments for Vx=2m/s

Phi	Theta	Mx	My	Mz
0	0	6,29388	4,47737	-0,0587129
0	30	1,72988	-4,83305	-0,105526
30	0	6,1745	3,43097	-2,75223
30	30	5,13976	-11,0544	3,3827
0	60	3,31344	-12,1964	1,5232
60	0	14,0361	-16,9253	-2,80274
60	60	4,66873	-15,3034	13,7497

5.1.2 Simulations for a velocity of Vy = 2m/s.

In the case of Vy = 2m/s the following results of forces and moments are obtained:

Table 5 Resulting forces for Vy=2 m/s.

Phi	Theta	Fx	Fy	Fz
0	0	14,1445	-138,997	7,70395
0	30	-11,4888	74,2553	-16,2557
30	0	-41,6532	271,992	-14,8513
30	30	-80	174,197	47,077
0	60	15,2633	88,4803	12,0819
60	0	-64,4668	207,119	-6,93012
60	60	-70,572	203,214	33,0702

Table 6 Resulting moments for Vy= 2 m/s.

Phi	Theta	Mx	My	Mz
0	0	-42,8195	-8,90238	16,0396
0	30	28,57136	-9,89297	11,5685
30	0	50,8471	-34,8416	-18,4054
30	30	37,2257	-15,61	37,2257
0	60	22,585	-3,66538	28,0404
60	0	3,57011	-8,881379	-5,06075
60	60	13,667	0,726911	-1,34065

5.1.2 Simulations with speed Vz = 2m/s.

In the case of Vz=2m/s the following results of forces and moments are obtained:

Table 7 Resulting forces for Vz=2m/s.

Phi	Theta	Fx	Fy	Fz
0	0	56,6411	-3,34174	212,765
0	30	-65,3505	8,93247	195,945
0	60	-36,3314	0,372523	266,879
30	0	43,4961	-26,3405	237,458
30	30	-63,2626	39,6996	163,389
60	0	24,6154	-42,4436	209,086
60	60	-21,058	31,8106	247,884

Table 8 Resulting moments for Vz=2m/s.

Phi	Theta	Mx	My	Mz
0	0	-1,7288	13,923	0,501148
0	30	-27,687	8,89877	-7,63337
0	60	-0,314053	10,5907	0,331353
30	0	9,93746	14,356	0,085281
30	30	-11,5506	16,5153	1,62998
60	0	13,0901	4,81768	0,120922
60	60	11,2462	4.62841	1.18314

5.2 Interpolation of the coefficients (Cx, Cy, Cz, Cmx, Cmy, Cmz).

For each velocity there have been carried out seven simulations in seven different configurations, with those data it is wanted to obtain the dimensionless coefficients in function of the configuration of Euler angles Euler (ϕ_e, θ_e, ψ_e), for the group formed by the helm-ring and the linear actuators

The reason of using dimensionless coefficients instead of values of force is that the forces depend on the magnitude of the speed for which are calculated, while the dimensionless coefficients don't depend on this speed. In base to the CFD hydrodynamics simulations we expected to obtain the coefficients in function of the configuration, that is to say, in function of the position and orientation of the group formed by the helm ring and the linear actuators

In the case of a parallel robot, the end-effector (helm ring) has 6 grades of freedom, what would lead to have to consider 6 variables of those that each hydrodynamic coefficient would depend on.

To simplify the problem, we can eliminate the position variables, due to the following causes:

- The margin of displacement of the linear is 400 mm. Approximately, this magnitude is smaller than the characteristic longitude of the simulate robot, because of that the +/- 200 mm. variation in relation to the total longitude is much smaller. This justifies the elimination of the variable.
- The margin of displacement of the final efector on the axis *OY* is still smaller due to the operation of the platform S-G. Also, this type of configurations would not be habitual in a underwater robot, since he/she would move the center of gravity and of flotation toward a side, what would cause swinging of the group. This justifies the elimination of the variable.
- Something similar happens with the displacement in the *OX* axis of the end-effector (helm ring), since this displacement is very small and it would cause pitching the robot. This justifies the elimination of the variable.
- Turning around the OZ axis of the effector (),also eliminate. The main reason is that although that movement could be useful in parallel robots with other applications (for example in construction applications), it would not be useful in underwater robots. A configuration with would generate a moment around of the *z* axis that could make unstable The UPR robot in some case.

With these simplifications we only have two parameters in which the coefficients dimensionless depend: .

5.3.1 Interpolation method.

To carry out the interpolations the computer program MATLAB has been used. This program has an utility that allows to work with Excel charts, called Excel link. This is possible to carry out operations of MATLAB from a leaf of Excel.

The work process has consisted on creating a calculation leaf in Excel that contains the charts of forces and moments, and starting from those data to interpolate with the MATLAB´s commands. In MATLAB exists different interpolation methods, but the "cubic" methods and "Matlab exist 4" are those that produce more softened surfaces.

The interpolation process consists of the following phases:

- Starting from the data of forces and moments of simulations to calculate the dimensionless coefficients. It is necessary to have the characteristic area, the characteristic density and the characteristic speed.
- Definition of values in which we want to obtain interpolated data.
- To use the Excel link to transmit the information to MATLAB, to carry out the interpolation and to keep the results.

5.3.2 Dimensionless hydrodynamics coefficients calculation.

The definition of the dimensionless coefficients has been described in the equations (10), (11). The most complicated aspect is to know the projected underwater area of the UPR robot for each configuration. The area is projected according to the address of the speed. Therefore, we should know the projected area of the end efector (helm ring) and linear actuators, for the three axes account different orientations the helm ring and linear actuators. To solve the problem it is appealed to the transformation of reference systems by means of the rotation Euler matrix. As we can see next, the areas can be obtained projecting to the axes according to the system of reference of the helm ring. The projected area can be calculated with CAD programs to obtain the values of. If we carry out a configuration change a rotation of the piece he/she will take place. Each projected area can be projected at the same time in turn on each one of their new axes. You can represent the projected area in vectorial form. Being the unitary vectors in each one of the addresses of the new reference axes, namely, the area projected on the new axis OX will be the sum of the first component of each vector.

Table 9 Area (projected) for a profile of velocity on the axis X: V_x (m^2).

Phi	Theta	Ax
0	0	0,10143713
0	30	0,1283
30	0	0,1274
30	30	0,1509
0	60	0,1209
60	0	0,1193

Table 10 Area (projected) for a profile of velocity on the axis Y: V_y (m^2).

Phi	Theta	Ay
0	0	0,0791
0	30	0,0791
30	0	0,1193
30	30	0,1193
0	60	0,0791
60	0	0,1274
60	60	0,1274

Table 11 Area (projected) for a profile of velocity on the axis Z: V_z (m^2).

Phi	Theta	Az
0	0	0,081
0	30	0,1209
30	0	0,1283
30	30	0,081
0	60	0,1339
60	0	0,081
60	60	0,1438

With the previous data of the front area the dimensionless coefficients can be obtained as:

Table 10 Dimensionless force damping coefficients for a profile of velocity in the axis X: V_x

Phi	Theta	Cx	Cy	Cz
0	0	0,64206765	-0,0182831	0,2010536
0	30	0,57786048	0,00686925	-0,0429848
30	0	0,42921507	-0,11644231	0,13732928
30	30	0,12374188	-0,01343135	-0,1755106
0	60	0,69978081	0,037733	-0,13625848
60	0	0,47755658	-0,11893881	-0,10029547
60	60	0,39375963	-0,06748151	0,04212057

Table 113 Dimensionless moments damping coefficients for a profile of velocity in the axis X: V$_x$

Phi	Theta	cmx	cmy	cmz
0	0	0,03102355	0,02206968	-0,00028941
0	30	0,00674154	-0,01883496	-0,00041125
30	0	0,02423273	0,01346535	-0,01080153
30	30	0,01703035	-0,03662823	0,01120842
0	60	0,01370323	-0,05044003	0,00629942
60	0	0,05882691	-0,07093588	-0,01174661
60	60	0,01798432	-0,05894992	0,05296495

Table 12 Dimensionless force damping coefficients for a velocity in the axis Y: V$_y$

Phi	Theta	Cx	Cy	Cz
0	0	0,08940898	-0,87861568	0,0486975
0	30	-0,072622	0,46937611	-0,1027541
30	0	-0,17457334	1,13994971	-0,0622435
30	30	-0,33528919	0,73007963	0,1973051
0	60	0,09648104	0,55929393	0,0763711
60	0	-0,25300942	0,81286892	-0,0271983
60	60	-0,27697017	0,79754317	0,1297889

Table 133 Dimensionless moments damping coefficients for a profile of velocity in the axis Y: V$_y$

Phi	Theta	cmx	cmy	cmz
0	0	-0,27066688	-0,05627295	0,1013881
0	30	0,18060278	-0,06253458	0,0731258
30	0	0,21310604	-0,14602515	-0,0771392
30	30	0,15601718	-0,0654233	0,1560172
0	60	0,14276233	-0,02316928	0,1772465
60	0	0,01401142	-0,03485628	-0,0198617
60	60	0,05363815	0,00285287	-0,0052616

Table 143 Dimensionless damping coefficients for a profile of velocity in the axis Z: V$_z$

Cx	Cy	Cz	Cmx	Cmy	Cmz
0,34963642	-0,02062802	1,3133642	-0,0106716	0,08594444	0,00309351
-0,27026675	0,03694156	0,8103598	-0,11450372	0,03680219	-0,03156894
-0,14158769	0,00145177	1,04005846	-0,0012239	0,04127319	0,00129132
0,26849444	-0,16259568	1,46579012	0,06134235	0,08861728	0,00052643
-0,23623077	0,14824347	0,61011576	-0,04313144	0,06167028	0,00608656
0,15194691	-0,26199753	1,29065432	0,08080309	0,02973877	0,00074643
-0,07321975	0,11060709	0,86190542	0,03910362	0,01609322	0,00411384

5.4 Generation of the interpolated hydrodynamics coefficients.

The most comfortable form of storing the interpolated data is in the matricial form. It has been considered that the precision of a grade is more than enough, as a result the index of the files represent the angle and the columns the angle.
For example, the matrix contains the interpolated data of the coefficient C_x. The element will be the coefficient C_x for the configuration.

The resulting matrix will be of dimension 61 x 61, and describes the coefficients when the angles of the helm-ring are rotate between 0 and 60 grades. The behaviour in the negative part (0 up to -60 grades) should be analyzed carefully.

In the following pages some 3D surfaces showed the interpolated values for the hydrodynamic coefficients, in the case of a profile of speeds $V_x = 2$ m/s.
Although in this paper is not possible to show all the interpolated surface (because many interpolated curves exist), for example, in the case of the hydrodynamics coefficients resulting of the velocity V_y, it is possible to conclude that the results of the variations of the angle *theta* have a low influence in the hydrodynamic induced forces. This is because of the variations in the angles *theta* don't produce a change in the surface faced to the flow. This reasoning is contrasted with most of the projection figures according to theta that has been obtained. One can observe that the projections in some cases come closer to a curve, to be precise, a curve that would depend only on phi, and less of theta.

5.4 Curves of interpolation for the velocity of: Vx=2m/s.
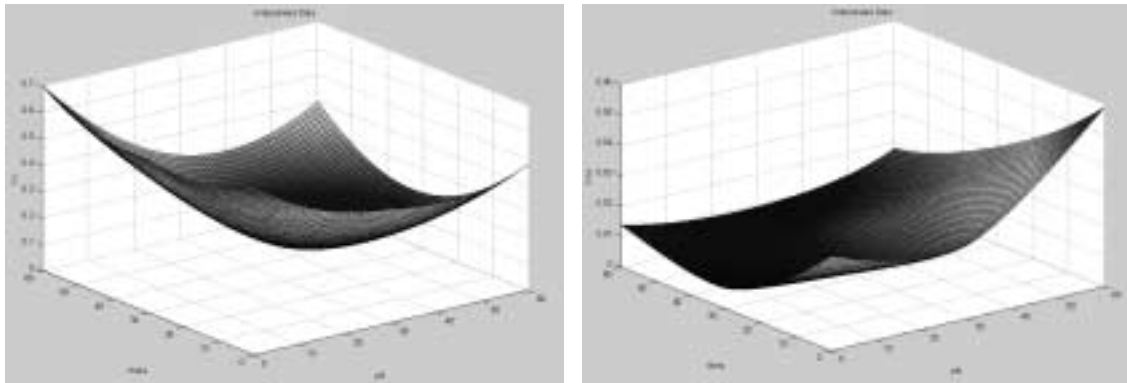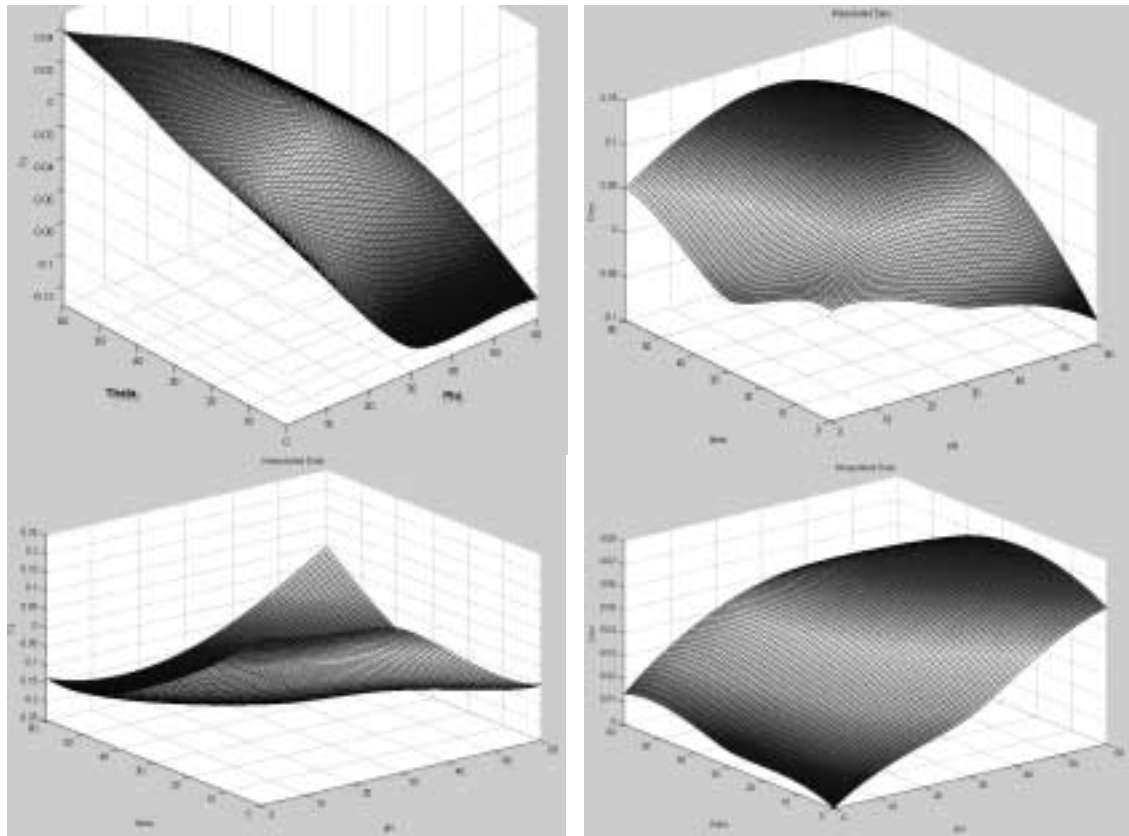
Figure 11 Curves of force and moments dimensionless damping coefficients

In the case of Vz speed a similar situation is given, but in this case with the phi angle. In the projections of the obtained surface we have some changes in the projection of the curve on the *phi* axis, and a low influence of theta.

Finally, according to the curves shows, in the case of Vx speed, we cannot apply a similar reasoning, because the phi angle and theta affects in a different way, and anyway modifications of one of the angles vary the front area.

5.5 Simulations with angular speed.

The dimensionless coefficients due to rotations can be obtained starting from the coefficients before that have already been calculated. The method is based in the rotation around an axis becomes in a translation motion whose speed is proportional to the distance of the turn axis. The caused force can be obtained if they are integrated along the vehicle with the obtained forces around rotation speed.

In the case of the end-effector (helm ring) of the UPR robot we can conclude that the longitude of the turn axis to this element is much bigger that width of the robot in relation of the axis OY and OZ. In these cases the forces could be calculated in the following way for a rotation in axis OY with angular speed q:

$$Fx = \frac{1}{2}\rho Af \cdot Cxw \cdot (r_e q)^2$$

$$Fy = \frac{1}{2}\rho Af \cdot Cyw \cdot (r_e q)^2$$

$$Fz = \frac{1}{2}\rho Af \cdot Czw \cdot (r_e q)^2$$

$$Mx = \frac{1}{2}\rho Af \cdot Cmxw \cdot (r_e q)^2 \qquad (15)$$

$$My = \frac{1}{2}\rho Af \cdot Cmyw \cdot (r_e q)^2$$

$$Mz = \frac{1}{2}\rho Af \cdot Cmzw \cdot (r_e q)^2$$

In the case of turn respect to the axis *z* with angular speed r:

$$Fx = \frac{1}{2}\rho Af \cdot Cxv \cdot (r_e r)^2$$

$$Fy = \frac{1}{2}\rho Af \cdot Cyv \cdot (r_e r)^2$$

$$Fz = \frac{1}{2}\rho Af \cdot Czv \cdot (r_e r)^2$$

$$Mx = \frac{1}{2}\rho Af \cdot Cmxv \cdot (r_e r)^2 \qquad (16)$$

$$My = \frac{1}{2}\rho Af \cdot Cmyv \cdot (r_e r)^2$$

$$Mz = \frac{1}{2}\rho Af \cdot Cmzv \cdot (r_e r)^2$$

Where r_e is the distance between the turn axis and the centre of the helm ring

6 CONCLUSIONS

In this paper are presented some criteria about of the conception and modeling of underwater parallel robots (UPR-robot). One of the more important obstacles to develop a variable geometry underwater robot is to have a methodology to modeling its hydrodynamics. Several hydrodynamics parameters can change with the geometry changes of the robot, the hydrodynamics damping coefficients are ones of those more important. In this paper is suggested a method for the computational estimation of the damping coefficients. The coefficients have been estimated in base to the hydrodynamics forces and moments that results of a CFD simulation of the UPR robot, for a series of velocities and intermediate geometric configurations. Although other hydrodynamics parameters must be calculated for solve the dynamics, such as: the added-mass matrix, or the centripetal-coriolis matrix, the damping coefficients can be calculated only by computational methods or experimental tests. Finally, apparently the computational methods to calculate the damping coefficients, it seems to be a very useful technique.

ACKNOWLEDGEMENT

REFERENCES

1. A. Alessandri, R. Bono, M. Caccia, G. Indiveri, G. Veruggio. "Experiences on the Modelling and Identification of the Heave Motion of an Open-frame UUV". Proceedings of IEEE OCEANS '98, Niza, Francia, Septiembre 1998.
2. A. Alessandri, M. Caccia, G. Indiveri, G. Veruggio. "Application of LS and EKF techniques to the identification of underwater vehicles". CNR-IAN. Instituto de automatización naval. Conferencia sobre aplicaciones de control 1998, Italy
3. Betlehem, T. "Autonomous Sumersible Robot: State Estimation System". Master Thesis. Department of Engineering, Australian National University.
4. Brutzman, Donald P., "A Virtual World for an Autonomous Underwater Vehicle", Dissertation, technical report NPS-CS-010-94, Naval Postgraduate School, Monterey California, December 1994. The accompanying public electronic distribution of this reference includes source code and executable programs. World-Wide Web (WWW) Uniform Resource Locator (URL) is *ftp://taurus.cs.nps.navy.mil/pub/auv/auv.html*.
5. Brutzman D., Doucy O., Healy A. "Near Surface Manoeuvring and Station-Keeping for an Autonomous underwater vehicle". NATO symposium. Applied Vehicle Technology Panel.
6. Exa Corporation. "PowerFlow user's guide. Release 3.4". 2002. Fossen, Thor I., Sagatun Svein I., "Lagrangian Formulation Of Underwater Vehicles' Dynamics". ISSN # 0-7803-0233-8/91 1991 IEEE.
7. Fossen, Thor I., "Guidance and Control of Ocean Vehicles", John Wiley & Sons, Chichester England, 1994.
8. Fossen,Thor I., "Marine Control Systems", John Wiley & Sons. ISBN 82-92356-00-2
9. Healey, A.J., McGhee, R.B., Cristi, F., Papoulias, F.A., Kwak, S.H., Kanayama, Y., Lee, Y., Shukla, S. and Zaky, A., "Research on Autonomous Underwater Vehicles at the Naval Postgraduate School," Naval Research Reviews, Office of Naval Research, Washington DC, vol. XLIV no. 1, Spring 1992.
10. J.N. Newman. "Marine Hydrodynamics". The MIT Press. ISBN 0-262-14026-8.
11. R.Aracil, R. Saltaren, O. Reinoso Parallel robots for autonomous climbing along tubular structures *Robotics and Autonomous Systems.* Vol. 42/2 pp. 125-134. January 2003
12. D. Stewart, "A platform with six degrees of freedom," *Proc. Instr. Mech.Engs.*, vol. 180-1, no. 15, pp. 371–386, 1965.
13. Dean Steinke "Numerical Modeling of an Underwater Vehicle Mech 499 Final Report". April 26, 2003.D. Wettergreen, C. Gaskett, A. Zelinsky "Autonomous Guidance and Control for an Underwater Robotic Vehicle".
14. D. Wettergreen, C. Silpa-Anan, S. Abdallah. "Autonomous Guidance and Control for an Underwater Robotic Vehicle".

Chapter 14

Climbing Robots for the Maritime Industries

M ARMADA, M PRIETO, T AKINFIEV, R FERNÁNDEZ, P GONZÁLEZ DE SANTOS, E GARCÍA,
H MONTES, S NABULSI, R PONTICELLI, J SARRIA, C SALINAS, J ESTREMERA, and S ROS
Instituto de Automática Industrial (CSIC), Arganda del Rey, Madrid, Spain
J GRIECO, G FERNANDEZ
Instituto de Ingeniería, Grupo de Mecatrónica, Caracas, Venezuela

Modern robotic systems are increasingly powerful in terms of sensor fusion and mobility. The progress allows advanced robots to cope progressively more better also with complex environments which are frequently found in the maritime industries. An overview of the development of mobile robots (climbing) is given with examples taken from the maritime industries applications, coming mostly from the experience of IAI-CSIC in different projects.

1 INTRODUCTION

The Automatic Control Department of the Industrial Automation Institute (IAI-CSIC) has been carrying out research and development projects in the field of robotic systems for more than twenty five years. Since late seventies this activity began with the realisation of industrial robots, what provided the research team with a wide experience and reputation in robot kinematics, dynamics, mechanical design, and control systems. After some successful developments in that field, the department focused its interest in the area of robots for hostile/hazardous environments. In these kind of environments it is necessary to carry out a variety of tasks (inspection, manipulation, welding, grinding, etc.), what implies human operators are exposed to hard working conditions. Also there are a great number of potential applications that cannot be performed directly by human operators because of difficulties in reaching working positions in a proper and safe way. This situation yields, in a natural way, to the utilisation of remotely controlled devices, where tele-robots can be considered as the most advanced and promising solutions. Doing so a number of advantages will come: improved working conditions, improved safety, automation of repetitive tasks, and opening the possibility of providing innovative solutions to emerging applications.

However, although many applications can be solved by means of an appropriate tele-manipulator, equipped with the right tools and with the concurrence of the human operator skills, many others cannot be solved in this way due to working position difficult access. The problem of accessing to more or less remote job sites presents major difficulties and prevents automation. There are, reported in the literature, interesting solutions to this situation, for example very long reach manipulators. Other, not less interesting approach is to provide a transport mean for the tele-manipulator. Such a transport mean includes wheeled or tracked vehicles, and more recently, legged-machines (climbing or walking).

Nowadays shipbuilding industry is being forced to adapt its production to new technical specifications, shorter delivery time and new safety regulations, so that the ships have to be built faster, more economically and under better environmental condition for operators. New robotic systems are improving these features. Especially, robot manipulators are helping to enhance the quality of welding, decrease arc time, and avoid operators be exposed to fume concentration. However, current robotic systems cannot accomplish some industrial applications, especially those related with mobility in complex environments. These scenarios appear in some stages of the ship construction such as are the operations in the dry dock, and also in the ship repairing yards in what respects ship cleaning and inspection. In this chapter some solutions are presented dealing with specially tailored climbing and walking robots for the maritime industries. These robotic systems have been mostly developed in the framework of European funded projects.

In the field of shipbuilding there are three main stages in the ship erection process:

- Block's construction in the workshop.
- Transportation of blocks to the dry dock or to the slip-way using cranes and especial vehicles.
- Connection of consecutive blocks in the dry dock or slip-way.

The first activity consists of the construction and assembly of huge ship blocks. This work is performed in highly automated workshops with a relatively good productivity, which is being increased by current research in this area. After the transportation of the blocks, which is performed in the second stage, the third involves joining two consecutive blocks by welding together all the longitudinal reinforcements and all the vertical bulkheads.

For environmental safety, most ships, especially tankers and bulk carriers are built with a double bottom and double hull so the cargo will not spill out if the hull is breached. This double structure forms cells all over the ship's hull. There are two important welding problems in ship erection: butt-welding in position along the near-flat external hull surface, and butt/fillet welding for joining double hull cells. In the last years IAI-CSIC has been involved in several projects dealing with welding automation in shipbuilding. Three main results are briefly reported in this work: one six-legged and one four-legged climbing robots for butt-welding of ship hull skin, and one robotic system for welding inside the double hull vertical cells (ROWER 2). All robots have been equipped with industrial welding units and special sensors for seam tracking. A fourth climbing robot, this time underwater, intended for sea adherence cleaning and hull inspection will be the subject of the last part of this chapter.

2 REST 1 CLIMBING ROBOT

The REST 1 climbing robot has six reptile-type legs with three degrees of freedom each one, actuated by dc motors through appropriate gearing. The leg kinematics is of *scara* type, with two rotational articulations and a prismatic one that holds at its end the foot. Feet at the end of legs are provided with special grasping devices based on electromagnets, securing the robot to ferromagnetic-material walls with intrinsic safety. Some degree of compliance has been provided to the feet, by means of an extra passive degree of freedom, so that the robot can

adapt itself to a certain extent of surface unevenness. The climbing robot carries on board his control system that consists on an industrial PC that serves as a master for a bunch of slave processors that controls in real time the 18-degrees of freedom. One of the main features is the combination of 6 low-cost/high-performance digital control and 6 power electronic cards (one per leg, each one providing control for 3 joints), specifically developed for this project, and that are the responsible of the just mentioned control of each one of the 18 degrees of freedom of the robot.

The main specifications of the REST 1 climbing robot are:

- Leg number: 6
- Degrees of freedom: 18
- Body frame length: 1100 mm
- Body frame width: 600 mm.
- Robot weight: 220 Kg.
- Robot payload: up to 100 Kg.

Different gaits and control algorithms has been implemented and evaluated. A detail on algorithm preparation is presented in next chapter sections.

2.1 The problem of climbing

The displacement of a climbing robot is the result of a co-ordinate motion of its legs. This motion is defined by some climbing gait that reflects specifications such as speed, direction etc. There are two phases clearly differentiated in the contribution of each leg to the robot motion. During the support phase every leg should be able to exert a certain force over the climbing surface, in order to provide the necessary forces to the body allowing moving it according to a predetermined path. Later on, during the transfer phase, the leg should displace toward its next support point in order to re-establish the sequence of motion. Each phase imposes a set of requirements to the leg operation. So, during the support phase the leg must have a great capability of force generation, while in the transfer phase the main requirement is the return speed.

The speed and force demand are straight related with the task to be carried out by the climbing robot as well as by the robot location on its environment. Once a task has been defined, the path is established and must be followed by the robot in its working space. The gait will define the state transitions for every leg. Nevertheless, the leg trajectory during the support phase is determined by the body trajectory. There are an infinite number of these trajectories that can be used to obtain the desired robot motion. In order to simplify this selection some authors do the assumptions that: (1) the reachable range of each foot is a rectangular prism, and the feet ranges take up symmetric positions and, (2) each trajectory symmetrically passes the centre C_i of the plane that is the horizontal projection of the reachable area [1,2]. These assumptions, which are based only on the leg mobility, work well for a walking machine on a regular terrain but there are not appropriate for a climbing machine.

One of the big distinctions among the walking and climbing robots reside in the influence of the gravity forces into the robot operation. Depending on the climbing direction, It could be generated some violation of the torque availability conditions associated with the robot's motors. For climbing robots a more reasonable approach towards the selection of foot trajectories should be based on a torque and speed optimisation process along the leg trajectory. The trajectory optimisation problem has been studied widely in the robotics literature [3,4]; generally, the initial and final points are known and the problem is to determine the optimum trajectory that joins both points according with some criterion. The problem exposed in this paper is different since the kind of trajectory is known (i.e. a straight line) while it should be decided its location in the work space, that is to determine the initial position of the leg so that the path is carried out with minimum cost. In this paper we use a torque optimisation approach and a minimum leg velocity criterion in order to select the optimum climbing trajectories during the leg support phase. Later on, we review the influence of the torque restriction over the workspace. Finally, we determine the greatest stroke allowed as a function of the climbing direction.

2.1.1 Leg placement. An optimum approach

In climbing robot the acceleration force/ support force ratio is very small. For that reason, in this paper a static force approach is used in order to find the best place for the legs during the support phase.

Defining the objective function

Consider a climbing robot, which is hanging on the wall. Let F_i the force applied by the *ith* leg in such a way that the robot centre of gravity remains in equilibrium. The static support torque is given by,

$$\tau_i = J_i(q_i)^T \cdot F_i \qquad \text{Eq. 1}$$

Lets $\Psi(x,y)$ the cost function considering the energy of a leg in support phase positioned in coordinates x,y in its workspace, then it can be defined as,

$$\Psi(x,y) = \tau^T \cdot \tau = F^T \cdot J \cdot J^T \cdot F \qquad \text{Eq. 2}$$

where JJ^T is given by,

$$JJ^T = \begin{bmatrix} (l_1 s_1 + l_2 s_{12})^2 + (l_2 s_{12})^2 & -(l_1 s_1 + l_2 s_{12})(l_1 c_1 + l_2 c_{12}) - l_2^2 c_{12} s_{12} & 0 \\ -(l_1 s_1 + l_2 s_{12})(l_1 c_1 + l_2 c_{12}) - l_2^2 c_{12} s_{12} & (l_1 c_1 + l_2 c_{12})^2 + (l_2 c_{12})^2 & 0 \\ 0 & 0 & 1 \end{bmatrix} \qquad \text{Eq. 3}$$

for a SCARA type leg. Thus, the objective function can be stated as,

$$\Psi(x,y) = \left[(l_1 s_1)^2 + 2(l_2 s_{12})^2 + 2 l_1 l_2 s_1 s_{12} \right] F_X^2 + \left[(l_1 c_1)^2 + 2(l_2 c_{12})^2 + 2 l_1 l_2 c_1 c_{12} \right] F_Y^2 -$$
$$2 \left[l_2^2 s_{12} c_{12} + l_1 l_2 s_{12} c_1 + l_1 l_2 s_1 c_{12} + l_1^2 s_1 c_1 \right] F_X F_Y + F_Z^2 \qquad \text{Eq. 4}$$

Finally, using the kinematic equations for a SCARA leg it is obtained,

$$\Psi(x,y) = \left[y^2 + l_2^2 s_{12}^2 \right] F_X^2 + \left[x^2 + l_2^2 c_{12}^2 \right] F_Y^2 - 2 \cdot \left[x \cdot y + l_2^2 s_{12} c_{12} \right] F_X F_Y + F_Z^2 \qquad \text{Eq. 5}$$

256

Vertical climbing motion
The objective function varies not only with the x,y coordinates of the leg but also with the F force which in turn depends in the climbing gait. This suggests that for every climbing gait an optimum path will exist that minimise the actuator torque for the leg. In order to solving the foot placement problem it should be necessary to establish it certain considerations. Of the forces that provide support and motion to the climbing robot, the higher contribution belongs to the vertical force. A first approach to the foot positioning problem could be to consider only this force so then the objective function is given by,

$$\Psi(x,y)=\left[x^2+l_2^2 c_{12}^2\right]F_Y^2 \qquad \text{Eq. 6}$$

Consider the support phase time T_a and the leg stroke R. The objective function associated with a x(t), y(t) trajectory could be obtained evaluating the equation (6) along the path. Therefore the trajectory objective function is given by,

$$\Psi_{TRAY}(x_c,y_c,T_a)=F_Y^2\cdot\int_0^{T_a}\left(x(t)^2+l_2^2 c_{12}(t)^2\right)dt \qquad \text{Eq. 7}$$

where,

$$c_{12}(t)=\frac{x(t)\cdot(l_1-D(t)\cdot l_2)-y(t)\cdot l_2\cdot\sqrt{1-D(t)^2}}{x(t)^2+y(t)^2} \qquad \text{Eq. 7b}$$

$$D(t)=\frac{x(t)^2+y(t)^2-l_1^2-l_2^2}{-2\cdot l_1\cdot l_2} \qquad \text{Eq. 7c}$$

Including the constraints
Some constraints must be considered in the optimisation process because of the leg structure and the environment in which the robot moves.

Figure 1 show the workspace for the front leg of an hexapod robot during vertical climbing and different constraints for and specific task (welding on a ship hull). For this task, the environment constraints can be defined as,

$$-0.18 < \mathrm{x}(t) < 0.280 \qquad \text{Eq. 8}$$

The structural constraints are due to physical limitation of the leg joints. For the REST robot these are: hip joint (± 90º), knee joint (± 130º), link length (250mm).
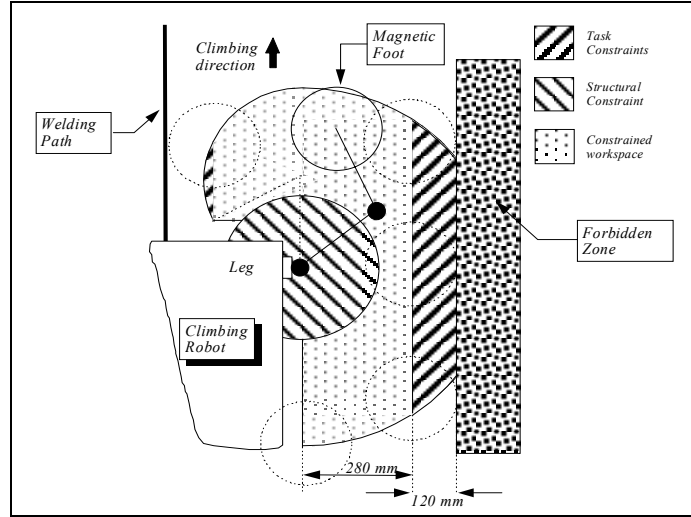
Figure 1 Workspace and structural and task constraints for a hexapod robot

Getting the location for the optimum leg placement

Once the constraints are established and the leg path (i.e. a straight line motion) is defined, then the foot placement problem can be formulated as a non linear optimisation problem defined as,

$$\underset{x_c,y_c}{\text{minimize}}\ \Psi\left(x_c,y_c,R,T_a\right) = \int_0^{T_a}\left(x(t)^2 + l_2^2\, c_{12}(t)^2\right)dt$$

subject to:

$$x^2 + y^2 < L^2$$

$$-2.27\,\text{rad} < \tan^{-1}\left(\frac{\sqrt{1-D^2}}{D}\right) < 2.27\,\text{rad} \qquad\qquad \text{Eq. 9}$$

$$-\frac{\pi}{2} < \tan^{-1}\left(\frac{y}{x}\right) - \tan^{-1}\left(\frac{\sqrt{1-D^2}}{1-D}\right) < \frac{\pi}{2}$$

$$-0.18 < x < 0.280$$

This is solved numerically using the Optimisation Toolbox of MATLAB [5].

Numerical results

In a climbing robot using a periodic continuos gait the robot velocity is

$$V = \frac{R}{\beta \cdot T} \qquad\qquad \text{Eq. 10}$$

so, keeping the ratio βT constant (the robot support forces depend on the duty factor) its possible to increase the velocity changing the leg stroke. Nevertheless, different legs stroke have different positions of the contact point for the legs that gets minimum actuator torque.

Figure 2 show the constraint workspace and the objective function for a leg stroke of R=0.2 mts. and (x,y) trajectory centre.
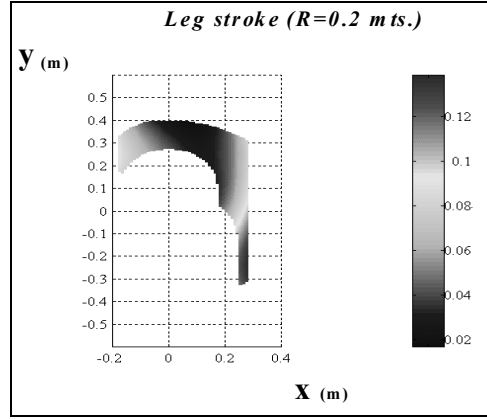
Figure 2 Objective function for a front leg with a stroke of 0.2 m.

In order to study the dependency of the optimum foot contact position with the leg stroke, it was necessary to run many simulations for different strokes. Figure 3 show the locations of the optimum foot contact position as a function of the leg stroke.
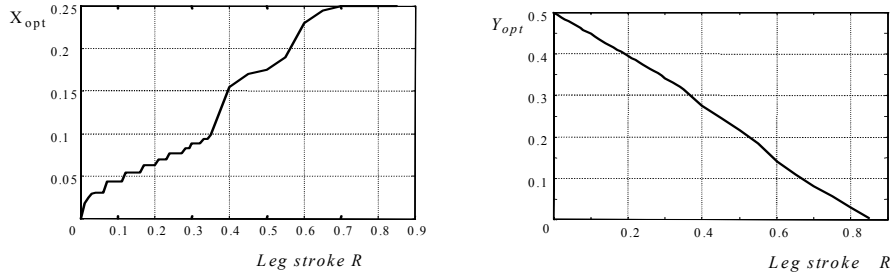
Figure 3 Optimum leg contact position during vertical climbing.

Omnidirectional climbing.
In omnidirectional climbing mode the robot can ascend in any direction. This section deal with the foot placement optimisation problem when a climbing robot moves following a straight line and the robot's longitudinal axis set a particular angle α with respect to the vertical climbing.

If two walking robot move following a straight line, over a regular terrain, and use the same gait parameter, changing only the walking directions, they will have the same power requirements. However, this is not true for climbing robots due to gravity force. This suggests that the optimum foot placement depend not only on the leg stroke but also on the climbing angle.

Figure 4 show a climbing robot with an α angle motion direction. Let F_{Ti} be the support force for the *ith* leg and let F_m be the acceleration force so the robot can follow the desired trajectory. The acceleration force can be considered proportional to the support force so $F_{mi} \approx \kappa F_{Ti}$. Thereby, the *ith* foot force is given by,

$$F_x = F_{Ti} \cdot sen\alpha$$
$$F_y = F_{Ti} \cdot cos\alpha + F_{mi}$$

Eq. 11

259

Using eq. 11 and eq.5 the objective function is,

$$\Psi(x,y,\alpha,\kappa)=\left\{ \begin{array}{c} \left[y^2+l_2^2 s_{12}^2\right]sen(\alpha)^2+\left[x^2+l_2^2 c_{12}^2\right]\left[cos(\alpha)+\kappa\right]^2- \\ \\ 2\cdot\left[x\cdot y+l_2^2 s_{12} c_{12}\right]sen(\alpha)\cdot\left[cos(\alpha)+\kappa\right] \end{array} \right\}\cdot F_{Ti}^2 \qquad \text{Eq. 12}$$

For a continuos climbing gait with constant velocity the objective function it is simplified by the condition $\kappa=0$.
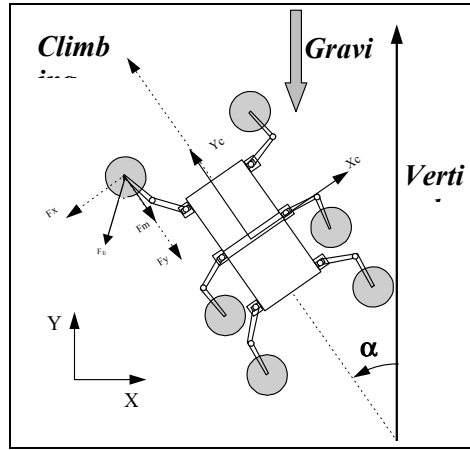
Figure 4 Diagonal climbing robot

Let T_a the support time and R the leg stroke then, the motion cost can be obtained minimising the objective function along the trajectory { $x(t) = X_c$, $y(t) = Y_c+R/2-Rt$ } with coordinate value (X_c,Y_c) for the trajectory centre. This can be formulated as a non-linear optimisation problem defined as,

$$\underset{x_c,\ y_c}{\text{minimise}}\ \Psi_{Traj}\left(x_c,y_c,\alpha,R,T_a\right)=\int_0^{T_a}\Psi\left(x,y,\alpha,\kappa=0\right)dt$$

subject to:

$$x^2+y^2<L^2$$

$$-2.27\,\text{rad}<\tan^{-1}\left(\frac{\sqrt{1-D^2}}{D}\right)<2.27\,\text{rad} \qquad \text{Eq. 13}$$

$$-\frac{\pi}{2}<\tan^{-1}\left(\frac{y}{x}\right)-\tan^{-1}\left(\frac{\sqrt{1-D^2}}{1-D}\right)<\frac{\pi}{2}$$

Numerical results

Some simulations have been carried out in order to find the optimum contact point for different climbing directions. All the solutions are based in a leg stroke R=0.25 mts. The robot symmetry permits simplify the problem and solutions for leg pairs (1-6) and (2-5) are the same. Figure 5 shows the optimal coordinates for the trajectory centre for legs 1-2-5-6 as a function of the climbing angle. The discontinuity presented for α = 0.669 rad is related with the structural restrictions.
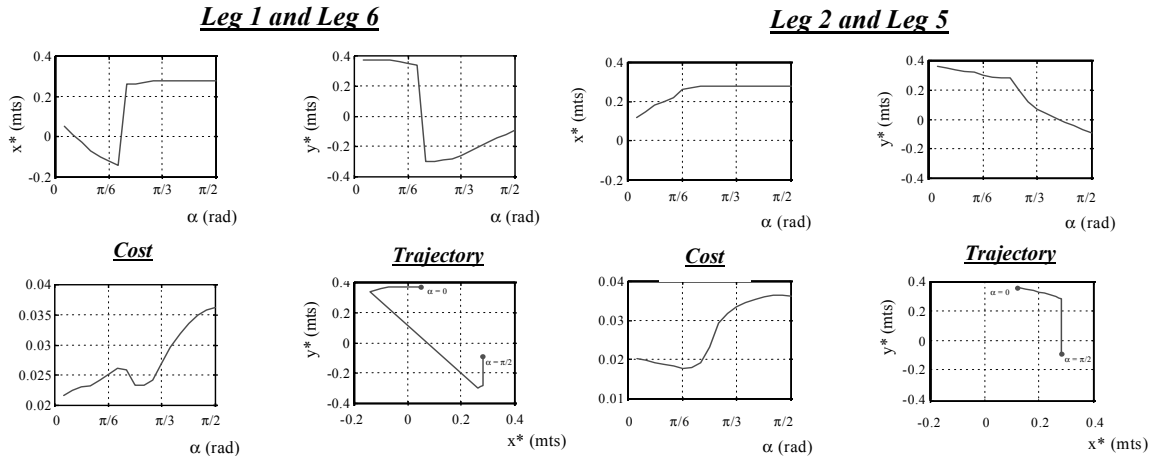
Figure 5 Optimal position for an SCARA type leg of an Hexapod robot

Figure 6 shows the optimal positions for the central legs 3-4 of the hexapod REST.
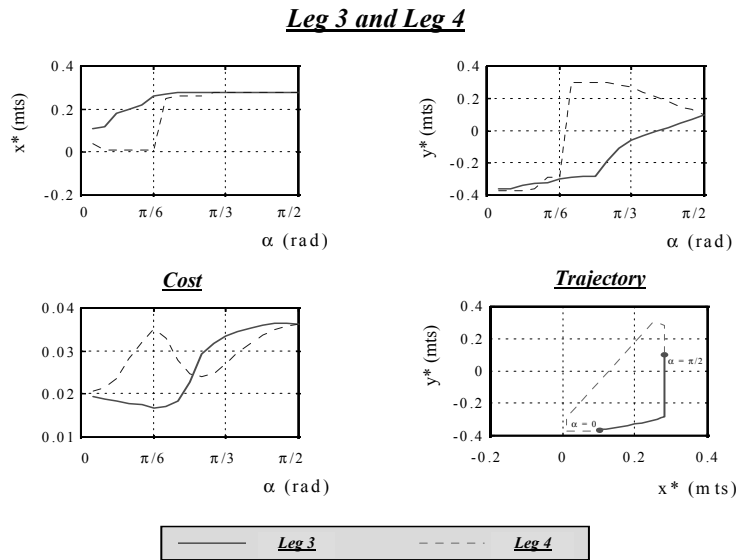
Figure 6 Optimal position for an SCARA type leg of an Hexapod robot. Legs 3-4

Figure 7 show the climbing sequence for an hexapod robot using optimal foot placement solution for a climbing angle $\alpha = 0.61$ *rad* with a leg stroke $R = 0.25$ *mts.* It can be seen the difference between a climbing robot with optimal contact position and a walking robot using standard leg positioning. In this figure the climbing robot use a Sawing Gait [6] with leg motion sequence {6-3-2-5-4-1}.

Finally, using SIDIREST [7] a comparison between the requirements for a horizontal climbing mode and a vertical climbing mode has been carried out. Figure 8 shows the simulation results for a front leg of the REST hexapod [6] using a wave gait with $\beta=5/6$,

R=0.3 m and a cycle time T_c=12 sec. Figure 8 is an example of duality between the kinematic differential equations (velocity) and static equation (force).
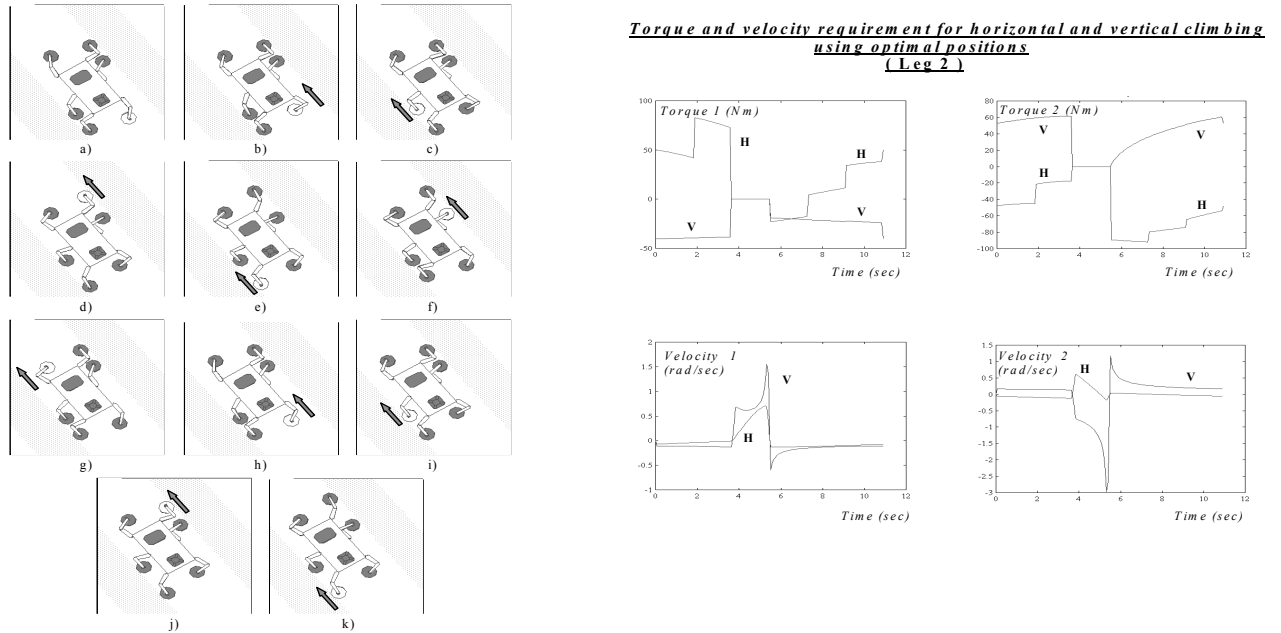
Figure 7 (left) Motion sequence for a climbing robot using optimal foot placement.
Figure 8 (right) SIDIREST simulation for horizontal and vertical climbing.

Additionally to the torque requirement sometimes is necessary to consider the actuator velocity in order to keep tracked the desired trajectory. The velocity depends on the climbing gait. During the support phase the leg and robot velocity are the same and it is determined for the task while during the leg return phase the leg velocity and the robot velocity follow the relation,

$$V_{leg} = \frac{\beta}{1-\beta} \bullet V_{body}$$ Eq. 14

If a duty factor β=11/12 is used, then the leg velocity is 11 times greater than the robot velocity. In this case the velocity must be taking in account in order to satisfy the requirement. The next section deal with the multicriteria optimisation based on torque and velocity requirement.

Multi-objective Optimisation

Consider a climbing robot, which is hanging on the wall. Let $\dot{x}_i$ the tip velocity of the *ith* leg during the return phase. The joint velocity are given by,

$$\dot{q}_i = J_i (q_i)^{-1} \cdot \dot{x}_i$$ Eq. 15

Lets $\Gamma(x,y)$ the cost function for a coordinate point (x,y) in the leg's workspace considering the velocity at the foot, then it can be defined as,

$$\Gamma(x,y)= \dot{q}_i{}^T \cdot \dot{q}_i = \dot{x}_i{}^T \cdot \left(J_i\,(q_i\,)\cdot J_i\,(q_i\,)^T \right)^{-1} \cdot \dot{x}_i \qquad \text{Eq. 16}$$

where $(JJ^T)^{-1}$ is,

$$\left(JJ^T\right)^{-1} = \frac{1}{l_2^2\cdot(y\cdot c_{12} - x\cdot s_{12})^2} \cdot \begin{bmatrix} x^2 + (l_2 c_{12})^2 & x\cdot y + l_2^2 c_{12} s_{12} & 0 \\ x\cdot y + l_2^2 c_{12} s_{12} & y^2 + (l_2 s_{12})^2 & 0 \\ 0 & 0 & l_2^2\cdot(y\cdot c_{12} - x\cdot s_{12})^2 \end{bmatrix} \qquad \text{Eq. 17}$$

and $\dot{x}_i = [\,\dot{x}_{xi}\ \dot{x}_{yi}\ \dot{x}_{zi}\,]^T$.

During the return phase the leg follow the trajectory given by $x_i(t)$ and $\dot{x}_i\,(t)$ which depend on gait parameter.

Defining the objective function
Using a similar procedure of the previous section and considering the eq. 17, the objective function, evaluated on point (x,y) of the return trajectory, can be stated as,

$$\Gamma(x,y) = \frac{\left[y^2 + l_2^2 s_{12}^2\right]}{l_2^2\cdot(y\cdot c_{12} - x\cdot s_{12})^2} V_y^2(x,y) \qquad \text{Eq. 18}$$

An important attribute of this functional is its not dependency with the climbing direction. Considering the return phase time T_r, the leg stroke R and a constant velocity V_r, then, the objective function could be obtained evaluating the equation (18) along the path. Therefore the trajectory objective function is given by,

$$\Gamma_{TRAY}(x_c, y_c, T_r) = V_y^2 \cdot \int_0^{T_r} \frac{\left[y(t)^2 + l_2^2 s_{12}(t)^2\right]}{l_2^2\cdot(y(t)\cdot c_{12}(t) - x(t)\cdot s_{12}(t))^2}\, dt \qquad \text{Eq. 19}$$

Therefore, considering the objective functions $\Psi(x,y)$ and $\Gamma(x,y)$ the multicriteria optimisation problem can be defined as,

$$\text{Let}\quad \Omega = [\,\Psi_{TRAY}\,(x_c\,,y_c\,,R,T_a\,)\ \Gamma_{TRAY}\,(x_c\,,y_c\,,R,T_r\,)\,]$$

$$\underset{x_c\,,y_c}{\text{minimize}}\ \Omega(x_c\,,y_c\,,R,T_a\,,T_r\,)$$

$$\text{subject to:}$$

$$x^2 + y^2 < L^2$$

$$-2.27\,\text{rad} < \tan^{-1}\left(\frac{\sqrt{1-D^2}}{D}\right) < 2.27\,\text{rad}$$

$$-\frac{\pi}{2} < \tan^{-1}\left(\frac{y}{x}\right) - \tan^{-1}\left(\frac{\sqrt{1-D^2}}{1-D}\right) < \frac{\pi}{2}$$

$$-0.18 < x < 0.280$$

Eq. 20

There are many methods to resolve a multi-objective optimisation problem. In this paper it is used a weighted sum strategy to convert the multi-criteria optimisation of the Ω vector into a scalar one by means of weight associated with each objective. Thus, the multi-criteria optimisation can be defined as,

$$minimize \quad \widetilde{\Omega} \quad = \quad \alpha_1 \cdot \Psi_{TRA}(x_c, y_c, R, T_a) + \alpha_2 \cdot \Gamma_{TRA}(x_c, y_c, R, T_r)$$

Eq. 21

$$subject \quad to \quad constraint \; Eq \quad 20$$

Numerical results for multi- objective optimisation

In this section it is considered the same importance for torque and velocity objective. This is established doing $\alpha_1 = \alpha_2 = 0.5$. Those interested readers can see [8] for a general selection of (α_1, α_2) based on climbing parameters.

The optimisation was carried out for different leg strokes, from 0.01m to 0.8 m. Figure 9 shows the optimum foot contact point for the REST robot during vertical climbing as a function of the leg stroke. It can be see that for a big leg stroke the multi-criteria optimisation converge to the torque optimisation due to restriction in the workspace. For a small leg stroke, R<0.5m, there are fewer motion restrictions. In order to have a general rule to get the foot placement positions an approximated solution was obtained using a fitting least square ninth degree polynomial.
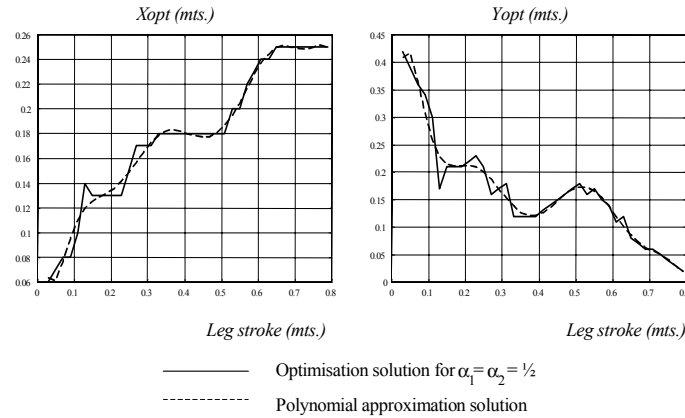
Figure 9 Optimum foot placement for a multi objective optimisation. Vertical climbing

Influence of the climbing direction on the leg stroke

Determination of the maximum leg stroke

Let us consider a climbing robot moving on a direction forming an angle α. The effective leg workspace varies in accordance with its configuration, with the direction angle and with the support force. In order to estimate the climbing stroke -R_{max} - is required to calculate the maximum stroke- R^i_{max} – that it is associated to robot leg i; taking in account that all supporting legs must use the same stroke during the locomotion cycle, then R_{max} is determined by $min\{R^i_{max}\}$.

Due leg configuration affects directly to R_{max}, then it is possible to determine the n-legs configuration that permits to obtain the maximum value for R_{max}. Let F_i the feet support phase force, and let be τ_{imax} the maximum torque that can be generated by the i-*th* leg actuators. The support trajectory centre is given by the x_c,y_c point. The stroke is r. Determination of R^i_{max} can be posed as:

$$R^i_{max} = \max_{x_a, y_a, r} \; r$$

subject to:

$$a)\; x_a^2 + (y_a - \omega \cdot r)^2 < L^2$$

$$b)\; -\frac{13\pi}{18} < q_{2i}(x_a, y_a - \omega \cdot r) < \frac{13\pi}{18}$$

$$c)\; -\frac{\pi}{2} < q_{1i}(x_a, y_a - \omega \cdot r) < \frac{\pi}{2}$$

$$d)\; J_i(x_a, y_a - \omega \cdot r) \cdot F_i(\alpha) < \tau_{i\,max}$$

Eq. 22

$$\forall \omega \in [0,1]$$

where a), b) and c) are leg kinematic restrictions, while d) represents the associated restriction to the maximum torque allowed through the trajectory. Once determined the values of R^i_{max} for each leg it can be determined R_{max} such,

$$R_{max} = \min\left\{ R^i_{max} \right\} \qquad i = 1,2,...,n$$

Eq. 23

Optimisation results

Two different leg configurations have been study. The configuration A represents an "elbow down" leg configuration referred to the first quadrant while configuration B exhibits an "elbow up" disposition referred to the same quadrant. Table 1 presents the obtained results for each leg in the REST robot.

Table 1. Maximum leg stroke depending on the leg disposition.

Leg	Configuration A			Configuration B			Stroke Max.
	P_X(cm)	P_Y(cm)	R(cm	P_X(cm)	P_Y(cm)	R(cm)	
1	3.47 -24.35	26.75 -35.75	20.2 14.62	-24.58	12.13	16.97	14.62-16.97 20.20
3	-2.5 -24.35	25 -35.75	16.24 14.62	-24.58	12.13	16.97	14.62-16.24 16.97
5	-2.5 -24.35	25 -35.75	16.24 14.62	-24.58 16.17	12.13 -12.7	16.97 14.49	14.62-16.24 16.97
2	24.58 -16.17	-12.13 12.7	16.97 14.49	2.5 24.35	-25 35.75	16.24 14.62	14.62-16.24 16.97
4	24.58	-12.13	16.97	2.5 24.35	-25 35.75	16.24 14.62	14.62-16.24 16.97
6	24.58	-12.13	16.97	-3.47 24.35	-26.75 35.75	20.2 14.62	14.62-16.97 20.20

Previous results exhibit how the maximum leg stroke, to be employed during the climbing motion with angle $\alpha = \pi/3$, is $R_{max} = 16$cm. This distance can be reached with any of the possible leg configurations, as it is shown in the Table 1.

Rmax variation with the climbing angle

Figure 10 represented the variation of maximum leg stroke depending with the climbing angle. It can be seen a strong discontinuity, close to 30º. Starting from this angle the leg's workspace consist of two separated areas reducing the maximum stroke.
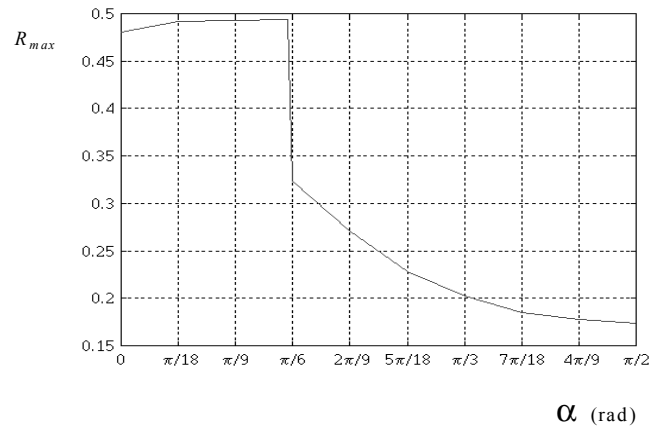
Figure 10 Leg stroke variation with climbing angle

The optimum foot placement problem for climbing robot has been formulated as a non-linear optimisation problem subject to kinematic and environment constraints. The technique permit to select the optimal placement from an energetically point of view. The diagonal climbing has been studied and different foot positions have been established for climbing direction ranging from vertical to horizontal. A multi objective optimisation is proposed in order to consider the velocity requirements during climbing tasks. Finally, the influence of climbing direction in the maximum leg stroke was presented.
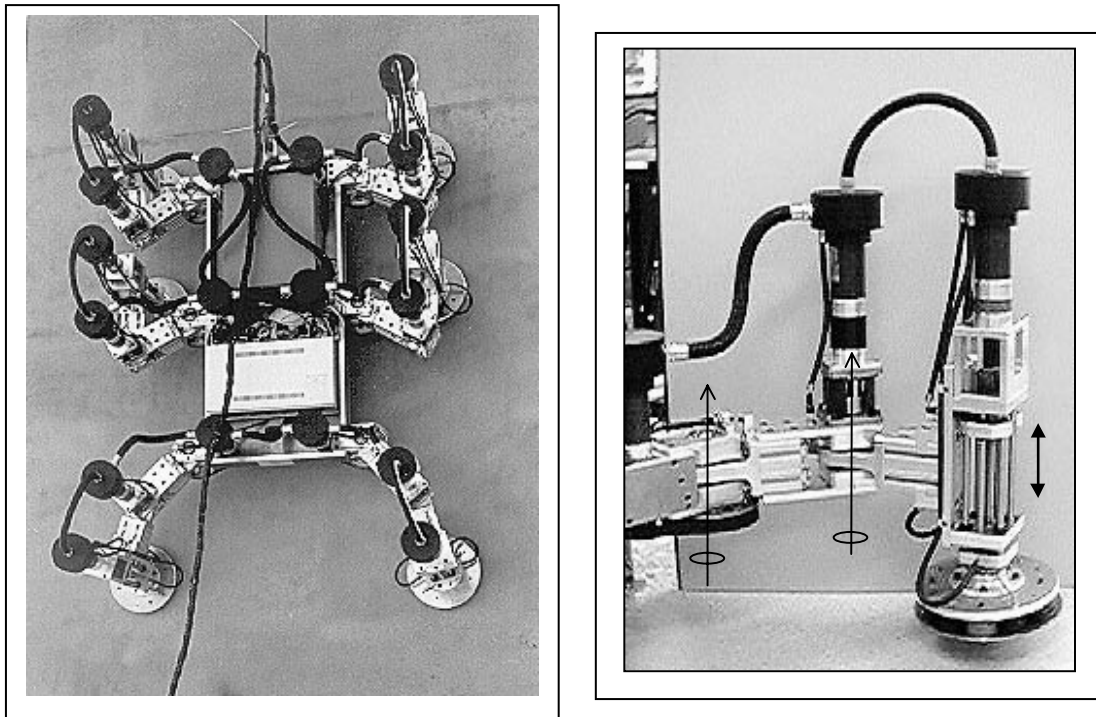
Figure 11 REST 1 climbing robot under experimental testing.

Figure 11 left illustrates the experimental testing of REST 1 six-legged climbing robot, right side shows a detail of the scara type legs.

3 REST 2 CLIMBING ROBOT

Following REST 1, a second prototype of climbing robot that moves continuously along the wall, named REST 2 has been constructed. It uses a variation of the well known wave gait in order to obtain fast continuous movement on softly undulated terrain together with foothold selection to handle obstacles and irregularities during climbing. The robot uses electromagnets to attach itself to ferromagnetic walls and has four legs (12 degrees of freedom) that resemble properties from sliding frames and true legged climbers. The novel leg design and geometrical configuration allows for fully overlapping workspaces. As a result of this novel leg and robot design, it was possible to achieve a much better payload to weight ratio, increased velocity, better inertial properties and reduced energy consumption. Our approach to reliability was to simplify the robot structurally and to support modularity of parts and connections.

REST 2 has been designed to carry on a light manipulator for butt welding. The robot weights less than 50 Kgs. Figures 12 and 13 shows a comparison of both climbing machines.

Figure 12. REST 1 climbing robot welding ship hull.
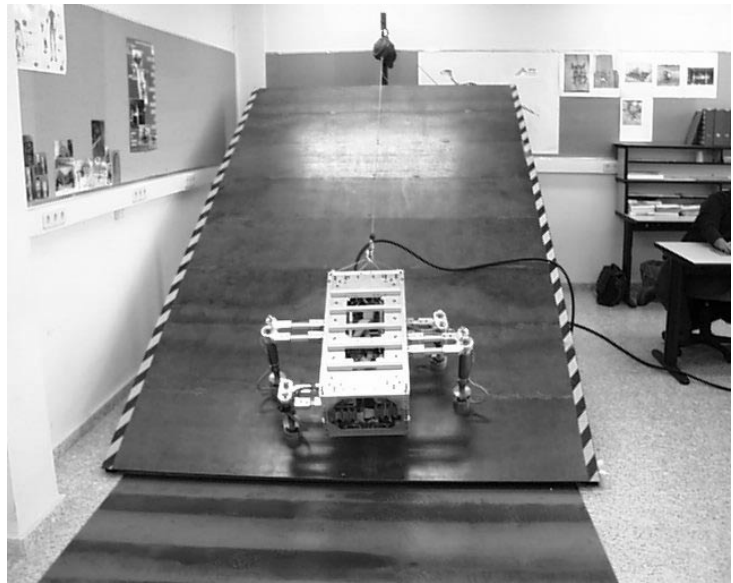
Figure 13. REST 2 climbing robot during testing

267

4 ROWER 2

A second development (after ROWER 1) was intended for contributing the problem of welding automation inside the double-bottom vertical cells. So further developments yielded to ROWER 2 (Figure 14), where a light manipulator is moved in the vertical direction for welding the double hull vertical cells.
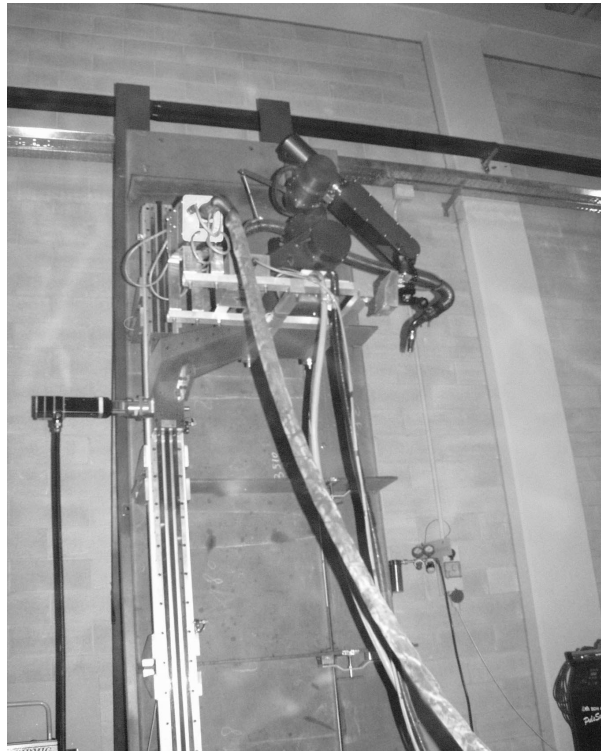
Figure 14. ROWER 2 system.

5 AURORA UNDERWATER CLIMBING ROBOT

It is well known that all kind of ship's underwater hull become overgrown with sea adherence (weed, barnacles) very fast. This means raise of fuel consumption, and freeing atmosphere an extra amount of CO_2 (incrementing greenhouse effect) and of sulphur dioxide (acid rain), apart from deterioration of ability of ship's control. This situation becomes important even after six months of ship activity. For recovery of ship's required operational performance, it is necessary for Ship-Repairing and Conversion Industries to dry dock a ship and proceeds to cleaning. This procedure is very time consuming and of high cost, but it is the only available solution nowadays for SRYs. On the other hand, this cleaning activity is the first to be done when a ship needs maintenance and/or some repairing, being the last the main activity of SRYs. So hull treatment is required and, at present time, is done manually in dry-dock using

different adapted methods like grit blasting or water jet, and it has to be noticed that, in itself, it is a very contaminant operation (dust contains always painting particles), it is harmful for human operators health and it is a very uncomfortable job.

To provide a solution to these problems an EC funded project (G3RD-CT-000-00246) was organised: AURORA (Auxiliary Climbing Robot for Underwater Ship Hull Cleaning of Sea Adherence and Surveying). The project partnership brings together 7 partners with complementary roles: the Industrial Automation Institute (IAI-CSIC) which is the Project co-ordinator, two ship-repairing yards, T. Kalogeridis&Co. Inc. and Unión Naval de Barcelona, Algosystems S.A., the Division of Robotics, Department of Mechanical Engineering, from Lund University, SAIND, manufacturer and vendor of equipment for shipyards, and Riga Technical University.

AURORA scenario consists in the underwater hull that after some time of ship operation is plenty of marine incrustations, where a new kind of underwater climbing robot equipped with special tools should perform cleaning and surveying tasks. That scenario presents large dimensions and exhibits some areas of very difficult reach-ability and poses some additional technical difficulties. As it has been conceived the underwater climbing robot control is a human-in-the-loop process. Human-Machine Interface (HMI) design takes this into consideration whether using direct control or supervised control. This interface includes a control command set used to select the machine trajectory and a graphic representation used to get information about the robot and its environment. Figure 15 shows the concept of AURORA project and some view of the teleoperation station. Figure 16 shows overall system architecture. The system has demonstrated excellent performance.
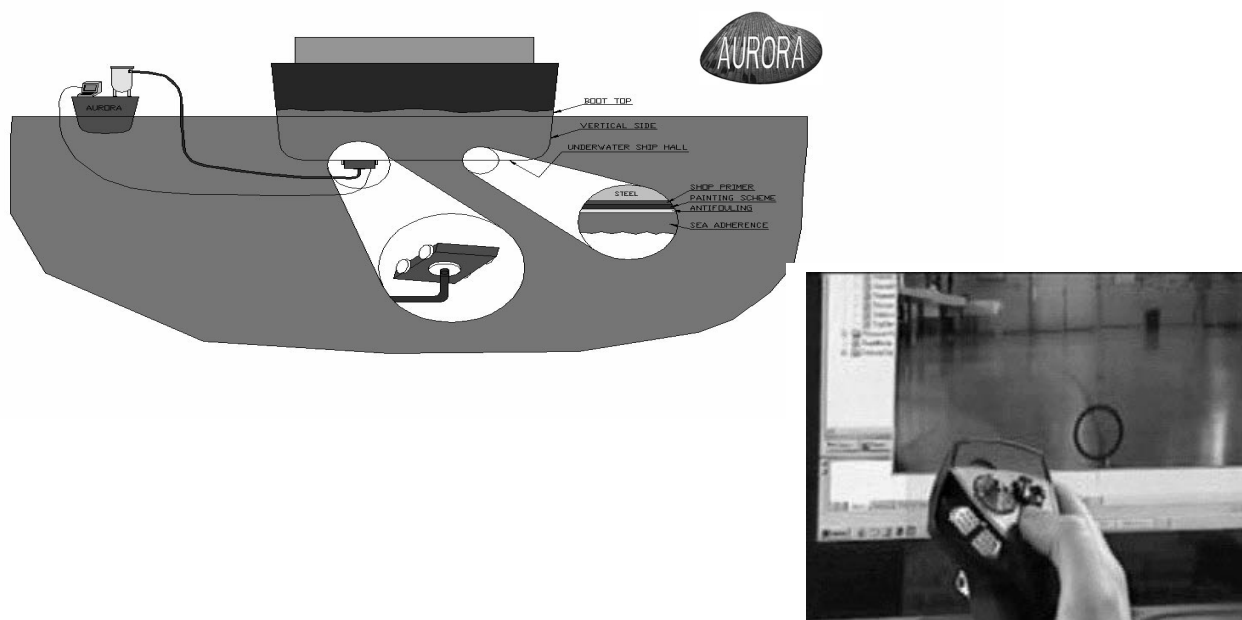
Figure 15. AURORA concept and remote control
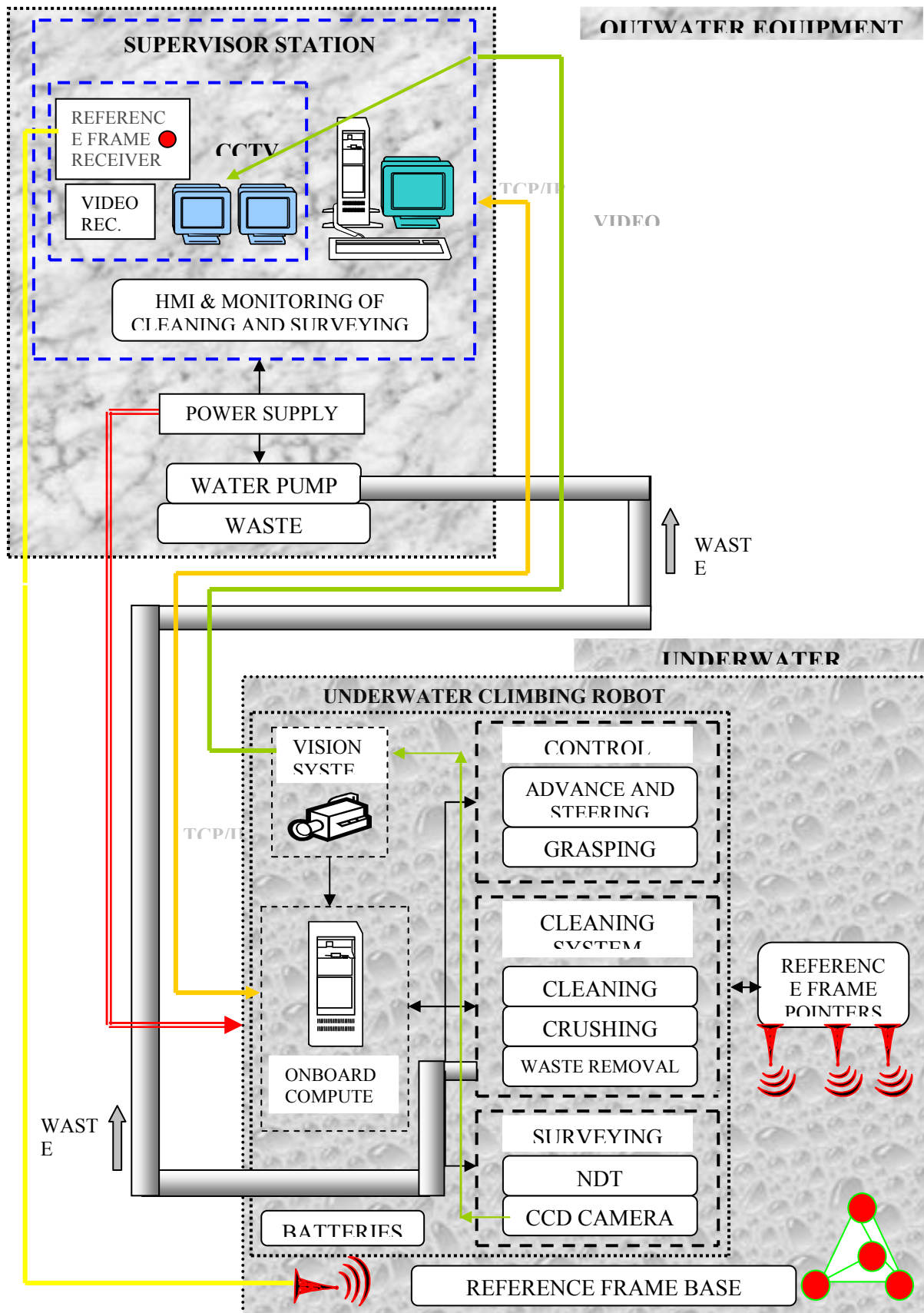
Figure 16. AURORA architecture.

6 CONCLUSIONS

Some achievements in the field of climbing robots related to the maritime industries in the last years have been presented. Most of the systems have being conceived to solve practical problems, but a lot of research is underlying and there are still many open questions.

ACKNOWLEDGEMENTS

REFERENCES

[1] Zhang, C. and Song, S.M. "Gaits and Geometry of a Walking Chair for the Disabled". J. of Terramechanics. Vol.26, Nº3/4 1989.

[2] Lee, J.K. and Song, S.M. "Path Planning and Gait of Walking Machine in an Obstacle-Strewn Environment". J. Rob. Syst., Vol.8, Nº 6. 1991.

[3] Kawato, M., Uno, Y. and Suzuki, R. "Formation and Control of Optimal Trajectory in Human Multijoint Arm Movement". Biological Cybernetics. Vol. 61. 1989.

[4] Zefran, M., Kumar, V. and Yun X. "Optimal Trajectories and Force Distribution for Cooperating Arms". Proc. IEEE Int. Conf. Rob. Autom. pp.1005-1012. San Diego 1994.

[5] Grace, A. "Optimization Toolbox User's Guide". The MathWorks Inc. Mass. USA. 1994.

[6] Grieco, J.C.; Prieto, M.; Armada, M.; González de Santos, P. "A Six-Legged Climbing Robot for High Payloads". 6th IEEE Conference on Control Applications ICCA'98. Trieste, Italy. September 1-4, 1998.

[7] Grieco, J.C., Armada, M., González de Santos, P. and Guerrero, A. "Computer-Aided-Design of a Climbing Robot for Harsh Environment". IFAC Workshop on Human-Oriented Design of Advanced Rob. Syst. DARS 95. Vienna, Austria. September 1995.

[8] Grieco, J.C.; "Robots escaladores. Consideraciones acerca del diseño, estabilidad y estrategias de control.". Tesis Doctoral. Universidad de Valladolid, Spain. 1997.

Author´s Index

273